

The plasma membrane attachment of Remorin
microdomain marker proteins is stabilized by
S-acylation



Dissertation

An der Fakultät für Biologie der
Ludwig-Maximilians-Universität München

Institut für Genetik

vorgelegt von

SEBASTIAN STEFAN ALOIS KONRAD

aus München

2015

Die vorliegende Arbeit wurde im Bereich Genetik der Arbeitsgruppe von Herrn Prof. Dr. Thomas Ott angefertigt.

Erstgutachter: Herr Prof. Dr. Thomas Ott

Zweitgutachter: Herr Prof. Dr. Marc Bramkamp

Tag der Abgabe: 23.06.2015

Tag der mündlichen Prüfung: 20.10.2015

Für meine Eltern

Sometimes feeling small is necessary. It helps you grow.

-Chris Burkard

Eidesstattliche Versicherung

Hiermit erkläre ich an Eides statt, dass ich die vorliegende Arbeit selbstständig, und ohne unerlaubte Hilfe von Dritten angefertigt habe.

München, den

(Sebastian Stefan Alois. Konrad)

Erklärung

Ich habe weder anderweitig versucht, eine Dissertation einzureichen oder mich einer Doktorprüfung zu unterziehen, noch habe ich diese Dissertation oder Teile derselben einer anderen Prüfungskommission vorgelegt.

München, den

(Sebastian Stefan Alois Konrad)

Table of contents

1	Summary	11
1.1	Summary	11
1.2	Zusammenfassung	13
2	Introduction	15
2.1	The plasma membrane is an interface for cell signalling.....	15
2.1.1	Physical interactions and behaviour of plasma membrane components.....	16
2.2	Membrane compartmentalization.....	28
2.2.1	Lipid raft hypothesis.....	28
2.2.2	Extrinsic factors alter membrane compartmentalization.....	30
2.2.3	Diversity of membrane domains	34
2.3	Remorins as a model to label membrane domains.....	39
3	Results	43
3.1	Overview of Publications.....	43
3.2	Publication I: Plasma Membranes are Sub-compartmentalized into a Plethora of Coexisting and Diverse Microdomains in <i>Arabidopsis</i> and <i>Nicotiana benthamiana</i>	45
3.3	Publication II: S-Acylation anchors remorin proteins to the plasma membrane but does not primarily determine their localization in membrane microdomains	73
3.4	Publication III: Knockin' on pollen's Door: Live cell imaging of early polarization events in germinating <i>Arabidopsis</i> pollen	99
3.5	Manuscript: Dissecting the multi-component assembly of a meso-scale membrane domain that controls host cell infection in <i>Medicago truncatula</i>	127
3.6	Current projects.....	171
3.6.1	Results	171
3.6.2	Material and Methods	177
4	Discussion	183
4.1	Membrane domains represent a new layer of compartmentalization.....	183
4.1.1	The role of Remorin lipidation.....	183

4.1.2	The diversity of Remorin labelled membrane domains opens new possibilities to investigate PM sub-compartmentalization	186
4.1.3	The influence of the cytoskeleton and cell-wall on membrane dynamics.....	187
4.1.4	Investigating the biological function of punctate membrane domains by active mislocalization of the immune receptor FLS2 within the PM	189
5	Abbreviations.....	193
6	Danksagung.....	195
7	References	197
8	Curriculum Vitae	217

Additionally to the indicated publications, parts of the introduction and discussion of this work have been published in:

Konrad, S. and Ott, T.(2015). Molecular principles of membrane microdomain targeting in plants. *Trends in Plant Science*. **20**: 351–361.

The manuscript underlying this publication was written by Sebastian S. A. Konrad

I hereby confirm the above mentioned statements:

.....

Prof. Dr. Thomas Ott

.....

Sebastian S. A. Konrad

1 Summary

1.1 Summary

Prokaryotic as well as eukaryotic cells are always surrounded by a lipid bilayer, the plasma membrane. This membrane enables the cell to sustain a defined reaction volume and prevent the loss of metabolic products. Plasma membranes are special as they are areas of information exchange between the cell and its environment. They are complex multi-component systems composed of lipids and proteins. Non-random segregation of lipids as well as proteins into distinct areas, so-called membrane domains, was shown in various cell-biological model organisms. Up-to-now, the basic principles of membrane domain formation and the physiological relevance of these areas in plants have been unanswered. Using modern microscopy techniques, the occurrence of different classes of membrane domains has been demonstrated. Mesoscale microdomains are the most commonly observed pattern of membrane domains. Sizes, close to the resolution limit of advanced light microscopy are specific for this type of membrane domain. In this work, Remorin proteins of the model organism *Arabidopsis thaliana*, are established as marker proteins for different plant plasma membrane microdomains. Quantitative image analysis revealed that microdomains labelled by Remorin proteins differed in size, fluorescence intensity, circularity, domain density as well as in lateral diffusion behaviour. Comprehensive co-localization analysis demonstrated that phylogenetically closely related Remorins also labelled more similar types of membrane domains compared to those targeted by distantly related ones. This set of marker proteins provides a useful tool for further characterization of plant microdomains.

Furthermore, the membrane binding mechanism of Remorin proteins was investigated during this work. The covalent binding of lipid anchors was shown to be a key feature of membrane attachment for Remorin proteins. Contrasting to other proteins, this so-called S-acylation reaction happens at the carboxy-terminal end of Remorins. Even though S-acylation often correlates with protein localization to membrane domains, it was shown that this post-translational modification does not enhance localization of Remorin proteins to microdomains. Thereby this work contributed important information on the constitution of membrane domain resident proteins in plants.

In summary, this work has provided the basis for future studies to investigate the influence of protein sub-organization during signal transduction of extracellular stimuli.

1.2 Zusammenfassung

Pro- und eukaryotische Zellen sind grundsätzlich von einer Lipiddoppelschicht umgeben. Diese Biomembranen ermöglichen es einer Zelle, ein definiertes Reaktionsvolumen aufrecht zu erhalten und verhindern den Verlust von Syntheseprodukten zellulärer Stoffwechselreaktionen. Die eine Zelle umschließende Plasmamembran ist ferner ein Ort des regen Informationsaustausches zwischen der Zelle und ihrer Umgebung. Speziell diese Plasmamembran ist ein komplexes Mehrkomponentensystem aus Lipiden und Proteinen. Die Unterteilung von Plasmamembranen in voneinander abgegrenzte Bereiche, den sogenannten Membrandomänen, konnte in verschiedensten zellbiologischen Modellorganismen gezeigt werden. Jedoch sind bis zum heutigen Tag die grundlegenden Mechanismen, welche zur Bildung dieser Bereiche beitragen, sowie deren physiologische Relevanz nicht abschließend geklärt. Anhand mehrzelliger Organismen, wie beispielsweise Pflanzen, konnten in den letzten Jahren verschiedener Klassen von Membrandomänen identifiziert werden. Die am häufigsten beobachtete Membrandomänenklasse sind sogenannte Mikrodomänen, welche sich vor allem durch ihre Größe nahe der Auflösungsgrenze fortgeschrittener optischer Mikroskopieverfahren auszeichnen. Remorine sind pflanzenspezifische, plasmamembranständige Proteine und lokalisieren in eben jene Mikrodomänen. In dieser Arbeit konnten Remorine des zellbiologischen Modellorganismus *Arabidopsis thaliana* als Markerproteine für unterschiedliche Mikrodomänen der pflanzlichen Plasmamembran etabliert werden. Mikrodomänen, welche von unterschiedlichen Remorin Proteinen markiert werden, unterscheiden sich durch Größe, Signalintensität, Form, Dichte der Domänen, sowie die lateralen Diffusionsgeschwindigkeiten. Dieses Markerproteinset ist ein nützliches Werkzeug für zukünftige Charakterisierungen pflanzlicher Mikrodomänen.

Im Weiteren wurde im Rahmen dieser Arbeit die Ursache der Membranlokalisierung von Remorin Proteinen untersucht. Hierbei konnte gezeigt werden, dass die kovalente Bindung eines Fettsäurerestes ein essentieller Bestandteil des Membranbindemechanismus von Remorinen ist. In Remorinen findet dieser als S-Acylierung bekannte Mechanismus ausschließlich in der Carboxy-terminalen Region der Proteine statt. Obwohl S-Acylierung ein bekanntes Motiv Mikrodomänen-assoziiierter Proteine ist humaner Zellen ist, konnte gezeigt werden, dass diese post-translationale Modifikation nicht primär zur Lokalisation von Remorinen in Mikrodomänen beiträgt. Durch diese Ergebnisse bildet diese Arbeit die Grundlage für zukünftige Studien, welche sich mit dem Einfluss von Membrandomänen auf Signal-Weiterleitungsprozesse aufgrund von extrazellulären Stimuli beschäftigen.

2 Introduction

2.1 The plasma membrane is an interface for cell signalling

The confinement of a defined environment was a vital achievement of cellular life. In all living organisms, this task is conferred by biological membranes. These membranes act as selective barriers that enable a cell to concentrate nutrients extracted from its environment and retain the products it synthesizes for its own use. Without membranes, a cell could not maintain its integrity as a coordinated chemical system.

Eukaryotic cells have evolved a sophisticated intracellular membrane system that further subdivides the interior of a cell into several cell organelles. These organelles spatially separate various compartments, allowing diverse functions such as transport, post-translational modifications or metabolic reactions. The outermost membrane, the plasma membrane (PM) is the major interaction interface of a cell with its environment. Numerous proteins embedded or associated with the PM act as sensors, allowing the cell to alter its behaviour in response to external signals.

Receptor-like kinases (RLKs) are one example of PM receptors that initiate the activation of multi-staged signalling cascades that transduce extracellular signals into the intracellular space. The structure of RLKs commonly consists of an amino (N)-terminal extracellular domain and a carboxy (C)-terminal kinase domain, which are connected by a membrane spanning transmembrane domain (Walker, 1994). Plant RLKs and the homologous animal Pelle-kinases evolved from a common ancestor. Yet in plants, the collection of RLKs has enormously diversified. Only 4 RLK representatives are found in humans while, over 600 members of the RLK protein superfamily are annotated in the *Arabidopsis thaliana* genome (Shiu and Bleecker, 2001a; Shiu and Bleecker, 2001b; Gish and Clark, 2011). One of these *A. thaliana* RLKs is the Brassinosteroid receptor BRASSINOSTEROID INSENSITIVE 1 (BRI1) (Li and Chory, 1997; Wang et al., 2001). BRI1 is a PM localized RLK with a large extracellular Leucine-rich repeat (LRR) domain that is capable of binding 24-(epi)-brassinolide with high affinity (He et al., 2000; Kinoshita et al., 2005). BRI1 mediated brassinolide signalling depends on the interaction of BRI1 with a second LRR-RLK, the BRI1-ASSOCIATED KINASE 1 (BAK1) (Li et al., 2002; Nam and Li, 2002) and regulates plant development and physiology (Zhu et al., 2013). Besides its role in brassinolide signalling, BAK1 has also been found to be an important component of signalling complexes that are essential for plant-pathogen resistance, where it acts as a co-receptor with several pattern recognition receptors, including FLAGELLIN INSENSITIVE 2 (FLS2) and EF-TU RECEPTOR-1 (EFR) (Chinchilla et al., 2007; Heese et al., 2007; Chinchilla et al., 2009; Postel et al., 2010).

BAK1 is only one example of a PM kinase receptor that is involved in several very different

signalling processes. Yet, cellular responses to external stimuli can be measured within minutes after signal perception (Asai et al., 2002). This is astonishing, considering the entanglement of different signal transduction cascades and that availability of receptors and their interaction partners is limited (van Esse et al., 2011). It also highlights a major question that biology is facing: How is it possible that signalling events are efficiently orchestrated and rapidly transduced, when there's an abundance of putative interaction partners available?

Observations on several membrane components have led to the hypothesis that an organized sub-compartmentalization of cellular membranes is present and may be responsible for efficient cellular signalling events (Simons and Ikonen, 1997). While PM sub-compartmentalization is nowadays widely accepted, its underlying mechanisms as well as functional implications are still a matter of debate (Kraft, 2013). In order to understand membrane sub-compartmentalization, fundamental properties of membranes and their components should be considered, which will be done in the first part of this work. The second part deals with examples that illustrate the variety of membrane sub-compartmentalization in plants known today.

2.1.1 Physical interactions and behaviour of plasma membrane components

2.1.1.1 Lipid-lipid interactions define major principles within a 2-dimensional liquid

Despite their diverse functions, all biological membranes share a common structure, which is a $\sim 45 \text{ \AA}$ thick double layer containing lipids and proteins. Lipids are the major building blocks of membranes because their physical properties dictate the shape and characteristics of every membrane. Lipid molecules are amphiphilic, meaning that they consist of a hydrophilic, so called "head group" and a hydrophobic "tail". The most abundant lipid molecules are phospholipids of which phosphatidylcholine (PtdCho), phosphatidylethanolamine (PtdEtn), phosphatidylserine (PtdSer) and Phosphatidylinositol (PtdIns) are the major representatives in eukaryotic membranes (van Meer et al., 2008).

A three-carbon glycerol molecule acts as the backbone of phospholipids, which is connected to the hydrophilic head via a phosphate group. These head groups mostly consist of simple organic molecules such as choline or serine. Head groups are of structural and in some cases functional importance for the cell (van Meer et al., 2008). A subgroup of phospholipids, the phosphoinositides for example have a *myo*-inositol head group that can be phosphorylated on positions 3, 4 and 5 of its cyclohexane ring which serves as a binding site for proteins and can act as a messenger molecule (Mueller-Roeber and Pical, 2002; Meijer and Munnik, 2003; Shisheva, 2008).

The hydrophobic tail of phospholipids consists of two hydrocarbon (or acyl-) chains, which are covalently linked to the phospholipid glycerol backbone via an ester bond. These acyl chains can

differ in length as well as in the amount of *cis*-double bonds. Acyl chains that contain no *cis*-double bond are called “saturated” whereas “unsaturated” hydrocarbon chains contain at least one *cis*-double bond that introduces a small kink in the molecule (Jain, 1989). Differences in length and saturation status of the lipids hydrocarbon chains determine how phospholipids pack against one another, thereby affecting the fluidity of the membrane. Especially unsaturated hydrocarbon chains decrease the possible packing density of membrane phospholipids because they require more space than saturated hydrocarbon chains (Jain, 1989). Plants synthesize a huge variety of hydrocarbon chains including very long acyl chains with more than 18 carbon atoms. The most abundant acyl chains in *Arabidopsis thaliana* 5 week old leaves are the 18 carbon, 3 *cis*-double bond gamma linoleic acid (18:3), linolenic acid (18:2) and palmitic acid (16:0) (Yonghua et al., 2013).

Long-chain hydrocarbon chains are often found in sphingomyelins (SM). SMs are special phospholipids, as their backbone structure does not consist of glycerol but of ceramide. This backbone, is built of a sphingoid base, such as sphingosine that is an amide linked to a saturated acyl chain typically 16-24 carbon atoms long. However, SMs are classified as phospholipids due to their head-groups being linked to the glycerol via a phosphate group. Often found head groups include phosphocholine or phosphoethanolamine (Fahy et al., 2005).

Sterol lipids are the third major group of structurally important biomembrane lipids. They generally consist of a tetracyclic structure with a polar group at the equatorial position of its first ring and a short hydrophobic acyl chain that branches from the 4th (“D”) ring. Cholesterol is the main sterol present in mammals and ergosterol is the predominant sterol species in fungi. Plants usually possess more complex sterol compositions with cholesterol, stigmasterol and sitosterol being the most abundant membrane sterols (Yonghua et al., 2013).

Within a membrane, lipids are able to move in various ways. Using artificial membranes lipids have been observed to rotate around a central axis, wobble from side to side, and last - but most importantly - laterally diffuse (Sergent et al., 2012). In general, lipid membranes can be regarded as a two dimensional liquid, however all movements of membrane components are restricted by the composition of membrane lipids and the packing density of membrane components. Since membranes are mixtures of a vast number of different components, they can be seen as “peculiar” liquids. In fact, membranes are able to adopt several states of fluidity, or so called “lipid phases” (Veatch et al., 2008; Honerkamp-Smith et al., 2009). These phases have specific characteristics that determine the orientation and mobility of membrane lipids as well as proteins within the membrane. Mixtures that are enriched with glycerophospholipids, which possess mostly unsaturated acyl chains, adopt a so-called “liquid disordered” phase where the packing density within the membrane core is low but individual lipids have a large freedom of movement and therefore are able to diffuse relatively fast (Bagatolli et al., 2010). In contrast, membrane mixtures enriched

Introduction

in sphingolipids that harbour long chain saturated acyl chains, tend to adopt so-called solid-gel phases with high packing densities and low diffusion rates (Bagatolli et al., 2010). Astonishingly, when sterols are introduced into membrane mixtures of phospholipids, a liquid-ordered phase is formed. This phase has a high packing density like solid-gel phases but retains the high diffusion capacity of liquid-disordered phases (Ipsen et al., 1987).

Since individual lipids undergo strong intermolecular interactions, large artificial bilayer assemblies display several regions of different lipid phases, thereby compartmentalizing the membrane into compositionally different areas. This phenomenon called “phase separation” is a product of lipid unmixing and frequently observed in artificial as well as cellular derived membrane preparations (Bagatolli et al., 2010). Importantly, lipid unmixing does not generate a fixed state. Phase transitions of lipids continuously form and fall apart. This effect can be best described as a condition close to a critical point. Observations on giant plasmamembrane vesicles (GPMVs), which are chemically induced blebs of plasma membranes, showed that plasma membranes exist close to a critical point of miscibility where density fluctuations are large, which might give an explanation for dynamic assembly of lateral membrane compartments (Veatch et al., 2008; Honerkamp-Smith et al., 2009) .

Importantly it has to be noted that experimental evidence for phase transition in living cells is still missing and even the exact properties of liquid-ordered phases are under debate (Fidorra et al., 2006; Subczynski et al., 2007). While some neglect the existence of liquid-ordered phases *in vivo*, it might well be that they are too small to observe with currently available techniques (Subczynski et al., 2007; Feigenson and Buboltz, 2008; Lee et al., 2015).

Besides the intrinsic complexity of every membrane it is apparent that even different membranes within a cell have very distinct lipid compositions. Late endosomes of mammalian cells for example have a considerable lower sterol content compared to overall phospholipid abundance, than the PM (van Meer et al., 2008). Moreover, biological membranes are highly asymmetric. The PM for example maintains a high PtdCho and SM content at the outer leaflet and high PtdEtn and PtdSer concentration at the inner membrane leaflet (Rothman and Lenard, 1977; Tejos et al., 2014).

Phase separation of lipids and hydrophobic mismatch are believed to represent major forces that drive the subcompartmentalization of biological membranes. However, the complexity of distribution and intermolecular interactions of basic membrane components have so far been underestimated and proven to be a major obstacle when studying membrane organization. Moreover, biological membranes do not only consist of lipids. They are an almost equimolar mixture of proteins and lipids (Wallin and von Heijne, 1998; Komatsu, 2008; Almén et al., 2009). Therefore, besides being functional components, proteins as well have to be considered as

important building units of biological membranes. To understand the relationship between proteins and lipids, one has to look at the various mechanisms of how proteins can attach to a membrane.

2.1.1.2 Membrane proteins are in close interaction with their solvent

2.1.1.3 Membrane attachment mechanisms – integral membrane proteins

Approximately 30% of all human gene products and 25% of *A. thaliana* proteins are integral parts of membrane systems (Schwacke et al., 2003). There are several ways how proteins can be attached to a membrane. Many important signalling and transport proteins pass between the lipid bilayer with a helical transmembrane domain (TMD) (Figure 1 A). Like the lipids that surround them, these TMDs are amphiphilic. The amino acids composing TMDs are in tight contact with the acyl chains of membranes lipids. In order to adapt to the steep hydrophobicity gradient at the lipid/water interface, amino acids containing large charged side chains such as Lysine or Arginine are commonly found in these particular regions. While the aliphatic part of these amino acids prefers the localization within the bilayer, the charged end has a preference to locate in a polar environment (Killian and von Heijne, 2000). Aromatic residues like Tryptophane and Tyrosine form an aromatic belt that is proposed to interact with lipid headgroups (Killian and von Heijne, 2000). TMDs are usually 15-20 amino acids long and most commonly form α -helical structures, with 3.6 amino acids per turn (Alberts et al., 2007). In addition to α -helical structures other helical secondary structures such as the 3_{10} -helix or the energetically favourable π -helix can also be rarely found (Alberts et al., 2007).

Sensory proteins such as RLKs are often single-pass transmembrane proteins that span the plasma membrane via one TMD (Shiu and Bleecker, 2001a; Shiu and Bleecker, 2001b). This enables proteins to connect extracellular sensory domains with cytosolic signal transducing kinase domains (Shiu and Bleecker, 2001a; Shiu and Bleecker, 2001b). Some proteins pass more than once through the PM and are referred to as polytopic transmembrane proteins. Very often, weak hydrogen bonds between different TMDs are observed, which helps to stabilize the tertiary structure of polytopic TMD proteins (Figure 1 B). Many mammalian receptor proteins contain polytopic TMDs (Fredriksson et al., 2003).

In plants, proteins that are responsible for selective solute transport for molecules such as sugars, hormones, often introduce passages into the membrane via multiple amphipathic α -helices. The pore forming TMDs can be derived from one polytopic peptide, or may be composed of different subunits of one protein complex. Examples of membrane proteins with multiple TMDs are plant aquaporins, RESPIRATORY BURST OXIDASE HOMOLOGUE D (RBOHD) and F (RBOHF)

Introduction

as well as SWEET sugar transporters and DHHC-motif containing protein S-acyl transferases (Torres et al., 1998; Maurel et al., 2009; Chen et al., 2010; Batistič, 2012).

Membrane attachment via α -helical structures does not necessarily result in membrane spanning. Some proteins contain so-called “membrane dipping” loops that penetrate only one layer of the membrane (Gonen et al., 2004; Van den Berg et al., 2004; Yernool et al., 2004). Others contain amphipathic helices, which also insert into only one membrane leaflet (Figure 1 C). Besides being α -helical, transmembrane segments may also be formed by several β -sheets, resulting in a cylindrical structure called the β -barrel (Figure 1 H). Even though the basic principles of amino acid compositions are the same for α -helices and β -barrel, the later always introduces a pore in the membrane and is therefore a common motif found in ion channels and transporter proteins.

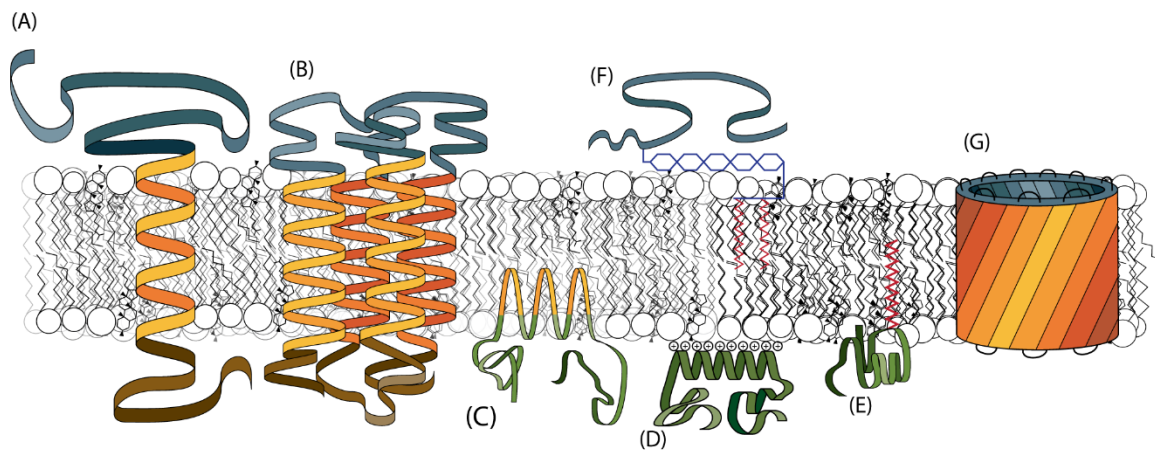


Figure 1: Different modes of membrane attachment.

Proteins can bind to membranes through various mechanisms. (A) Helical TMDs span the lipid bilayer. This motif is often found in surface receptors such as the RLK FLS2. (B) Polytopic transmembrane proteins surpass membranes using several helical TMDs. Hydrogen bond interactions often stabilize the tertiary structure of these proteins. (C) Amphipathic helices insert only into one membrane leaflet by concentrating amino-acids with hydrophobic side-chains at one side of the helix. (D) Polybasic stretches of amino-acids do not enable direct membrane attachment, but confer weak associations to negatively charged membranes via electrostatic interactions. (E) Depending on the type of lipid, post-translational lipidations can confer weak to very strong attachment to the membrane. (F) GPI-anchored proteins are soluble proteins, covalently linked to this lipid anchor. They are exclusively found at the outer membrane surface. (G) Amphipathic amino-acid stretches might also fold into a barrel-like structure that is often found in ion-channels or transporter proteins.

In addition polybasic stretches of amino acids can confer a weak but significant affinity of a peptide towards membranes (Jack et al., 2008). They are particularly interesting because post-translational modifications such as phosphorylation may alter the charge of polybasic amino acid stretches and thereby vary the membrane affinity of the protein (Figure 1 D) (Goldenberg and Steinberg, 2010; Maures et al., 2011)

Apart from intrinsic protein composition other modes of membrane attachment have been identified. Post-translational modifications are commonly known to be important regulators of protein function. Besides the direct impact on protein function, post-translational modifications can also alter protein localization and affinity to membrane environments. In particular, protein lipidations are post-translational modifications, where hydrophobic molecules are attached to a protein, resulting in its membrane attachment (Figure 1 E). Among the added moieties are the polyisoprene lipids farnesyl and geranylgeranyl as well as fatty acids such as myristate, stearate or palmitate. The chemical nature of protein lipid modifications is very similar to lipids that are associated to membrane domains. Therefore it may not be surprising that lipidated proteins are often found to be associated with membrane subcompartmentalization (Levental et al., 2010; Hemsley et al., 2013).

Among all lipid modifications, glycosylphosphatidylinositol (GPI)-anchored proteins are special (Figure 1 F). This lipid modification of proteins consist of a phosphodiester linkage of a protein to the glycolipid glycosylphosphatidylinositol. It is conferred by a transamidase complex, located at the luminal side of the endoplasmic reticulum (ER). Consequently GPI-anchored proteins are always localizing to the ER lumen or the apoplast. In plants, a special variant with a glycosylinositolphosphoryl ceramide glycoprotein has been identified, which serves the same function but has not been described in animal systems (Sperling et al., 2004). The term “anchor” is specifically adequate because the GPI-moiety introduces a substantial distance between the protein and the membrane it is attached to. Enzymatic cleavage by several phospholipases is known to release GPI-anchored proteins from their lipid binding motif in animals and similar mechanisms have been described in plants (Elortza et al., 2006).

GPI-anchored proteins are widespread in eukaryotes. The most prominent example of GPI-anchored proteins are the variable surface glycoproteins (VSG) of several *Trypanosoma* species. Trypanosomes are parasitic single celled organisms of which some species are the causative organism of human sleeping sickness. VSG-proteins are highly variable in their amino acid sequence as well as their glycosylation pattern, and constitute the major mechanism by which Trypanosomes evade the host immune system (Vanhamme et al., 2001). In *Arabidopsis* there are 248 membrane proteins that are predicted to be GPI/GIPC-anchored (Borner et al., 2003). Among these are proteins related to cell-wall modification, receptor-like proteins and various proteases and

phytoeyanins (Borner et al., 2003).

The addition of 14 carbon myristoyl chains to an N-terminal glycine via an amide bond is known as myristoylation (Figure 2). The reaction is catalysed by N-myristoyl transferases (NMTs), which are represented by 2 isoforms in *Arabidopsis* (Boisson et al., 2003). N-myristoylation is usually a co-translational modification but can also occur when internal glycines are exposed due to post-translational proteolytic processing (Boisson et al., 2003). In *Arabidopsis*, 319 proteins are predicted to be N-myristoylated (Podell and Gribskov, 2004). With 1.7% of the complete proteome putatively being N-myristoylated, plants contain a larger myristoylome than expected from comparisons to metazoans and fungi (Marmagne et al., 2007). Surprisingly the *Arabidopsis* myristoylome contains many unusual protein families such as thioredoxins and transcription factors but also components involved in innate immunity, protein degradation and 6-phosphofructo-2-kinase/fructose-2,6-bisphosphate 2-phosphatase (F2KP) a central regulatory component of glycolysis (Boisson et al., 2003).

Regardless of its predicted abundance, myristoylation has been biochemically demonstrated for only few proteins (Running, 2014). Even though myristoylation is functionally important for some proteins such as the SnRK1 kinase (Pierre et al., 2007), this lipidation primarily increases membrane affinity of polypeptides. Moreover, recent work correlates the efficiency of N-myristoylation with membrane association of h-type thioredoxins (TRX). Since only a sub-fraction of the cellular TRX protein population resides at the PM it remains to be elucidated whether the membrane anchoring capability mediated by N-myristoylation is too weak, or if myristoylation correlates with the activation status of different TRX family members (Traverso et al., 2013).

The covalent addition of the 15- or 20-carbon isoprenoids farnesyldiphosphate or geranylgeranyldiphosphate via a thioether bond to one or more cysteine residues, close to the C-terminus of target proteins is known as prenylation (Figure 2) (Zhang and Casey, 1996). Prenylation is an abundant post-translational modification with 950 putative target proteins in *Arabidopsis* (Running, 2014). Three enzymes, the protein farnesyltransferase (FTase), protein geranylgeranyltransferase and Rab geranylgeranyltransferase (GGTases) catalyse prenylation reactions (Maurer-Stroh et al., 2003; McTaggart, 2006). Examples of prenylated proteins are the membrane anchored ubiquitin fold (MUB) family of proteins, which are likely to be farnesylated, as well as ROP6, a small GTPase that has been shown to be geranylgeranylated (Downes et al., 2006; Sorek et al., 2007).

During S-acylation acyl chains such as palmitoyl or stearyl are attached to cysteine residues, a reaction that can occur along the whole protein (Figure 2). The post translational addition of acyl chains is mediated by the action of protein acyl transferases (PATs) (Roth et al., 2002; Huang et al., 2004; Hemsley et al., 2005). PATs are represented by 24 family members in *Arabidopsis*. Individual

gene products of this large gene family localize to almost every membrane of the cell and are ubiquitously found in all tissues and throughout development (Schiefelbein et al., 1993; Ryan et al., 1998; Hemsley et al., 2005; Batistič, 2012; Zhou et al., 2013). The only two mutant alleles described for PAT enzymes show pleiotrophic phenotypes, indicating that both enzymes PAT24 and PAT10 have a broad range of target proteins (Schiefelbein et al., 1993; Ryan et al., 1998; Hemsley et al., 2005; Zhou et al., 2013). As with all lipidation reactions, a weak interaction of peripheral proteins with the membrane is necessary to enable the substrates to interact with their cognate PAT and subsequently their lipidation (Rocks et al., 2010).

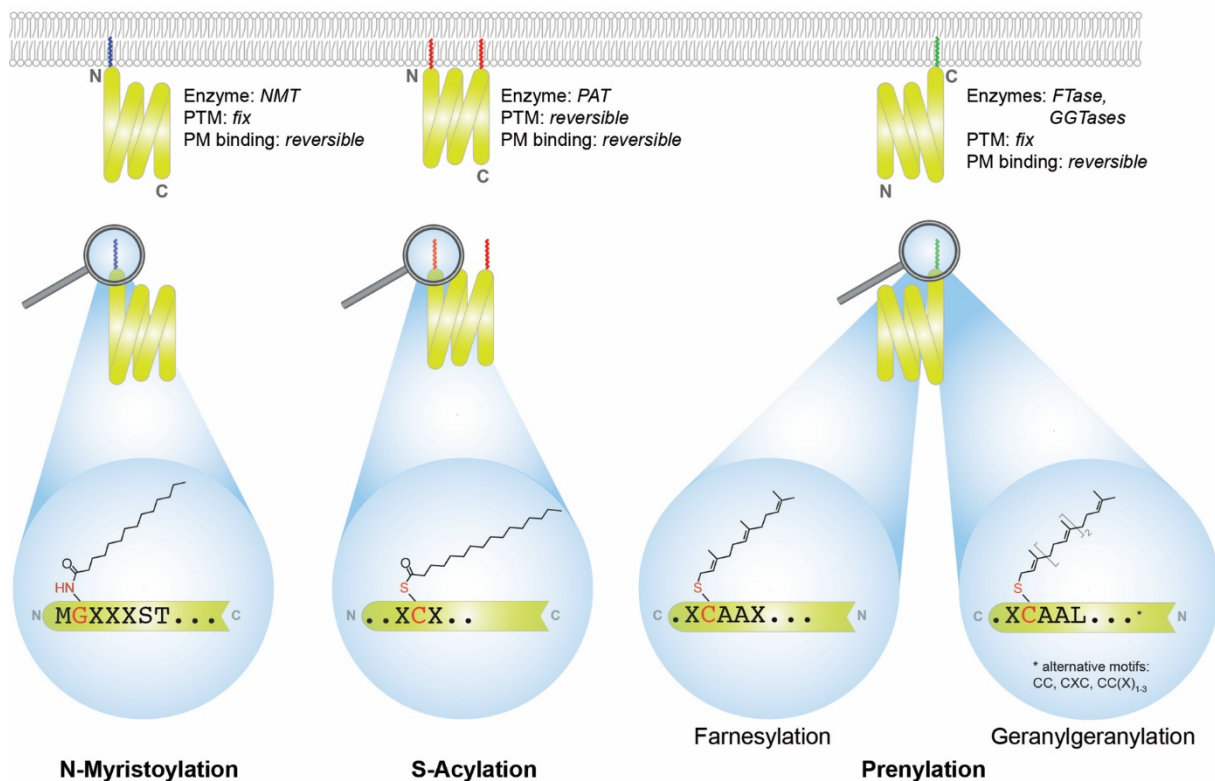


Figure 2: Common post translational protein lipidations.

N-myristoylation is conferred by N-myristoyl transferases (NMTs) at N-terminal glycine residues in position 2 of the peptide. The amide-linked myristoyl group confers a weak affinity to lipid bilayers. S-acylation of proteins on the other side enables a strong attachment to membranes. Here, palmitoyl or stearoyl groups are bound to cysteine residues via thioester linkages by the action of protein acyl-transferases (PAT). The enzymatic action of acyl-protein thioesterases (APT) may cleave this bondage, making S-acylation the only reversible post-translational protein lipidation. Farnesyl- or Geranylgeranyltransferases catalyze the attachment of Farnesyl or Geranylgeranyl groups during prenylation. S-acylation and prenylation can occur throughout the protein. (Adapted from Konrad and Ott (2015))

Introduction

In contrast to other lipidations, S-acylation is reversible, a reaction which is catalysed by the action of acyl-protein thioesterases (APTs) and palmitoyl protein thioesterases (PPTs) that cleave the thioester bond between the S-acylated protein and the acyl chain (Camp and Hofmann, 1993). Thioesterase activity allows dynamic modulation of membrane affinities and chemical properties of S-acylated proteins (Camp and Hofmann, 1993). This permits protein shuttling between cellular compartments (Roy et al., 2005; Zeng et al., 2007). S-acylation has been shown to be required for processes such as subcellular sorting, protein-protein interactions, trafficking and protein activation (Hemsley et al., 2013). For example, it is crucial for the functionality of the immune receptor FLS2 (Hemsley et al., 2013), for activation of the defence related proteins RAC-LIKE GTP-BINDING PROTEIN 1 (RAC1) (Kawano et al., 2014) and RPM1 INTERACTING PROTEIN 4 (RIN4) (Kim et al., 2005) and membrane localization of the bacterial effectors AvrRpm1 and AvrB (Nimchuk et al., 2000).

N-myristoylation and prenylation are often observed to appear in combination with S-acylation. For example, proteins like ROP6 and the heterotrimeric G-protein γ -subunits AGG1 and AGG2 which are type-I ROPs, the rho equivalent kinases in plants, are found to be prenylated as well as S-acylated (Sorek et al., 2007; Zeng et al., 2007). Examples of N-myristoylated and S-acylated proteins can be found in many well studied protein classes such as calcium-dependent protein kinases (CPKs), calcineurin-B like proteins (CBLs) and receptor-like cytoplasmic protein kinases (Martín and Busconi, 2000; Batistič et al., 2008; Hemsley et al., 2013). This may be due to the fact that the addition of a single palmitoyl moiety contributes to a membrane affinity that is 5 times stronger than a single geranylgeranyl group, 10 times stronger than a myristoyl moiety and 100 times stronger than a farnesyl group and longer S-acyl chains even increase the strength of membrane interaction (Silvius and l'Heureux, 1994; Shahinian and Silvius, 1995). In fact, S-acylated proteins are often as insoluble during protein purifications as TMD containing proteins (Hemsley and Grierson, 2008).

It can be speculated, whether these double lipid modifications are crucial auxiliary effects for membrane association or provide a functional component. Considering the fact that all types of post-translational lipid modifications can be dynamically modified through lipid and electrostatic switches, these membrane attachment mechanisms appear to be highly dynamic, arguing for a functional involvement (Resh, 2006). This functional aspect may not only be restricted to an on/off status of membrane localization. Recent advances in membrane research showed that membrane proteins are actively interacting with their lipid environment. These interactions highly influence the lipid composition in the protein's vicinity (see 2.1.1.1 and 2.1.1.4). Therefore it has been speculated that protein-lipid modifications confer functionality by recruiting specific lipids into the proximity of the lipidated protein. This recruitment is thought to nucleate the formation of a

microenvironment that accommodates other proteins with related miscibility properties. The process of lipid environment shaping may be one mechanism to organize the membrane, allowing dynamic attraction and exclusion of components into membrane compartments (Hurst and Hemsley, 2015). Protein-lipid interactions that are the basis of these considerations are discussed in the next chapters.

2.1.1.4 Protein-lipid interactions

Proteins embedded or attached to the lipid bilayer interact with their solvent. The nature of these interactions is diverse and may appear as an indirect response to circumvent thermodynamically unfavourable conditions or as attempts to actively shape the lipid bilayer composition. Moreover, protein-lipid interactions may involve direct binding, which is a common feature to facilitate signalling events.

2.1.1.4.1 Indirect protein-lipid interactions

Indirect protein-lipid interactions are a result of the disturbance that a membrane protein imposes on lipid bilayers and is primarily driven by hydrophobic effects. Amino acids within a TMD that are located inside the lipid bilayer are in tight contact with the fatty acid chains of membrane lipids. Even though these amino acids share the same hydrophobicity as the hydrocarbon chains of a membrane's inner core region, they have considerable effects on the behaviour of surrounding lipids (Killian and von Heijne, 2000; Lee, 2003; Ernst et al., 2010).

The relative residence time of a particular lipid at the protein-lipid interface is often used to describe different types of interactions. So-called 'bulk lipids' show a short relative residence time close to membrane proteins and therefore a low degree of interaction with them. However, if lipids interact with membrane proteins, they display a significantly higher relative residence time in the vicinity of the protein-lipid interface. Electron spin resonance experiments showed lipids to have up to 10 times higher relative residence times within the proximity of a membrane protein compared to their diffusion in the rest of the bilayer (Marsh and Watts, 1982; Lee, 2003). This anomalous diffusion has also been observed in living cells using Fluorescence Correlation Spectroscopy (FCS) (Schwille et al., 1999). The composition of these lipids is protein specific and not necessarily homogeneous. For some proteins, the composition of these so-called 'annular lipids' even changes during different activation states (Soubias and Gawrisch, 2013).

Membranes are under constant stress to minimize the interfacial surface between aliphatic acyl chains and hydrophobic regions exposed by proteins. This hydrophobic mismatch is known as an indirect interaction of transmembrane proteins and the lipid bilayer that is the driving force in

Introduction

protein-sorting events and it is considered to have major implications on membrane lipid distribution. The concept of hydrophobic mismatch assumes that membrane spanning hydrophobic regions have to match the local membrane thickness (Mouritsen and Bloom, 1984). Experiments on the Na,K-ATPase illustrate nicely the functional implications of hydrophobic mismatch. Transporter activity is most efficient in membranes composed of lipids with 22 carbon long acyl chains. If transport kinetics are measured in thinner membranes, transport is prohibited but can be restored by addition of cholesterol, which thickens the membrane (Cornelius, 2001).

The thermodynamically unstable condition of hydrophobic mismatch can be solved by several mechanisms. The protein may diffuse to a membrane region with a fitting thickness or the lipid environment around the protein can change in a way that fits the proteins hydrophobic needs. Indeed it has been shown that the bilayer close to a protein differs from distant regions that proteins can induce local heterogeneities in lipid composition and drive phase separation in artificial membranes (Pink et al., 1984; Gawrisch et al., 1995; Vidal and McIntosh, 2005; McIntosh et al., 2008; Kaiser et al., 2011).

Apart from these local effects, proteins are also able to induce large-scale alterations to the membrane. If an amphipathic helix is introduced in only one leaflet of the lipid bilayer, the surface area from one side of the bilayer increases. This has to be counteracted by a bending of the bilayer to circumvent exposure of hydrophobic areas to an aqueous environment. This effect is playing a vital role in several membrane-bound processes. For example, during vesicle budding of COPI and COPII mediated retrograde and anterograde transport, membrane curvature is induced by the insertion of amphipathic helices of the small GTPases SAR1 and ARF1 (Antonny et al., 1997; Goldberg, 1998; Antonny et al., 2001). Many more examples of active membrane shaping can be found in vesicle budding mechanisms (Fromme et al., 2008; Spang, 2008).

Hydrophobic mismatch has also been observed to be important during protein sorting processes. The TMDs length of human transmembrane protein LINKER FOR ACTIVATION OF T-CELLS (LAT), greatly determines their targeting into sphingolipid and sterol enriched sites (Mouritsen, 2011; Diaz-Rohrer et al., 2014). Similar observations have been previously made for the directed targeting of TMD proteins to the PM or the ER membrane (Sharpe et al., 2010). Targeted trafficking and a mode by which the TMD composition orchestrates protein localization are well illustrated by the *A. thaliana* protein RESISTANCE TO POWDERY MILDEW 8.2 (RPW8.2). RPW8.2 localizes to the so-called extrahaustorial membrane that surrounds invading structures of pathogenic fungi and oomycetes (Wang et al., 2009). Targeted trafficking to this membrane is not only VAMP-dependent (Kim et al., 2014) but also relies on few residues within the TMD of RPW8.2 as demonstrated by site-directed mutagenesis (Wang et al., 2009). The

observation that mutation variants of the RPW8.2 TMD accumulate in various cellular compartments is in accordance with other studies that suggest a TMD-dependent pre-sorting of proteins at the ER (Sharpe et al., 2010; Cosson et al., 2013).

The general picture that emerges from these observations is that proteins induce locally restricted alterations in membrane lipid composition but membrane structure dictates localization of proteins.

2.1.1.4.2 Direct protein-lipid interactions

Apart from indirect interactions with membrane components TMDs have also been shown to directly interact with certain lipids that penetrate deep into the structure of the protein. In order to match the rough surface of a membrane protein, the lipid acyl chains of so-called ‘structural lipids’ bend and therefore prevent poor packing of the membrane. In some cases, structural lipids dramatically influence protein function. The binding affinities involved in these interactions can be so tight that structural lipids are able to be co-crystallized, as is possible with the potassium channel KIR2 or the TMD of the COPI machinery protein p24 (Hansen et al., 2011; Contreras et al., 2012). The binding of KIR2 to a phosphorylation species of PtdIns via a phospholipid binding domain within the protein’s TMD results in a large conformational shift of about 6 Å, which leads to an opening of the channel (Hansen et al., 2011).

A more general mechanism of lipid binding has been identified by Contreras and colleagues. Here, the binding signature VXXTLXXIY within the TMD of p24, a part of the COPI vesicle biogenesis complex, confers binding to specific SM classes. This interaction depends on both, the acyl chain as well as the head group of SM. Based on this binding signature, several more proteins were identified to bind SM. One of them, the interferon gamma receptor INGR1 was demonstrated to bind SM in a ligand dependent manner (Contreras et al., 2012).

Besides integral membrane proteins, peripheral proteins can also interact with membrane lipids via lipid-binding domains (LBDs). Direct lipid binding is especially important during phosphoinositide (PI) signalling, a common signalling pathway found in all eukaryotic cells that utilizes phosphorylation variants of PtdIns as second messenger molecules. PI signalling has been shown to be important during regulation of cytoskeletal dynamics, membrane trafficking and signalling processes (Janmey and Lindberg, 2004; Balla, 2006; Di Paolo and De Camilli, 2006; Krauß and Haucke, 2007). LBDs usually interact with negatively charged lipid headgroups but Ca²⁺ dependent interaction surfaces have also been reported (Yoshida et al., 1994; Ford et al., 2001; Jensen et al., 2001). The importance of lipid binding is illustrated by the fact that the *Saccharomyces cerevisiae* genome currently accommodates 172 proteins annotated to contain LBDs which bind to all major

lipid classes (Oriol et al., 2010). Unfortunately, *in vivo* data for LBDs binding specificities are missing for most LBDs (Oriol et al., 2010).

2.2 Membrane compartmentalization

The “fluid mosaic” model, introduced by Singer and Nicolson in 1972 became the first generally accepted model of membrane organization and the primary assumptions of the model are still valid (Singer and Nicolson, 1972). With this, the framework of basic physical interactions that hold biological membranes together, was set: Membranes can be regarded as 2-dimensional liquids composed of lipids and proteins. In their model, a membrane was believed to form a bilayer mixture of homogeneously distributed lipids that acts as a solvent for embedded or associated proteins. Based on experiments by Frye and Edidin, who fused mammalian cells and observed that within 40 min, proteins originating from two different cells were equally distributed over the fused PM (Frye and Edidin, 1970), they concluded that proteins must be able to diffuse freely within the membrane plane. Even though the fluid mosaic model assumed general uniformity within the membrane, Singer and Nicolson acknowledged the possibility of non-random distribution due to certain “mechanisms” (Singer and Nicolson, 1972) and indeed in the following years showed that components of the membrane can be unevenly distributed (Lucas and Smith, 1973; Bretscher, 1983; van Meer et al., 1987).

With an increasing number of scientists getting involved in the investigation of lateral membrane organization, it became apparent that many, if not the majority of membrane-resident proteins and lipids are unevenly distributed. Membrane compartmentalization appears to be an underlying organization principle of PMs in eukaryotic and prokaryotic cells (Harder, 2003; Ghossoub et al., 2011; Spira et al., 2012; Bach and Bramkamp, 2013; Reuter et al., 2013). These observations are the foundation of the current generally accepted opinion that membranes – especially the PM – are sub-organized into distinct compartments, most generally called ‘membrane domains’. However, these membrane domains exhibit a great plasticity with respect to parameters like size, shape and cell-type specificity (Brown and Rose, 1992; Homann et al., 2007; Haney et al., 2011; Roppolo et al., 2011; Spira et al., 2012; Hao et al., 2014; Pfister et al., 2014).

2.2.1 Lipid raft hypothesis

The lipid raft hypothesis postulated by Simons and Ikonen was the first model to provide a functional explanation of membrane inhomogeneities and gave a very elegant and relatively simple explanation of membrane organization which was based on the self-assembling forces of lipids

(Simons and Ikonen, 1997).

According to the lipid raft hypothesis, the clustering of glycosphingolipids, nucleates the formation of lipid microdomains that are further stabilized by cholesterol to form a liquid ordered domain ((Simons and Ikonen, 1997), see 2.1.1.1). These so-called lipid rafts are densely packed lipid assemblies and are functionally different from the rest of the membrane (Simons and Ikonen, 1997). Lipid-rafts were defined as small, sphingolipid- and cholesterol-rich compartments of liquid ordered phase, supposedly found in all cellular membranes (Simons and Ikonen, 1997). The distinct lipid environment of lipid rafts was thought to act as sorting platform for proteins, due to their affinity to lipid-raft or non-raft environments. Experimental evidence for their hypothesis was primarily drawn from the observations of non-random lipid distributions within epithelial cells and during caveolae formation. Caveolae are small invaginations of the PM that are involved in endocytosis but are devoid of clathrin coats (Parton, 1996). Caveolae were found to contain clusters of glycosphingolipids and the occurrence of caveolae depends on the presence of cholesterol (Rothberg et al., 1990). It was suggested that lipid rafts confer the sorting of caveolae-associated proteins, thereby being an important functional component of endocytosis.

Comparably, it was suggested that lateral sorting events in the ER due to lipid rafts were responsible for the direct delivery of newly synthesized glycosphingolipids and GPI-anchored proteins in epithelial cells to the apical PM (Simons and van Meer, 1988). Epithelial cells are a special cell type that grows as a polarized monolayer with distinct functional discrimination of apical and basal surfaces. According to this functional discrimination, glycosphingolipids as well as GPI-anchored proteins are exclusively found at the apical PM surface (van Meer et al., 1987).

The small and dynamic nature of lipid-rafts made it challenging to provide direct evidence for the lipid raft hypothesis. Brown and Rose developed a biochemical method of isolating the apical surface membrane compartment of epithelial cells, the lipid composition of which resembled lipid-rafts (Brown and Rose, 1992). The extraction of membrane fractions with Triton X-100 at 4°C and subsequent equilibrium gradient centrifugation yielded so-called “detergent insoluble membranes” (DIM) that contained proteins found in the apical membrane compartment and were therefore suggested to be the biochemical counterpart of what was later named lipid-rafts (Brown and Rose, 1992). Generalization of this protocol to other cell types and implication on other model systems led to the identification of numerous “raft-proteins” in almost every organism studied. However, it turned out that DIM fractionations do not contain what could be the equivalent of membrane structures of living cells and that DIMs determine the solubility of a protein rather than its association to specific lipids (Zurzolo et al., 2003; Kierszniowska et al., 2009; Simons and Gerl, 2010; Tanner et al., 2011).

A substantial amount of research on the formation of lipid-rafts has been carried out in artificial

membranes. In this system, phase separation of lipids has been shown numerous times and can be predicted with computational models (Illya et al., 2006). These results cannot be easily applied to living systems. Up to date, lipid phase separation has not been undoubtedly shown *in vivo* (Lee et al., 2015). Just as well, evidence for co-clustering of transmembrane proteins with liquid ordered membrane domains *in vivo* is missing (Fidorra et al., 2006; Subczynski et al., 2007).

Besides experimental approaches, the lipid-raft hypothesis also has several conceptual issues. The behaviour of glycosphingolipids and GPI-anchored proteins only takes PM components into account that localize to the extracellular side of a cell. This may represent a very special case of membrane organization especially considering the asymmetry of the PM (see 2.1.1.1). Phase-transition of lipids, which is crucial for the formation of lipid-rafts, is a concentration-dependent mechanism. The model therefore assumes that membranes consist for the most part of lipids. Estimations on the PM of human erythrocytes or synaptic vesicles however suppose that the membrane can in some cases be less fluid than expected by Singer and Nicolson because it is tightly packed with proteins (Takamori et al., 2006; Dupuy and Engelman, 2008). Finally, the lipid-raft hypothesis does not consider the perturbations of the membrane due to the presence of proteins. It overemphasises the role of lipid-lipid interactions as the only force in membrane compartmentalization and does not consider the effects of membrane proteins on lipids, as well as other proteins.

These issues led to several amendments to the original lipid-raft hypothesis. Up-to-date, lipid rafts are defined to be small, dynamic congregations that consist of cholesterol, sphingolipids and proteins and may associate into larger structures as a result of interactions between lipids, lipids and proteins as well as proteins (Lingwood and Simons, 2010). However, the term “lipid-raft” still implies a lipid centric view on membrane compartmentalization. Therefore the unbiased term “membrane domains” is more applicable to name non-random distributions of membrane components especially when investigating meso-scale assemblies.

2.2.2 Extrinsic factors alter membrane compartmentalization

Membrane domain formation is always connected to the diffusion of proteins and lipids within the membrane plane. However, as mentioned above, diffusion of lipids and proteins is intrinsically affected by interactions between these components and local protein crowding. Additionally, extrinsic factors such as the cytoskeleton and the cell wall are also considerable obstacles of free diffusion. Unexpected diffusion behaviours of membrane lipids prompted Akihiro Kusumi to propose a hierarchical model of membrane compartmentalization within the mesoscale of 2-300 nm. The model not only considers the principles proposed by the lipid-raft hypothesis but also his

findings on protein dependent diffusion corrals.

High-speed tracking in living human cells revealed that membrane proteins as well as lipids do not diffuse freely within the PM but follow a restricted diffusion mode (Fujiwara et al., 2002). Notably, this “hop-diffusion” was also observed for non-raft phospholipids (Fujiwara et al., 2002). Since depolymerisation of the actin cytoskeleton led to linear diffusion it appears that other components contribute to membrane compartmentalization beyond raft domains (Fujiwara et al., 2002). Based on these observations, Kusumi *et al* proposed the “anchored membrane protein picket model”. In this model, the membrane adjacent cytoskeleton forms a mesh like “fence” at which attached transmembrane proteins form “picket”-like barriers against the free diffusion of phospholipids (Nakada et al., 2003; Kusumi et al., 2005). The hydrodynamic friction imposed by these TMD proteins divides the PM into many 40-300nm wide sub-compartments in this “picket –fence” illustration of the PM (Kusumi et al., 2011). Notably, diffusion of components from one compartment to another is not prohibited *per se*, but relies on comparably rare occasions where the distance between two picket forming transmembrane proteins is large enough to allow passage of membrane components between compartments or the dynamic nature of the cytoskeleton creates diffusion windows (Kusumi et al., 2005). These mechanisms then give rise to the observed non-linear hop-diffusion events (Kusumi et al., 2011).

The cytoskeleton induced membrane compartments represent the first layer in the hierarchical model of the PM proposed by Kusumi et al. (Figure 3 B) (Kusumi et al., 2005). Within these large compartments, the raft-domains postulated by Simons and colleagues (see 2.2.1) are still predicted to form (Figure 3 C) (Kusumi et al., 2005). These represent the second tier of membrane compartments predicted to be within 2-20nm large, even though the size dimensions of lipid rafts may be greatly affected by raft composition and membrane compartment size (Kusumi et al., 2011). As a matter of completeness, Kusumi *et al.* included temporary complexes of proteins due to di- and oligomerization events as the third and last layer of membrane compartments formation into their model (Figure 3 A) (Kusumi et al., 2005).

The importance of actin dependent membrane sub-compartmentalization has been shown for the CD36 receptor. This surface receptor is expressed in several cell types such as endothelial cells and macrophages, binds multivalent ligands including oxidized low –density lipoprotein or apoptotic cells (Febbraio et al., 2001). Clustering of CD36 upon ligand perception is a key event to trigger signal-transduction for this receptor and receptor-ligand internalization (Daviet et al., 1997; McGilvray et al., 2000). Single-molecule tracking experiments of CD36 revealed its actin dependent hop-diffusion (Jaqaman et al., 2010). Strikingly, the receptors efficiency of signal transduction initiation, as well as ligand uptake, was greatly impaired in the presence of during cytoskeleton destabilizing drugs even though general endocytosis was not inhibited (Jaqaman et al., 2010).

Introduction

Therefore, it is generally accepted that the actin cytoskeleton controls at least one layer of membrane compartmentalization in animal cells.

In contrast to animal systems, plasma membrane proteins in plants are rather immobile. Proteins such as KAT1, PIN2, KNOLLE, BOR1 or NIP5;1 have been found to display very low lateral mobility with only a small sub-fraction of these proteins displaying mobile behaviour (Sutter et al., 2006; Men et al., 2008; Takano et al., 2010; Roppolo et al., 2011; Boutté and Moreau, 2014). However, restricted diffusion is not a default state as several proteins are able to change their diffusion behaviour. The aquaporin PIP2;1 for example can switch between Brownian diffusion to a restricted diffusion mode upon salt stress (Li et al., 2011). RBOHD, a NADPH-oxidase, changes its speed of diffusion in a Ca^{2+} and phosphorylation dependent manner. Both play important roles in regulating RBOHD function (Hao et al., 2014).

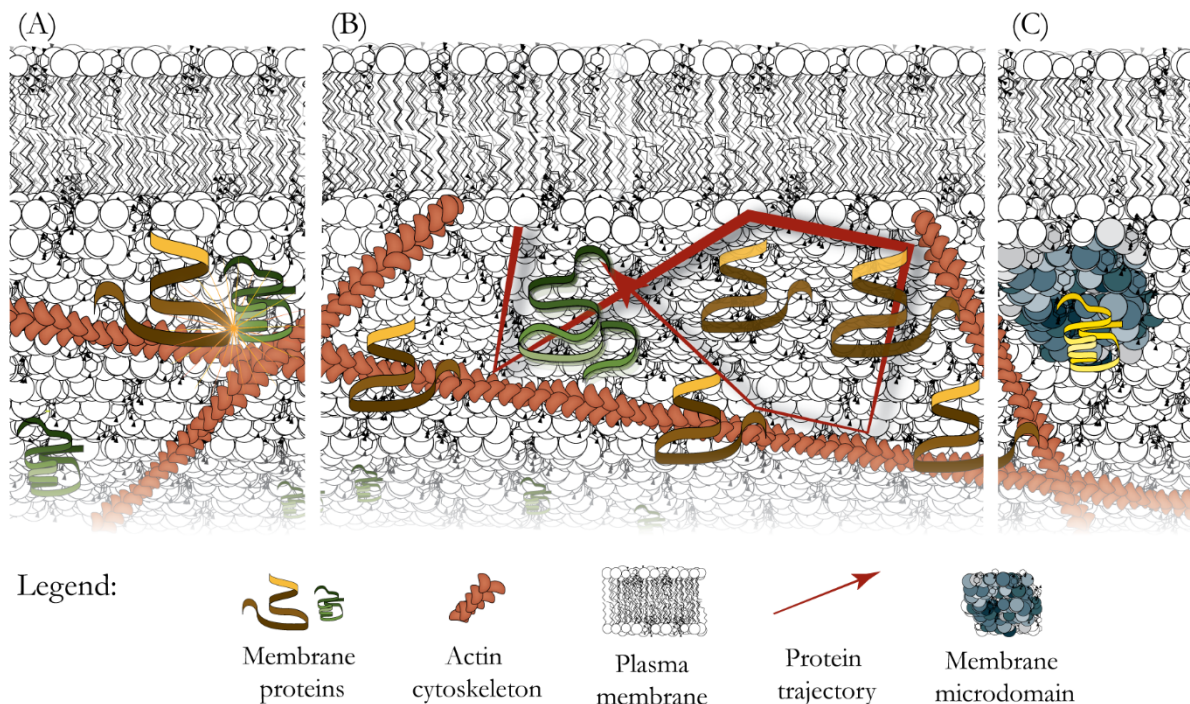


Figure 3: The three-tiered picket-fence model of membrane sub-compartmentalization.

This model adapted from Kusumi *et al.* differentiates three stages of membrane sub-compartmentalization that all contribute to the lateral organization of the PM. (A) Short-lived protein complexes that form upon di- or oligomerization events represent one layer of membrane organization. (B) Membrane adjacent cytoskeletal structures and proteins attached to it form barriers that proteins, trapped within these compartments cannot pass. Rare passage from one compartment into another is only possible, if the distance between two picket-forming transmembrane proteins is large enough or if diffusion windows are open by the dynamic nature of the cytoskeleton. (C) Within these compartments, “raft-domains” as postulated by Simons *et al.* may form as a consequence of interactions between lipids and proteins.

Similar to mammalian cells, there are examples, where the cytoskeleton is involved in limiting diffusion of membrane proteins. For example, lateral mobility of MIDD1, a microtubule binding protein, is restricted to individual compartments that are surrounded by the microtubular cytoskeleton (Oda and Fukuda, 2012). Also, the cell wall synthesizing complex (CSC) (McFarlane et al., 2014) associates with the microtubule cytoskeleton via the cellulase KORRIGAN and a protein of unknown function called POM2 (Martin et al., 2012; Vain et al., 2014). The CSC is comprised of 12-36 CESA membrane-spanning glycosyltransferases. It can be visualized microscopically and appears as a punctate homodomain (Park et al., 2011). Like other punctate membrane domains alteration of lipid composition and disturbance of the microtubular cytoskeleton both impair CSC patterning on the plasma membrane (Lalanne et al., 2004; Schrick et al., 2004; Paredez et al., 2006).

In plant cells, the high turgor pressure actively compresses the PM against the cell wall (Wang et al., 2006a), which is a major difference to animal cells that have a comparably weak association to the extracellular matrix. Therefore, the PM and the cell wall are in tight contact, creating biophysical constraints that might affect the behaviour of plant membrane proteins. In fact, a very elegant study showed that the plant cell wall extensively constrains diffusion of membrane proteins and that the effect is particularly pronounced for membrane proteins that extend into the apoplastic space (Martinière et al., 2012). Moreover, in experiments where seedlings were treated with isoxaben, a cellulose synthase inhibiting drug, the mobility of transmembrane proteins significantly decreased. This implies, that not only the presence but also the organization of the cell wall is actively influencing protein dynamics at the PM (Martinière et al., 2012). A predominant impact of the cell wall over the cytoskeleton has also been reported for the potassium channel KAT1. In the PM of *Vicia faba* stomatal guard cells, KAT1 localizes to radial structures that do not resemble actin or microtubular structures. Moreover, destabilization of the cytoskeleton did not affect KAT1 localization. However, KAT1 localization follows the pattern of cellulose fibrils and radial distribution is lost in hypertonic conditions, where the PM is detached from the cell wall (Homann et al., 2007).

By now a picture emerges where in plants the cell wall may have the same functional implications as the cytoskeleton with respect to plasma membrane compartmentalization (Martinière et al., 2012). This can occur via direct protein-cell wall interactions as shown for proteins such as the *Arabidopsis* Formin1 or members of the wall-associated kinase (WAK) family (Steinwand and Kieber, 2010; Martinière et al., 2011). Alternatively the cell wall may indirectly influence lateral mobility when freely diffusing proteins interact with cell wall associated ones. The cell wall should therefore be considered as a less static structure as it was historically perceived but rather as a dynamic structure. This is illustrated by spatio-temporally regulated cell-wall alterations such as

callose depositions upon pathogen infection or loosening upon symbiont accommodation (Ridge and Rolfe, 1985; Luna et al., 2011). Even though it remains to be proven to what extent this can be compared to the dynamics of cytoskeleton components, various examples of proteins connecting the cell wall and the cytoskeleton show that cell wall, plasma membrane and cytoskeleton should not be regarded as single-acting components, but rather as a uniform continuum, exhibiting concerted actions (McKenna et al., 2014).

2.2.3 Diversity of membrane domains

Membrane domain localization is not restricted to certain functional protein classes. Non-uniform distribution of functional components has been reported during various processes such as hormone signalling, endocytosis or plant-microbe interactions (Bhat et al., 2005; Men et al., 2008; Raffaele et al., 2009; Lefebvre et al., 2010; Bozkurt et al., 2014; Moling et al., 2014). This diversity most likely reflects the co-existence of different membrane domain types in the same cell and suggests functional specification of these sites (Brown and Rose, 1992; Homann et al., 2007; Haney et al., 2011; Roppolo et al., 2011; Spira et al., 2012; Hao et al., 2014; Pfister et al., 2014).

2.2.3.1 Polar domains

The most well-known membrane structures are polar membrane domains that occur in polarized cells. Members of the PIN-FORMED (PIN) auxin efflux carriers are the most prominent marker proteins of these comparably large domains (reviewed in Kania et al. (2014)). Polar localization of PINs is required to maintain concentration gradients of the phytohormone auxin that regulates a wide spectrum of developmental processes within plant cells and tissues (Finet and Jaillais, 2012; Jeong et al., 2012; Lau et al., 2012; Barbez and Kleine-Vehn, 2013; Pierre-Jerome et al., 2013). Depending on the direction of auxin fluxes in a specific cell type or tissue, most of these domains can be relocated to any cell pole. Polarity of cells, and consequently the maintenance of polar membrane domains is normally achieved by the action of S-acylated and dimeric RAC/ROP GTPases that also serve as canonical marker proteins for these domains (Sorek et al., 2007; Yang and Lavagi, 2012). In most cases polar localized proteins reach their destination by directed, mostly clathrin-dependent vesicle trafficking from the endoplasmic reticulum (ER) and Golgi apparatus to the PM (Kleine-Vehn and Friml, 2008; Grunewald and Friml, 2010; Kleine-Vehn et al., 2011; McMahon and Boucrot, 2011; Luschnig and Vert, 2014). While this mechanism does not ultimately require specific lipid-binding characteristics of these proteins, lipid distribution is crucial to maintain polarity. This hypothesis is supported by findings that polar distribution of phosphoinositides coincides with PIN polarity (Tejos et al., 2014) and that localization of PIN2 is sterol-dependent (Men et al., 2008). Another example of proteins in polar domains is the iron

transporter IRT1 which conditionally localizes to the outer lateral PM domain in root epidermal cells (Barberon et al., 2014). The localization of IRT1 is controlled by the phosphoinositol binding protein FYVE and sensitive to the availability to metal substrates of IRT1 such as zinc, manganese or cobalt (Barberon et al., 2014)

Besides environmental or developmental factors, the phosphorylation status and/or the polar localization of kinases such as the D6 protein kinase (Wisniewska et al., 2006; Michniewicz et al., 2007; Pumplin et al., 2012; Barbosa et al., 2014) may represent control checkpoints during polar trafficking as polar localization of other proteins depend on them. Additionally polar recycling (transcytosis) plays important roles in establishing and maintaining of polar membrane domains. For example polar localized membrane domains are marked by the boric acid channel NIP5;1 or the boric acid/borate transporter BOR1 (Takano et al., 2010). Both proteins are involved in the homeostasis of boron, which is crucial for plant growth but is toxic when present in excess concentrations (Nable et al., 1997; Takano et al., 2010). NIP5;1 localizes to the distal PM of lateral root cap cells as well as epidermal cells of the meristem and elongation zones, which physiologically reflects its function in boron import (Takano et al., 2006; Takano et al., 2010).

The boric acid/borate exporter BOR1 on the other hand can be found at proximal PMs in the columella, the lateral root cap, the epidermis and the endodermis in root tip regions as well as in the epidermis and endodermis of the elongation zone (Takano et al., 2002; Takano et al., 2010). Phosphorylation seems to be one selective driving force in the polar distribution maintenance machinery of BOR1, as polar distribution is abolished in a phosphorylation mutant version of BOR1 (Takano et al., 2010). Strikingly, this phosphorylation-dependent membrane domain localization is not dependent on endocytotic recycling of BOR1, because BOR1 phospho-mutants are still able to enter the same endocytotic pathway as native BOR1 (Takano et al., 2010).

In addition to or as an alternative to post-translational modifications, polar trafficking of proteins can be mediated by spatio-temporal regulation of promoter activity. This is nicely illustrated by specific localization patterns of the phosphate transporter PT4 from *Medicago truncatula* (Pumplin et al., 2012). PT4 is specifically targeted to the periarbuscular membrane (PAM), the membrane that surrounds the fungal arbuscule, which serves as the symbiotic interface between the host plant and the fungus. Controlling expression of other transporter proteins that naturally localize to the peripheral PM using the PT4 promoter allows redirection of these proteins to the PAM, demonstrating the importance of spatial timing for polar secretion of proteins following the endocytotic pathway (Pumplin et al., 2012). Further examples of specific targeting of proteins to perimicrobial membranes have been reviewed recently (Dörmann et al., 2014).

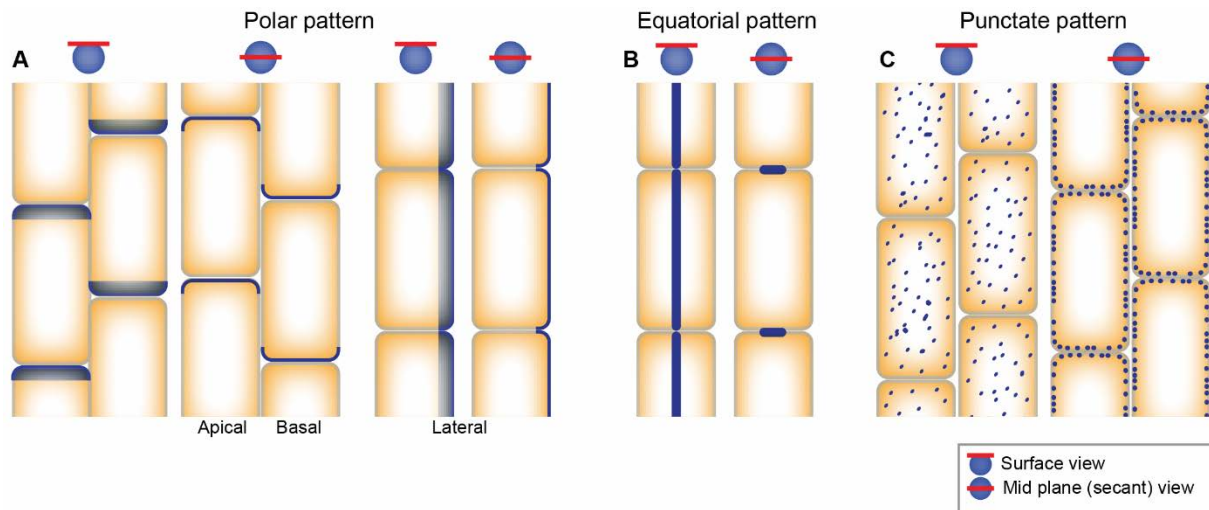


Figure 4: Overview of different membrane domain types found in plants.

(A) Polar membrane domains can be found in apical or basal membranes as in case of PIN auxin transporter proteins, but can also occur at lateral membranes. (B) Proteins essential for the establishment of the Casparian strip like DR1PA localize to equatorial membrane domains. (C) The most commonly observed membrane domain are punctate domains such as labelled by Remorins or Flotillins. Adapted from Konrad and Ott (2015).

2.2.3.2 Equatorial domains

Some polarized membrane domains exhibit an equatorial pattern and are capable of dividing a cell into separate functional sides.

The most prominent example of equatorial domains has been described at the plant root endodermis. This specialized cell layer is characterized by the presence of the “Casparian strip” (CS), a modification of the primary cell wall (Enstone et al., 2003). It forms a belt-like structure that prevents free diffusion of solutes from the soil to the apoplastic space in the stele (Moon et al., 1986; Peterson, 1987; Enstone et al., 2003). The CS is accompanied by a highly specific and protein-rich “Casparian strip domain” (CSD). The CSD is in tight conjunction with the CS as it remains attached to the cell wall during plasmolysis (Bonnett, 1968). It also prevents free diffusion of PM proteins as well as the lipophilic dye FM4-64 and is therefore thought to be a major barrier for most endodermal PM components (Alassimone et al., 2010). CASPARIAN STRIP MEMBRANE DOMAIN PROTEINs (CASPs) are the most prominent marker proteins for the CSD. They are thought to act as major scaffold components of the CSD due to their ability to interact with themselves and the fact that they are laterally immobilized. However, the plasticity of CASP localization during the development of the CS points to an extrinsic component that is responsible for CSD formation (Roppolo et al., 2011). As the normal CSD localization pattern is altered to a patchy pattern in *schengen3* (*sgn3*) mutant plants, the leucine-rich repeat receptor-like kinase encoded by *JGN3* contributes to CSD organization (Pfister et al., 2014).

2.2.3.3 Punctate, meso-scale membrane domains

Punctate membrane domains mostly show a distribution over the entire PM that appears to be isotropic in nature at first glance. Targeting to these domains may be universal for single- or multi-pass transmembrane-domain (TMD) containing proteins as shown for the *Medicago truncatula* LYSIN MOTIF RECEPTOR-LIKE KINASE 3 (LYK3) (Haney et al., 2011; Moling et al., 2014), the *Solanum tuberosum* sugar transporter SUT1 (Krügel et al., 2008), the SLOW ANION CHANNEL 1 (SLAC1) HOMOLOG 3 (SLAH3) (Demir et al., 2013), the RESPIRATORY BURST OXIDASE HOMOLOG D (RBOHD) (Hao et al., 2014), the functional tetrameric aquaporin PIP2;1 (Törnroth-Horsefield et al., 2006; Wang et al., 2006b; Wan et al., 2011) from *Arabidopsis thaliana* or the *Vicia faba* potassium channel KAT1 (Homann et al., 2007). It remains to be shown whether these proteins are targeted to the same or to different types of membrane domains and if this specific targeting is dependent on distinct lipid species.

Besides intrinsic membrane proteins a range of peripheral membrane proteins such as Flotillins (FLOTs) are also targeted to punctate membrane microdomains and are frequently used as marker proteins (Lang et al., 1998; Morrow et al., 2002; Blonder et al., 2004; Haney et al., 2011; Nixon et al., 2011; Li et al., 2012). FLOTs – also known as Reggie proteins – are widespread among metazoans as well as prokaryotes and encoded by three genes in *A. thaliana* (At5g25250, At5g25260 and At5g64870) (Rivera-Milla et al., 2006; Bach and Bramkamp, 2013; Reuter et al., 2013). They have been shown to label mesoscale microdomains in *A. thaliana* and *M. truncatula* (Haney et al., 2011; Li et al., 2012) and may be involved in clathrin-independent endocytosis in *Arabidopsis* (Li et al., 2012). For animal FLOTs, members of the SPFH/Band 7/PHB domain containing proteins, myristoylation is crucial for targeting to membrane domains (Morrow et al., 2002; Neumann-Giesen et al., 2004; Traverso et al., 2013). In contrast, the FLOT homologs from *A. thaliana* and *M. truncatula* do not contain the required N-terminal glycine residue in position 2 and are unlikely to be myristoylated, even though other members of the SPFH/Band 7/PHB domain containing proteins in *Arabidopsis* were shown to be myristoylated (Boisson et al., 2003).

Two FLOT homologues from *M. truncatula* play vital roles in the successful establishment of functional root nodule symbiosis (RNS) (Haney and Long, 2010). The symbiotic interaction of legumes and their rhizobial symbionts happens within a newly developed organ, the root-nodule. Development of root nodules starts soon after rhizobial cells are accommodated into the root via the passage through a so-called infection thread within root hair cells. Initiation of infection threads usually happens within curled root hairs that entrap bacteria, which form a microcolony at this stage (Oldroyd and Downie, 2004). However, if FLOT2 or FLOT4, transcripts are reduced by expression of small interfering RNAs, root systems develop fewer nodules and infection threads. In particular the silencing of FLOT4 leads to abortion of almost 90% of initiated infection threads

Introduction

underlining its importance for this process. Fluorescence microscopy revealed that FLOT2 and FLOT4 both localize to punctate membrane domains within epidermal or root hair cells of *M. truncatula* where they are distributed randomly over the entire cell surface. At least for FLOT4, this changes dramatically in the presence of symbiotic bacteria. On a big scale, the majority of the fluorescence signal originating from FLOT4 moves to the root hair tip (Haney and Long, 2010). Only in the presence of the symbiont, does FLOT4 signal overlap with signal originating from fluorescently tagged LYK3, an essential RLK involved in RNS signal perception which also localizes to punctate membrane domains (Haney and Long, 2010). These data show that signal perception triggers the re-localization of signalling components into one membrane domain. It also provides first insights into distinct compositional plasticity of individual membrane microdomains that likely determine their functional specificity.

2.3 Remorins as a model to label membrane domains

In his discussion about size and composition of small, punctate membrane domains, Akihiro Kusumi hypothesized that a large diversity of domains is expected to form because of the numerous multimolecular interactions involved in membrane domain formation (Kusumi et al., 2011). “Indeed, obtaining the full spatiotemporal spectrum of raft domains will be a Herculean task. Presently, the best we can do is to observe raft domains and report the data as quantitatively as possible (...)” (Kusumi et al., 2011).

To approach this task of deciphering the diversity, dynamics, function and formation of membrane domains, a versatile set of marker proteins has to be chosen. However, insights gained from proteins reported as being membrane domain resident are very often not comparable. This is due to the fact that they differ greatly in their membrane attachment mechanism as well as molecular function and therefore the mechanisms of membrane domain localization may not be universal.

Proteins of the Remorin family are excellent candidates to circumvent these problems. Remorins are PM associated proteins that are represented by a large, plant specific protein family with 16 members in *A. thaliana* (Farmer and Pearce, 1989; Jacinto et al., 1993; Reymond et al., 1996; Marmagne et al., 2004; Mongrand et al., 2004; Sazuka et al., 2004; Valot et al., 2005; Nelson et al., 2006; Valot et al., 2006; Raffaele et al., 2007). Based on their gene structure, Remorins have been divided into six subgroups (Raffaele et al., 2007). Remorins contain the canonical Remorin signature sequence in their highly conserved C-terminal region (Raffaele et al., 2007) that contains a high content of charged residues as well as a predicted coiled-coil domain (Reymond et al., 1996; Raffaele et al., 2007). As coiled-coil domains are principally found to confer protein oligomerization (Burkhard et al., 2001), the C-terminal region of remorins has unsurprisingly been identified to be important for protein-protein interactions (Marín et al., 2012; Tóth et al., 2012).

The majority of Remorins also feature a highly diverse N-terminal region which is speculated to confer functional specificity (Raffaele et al., 2007). For many Remorin proteins, this N-terminal region has been predicted to be intrinsically disordered (ID) (Marín et al., 2012). ID regions can be commonly found in eukaryotic proteins and have recently been identified in bacterial effector proteins (Marín et al., 2013; Marín and Ott, 2014). These protein regions follow an induced folding mechanism upon protein-protein interaction and are thereby thought to confer a high binding flexibility. It may allow one intrinsically disordered protein to interact with several structurally different partners (Marín and Ott, 2014). ID regions not only provide remorins with a structural element but are also dominant sites for protein phosphorylation (Marín et al., 2012).

Remorin proteins have frequently been reported to enrich in DIM fractions and were therefore thought to localize to membrane domains (Wang et al., 2001; Lefebvre et al., 2007; Kierszniowska

et al., 2009; Raffaele et al., 2009). However, DIM fractionations are able to determine the solubilisation properties of proteins but not of subcellular localization (see 2.2.1). Therefore the microscopically visible unequal distribution of remorins as seen for the *Solanum tuberosum* StRem1.3 in *Nicotiana benthamiana* or the symbiotic remorin of *Medicago truncatula* SYMBIOTIC REMORIN 1 (SYMREM1) demonstrate the membrane domain localization of Remorin proteins more convincingly (Raffaele et al., 2009; Lefebvre et al., 2010).

Remorin proteins are especially interesting, because they play highly specific roles during processes such as the regulation of viral spreading (Raffaele et al., 2009), symbiotic and pathogenic infections (Lefebvre et al., 2010; Bozkurt et al., 2012; Tóth et al., 2012), responses to the phytohormone ABA and abiotic stress (Checker and Khurana, 2013; Demir et al., 2013; Yue et al., 2014). What makes Remorins so suitable tools for membrane domain research is their functional specification paired with a promiscuous interaction capability. The best example to illustrate the functional specification of Remorins are the SYMREM1 proteins from *M. truncatula* and *Lotus japonicus*. Phylogenetically, these two homologous proteins belong to the Remorin group 2 which is only present in legume plants and poplar (Raffaele et al., 2007). Legumes are able to establish a symbiotic relationship with soil living bacteria the so-called “root nodule symbiosis” (RNS) in order to fix atmospheric nitrogen (Sprent, 2007; Markmann and Parniske, 2009). Both SYMREM1 proteins have been demonstrated to play important roles during RNS (Lefebvre et al., 2010; Tóth et al., 2012). While interaction of SYMREM1 with key RLKs of initial RNS signalling has been demonstrated for both proteins *in vivo*, the direct interaction of *L. japonicus* SYMREM1 with NOD FACTOR RECEPTOR1 (NFR1), NOD FACTOR RECEPTOR 5 (NFR5) and SYMBIOSIS RECEPTOR-LIKE KINASE (SYMRK) has been confirmed *in vitro*. Both NFR1 and SYMRK are able to directly phosphorylate SYMREM1 (Tóth et al., 2012). Without prohibiting it, the loss or overexpression of SYMREM1 both affect the formation of root nodules, the organ of symbiotic exchange (Lefebvre et al., 2010; Tóth et al., 2012). Therefore, SYMREM1 is speculated to be important for efficient receptor signalling, where they act as scaffold proteins to enable efficient receptor interaction and downward signalling (Lefebvre et al., 2007; Lefebvre et al., 2010; Tóth et al., 2012). The fact that group 2 Remorins are only present in plants that undergo RNS and their active role during that process demonstrates the functional specificity of Remorins (Popp and Ott, 2011).

Other members of the Remorin protein family have been demonstrated to be involved in various processes. Several group 1 Remorins have been identified to be differentially phosphorylated during perception of bacterial pathogen associated microbial patterns (PAMPs) or polygalacturonic acid (Farmer and Pearce, 1989; Benschop et al., 2007) and phosphorylated peptides of Remorin proteins are often found in large-scale proteomic studies (Nühse et al., 2007; Sugiyama et al., 2008; Reiland et al., 2009; Grimsrud et al., 2010; Nakagami et al., 2010). This implies that functional

specification takes place throughout the whole Remorin protein family. Similar to CASPs and flotillins, remorins have been hypothesized to function as molecular scaffold proteins (Jarsch and Ott, 2011) as they oligomerise to higher order structures (Marín et al., 2012; Tóth et al., 2012). This functional specification paired with the promiscuous interaction capability and their localization to membrane domains makes Remorins extraordinary interesting proteins to study membrane domains. Not only does the diversification of Remorin proteins itself allow to investigate the subcompartmentalization of plant plasma membranes. It gives us also the opportunity to study their functional importance during biotic and abiotic stresses. The capability of Remorins to interact with important signalling molecules may also be a valuable tool to identify new components of signal transduction networks.

3 Results

3.1 Overview of Publications

Publication I:

Jarsch, I.K., Konrad, S.S.A., Stratil, T.F., Urbanus, S.L., Szymanski, W., Braun, P., Braun, K.-H.H., and Ott, T. (2014). Plasma Membranes Are Subcompartmentalized into a Plethora of Coexisting and Diverse Microdomains in *Arabidopsis* and *Nicotiana benthamiana*. *The Plant Cell* **26**, 1698-1711

Status: published | Year 2014 | DOI: 10.1105/tpc.114.124446

Publication II:

Konrad, S.S.A., Popp, C., Stratil, T.F., Jarsch, I.K., Thallmair, V., Folgmann, J., Marín, M., and Ott, T. (2014). S-acylation anchors remorin proteins to the plasma membrane but does not primarily determine their localization in membrane microdomains. *The New Phytologist* **203**, 758-769.

Status: published | Year: 2014 | DOI: 10.1111/nph.12867

Publication III:

Vogler, F., Konrad, S.S.A., and Sprunck, S. (2015). Knockin' on pollen's door: live cell imaging of early polarization events in germinating *Arabidopsis* pollen. *Frontiers in Plant Science* **6**.

Status: published | Year: 2015 | DOI: 10.3389/fpls.2015.00246

Manuscript:

Thomas F. Stratil, Sebastian S.A. Konrad; Jessica Folgmann, Thomas Ott Dissecting the multi-component assembly of a meso-scale membrane domain that controls host cell infection in *Medicago truncatula*. In eLIFE

Status: submitted | Year: 2015 | DOI: N.N.

3.2 Publication I: Plasma Membranes are Sub-compartmentalized into a Plethora of Coexisting and Diverse Microdomains in *Arabidopsis* and *Nicotiana benthamiana*

Iris K. Jarsch,^a Sebastian S. A. Konrad,^a Thomas F. Stratil,^a Susan L. Urbanus,^a Witold Szymanski,^a
Pascal Braun,^c Karl-Heinz Braun,^a and Thomas Ott^{a,1}

Plant Cell **26**, 1698-1711 (2014)

DOI: 10.1105/tpc.114.124446

^a Ludwig-Maximilians-University of Munich, Faculty of Biology, Institute of Genetics, 82152 Martinsried, Germany

^b Max-Planck-Institute of Molecular Plant Physiology, 14476 Potsdam-Golm, Germany

^c Department of Plant Systems Biology, Center for Life and Food Sciences Weihenstephan, Technische Universität München, 85354 Freising-Weihenstephan, Germany

¹ Address correspondence to thomas.ott@bio.lmu.de.

Author contributions:

To this work, I contributed different aspects of it's conception and design. Furthermore, I performed parts of the research and analysed experimental data.

Experimentally I contributed by generating all Remorin clones, where gene expression was driven by the native promoters (Figure 2; Supplementary Figure 1) and performed the TIRF microscopy (Supplementary Figure 2). All image analysis of these figures was performed by me.

I hereby confirm the above mentioned statements:

.....

Prof. Dr. Thomas Ott

.....

Sebastian S. A. Konrad

Plasma Membranes Are Subcompartmentalized into a Plethora of Coexisting and Diverse Microdomains in *Arabidopsis* and *Nicotiana benthamiana*^{©LW}

Iris K. Jarsch,^a Sebastian S.A. Konrad,^a Thomas F. Stratil,^a Susan L. Urbanus,^a Witold Szymanski,^b Pascal Braun,^c Karl-Heinz Braun,^a and Thomas Ott^{a,1}

^aLudwig-Maximilians-University of Munich, Faculty of Biology, Institute of Genetics, 82152 Martinsried, Germany

^bMax-Planck-Institute of Molecular Plant Physiology, 14476 Potsdam-Golm, Germany

^cDepartment of Plant Systems Biology, Center for Life and Food Sciences Weihenstephan, Technische Universität München, 85354 Freising-Weihenstephan, Germany

Eukaryotic plasma membranes are highly compartmentalized structures. So far, only a few individual proteins that function in a wide range of cellular processes have been shown to segregate into microdomains. However, the biological roles of most microdomain-associated proteins are unknown. Here, we investigated the heterogeneity of distinct microdomains and the complexity of their coexistence. This diversity was determined in living cells of intact multicellular tissues using 20 different marker proteins from *Arabidopsis thaliana*, mostly belonging to the Remorin protein family. These proteins associate with microdomains at the cytosolic leaflet of the plasma membrane. We characterized these membrane domains and determined their lateral dynamics by extensive quantitative image analysis. Systematic colocalization experiments with an extended subset of marker proteins tested in 45 different combinations revealed the coexistence of highly distinct membrane domains on individual cell surfaces. These data provide valuable tools to study the lateral segregation of membrane proteins and their biological functions in living plant cells. They also demonstrate that widely used biochemical approaches such as detergent-resistant membranes cannot resolve this biological complexity of membrane compartmentalization in vivo.

INTRODUCTION

Plasma membranes (PMs) are highly organized structures that are partitioned in different types of membrane domains (reviewed in Kusumi et al., 2012; Malinsky et al., 2013). Prominent examples are the basolateral membrane of root epidermal cells that is labeled by the polarly localized PIN-FORMED auxin efflux carrier PIN2 (Müller et al., 1998), the Casparian strip that is targeted by CASP proteins (Roppolo et al., 2011), and focal accumulation of the MILDEW RESISTANCE LOCUS O protein at periaustorial membranes during plant–microbe interactions (Bhat et al., 2005). However, most of these higher order membrane regions are further subdivided. The largest unit, recently defined as the “membrane compartment,” is between 40 and 300 nm in diameter and mainly determined by cortical cytoskeleton elements that restrict the lateral diffusion of membrane-associated proteins (Kusumi et al., 2012). Similar structures have also been described in other eukaryotic cells such as *Saccharomyces cerevisiae* (yeast) (Malinsky et al., 2010; Spira et al., 2012). “Membrane rafts” can be found within these

compartments. They are substantially smaller (2 to 20 nm) and characterized by their enrichment in sterols and sphingolipids (Boutté and Grebe, 2009). The molecular interactions between these membrane components have been shown to lead to a spatial phase transition toward a more liquid-ordered state in model membranes. Targeting of proteins to membrane rafts is often achieved by posttranslational modifications such as the addition of glycosylphosphatidylinositol and S-acyl (palmitoyl) moieties (Levental et al., 2010a, 2010b) or by electrostatic interactions (van den Bogaart et al., 2011). Physical interaction between raft-localized proteins and/or molecular scaffolds can lead to the clustering of nanoscale domains into larger units, recently defined as “raft platforms,” or membrane microdomains (Lingwood and Simons, 2010). These domains can almost reach micrometer ranges and are believed to harbor defined sets of preassembled signaling protein complexes, including components of the innate immune system. In plants, unfortunately and misleadingly, for a long time membrane domains have been equalized with detergent-resistant membranes (DRMs). DRMs derive from a biochemical extraction with nonionic detergents such as Triton X-100 in the cold. However, the specificity of DRMs has been widely questioned over the years, as sterols have the biophysical tendency to aggregate into large sheets that do not reflect individual microdomains in vivo (Zurzolo et al., 2003; Tanner et al., 2011; Malinsky et al., 2013).

A number of recent cell biological approaches revealed membrane-associated proteins such as Flotillins and Remorins to label distinct microdomains in living cells (Raffaele et al., 2009; Haney and Long, 2010; Lefebvre et al., 2010; Haney et al.,

¹ Address correspondence to thomas.ott@bio.lmu.de.

The author responsible for distribution of materials integral to the findings presented in this article in accordance with the policy described in the Instructions for Authors (www.plantcell.org) is: Thomas Ott (thomas.ott@bio.lmu.de).

© Some figures in this article are displayed in color online but in black and white in the print edition.

© Online version contains Web-only data.
www.plantcell.org/cgi/doi/10.1105/tpc.114.124446

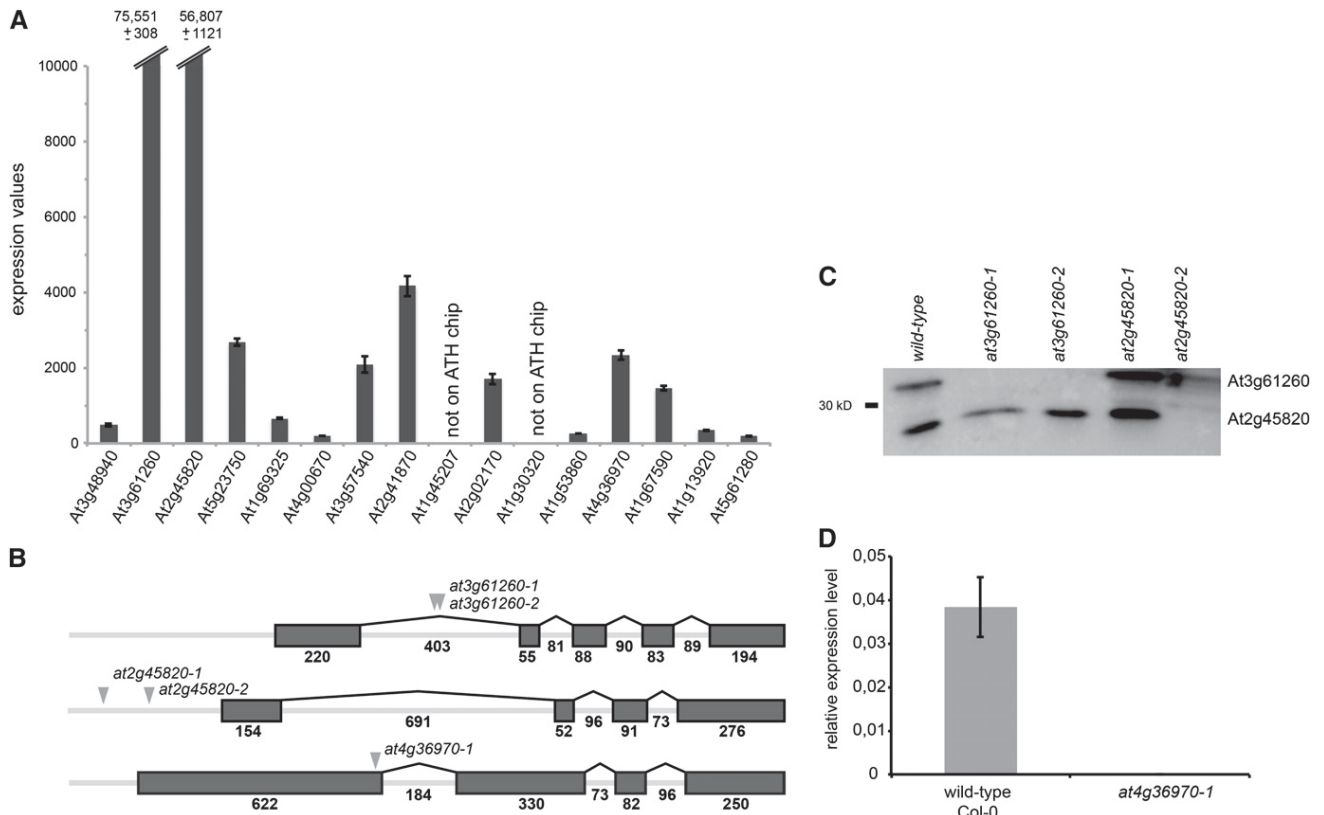


Figure 1. Remorin Expression Patterns and Identification of Homozygous Knockout Mutants.

(A) Data were obtained from the publicly available Genevestigator database (<https://www.genevestigator.com/gv/plant.jsp>). Error bars represent SE of three independent biological experiments. ATH chip, *Arabidopsis* Affymetrix chip.

(B) Schematic representation of the Remorin genes *At3g61260*, *At2g45820*, and *At4g36970*. Triangles indicate the T-DNA insertion sites, and gray boxes indicate the exons of the genes.

(C) Protein gel blot analysis of different *at3g61260* and *at2g45820* mutants confirmed the absence of the respective proteins in three of these lines. An α -REM antibody that was originally raised against the potato REM1.3 recognizes the two most closely related proteins in *Arabidopsis*.

(D) Quantitative real-time PCR analysis of three independent biological replicates confirmed the lack of transcript in the *at4g36970-1* mutant line. Error bars represent SE . Col-0, Columbia-0.

2011; Li et al., 2012; Demir et al., 2013). As in mammalian cells, Flotillins form a small gene family with only three members (*At5g25250*, *At5g25260*, and *At5g64870*) in *Arabidopsis thaliana*, while the plant-specific Remorin family comprises 16 genes (Raffaele et al., 2007). All Remorin proteins contain a canonical C-terminal region (Raffaele et al., 2007), and the majority of them contain an intrinsically disordered N-terminal segment that varies greatly in length and sequence but harbors almost all in vivo phosphorylation sites (Marín and Ott, 2012; Marín et al., 2012). Localization of single Remorins to membrane domains has been shown for ectopically expressed REM1.3 from potato (*Solanum tuberosum*), for an endogenous Remorin from tomato (*Solanum lycopersicum*; Raffaele et al., 2009), as well for the closely related protein from *Arabidopsis* (REM1.3/At2g45820) (Demir et al., 2013). Furthermore, immunolocalization of the legume-specific SYMBIOTIC REMORIN1 (SYMREM1) protein from *Medicago truncatula* revealed domain-localized patterns along infection threads that encapsulate symbiotic bacteria during root nodule symbiosis (Lefebvre et al., 2010). While the potato REM1.3 regulates viral movement (Raffaele et al., 2009),

SYMREM1 is required for successful infection by rhizobia and interacts via its predicted coiled-coil domain with receptor-like kinases such as the LYSIN-MOTIF RECEPTOR KINASE3 (LYK3) and the NOD FACTOR RECEPTOR1 (NFR1) (Lefebvre et al., 2010; Tóth et al., 2012). Interestingly, LYK3 also localizes to membrane domains. Upon perception of symbiotic rhizobia by the host plant, LYK3 mobility is laterally arrested, resulting in a colocalization with the domains labeled by the Flotillin protein FLOT4 (Haney et al., 2011). It remains to be shown whether both proteins interact physically in these membrane domains. However, such compartmentalized interactions have been demonstrated by fluorescence lifetime imaging microscopy between a number of proteins: the hyper-variable region of a small maize (*Zea mays*) GTPase ROP7 and the CALCIUM-DEPENDENT PROTEIN KINASE1 (CPK1) (Vermeer et al., 2004), for homooligomeric complexes of the brassinosteroid receptor BRASSINOSTEROID INSENSITIVE1 (BRI1), for BRI1 in a heteromeric complex with the SOMATIC EMBRYOGENESIS RECEPTOR KINASE3 (SERK3) (Rusinova et al., 2004), as well as for a complex between the AAA ATPase CDC48A and SERK1 (Aker

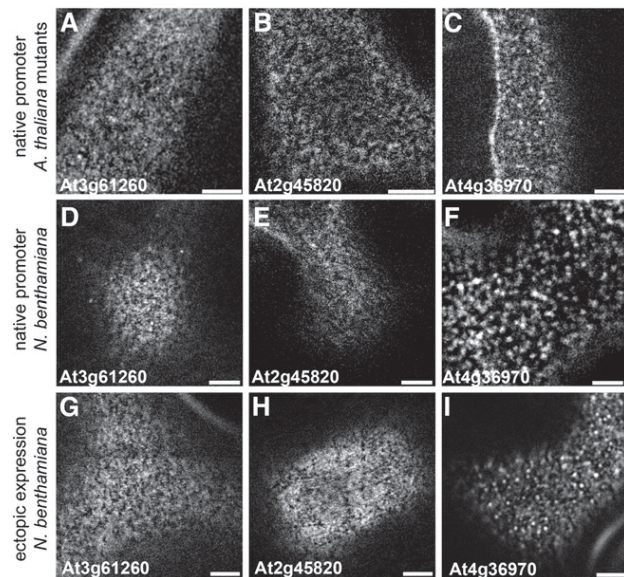


Figure 2. Labeling of Membrane Domains Can Be Consistently Observed in Different Biological Systems.

(A) to (C) Homozygous *Arabidopsis* knockout mutants were transformed with the respective fluorophore-tagged Remorins expressed under the control of their endogenous promoters. Bars = 5 μ m.

(D) to (F) Domain patterning was observed in *N. benthamiana* leaf epidermal cells where the respective genes were expressed under the control of the endogenous *Arabidopsis* promoter. Bars = 5 μ m.

(G) to (I) Domain patterning was observed in *N. benthamiana* leaf epidermal cells where the respective genes were ectopically expressed under the control of the cauliflower mosaic virus 35S promoter. Bars = 5 μ m.

et al., 2007). These data suggest that lateral segregation of proteins into membrane microdomains, either constitutively or in a stimulus-dependent manner, may be an integral determinant for their functionality. These studies ultimately raise the question of how heterogeneous PMs are. In plants, microdomains, especially when being targeted by proteins belonging to the same family, have so far been regarded as one uniform pattern. Here, we show that this concept has to be substantially refined, as single cell membranes in *Arabidopsis* and *Nicotiana benthamiana* are virtually covered with different types of microdomains. These may serve as platforms for interactions between different types of membrane-resident proteins and contribute to their functions.

RESULTS

Identification of Membrane Domain Patterns in Different Experimental Systems

As this study aims to characterize the diversity and dynamics of membrane domains in living plant cells by imaging-based approaches, we first validated our experimental systems carefully. Three Remorin genes (*At3g61260*, *At2g45820*, and *At4g36970*) were chosen based on available expression data. *At3g61260* and *At2g45820* are more than 20-fold higher

expressed compared with any other member of this multigene family (Figure 1A) and are the most studied ones. To select a structurally different Remorin (Raffaele et al., 2007), *At4g36970*, which is expressed at intermediate levels, was additionally used for this initial analysis. For these genes, *Arabidopsis* T-DNA insertion lines were obtained from the public stock center and homozygous mutant lines were selected. The respective insertion sites are illustrated in Figure 1B. To test if these lines were knockouts, protein or transcript levels were determined. Using the previously described α -REM antibody (Raffaele et al., 2009), which also recognizes the two most abundant *Arabidopsis* Remorins (*At3g61260* and *At2g45820*), we confirmed that both *at3g61260* mutant lines were null alleles, while the *At2g45820* protein was no longer expressed in only one line (*at2g45820-2*) (Figure 1C). Thus, this line was used for further analysis. As no antibody was available for *At4g36970*, transcript levels of this gene were determined using quantitative real-time PCR. Indeed, no *At4g36970* transcript was detectable in the *at4g36970-1* mutant (Figure 1D). Next, we transformed *at3g61260-2*, *at2g45820-2*, and *at4g36970-1* with constructs expressing the respective genes as N-terminally tagged fusion proteins under the control of their native promoters (e.g., *ProAt3g61260-YFP:At3g61260*). To obtain a detailed view of the membrane domains, confocal laser scanning microscopy (CLSM) was used to image the upper surface plane of rosette leaf epidermal cells of 3- to 4-week-old plants. A diffuse but structured labeling of the PM was observed for the two highly expressed Remorins *At3g61260* and *At2g45820* (Figures 2A and 2B). By contrast, *At4g36970* segregated into more distinct microdomains (Figure 2C). The same results were obtained upon expression of these constructs under the control of their native promoter (Figures 2D to 2F) or the constitutively active cauliflower mosaic virus 35S promoter (Figures 2G to 2I) in *N. benthamiana* leaf epidermal cells.

To further verify these results, the subcellular localization of another weakly expressed Remorin protein (*At5g61280*) was investigated. A *ProAt5g61280-YFP:At5g61280* construct was transiently transformed into leaf epidermal cells of a transgenic *Arabidopsis* line that expresses the bacterial effector *AvrPto* under the control of a dexamethasone-inducible promoter (*ProDex-AvrPto*) (Hauck et al., 2003). Induction of *AvrPto* expression leads to the degradation of plant immune receptors and thus allows efficient transient transfection of cells by *Agrobacterium tumefaciens* (Tsuda et al., 2012). In *Arabidopsis*, *At5g61280* was only weakly expressed but localized to distinct membrane domains (Supplemental Figure 1A).

As the observed patterns for *At3g61260* and *At2g45820* (Figure 2) did not resemble the results from a recent report where strong overexpression of *At2g45820* after ballistic transformation resulted in an accumulation of the protein in large clusters (Demir et al., 2013), we performed total internal reflection microscopy (TIRFM), which allows higher resolution in the z axis on our transgenic lines. Indeed, expression of both group 1 Remorins under the control of their endogenous promoters showed the same weakly structured pattern (Supplemental Figure 2) as observed by CLSM. To further verify the robustness of our experimental systems, we studied the localization of the previously reported potato Remorin REM1.3.

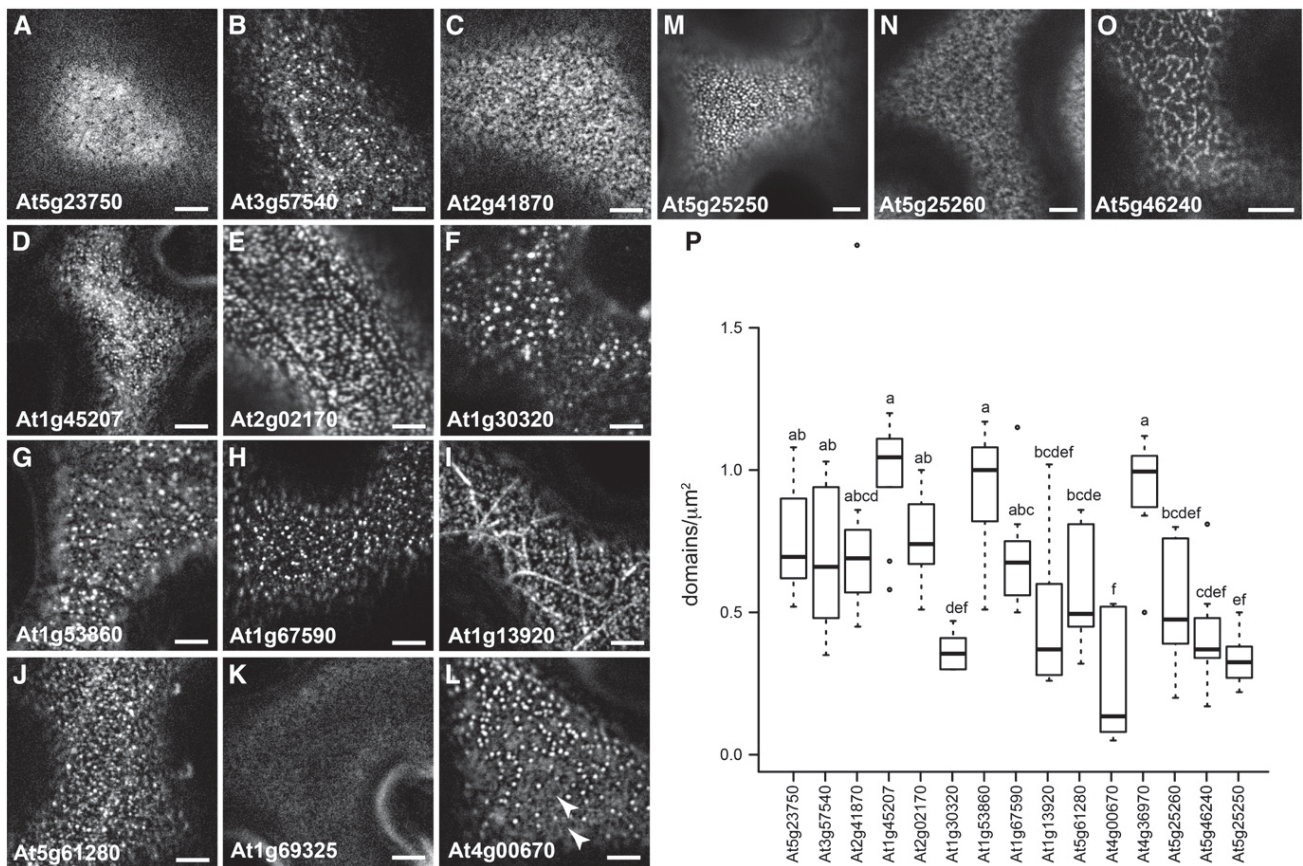


Figure 3. Remorin Proteins, Flotillins, and KAT1 Label a Variety of Distinct Membrane Domains in *N. benthamiana*.

(A) to (L) Surface imaging of upper leaf epidermal cell planes expressing 12 different fluorophore-tagged Remorin proteins using CLSM. Bars = 5 μm .

(M) and (N) Leaf epidermal cell planes expressing the fluorophore-tagged Flotillin proteins FLOT1A (M) and FLOT1B (N). Bars = 5 μm .

(O) Leaf epidermal cell plane expressing the fluorophore-tagged potassium channel KAT1. Bar = 5 μm .

(P) Quantitative image analysis revealed that the average density of membrane domains varied significantly between the different marker proteins. Letters indicate results of a one-way ANOVA followed by Tukey's honestly significant difference test.

Indeed, GFP-REM1.3 also localized to distinct microdomains in *N. benthamiana* leaf epidermal cells (Supplemental Figure 1B).

Similarly, the phylogenetically related SYMREM1 protein was also frequently found to label distinct membrane domains in this system (Supplemental Figure 1C).

Remorin and Flotillin Proteins Label a Large Variety of Membrane Domains

To globally assess the diversity of microdomains, 12 additional Remorins, the two *Arabidopsis* Flotillins FLOT1A (At5g25250) and FLOT1B (At5g25260), and the POTASSIUM CHANNEL IN ARABIDOPSIS THALIANA1 (KAT1) were cloned and ectopically expressed as yellow fluorescent protein (YFP)-tagged fusion proteins in *N. benthamiana* leaf epidermal cells (Figure 3). Imaging of single secant planes revealed PM association of all proteins (Supplemental Figure 3). However, At1g69325, At1g53860, At1g13920, and At5g61280 exhibited partial nuclear and minor cytosolic localization (Supplemental Figures 3D, 3K,

3N, and 3O, arrowheads). To further verify that the observed patterns were not caused by heterologous expression of the proteins, a representative subset (At4g00670, At3g57540, At1g45207, At2g02170, At1g30320, and At1g53860) was expressed in the above-mentioned *ProDex-AvrPto Arabidopsis* lines. All proteins displayed patterns similar to those observed in *N. benthamiana* (Supplemental Figures 1D to 1I).

To describe the patterns in more detail, 10 individual images per construct were subjected to quantitative image analysis. Parameters such as domain size, domain width, mean domain intensity, and circularity (Supplemental Figure 4) as well as domain density (Figure 3P) were determined. It should be noted that even if this analysis is restricted by the resolution limits of CLSM, domains observed in this study were generally larger (Supplemental Figure 4B). As expected, no domains were identified for the rather homogeneously distributed proteins At3g61260, At2g45820 (Figure 2), and At1g69325 (Figure 3K). However, At5g23750, which is phylogenetically close to At3g61260 and At2g45820, showed a more structured pattern

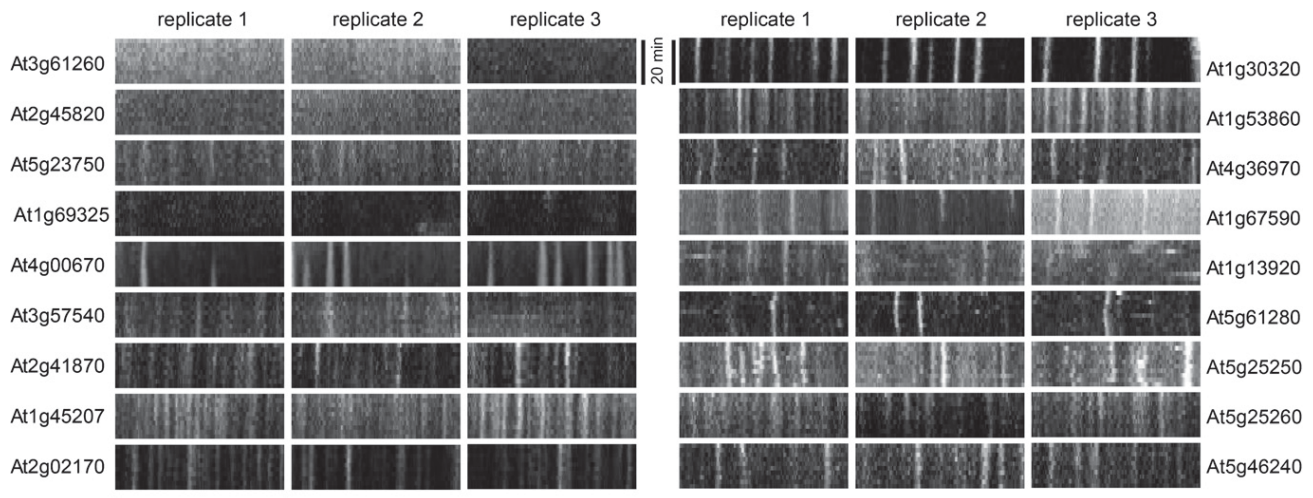


Figure 4. Kymographs Indicate the Lateral Stability of Membrane Domains.

The temporal and lateral mobility of membrane domains was investigated over 20 min in 2-min intervals. Vertical lines in kymographs indicate the lateral stability of most membrane domains. Movement was observed in the case of At1g13290 and partially in the case of At5g61280. The punctate structures appearing at single time points when imaging the Flotillin At5g25250 may represent endosomes. Bars = 20 μm (horizontal) and 20 min (vertical).

(Figure 3A), with an average domain size of $\sim 0.28 \mu\text{m}^2$ and an intermediate domain density of 0.75 domains/ μm^2 (Figure 3P; Supplemental Figure 4). All other proteins localized to distinct microdomains (Figures 3B to 3J) of different size, shape, and density. While most of the marker proteins labeled membrane domains of $\sim 0.25 \mu\text{m}^2$ on average, proteins like At3g57540, At4g36970, At5g61280, and At5g25260 targeted domains that were significantly smaller (Figure 3; Supplemental Figure 4). Two marker proteins, At4g00670 (Figure 3L) and At1g13920 (Figure 3I), showed more distinct patterns. In general, the fluorescence of domains observed for At4g00670 was more intense (Supplemental Figure 4C) and domain density was significantly reduced but varied greatly (Figure 3P) compared with all other marker proteins. Furthermore, this protein labeled a larger homogeneously distributed fraction at the PM in addition to distinct membrane domains (Figure 3L; Supplemental Figure 1D, arrowheads). Interestingly, we repeatedly observed that At1g13920 labeled filamentous structures while it additionally localized to more canonical membrane domains in the same cell (Figure 3I). In agreement with published data, the Flotillin proteins At5g25250 (FLOT1A) and At5g25260 (FLOT1B) labeled distinct microdomains (Figures 3M and 3N). FLOT1A-targeted domains varied significantly in size, while FLOT1B domains were relatively small (below $0.2 \mu\text{m}^2$) (Figure 3P; Supplemental Figure 4). When using another domain-localized protein, the potassium channel KAT1 (At5g46240), domains appeared stretched and network-like (Figure 3O). These observations are in full agreement with localizations reported for KAT1 earlier (Sutter et al., 2006).

Membrane Microdomains Are Temporally Stable Structures

Next, we asked whether the observed domains represent laterally stable structures. To assess this feature in more detail, we performed time-lapse experiments on all 18 marker proteins. PM

surfaces were imaged in 120-s intervals for 20 min, and kymographs were generated. Data obtained from these experiments clearly demonstrated high degrees of lateral stability for most of the observed membrane domains (Figure 4). Since At3g61260, At2g45820, and At1g69325 labeled the membrane more homogeneously (Figure 3), the temporal stability of these proteins could not be resolved by this method. Furthermore, a certain degree of lateral movement was observed for At4g36970, At1g13920, and At5g61280. For the latter two proteins, this may reflect the partial cytosolic protein fraction. However, microdomains for these proteins were also temporally stable, as indicated by the vertical lines (Figure 4). In addition, we observed some mobility in At5g25250 (FLOT1A)-expressing cells, which may represent endocytotic vesicles that were described for this protein earlier (Li et al., 2012).

Assessing Lateral Mobility by Fluorescence Recovery after Photobleaching

To characterize the lateral mobility of microdomain marker proteins in more detail, we performed extensive fluorescence recovery after photobleaching (FRAP) analysis on a subset of seven Remorin proteins (Figure 5A). For this, a circular region of interest (ROI) was bleached by high-intensity laser emission for 10 frames (~ 15 s). Fluorescence recovery on membrane surface areas was assessed over 5 min in 30-s intervals, and data were normalized to a reference ROI of equal size that was placed in close proximity to the bleached one. To compare these data with a cytosolic protein, we expressed soluble YFP in addition. In all samples, fluorescence recovered monoexponentially with coefficient of determination ($R^2 > 0.97$) (Figure 5A). In general, membrane surfaces labeled by domain marker proteins recovered significantly slower compared with the cytosolic YFP control, with half-times of 24.3 ± 1.4 s (At1g13920 filaments) to

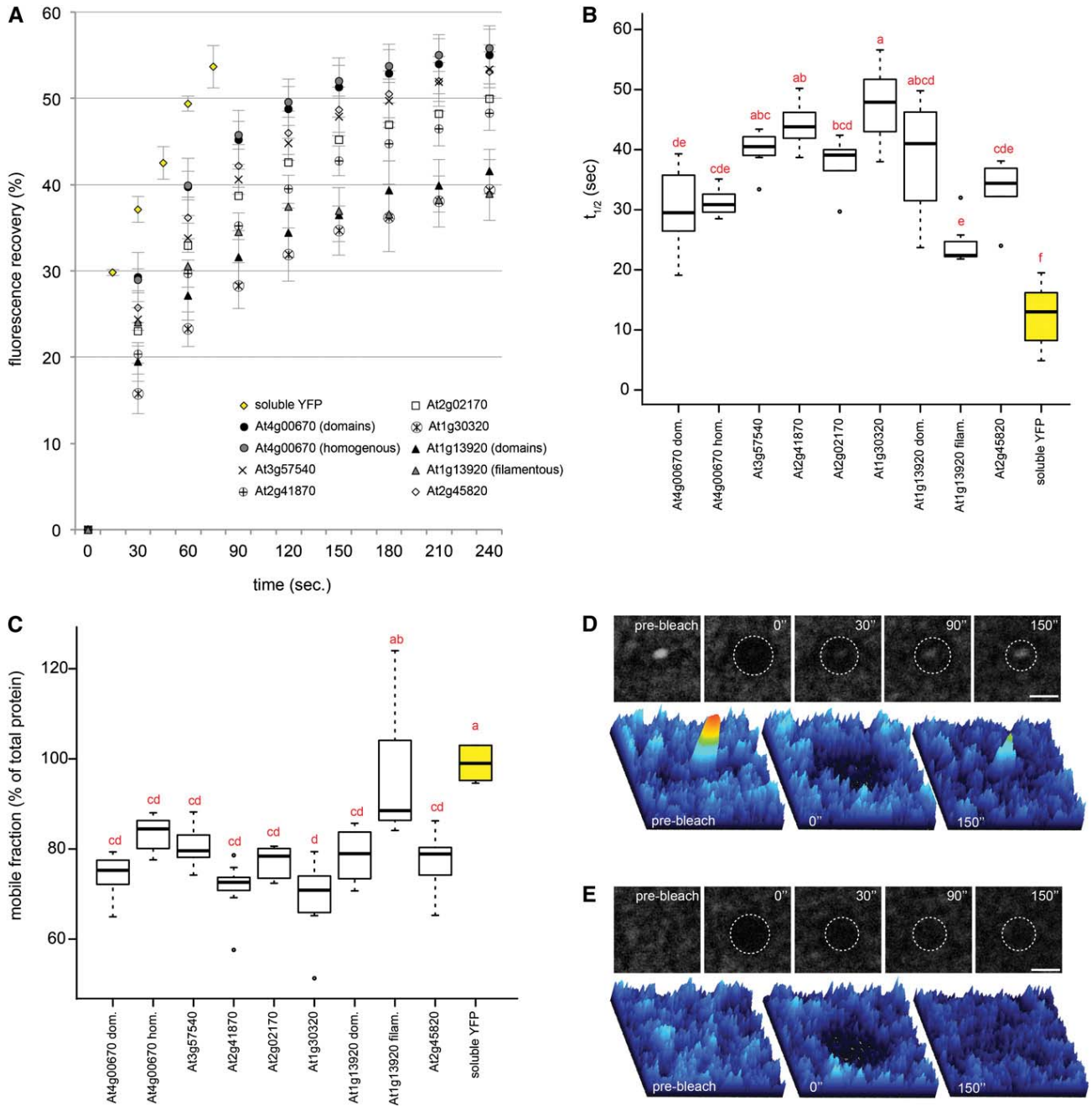


Figure 5. Assessing Protein Mobility by FRAP Analysis.

FRAP was used to investigate the mobility of different marker proteins.

(A) Fluorescence recovery was measured in a minimum of 12 independently bleached ROIs and normalized to nonbleached ROIs in their direct vicinity. Error bars show SE.

(B) and **(C)** Half-times ($t_{1/2}$) **(B)** and mobile fractions **(C)** were calculated for all proteins as described in Methods. Letters indicate results of a one-way ANOVA followed by Tukey's honestly significant difference test. dom., domain-localized protein fraction; hom., homogeneously distributed protein fraction; filam., filamentous protein fraction.

(D) Bleaching of individual membrane domains of At4g00670 resulted in recovery at the same position. Panels at top show the images that were used for plotting the corresponding pixel intensities (bottom). Numbers indicate seconds after bleaching. Bar = 2 μ m.

(E) Bleaching of the homogenous protein fraction of At4g00670. Fluorescence was centripetally recovered over time. Panels at top show the images that were used for plotting the corresponding pixel intensities (bottom). Numbers indicate seconds after bleaching. Bar = 2 μ m.

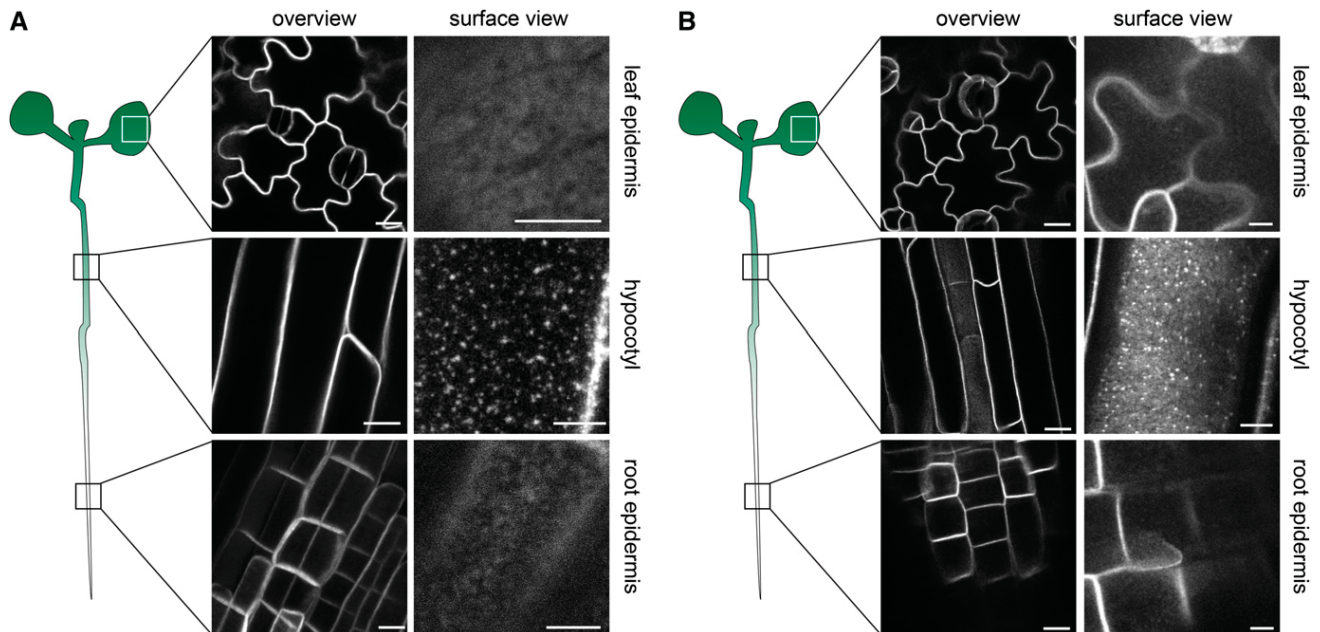


Figure 6. Tissue-Specific Formation of Membrane Domains.

(A) Upper planes of leaf epidermal cells (top panels), elongating hypocotyl cells (middle panels), and root epidermal cells (bottom panels) were imaged in 5-d-old seedlings of transgenic *Arabidopsis at3g61260-1* mutant plants expressing the Remorin protein At3g61260 as an N-terminally tagged YFP fusion protein under the control of its native promoter. Bars = 10 μ m (left column) and 5 μ m (right column).

(B) Localization studies as in **(A)** but of YFP-At2g45820 expressed in an *at2g45280-2* mutant background under the control of its native promoter. Bars = 10 μ m (left column) and 5 μ m (right column).

[See online article for color version of this figure.]

47.7 \pm 1.9 s (At1g30320) and 12.4 \pm 2.6 s, respectively (Figure 5B). However, significant differences were observed between the proteins, with At1g30320 being the most slowly diffusing protein. In the case of At4g00670, no difference in fluorescence recovery between the domain-associated fraction and the homogeneously PM-labeling fraction was observed (Figure 5B). Moreover, when bleaching single membrane domains labeled by At4g00670, proteins accumulated in the same position (Figure 5D) while non-domain-labeled PM segments recovered homogeneously (Figure 5E). This indicates a physical structure underlying protein accumulation in these distinct positions. Interestingly, At1g13920 again showed a significantly different pattern. While the domain-localized protein fraction overall recovered slowly, the half-time of filament-associated At1g13920 was significantly smaller (Figure 5B). This was also reflected in the mobile fraction, which was significantly increased for filament-associated At1g13920, while no differences were observed between the other Remorin proteins (Figure 5C).

As filament-like structures targeted by At1g13920 were stable over time (Supplemental Figure 5A), we assumed that they do not represent cytosolic strands. To test whether they are dependent on cortical cytoskeleton elements such as microtubules (labeled by MAP4; Supplemental Figure 5B) or actin (labeled by LifeAct; Supplemental Figure 5C), we depolymerized actin and microtubules by the drugs latrunculin B and oryzalin, respectively. While these structures entirely disappeared upon oryzalin treatment and resulted in a predominantly cytosolic

localization of At1g13920 (Supplemental Figure 5D), latrunculin B treatment did not alter the At1g13920-labeled filaments (Supplemental Figure 5E). These data indicate that microtubules affect the localization of At1g13920.

Tissue-Specific Labeling of Membrane Microdomains

As described above, At3g61260 and At2g45820 were not targeted to distinct membrane domains in mature rosette leaves in stable transgenic lines where both genes were expressed under the control of their endogenous promoters (Figures 2A and 2B). Thus, we tested whether membrane domains may be labeled in a tissue-specific manner. For this, we imaged different tissues in 3- and 5-d-old seedlings that were grown under sterile conditions. In both cases, we did not observe distinct membrane domains in leaf and root epidermal cells (Figure 6). By contrast, both proteins were occasionally targeted to distinct membrane domains in elongating hypocotyl cells (Figure 6, middle panels). There, they labeled foci in the PM that were similar to those observed for other Remorin proteins. These data indicate that membrane domains are dynamically formed or disintegrated under different environmental conditions or developmental stages.

Coexisting Microdomains Shape Multifaceted PMs

Using a subset of different domain marker proteins, we assessed the coexistence of microdomains on the same cell

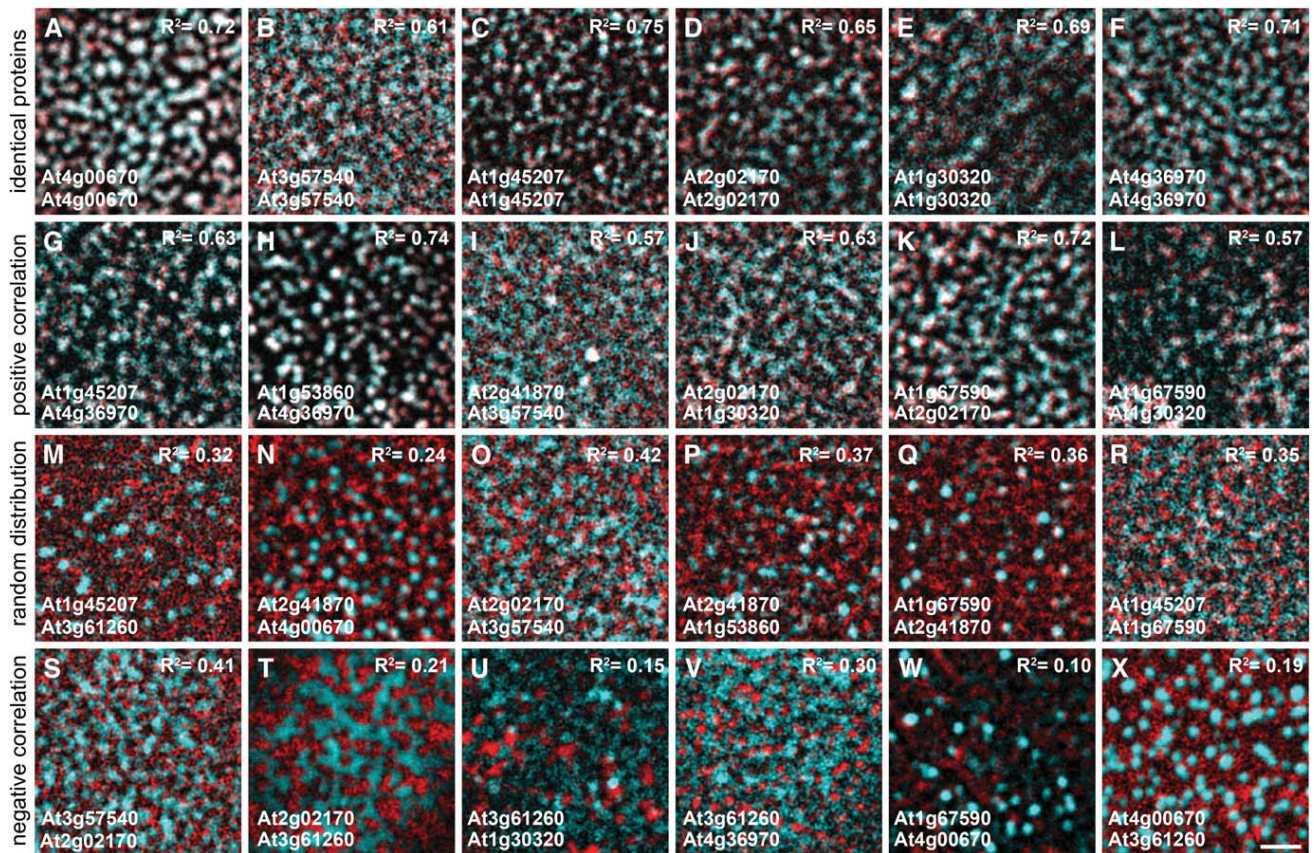


Figure 7. PMs Comprise a Wide Spectrum of Coexisting Microdomains.

(A) to (F) Representative images from control experiments where domains were labeled by the same proteins that were tagged with two different fluorophores, CFP (red) and YFP (cyan). R^2 values, which were significantly higher compared with those of the corresponding randomized images, indicate full colocalization of the proteins.

(G) to (L) Representative images of protein pairs that showed positive correlation. R^2 values were significantly higher compared with those of the corresponding randomized images. These proteins mutually excluded each other.

(M) to (R) Representative images of protein pairs randomly colocalized with each other. R^2 values were not significantly different from those of the corresponding randomized images.

(S) to (X) Representative images of protein pairs that showed negative correlation. R^2 values were significantly lower compared with those of the corresponding randomized images. These proteins mutually excluded each other.

Bar in (X) = 2 μ m for (A) to (X).

membrane. An extensive cross-comparison with a total number of 45 colocalization experiments was performed using different domain marker proteins tagged with either cyan fluorescent protein (CFP) or YFP. In all cases, the weakest expressing cells were chosen for image acquisition to minimize possible impacts by overexpression and to resemble the native situation as closely as possible. For each colocalization experiment, an average of 12 single images were subjected to quantitative image analysis. The R^2 (Manders et al., 1993) (Figure 7; Supplemental Table 1) and the standard Pearson correlation coefficient (Manders et al., 1992) (Supplemental Table 1) were calculated for each individual image. To determine the random overlap coefficient, each corresponding channel 2 image (YFP fluorescence) was flipped by 180° and merged with the original image from the CFP channel (Supplemental Figure 6). A Student's t test was then applied to determine whether the difference between

the two values was significant. Pairs with $R^2 > R^2$ random (positive correlations) were regarded as colocalizing and pairs with $R^2 < R^2$ random (negative correlations) were scored as excluding proteins. Combinations that did not pass the significance level ($P < 0.05$) were designated as randomly colocalized with each other and thus could not be assigned to either of the two categories.

To verify our approach, we first tested nine different pairs, where the same proteins were fused to YFP and CFP. On average, R^2 values of 0.645 were obtained, with the highest value at $R^2 = 0.752$ for At1g45207 (Figure 7C; Supplemental Table 1). These coefficients are fully consistent with the colocalization of microdomain-localized protein pairs previously described for living cells (Spira et al., 2012; Demir et al., 2013). Due to its homogenous distribution, At3g61260 showed the lowest value.

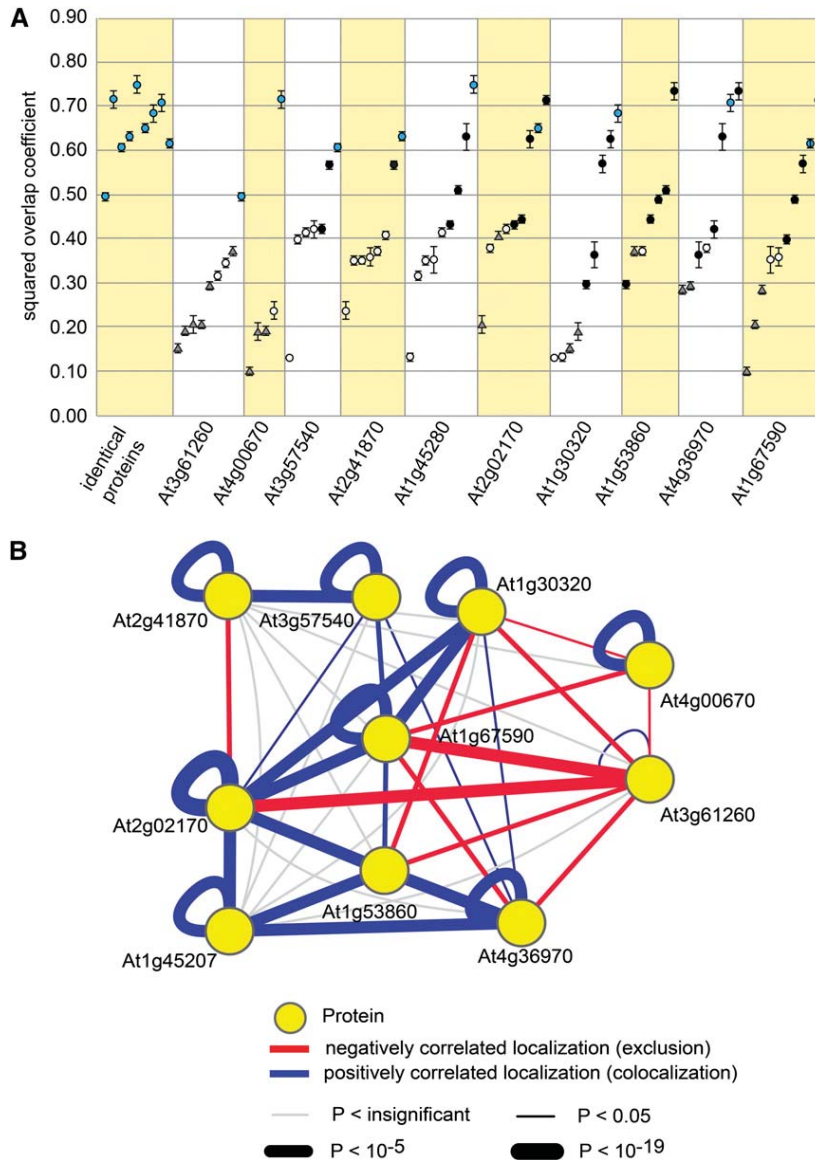


Figure 8. Quantifications and Network Analysis of Membrane Domain Colocalizations.

(A) R^2 values of all tested combinations were plotted in relation to individual proteins. The columns show R^2 values for identical protein pairs (blue circles) that all showed positive correlations. For all other combinations, positive correlations are depicted as black circles, randomly colocalizing combinations as white circles, and pairs with negative correlation as gray triangles. Error bars represent \pm SE.

(B) Network analysis of domain colocalizations revealed that Remorins of subgroup 6 often colocalized, while proteins such as At3g61260 and At4g00670 represent particular membrane domains or compartments.

Testing another 36 different combinations, we identified 14 colocalizing pairs and 12 combinations that strictly excluded each other (Supplemental Table 1). In all remaining cases, random colocalizations were observed. Most of the tested proteins showed a large dynamic range where the number of positive colocalizations exceeded the other categories (Figure 8A). Interestingly, we found a minimum of one colocalization for all tested proteins except At4g00670 (Figures 8A and 8B; Supplemental Table 1). This Remorin protein labeled a unique microdomain population that is highly distinct

from all other tested ones and showed colocalization only with itself. Similarly, the more evenly distributed At3g61260 did not colocalize with the majority of other domains (Figures 8A and 8B). In general, the number of significant R^2 values of colocalizing pairs greatly varied between the different proteins (Figure 8A). Proteins that are phylogenetically closely related (Raffaele et al., 2007) showed a tendency to increased colocalization (e.g., At2g41870/At3g57540 and At2g02170/At1g30320/At1g53860/At4g36970/At1g67590) (Figure 8B), implying that these microdomains may serve similar functions.

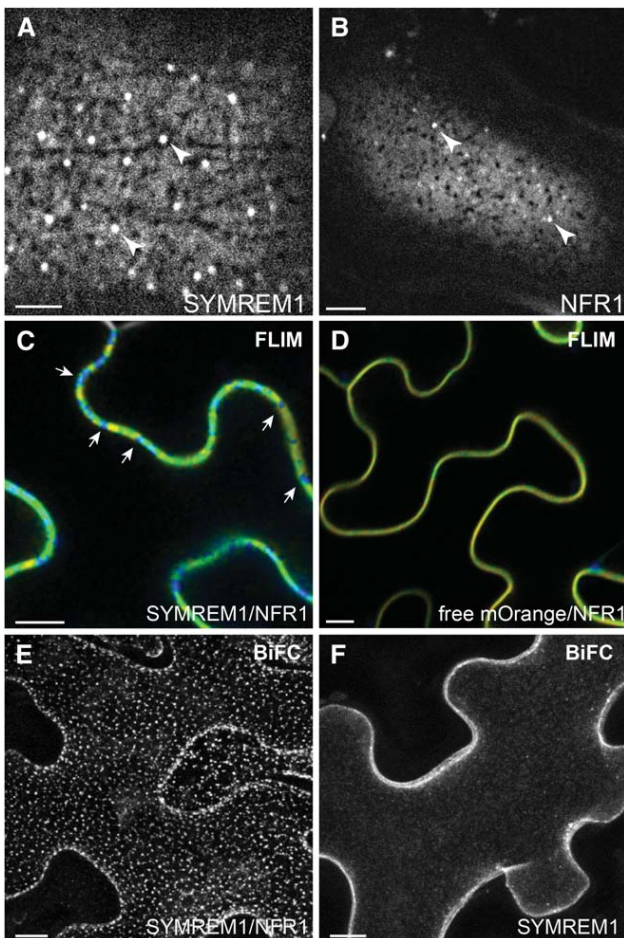


Figure 9. Membrane Domains May Provide Scaffolds for Protein-Protein Interactions.

(A) and (B) Heterologous expression of *L. japonicus* Remorin protein SYMREM1 (A) and NFR1 (B) in *N. benthamiana* leaf epidermal cells resulted in membrane domain labeling (arrowheads) at the cell surface. Bars = 5 μm .

(C) and (D) Donor fluorophore lifetime data obtained by fluorescence lifetime imaging microscopy (FLIM) and spectral photocounting on microscopic images. Cells expressing NFR1-Cerulean and SYMREM1-mOrange (C) and NFR1-Cerulean/free mOrange (D) showed interaction hotspots depicted in blue (decreased lifetime) (C) and homogeneously distributed background signal (D) along the PM of *N. benthamiana* leaf epidermal cells. Bars = 10 μm .

(E) and (F) Compartmentalized interaction between SYMREM1 and NFR1 was also observed using bimolecular fluorescence complementation (BiFC) in *N. benthamiana* leaf epidermal cells. Less intense domains were found in BiFC assays testing homooligomerization of SYMREM1 (F). Bars = 10 μm .

Perspectives: Protein-Protein Interactions Can Be Confined to Membrane Domains

Finally, we assessed whether receptor complex formation may be restricted to membrane domains. For this, we made use of an already described interaction between the Nod factor receptor NFR1 and the Remorin SYMREM1 from *Lotus japonicus*

(Lefebvre et al., 2010; Tóth et al., 2012). Expression of fluorophore-tagged SYMREM1 (Figure 9A) and NFR1 (Figure 9B) in *N. benthamiana* leaf epidermal cells frequently resulted in clear labeling of distinct microdomains (arrowheads) as well as a more uniformly distributed protein fraction across the entire PM (Figures 9A and 9B), as described for other Remorin proteins (Figure 3). Using fluorescence lifetime imaging microscopy and Förster resonance energy transfer, we already demonstrated physical interactions between NFR1 and SYMREM1 (Tóth et al., 2012). To analyze the spatial patterning of protein interactions on the PM, the obtained photon counts were mapped onto cell images to investigate lateral variation in donor lifetimes across the PM. Interestingly, distinct sites of reduced fluorescence lifetime of the donor fluorophore (NFR1:Cerulean) were identified (blue), indicating interaction hotspots in membrane domains (Figure 9C). Similar patterns were observed for the interaction between the ATPase CDC48A and the receptor-like kinase SERK1 (Aker et al., 2007). No such foci were found in control experiments where we coexpressed NFR1 with the soluble acceptor fluorophore mOrange (Figure 9D). Similar results were obtained when performing bimolecular fluorescence complementation assays. Here, the NFR1 receptor and SYMREM1 were fused to the N-terminal and the C-terminal halves of the YFP fluorophore, respectively. Fluorescence was exclusively observed in distinct and immobile membrane domains that were distributed over the entire inner PM leaflet of transformed cells (Figure 9E). To exclude the possibility that the fluorescence was only due to protein accumulation in membrane domains, we studied SYMREM1 oligomerization. Here, no domain-restricted fluorescence was observed (Figure 9F), suggesting that Remorin-receptor interaction may indeed be delimited to membrane domains. Overall, these data indicate that laterally defined membrane domains may provide physical rafts for receptor-scaffold and other protein-protein interactions.

DISCUSSION

A number of cell biological studies revealed domain localization of PM-associated proteins such as Remorins (Raffaele et al., 2009; Lefebvre et al., 2010), Flotillins (Haney and Long, 2010; Li et al., 2012), the potassium channel KAT1 (Sutter et al., 2006; Reuff et al., 2010), the anion channel SLAC1 HOMOLOG3 (SLAH3) (Demir et al., 2013), the LysM receptor LYK3 (Haney et al., 2011), the NADPH oxidase RBOHD (Lherminier et al., 2009), and the exocyst protein SECA3 (Zhang et al., 2013). So far, all studies in plants were restricted to the analysis of individual proteins or a single protein pair. First insights into the coexistence of different membrane domains in plants were provided by the stimulus-dependent colocalization of FLOT4 and LYK3 (Haney et al., 2011). This observation is in agreement with the proposed function of Flotillins, which act as molecular scaffold proteins that mediate the assembly of domain platforms and can confer anchoring of membrane domains to the cytoskeleton (Langhorst et al., 2007). Similar functions have been proposed for Remorin proteins (Lefebvre et al., 2010; Tóth et al., 2012). Here, we took advantage of the genetic expansion of the Remorin gene family with 16 members in *Arabidopsis* to assess the diversity of microdomains that are targeted by members of

one specific family. Indeed, cloning and expression of almost all Remorin proteins revealed that the great majority of them predominantly localized to immobile microdomain platforms (Figures 2 and 3; Supplemental Figure 3). The existence of these domains was confirmed in different biological systems (Figures 2 and 3; Supplemental Figure 1). We found that members of the Remorin subgroup 1 (At3g61260, At2g45280, and At5g23750) (Raffaële et al., 2007) exhibited a more homogenous labeling of the PM surface. Interestingly, proteomic approaches identified only members of this subgroup in *Arabidopsis* DRMs (Shahollari et al., 2004; Kierszniowska et al., 2009; Minami et al., 2009; Keinath et al., 2010). In addition, closely related proteins showed either a similar pattern (At1g69325; group 3) or, in the cases of SYMREM1 (group 2) and At4g00670 (group 3), frequently labeled membrane domains, the latter at low density (Figure 3P). Together with the finding that group 1 Remorins may be targeted to distinct membrane domains in a stimulus- or tissue-dependent manner (Figure 6), these data indicate that evolutionarily related proteins target similar types of membrane domains. This hypothesis is supported by the fact that closely related proteins such as At3g57540 and At2g41870 (Figures 7I and 8B) or Remorins with extended N-terminal domains of group 6 (At2g02170, At1g30320, At1g53860, At4g36970, At1g67590, At1g13920, and At5g61280) generally displayed higher degrees of colocalization compared with phylogenetically distinct proteins (Figure 8). These data are also in line with a recent report regarding yeast, where extensive colocalization studies revealed that proteins with similar functions (e.g., hexose transporters) showed increased tendencies to colocalize in the same membrane compartment (Spira et al., 2012). Such functional specification of membrane domains would be biologically preferred not only to support protein complex formation but also to physically separate enzymatic activities of physiologically unrelated processes. This hypothesis is supported by a recent study that demonstrated a colocalization of the *Arabidopsis* anion channel SLAH3 with the calcium-dependent protein kinase CPK21 in membrane microdomains. Interestingly, coexpression of the SLAH3/CPK21 complex with the PROTEIN PHOSPHATASE 2C (PP2C) phosphatase ABI1 led to a displacement from microdomains. This correlated with a loss of SLAH3 functionality (Demir et al., 2013). Similarly, mistargeting of the FERRO-O₂-OXIDOREDUCTASE Fet3 to the membrane domain labeled by PLASMA MEMBRANE PROTEIN1 (Pmp1) by transmembrane domain replacement resulted in impaired iron uptake in yeast even though full enzymatic activity of the Fet3-Pmp1 chimera needs to be demonstrated (Spira et al., 2012). For Remorin proteins that were analyzed in this study, these data imply that even though they may serve similar molecular functions, different members could be involved in distinct biological processes.

Almost all membrane domains investigated in this study formed structures that were immobile (Figures 4 and 5D). These domains are predominantly maintained by lateral protein diffusion, indicated by rather slow and centripetal fluorescence recovery (Figure 5), which has been reported for other PM-associated proteins before (Bhat et al., 2005; Martinière et al., 2012; Spira et al., 2012). Interestingly, no differences in recovery half-times and mobile fractions were observed between a membrane domain-associated fraction and a freely membrane-bound fraction

(Figures 5B and 5C). Two physical scaffolds may mediate such stability: the cell wall and the cortical cytoskeleton. Using protoplasts that continuously rebuild a cell wall after its enzymatic removal, a recent study showed that the lateral mobility of proteins was significantly altered during cell wall regeneration (Martinière et al., 2012). In addition, cortical actin and microtubule arrays can serve as fences or anchoring scaffolds for membrane domains (reviewed in Kusumi et al., 2005, 2012). In line with data from yeast, where microtubules stabilized membrane domains (Spira et al., 2012), at least a fraction of At1g13920 that targets a filament-like structure in the PM was also found to be sensitive to oryzalin treatment (Supplemental Figure 5D). However, while the role of actin in membrane domain stabilization remains to be demonstrated in plants, recent data from human cells suggest active roles of this cytoskeleton component in the lateral immobilization of membrane compartments (Dinic et al., 2013). Such dependence on the cytoskeleton may also explain why processes like the invasion of host cells by pathogenic fungi that are accompanied by cortical rearrangement (Henty-Ridilla et al., 2013) trigger the accumulation of sterol-rich membrane domains and resistance proteins at the site of cell penetration (Bhat et al., 2005; Underwood and Somerville, 2013). Therefore, it will be a future challenge to dissect the functional specification and diversity of membrane domains during plant-microbe interactions. Remorin- and Flotillin-labeled microdomains are likely to harbor unique sets of signaling proteins or to serve as signaling platforms (Figure 9) required for plant cell responses toward pathogenic and symbiotic microbes (Jarsch and Ott, 2011; Urbanus and Ott, 2012). Thus, the identification of the microdomain proteome will allow detailed understanding of supercomplexes and potential modes of regulation.

METHODS

Cloning and Constructs

For ectopic expression, 10 of the 16 *Arabidopsis thaliana* Remorins were obtained as cDNA clones from RIKEN (<http://www.brc.riken.jp/lab/epd/catalog/cdnaclone.html>). At5g23750, At1g69325, At1g67590, and At5g61280 were amplified from *Arabidopsis* cDNA generated by reverse transcription of RNA from *Nicotiana benthamiana* plants overexpressing the respective genomic constructs. At1g13920 was amplified from *Arabidopsis* genomic DNA. We created Gateway (GW)-compatible entry vectors for N-terminal fluorophore fusions. As destination vectors for ectopic overexpression, we used pAM-PAT-35SS:YFP:GW, pAM-PAT-35SS:CFP:GW, and pUBI-YFP:GW, respectively (Maekawa et al., 2008; Tóth et al., 2012). For the expression of N-terminally tagged fluorophore fusions under the control of the endogenous promoter, we created subclones of the putative 2-kb promoter region, the fluorophore, and the genomic coding sequence. Those fragments joined with *Bsa*I recognition sites and individual overhangs were blunt-end ligated into a modified puc57 and subsequently assembled via cut ligation into a modified pENTR-D. Expression vectors were created with pGWB1 (Binder et al., 2014). All primers used in this study are listed in Supplemental Table 2.

Plant Material and Quantitative Real-Time PCR

For stable transformations of N-terminally tagged Remorin constructs under the control of their respective endogenous promoters, the

following *Arabidopsis* T-DNA insertion lines were obtained: At3g61260 (SALK_117637.50.50.x), At2g45820 (SALK_17448.53.95.x), and At4g36970 (SALK_037050.55.00.x). For transient transformations of *Arabidopsis*, transgenic lines expressing a *ProDEX:AvrPto* construct (Hauck et al., 2003; Tsuda et al., 2012) were used. Transcript levels in the *at4g36970-1* mutant were determined by quantitative real-time PCR on cDNA of three independent biological replicates obtained from young rosette leaves of plants grown in a greenhouse using a SYBR Green assay. Data were normalized to the expression of PP2A as described elsewhere (Czechowski et al., 2005). Protein gel blot analysis was performed on plant material grown under the same conditions using the α -REM antibody at a 1:3000 dilution as described earlier (Raffaele et al., 2009).

Protein Expression for Fluorescence Microscopy

Agrobacterium tumefaciens-mediated transient transformation of *N. benthamiana* was performed as described earlier (Tóth et al., 2012). For single infiltrations, pAM-PAT 35S constructs were used. To avoid promoter silencing during coexpression, we used one construct driven by the 35S promoter and one driven by the pUbiquitin (pUbi) promoter. For infiltration of pUbi-driven constructs, we used final OD₆₀₀ values of 0.01 and 0.005; for pAM-PAT-35S, we used final OD₆₀₀ values of 0.2 to 0.4 for colocalization experiments and 0.01 for the expression of single proteins. *Agrobacterium*-mediated transient transformation of *Arabidopsis* was performed in stable lines carrying a *ProDEX:AvrPto* construct (Tsuda et al. 2012). For dexamethasone pretreatment, plants were sprayed with a 2 μ M dexamethasone solution containing 0.04% Silwet-77 24 h prior to transformation. Microscopical analysis was performed 2 d after infiltration as described below.

Plant Growth and Stable Transformation

N. benthamiana plants were grown 4 to 5 weeks under greenhouse conditions. *ProDEX:AvrPto Arabidopsis* plants were grown 5 to 6 weeks under short-day conditions (16 h of dark, 18°C/8 h of light, 20°C). *Arabidopsis* lines for stable transformation were grown 4 weeks under long-day conditions (8 h of dark/16 h of light) in the greenhouse. Shoots were cut back and plants regrown for 1 more week prior to floral dipping (Clough and Bent, 1998). Selection of stable transformants on hygromycin-containing plates was performed according to Harrison et al. (2006).

Confocal Microscopy and Quantitative Image Analysis

Standard confocal microscopy was performed with a Leica TCS SP5 confocal laser scanning microscope using an argon laser. YFP and CFP fluorophores were excited with the 514- and 456-nm laser lines, and emission was recorded in the range of 525 to 600 nm and 475 to 520 nm, respectively. Images were taken with a Leica DFC350FX digital camera.

For quantitative image analysis of individually expressed proteins, 10 images were segmented to differentiate between background and domains using a threshold of 0, 15 to 0, 22 and a background subtraction with a rolling ball radius of 20 pixels. The Fiji plugin Watershed was applied to separate overlapping intensities. The resulting image was used as a mask for an overlay on the original image. All quantitative measurements were then performed on the unprocessed image. Average values for domain size, mean domain intensity, circularity, and density were depicted as box plots using R. Statistical analysis was performed in R using ANOVA and Tukey's honestly significant difference.

For colocalization analysis, single images were subjected to a mean blur of 2 pixels and a background subtraction with a rolling ball radius of 20 pixels. Intensity correlation analysis using the respective plugin for

ImageJ provided by the Wright Cell Imaging Facility (Li et al., 2004) was performed to calculate both the Pearson correlation coefficient (Manders et al., 1992) and the R² (Manders et al., 1993). Mean values of an average of 12 repetitions were calculated. Simulations for random distribution patterns of each investigated protein pair were performed on reflected or rotated images, selecting ROIs containing relevant signal information in both channels. Between 8 and 17 values of colocalizing and randomized samples of one protein pair were used for a Student's *t* test to determine the significance of positive or negative correlations.

FRAP analysis was performed using FRAP Wizard implemented in the Leica LAS AF software. One frame was scanned prior to bleaching. Bleaching was performed on a circular ROI of 5 μ m in diameter in 10 frames with 100% laser intensity (~15 s). For single-domain bleaching (Figures 5D and 5E), this ROI was decreased to 2 μ m. Fluorescence recovery was imaged in 30-s intervals over 10 frames. FRAP values were fitted as described previously (Spira et al., 2012) using a simple exponential fit of $y = a \times (1.0 - \exp(-bx))$. Half times [$t_{1/2} = \ln(0.5)/b$] and mobile fractions [Mf = $(a \times 100)/\ln(\text{norm})$] were calculated for all FRAP experiments with a fit higher than 0.97. Surface plots were calculated from single ROIs in ImageJ.

For kymographs, films were acquired over a time frame of at least 20 min. Z-stacks with 15 to 18 slices of 1 μ m thickness were recorded every 2 min. Single images from Z-stacks of each time point were combined into stacks and transformed into Z-projects with maximal intensities in Fiji. All 10 Z-project images were again combined into a stack and corrected for eventual lateral shift of the sample via the Fiji plugin StackReg (Rigid Body). A line of 20 μ m was drawn, and the kymograph was created via the Reslice [L] tool of Fiji.

The colocalization network was visualized using Cytoscape software (Shannon et al., 2003). Layout of the network was done manually. As indicated in the figure legends, the line width indicates the probability of the observed correlation occurring by random (gray) and the color indicates whether the two proteins colocalized (blue) or were found in mutually exclusive localizations (red).

TIRFM

TIRFM was performed on leaves of 2-week-old seedlings grown sterile on plates. Images were acquired on an iMIC stand (Till Photonics) with an Olympus 100 \times 1.45 numerical aperture objective. A diode-pumped solid state laser (75 mW) at 488 nm (Coherent Sapphire) was selected through an acousto-optical tunable filter. A two-axis scan head was used to adjust incidence angles. Images were collected with an Andor iXON DU-897 EMCCD camera controlled by Live Acquisition (Till Photonics) software.

Drug Treatments

A 1 mM stock solution of oryzalin was prepared using DMSO as solvent and diluted to a final concentration of 5 μ M. Leaf discs were incubated for 4 h before imaging. For latrunculin B, a 2.4 μ M stock solution in ethanol was diluted in water to a final concentration of 50 nM. Leaf discs were incubated in the latrunculin B solution for 3 h before imaging. All controls were incubated in the respective solvent that was diluted accordingly.

Accession Numbers

Sequence data from this article can be found in the GenBank/EMBL data libraries under the following accession numbers: FLOT1A (At5g25250), FLOT1B (At5g25260), KAT1 (At5g46240), potato REM1.3 (NM_001288060), and SYMREM1 (JQ061257). Gene expression data (Figure 1A) are available in the Genevestigator database (repository identifiers GSM768250, GSM768251, and GSM768252) with the following accession numbers: *at3g61260-1* (SALK_117639), *at3g61260-2* (SALK_117637), *at2g45820-1* (SALK_011986), *at2g45820-2* (SALK_17448), and *at4g36970-1* (SALK_037050).

Supplemental Data

The following materials are available in the online version of this article.

Supplemental Figure 1. Membrane Domain Localization of Different Remorin Proteins in *Arabidopsis* and *N. benthamiana*.

Supplemental Figure 2. Total Internal Reflection Microscopy (TIRFM) of Upper Plasma Membrane Planes.

Supplemental Figure 3. Confocal Images of Secant Planes Illustrate the Plasma Membrane Localization of All 18 Marker Proteins.

Supplemental Figure 4. Quantification of Membrane Domain Parameters of All Marker Proteins.

Supplemental Figure 5. Filament-Like Localization of At1g13290 Is Dependent on Microtubules.

Supplemental Figure 6. Image Processing and Randomization for Quantitative Analysis of Colocalizations.

Supplemental Table 1. Data from Quantitative Image Analysis of Colocalization Experiments.

Supplemental Table 2. List of Primers Used in This Study.

ACKNOWLEDGMENTS

We thank members of our laboratory for fruitful discussions. We thank Macarena Marín and Claudia Popp for critical reading of the article, Guido Grossmann (Centre for Organismal Studies, Heidelberg, Germany) and Simon Brandner for valuable advice on image analysis, and Martina Ried for help with R. We also thank Jessica Folgmann for excellent technical assistance and Roland Wedlich-Söldner (Max-Planck-Institute for Biochemistry) for access to the total internal reflection microscope. The potato REM1.3 clone and the α -REM antibody were kind gifts from Sylvain Raffaele (Laboratoire des Interactions Plantes-Microorganismes, Toulouse, France) and Sebastien Mongrand (University of Bordeaux). The LifeAct template was provided by the laboratory of Stefanie Sprunck (University of Regensburg). This work was supported by the Deutsche Forschungsgemeinschaft from the Emmy-Noether Programme (Grant OT423/2-1) and the Collaborative Research Center 924 (Grant Sonderforschungsbereich 924), by the University of Bavaria (Ph.D. fellowships to I.K.J. and S.S.A.K.), and the Boehringer Ingelheim Foundation.

AUTHOR CONTRIBUTIONS

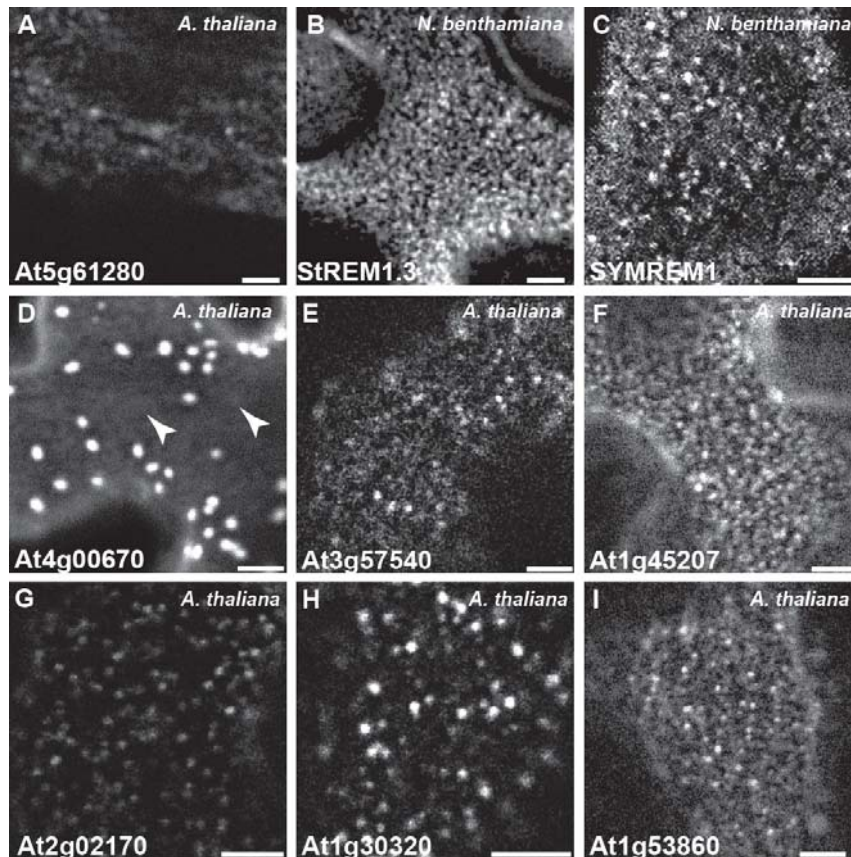
I.K.J., S.S.A.K., and T.O. designed the research. I.K.J., S.S.A.K., T.F.S., S.L.U., K.-H.B., W.S., and T.O. performed research. I.K.J., S.S.A.K., T.F.S., P.B., and T.O. analyzed data. I.K.J. and T.O. wrote the article.

Received February 18, 2014; revised March 17, 2014; accepted March 24, 2014; published April 8, 2014.

REFERENCES

- Aker, J., Hesselink, R., Engel, R., Karlova, R., Borst, J.W., Visser, A.J., and de Vries, S.C. (2007). In vivo hexamerization and characterization of the Arabidopsis AAA ATPase CDC48A complex using Förster resonance energy transfer-fluorescence lifetime imaging microscopy and fluorescence correlation spectroscopy. *Plant Physiol.* **145**: 339–350.
- Bhat, R.A., Miklis, M., Schmelzer, E., Schulze-Lefert, P., and Panstruga, R. (2005). Recruitment and interaction dynamics of plant penetration resistance components in a plasma membrane microdomain. *Proc. Natl. Acad. Sci. USA* **102**: 3135–3140.
- Binder, A., Lambert, J., Morbitzer, R., Popp, C., Ott, T., Lahaye, T., and Parniske, M. (2014). A modular plasmid assembly kit for multigene expression, gene silencing and silencing rescue in plants. *PLoS ONE* **9**: e88218.
- Boutté, Y., and Grebe, M. (2009). Cellular processes relying on sterol function in plants. *Curr. Opin. Plant Biol.* **12**: 705–713.
- Clough, S.J., and Bent, A.F. (1998). Floral dip: A simplified method for *Agrobacterium*-mediated transformation of *Arabidopsis thaliana*. *Plant J.* **16**: 735–743.
- Czechowski, T., Stitt, M., Altmann, T., Udvardi, M.K., and Scheible, W.R. (2005). Genome-wide identification and testing of superior reference genes for transcript normalization in Arabidopsis. *Plant Physiol.* **139**: 5–17.
- Demir, F., Horntrich, C., Blachutzik, J.O., Scherzer, S., Reinders, Y., Kierszniowska, S., Schulze, W.X., Harms, G.S., Hedrich, R., Geiger, D., and Kreuzer, I. (2013). Arabidopsis nanodomain-delimited ABA signaling pathway regulates the anion channel SLAH3. *Proc. Natl. Acad. Sci. USA* **110**: 8296–8301.
- Dinic, J., Ashrafzadeh, P., and Parmryd, I. (2013). Actin filaments attachment at the plasma membrane in live cells cause the formation of ordered lipid domains. *Biochim. Biophys. Acta* **1828**: 1102–1111.
- Haney, C.H., and Long, S.R. (2010). Plant flotillins are required for infection by nitrogen-fixing bacteria. *Proc. Natl. Acad. Sci. USA* **107**: 478–483.
- Haney, C.H., Riely, B.K., Tricoli, D.M., Cook, D.R., Ehrhardt, D.W., and Long, S.R. (2011). Symbiotic rhizobia bacteria trigger a change in localization and dynamics of the *Medicago truncatula* receptor kinase LYK3. *Plant Cell* **23**: 2774–2787.
- Harrison, S.J., Mott, E.K., Parsley, K., Aspinall, S., Gray, J.C., and Cottage, A. (2006). A rapid and robust method of identifying transformed *Arabidopsis thaliana* seedlings following floral dip transformation. *Plant Methods* **2**: 19.
- Hauck, P., Thilmony, R., and He, S.Y. (2003). A *Pseudomonas syringae* type III effector suppresses cell wall-based extracellular defense in susceptible Arabidopsis plants. *Proc. Natl. Acad. Sci. USA* **100**: 8577–8582.
- Henty-Ridilla, J.L., Shimono, M., Li, J., Chang, J.H., Day, B., and Staiger, C.J. (2013). The plant actin cytoskeleton responds to signals from microbe-associated molecular patterns. *PLoS Pathog.* **9**: e1003290.
- Jarsch, I.K., and Ott, T. (2011). Perspectives on remorin proteins, membrane rafts, and their role during plant-microbe interactions. *Mol. Plant Microbe Interact.* **24**: 7–12.
- Keinath, N.F., Kierszniowska, S., Lorek, J., Bourdais, G., Kessler, S.A., Shimosato-Asano, H., Grossniklaus, U., Schulze, W.X., Robatzek, S., and Panstruga, R. (2010). PAMP (pathogen-associated molecular pattern)-induced changes in plasma membrane compartmentalization reveal novel components of plant immunity. *J. Biol. Chem.* **285**: 39140–39149.
- Kierszniowska, S., Seiwert, B., and Schulze, W.X. (2009). Definition of Arabidopsis sterol-rich membrane microdomains by differential treatment with methyl-beta-cyclodextrin and quantitative proteomics. *Mol. Cell. Proteomics* **8**: 612–623.
- Kusumi, A., Fujiwara, T.K., Chadda, R., Xie, M., Tsunoyama, T.A., Kalay, Z., Kasai, R.S., and Suzuki, K.G. (2012). Dynamic organizing principles of the plasma membrane that regulate signal transduction: Commemorating the fortieth anniversary of Singer and Nicolson's fluid-mosaic model. *Annu. Rev. Cell Dev. Biol.* **28**: 215–250.
- Kusumi, A., Nakada, C., Ritchie, K., Murase, K., Suzuki, K., Murakoshi, H., Kasai, R.S., Kondo, J., and Fujiwara, T. (2005). Paradigm shift of the plasma membrane concept from the two-dimensional continuum fluid to the partitioned fluid: High-speed single-molecule tracking of membrane molecules. *Annu. Rev. Biophys. Biomol. Struct.* **34**: 351–378.

- Langhorst, M.F., Solis, G.P., Hannbeck, S., Plattner, H., and Stuermer, C.A. (2007). Linking membrane microdomains to the cytoskeleton: Regulation of the lateral mobility of reggie-1/flotillin-2 by interaction with actin. *FEBS Lett.* **581**: 4697–4703.
- Lefebvre, B., et al. (2010). A remorin protein interacts with symbiotic receptors and regulates bacterial infection. *Proc. Natl. Acad. Sci. USA* **107**: 2343–2348.
- Levental, I., Grzybek, M., and Simons, K. (2010a). Greasing their way: Lipid modifications determine protein association with membrane rafts. *Biochemistry* **49**: 6305–6316.
- Levental, I., Lingwood, D., Grzybek, M., Coskun, U., and Simons, K. (2010b). Palmitoylation regulates raft affinity for the majority of integral raft proteins. *Proc. Natl. Acad. Sci. USA* **107**: 22050–22054.
- Lherminier, J., Elmayan, T., Fromentin, J., Elaraqui, K.T., Vesa, S., Morel, J., Verrier, J.L., Cailleteau, B., Blein, J.P., and Simon-Plas, F. (2009). NADPH oxidase-mediated reactive oxygen species production: Subcellular localization and reassessment of its role in plant defense. *Mol. Plant Microbe Interact.* **22**: 868–881.
- Li, Q., Lau, A., Morris, T.J., Guo, L., Fordyce, C.B., and Stanley, E.F. (2004). A syntaxin 1, Galpha(o), and N-type calcium channel complex at a presynaptic nerve terminal: Analysis by quantitative immunocolocalization. *J. Neurosci.* **24**: 4070–4081.
- Li, R., Liu, P., Wan, Y., Chen, T., Wang, Q., Mettlich, U., Baluska, F., Samaj, J., Fang, X., Lucas, W.J., and Lin, J. (2012). A membrane microdomain-associated protein, *Arabidopsis* Flot1, is involved in a clathrin-independent endocytic pathway and is required for seedling development. *Plant Cell* **24**: 2105–2122.
- Lingwood, D., and Simons, K. (2010). Lipid rafts as a membrane-organizing principle. *Science* **327**: 46–50.
- Maekawa, T., Kusakabe, M., Shimoda, Y., Sato, S., Tabata, S., Murooka, Y., and Hayashi, M. (2008). Polyubiquitin promoter-based binary vectors for overexpression and gene silencing in *Lotus japonicus*. *Mol. Plant Microbe Interact.* **21**: 375–382.
- Malinsky, J., Opekarová, M., Grossmann, G., and Tanner, W. (2013). Membrane microdomains, rafts, and detergent-resistant membranes in plants and fungi. *Annu. Rev. Plant Biol.* **64**: 501–529.
- Malinsky, J., Opekarová, M., and Tanner, W. (2010). The lateral compartmentation of the yeast plasma membrane. *Yeast* **27**: 473–478.
- Manders, E.M., Stap, J., Brakenhoff, G.J., van Driel, R., and Aten, J.A. (1992). Dynamics of three-dimensional replication patterns during the S-phase, analysed by double labelling of DNA and confocal microscopy. *J. Cell Sci.* **103**: 857–862.
- Manders, E.M., Verbeek, F.J., and Aten, J.A. (1993). Measurement of co-localization of objects in dual-colour confocal images. *J. Microsc.* **169**: 375–382.
- Marín, M., and Ott, T. (2012). Phosphorylation of intrinsically disordered regions in remorin proteins. *Front. Plant Sci.* **3**: 86.
- Marín, M., Thallmair, V., and Ott, T. (2012). The intrinsically disordered N-terminal region of AtREM1.3 remorin protein mediates protein-protein interactions. *J. Biol. Chem.* **287**: 39982–39991.
- Martinière, A., et al. (2012). Cell wall constrains lateral diffusion of plant plasma-membrane proteins. *Proc. Natl. Acad. Sci. USA* **109**: 12805–12810.
- Minami, A., Fujiwara, M., Furuto, A., Fukao, Y., Yamashita, T., Kamo, M., Kawamura, Y., and Uemura, M. (2009). Alterations in detergent-resistant plasma membrane microdomains in *Arabidopsis thaliana* during cold acclimation. *Plant Cell Physiol.* **50**: 341–359.
- Müller, A., Guan, C., Gälweiler, L., Tänzler, P., Huijser, P., Marchant, A., Parry, G., Bennett, M., Wisman, E., and Palme, K. (1998). AtPIN2 defines a locus of *Arabidopsis* for root gravitropism control. *EMBO J.* **17**: 6903–6911.
- Raffaele, S., et al. (2009). Remorin, a Solanaceae protein resident in membrane rafts and plasmodesmata, impairs potato virus X movement. *Plant Cell* **21**: 1541–1555.
- Raffaele, S., Mongrand, S., Gamas, P., Niebel, A., and Ott, T. (2007). Genome-wide annotation of remorins, a plant-specific protein family: Evolutionary and functional perspectives. *Plant Physiol.* **145**: 593–600.
- Reuff, M., Mikosch, M., and Homann, U. (2010). Trafficking, lateral mobility and segregation of the plant K channel KAT1. *Plant Biol. (Stuttg.)* **12** (suppl. 1): 99–104.
- Roppolo, D., De Rybel, B., Tendon, V.D., Pfister, A., Alassimone, J., Vermeer, J.E., Yamazaki, M., Stierhof, Y.D., Beeckman, T., and Geldner, N. (2011). A novel protein family mediates Casparian strip formation in the endodermis. *Nature* **473**: 380–383.
- Russinova, E., Borst, J.W., Kwaaitaal, M., Caño-Delgado, A., Yin, Y., Chory, J., and de Vries, S.C. (2004). Heterodimerization and endocytosis of *Arabidopsis* brassinosteroid receptors BRI1 and AtSERK3 (BAK1). *Plant Cell* **16**: 3216–3229.
- Shahollari, B., Peskan-Berghoefer, T., and Oelmueller, R. (2004). Receptor kinases with leucine-rich repeats are enriched in Triton X-100 insoluble plasma membrane microdomains from plants. *Physiol. Plant.* **122**: 397–403.
- Shannon, P., Markiel, A., Ozier, O., Baliga, N.S., Wang, J.T., Ramage, D., Amin, N., Schwikowski, B., and Ideker, T. (2003). Cytoscape: A software environment for integrated models of biomolecular interaction networks. *Genome Res.* **13**: 2498–2504.
- Spira, F., Mueller, N.S., Beck, G., von Olshausen, P., Beig, J., and Wedlich-Söldner, R. (2012). Patchwork organization of the yeast plasma membrane into numerous coexisting domains. *Nat. Cell Biol.* **14**: 640–648.
- Sutter, J.U., Campanoni, P., Tyrrell, M., and Blatt, M.R. (2006). Selective mobility and sensitivity to SNAREs is exhibited by the *Arabidopsis* KAT1 K⁺ channel at the plasma membrane. *Plant Cell* **18**: 935–954.
- Tanner, W., Malinsky, J., and Opekarová, M. (2011). In plant and animal cells, detergent-resistant membranes do not define functional membrane rafts. *Plant Cell* **23**: 1191–1193.
- Tóth, K., Stratil, T.F., Madsen, E.B., Ye, J., Popp, C., Antolín-Llovera, M., Grossmann, C., Jensen, O.N., Schüssler, A., Parniske, M., and Ott, T. (2012). Functional domain analysis of the Remorin protein LjSYMREM1 in *Lotus japonicus*. *PLoS ONE* **7**: e30817.
- Tsuda, K., Qi, Y., Nguyen, V., Bethke, G., Tsuda, Y., Glazebrook, J., and Katagiri, F. (2012). An efficient Agrobacterium-mediated transient transformation of *Arabidopsis*. *Plant J.* **69**: 713–719.
- Underwood, W., and Somerville, S.C. (2013). Perception of conserved pathogen elicitors at the plasma membrane leads to relocalization of the *Arabidopsis* PEN3 transporter. *Proc. Natl. Acad. Sci. USA* **110**: 12492–12497.
- Urbanus, S.L., and Ott, T. (2012). Plasticity of plasma membrane compartmentalization during plant immune responses. *Front. Plant Sci.* **3**: 181.
- van den Bogaart, G., Meyenberg, K., Risselada, H.J., Amin, H., Willig, K.I., Hubrich, B.E., Dier, M., Hell, S.W., Grubmüller, H., Diederichsen, U., and Jahn, R. (2011). Membrane protein sequestering by ionic protein-lipid interactions. *Nature* **479**: 552–555.
- Vermeer, J.E., Van Munster, E.B., Vischer, N.O., and Gadella, T.W., Jr., (2004). Probing plasma membrane microdomains in cowpea protoplasts using lipidated GFP-fusion proteins and multimode FRET microscopy. *J. Microsc.* **214**: 190–200.
- Zhang, Y., Immink, R., Liu, C.M., Emons, A.M., and Ketelaar, T. (2013). The *Arabidopsis* exocyst subunit SEC3A is essential for embryo development and accumulates in transient puncta at the plasma membrane. *New Phytol.* **199**: 74–88.
- Zurzolo, C., van Meer, G., and Mayor, S. (2003). The order of rafts. Conference on microdomains, lipid rafts and caveolae. *EMBO Rep.* **4**: 1117–1121.



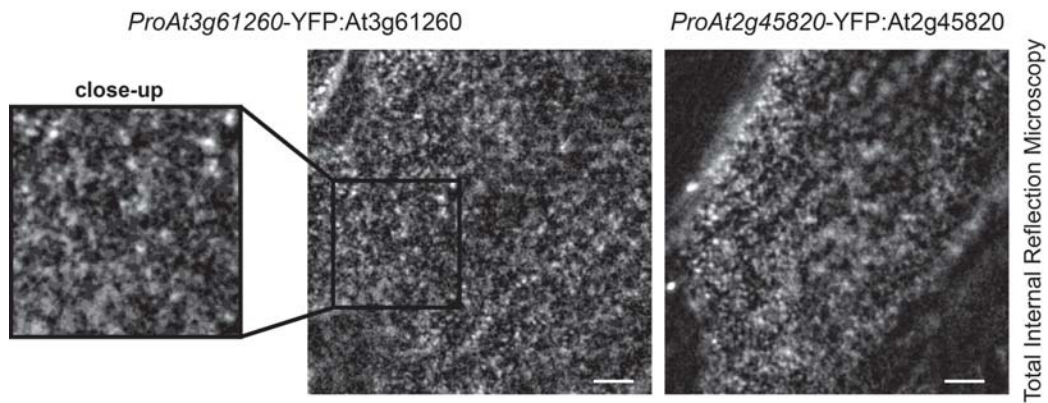
Supplemental Figure 1 online.

Membrane domain localization of different Remorin proteins in *A. thaliana* and *N. benthamiana*.

(A) Expression of At5g61280 under the control of its endogenous promoter in AvrPto DEX inducible *A. thaliana* resulted in labeling of distinct membrane domains. Scale bars indicate 5 μ m.

(B-C) Heterologous and ectopic expression of the potato REM1.3 (B) and *M. truncatula* SYMREM1 (C) in *N. benthamiana* leaf epidermal cells. Scale bars indicate 5 μ m.

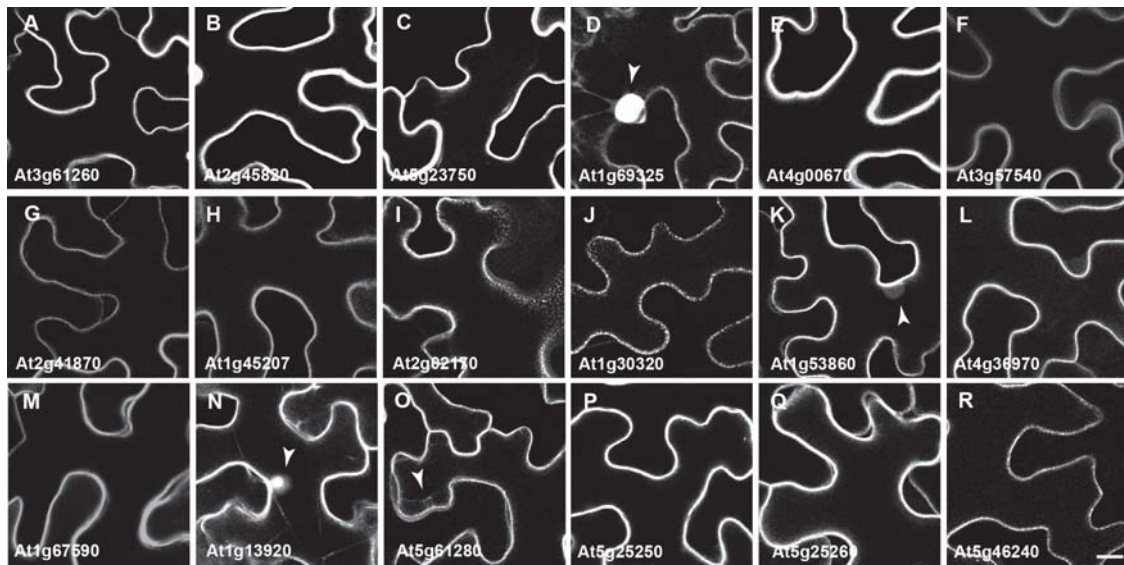
(D-I) Ectopic expression of different Remorins in leaf epidermal cells of transgenic *A. thaliana* plants transformed with a dexamethasone inducible AvrPto construct. Scale bars indicate 5 μ m.



Supplemental Figure 2 online.

Total Internal Reflection Microscopy (TIRFM) of upper plasma membrane planes.

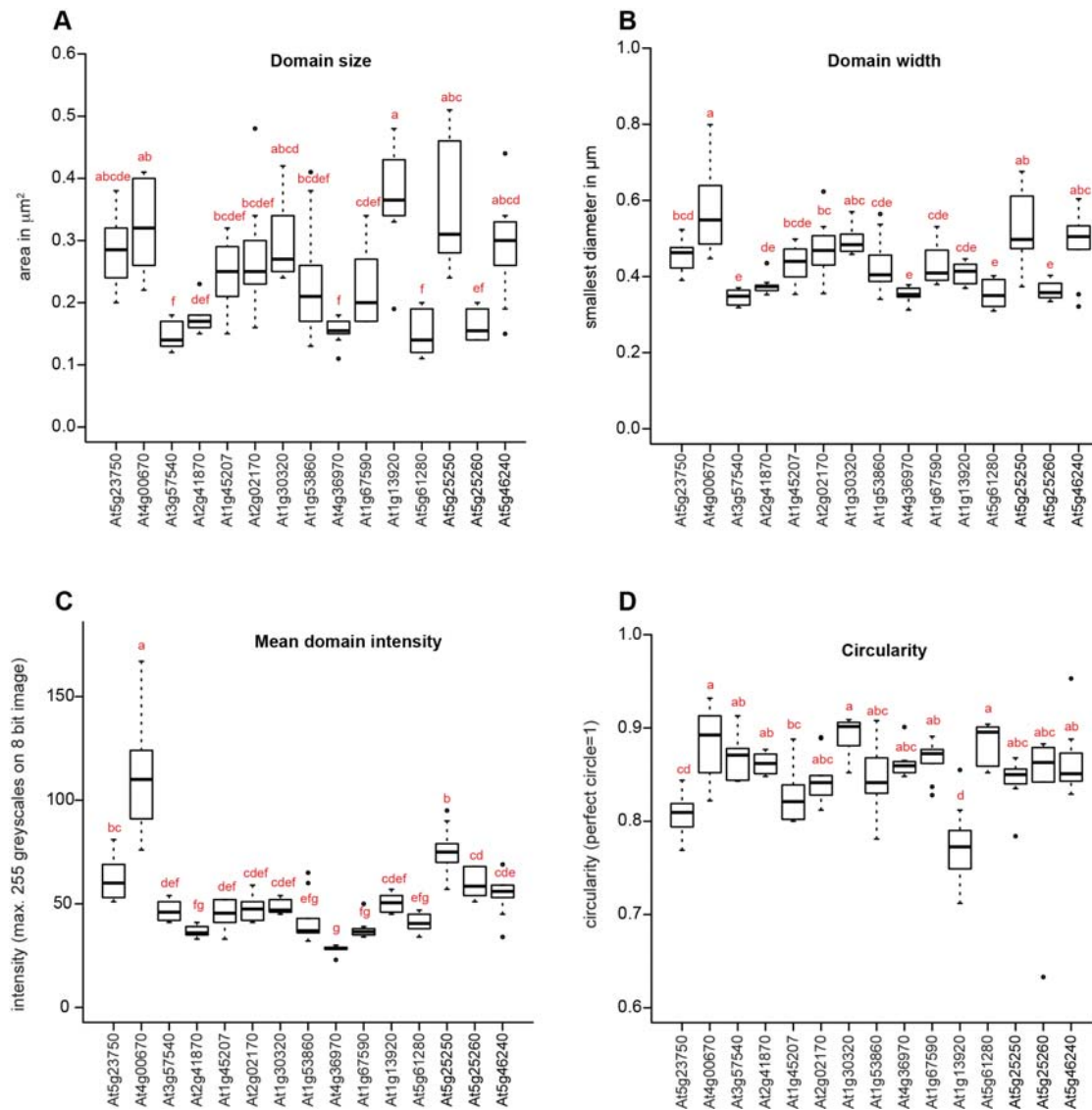
Null mutants expressing *At3g61260* and *At2g45820* as YFP fusion proteins were assessed by TIRFM. Both proteins localized to small yet highly mobile domains. Scale bars indicate 2 μm .



Supplemental Figure 3 online.

Confocal images of secant planes illustrate plasma membrane localization of all marker proteins.

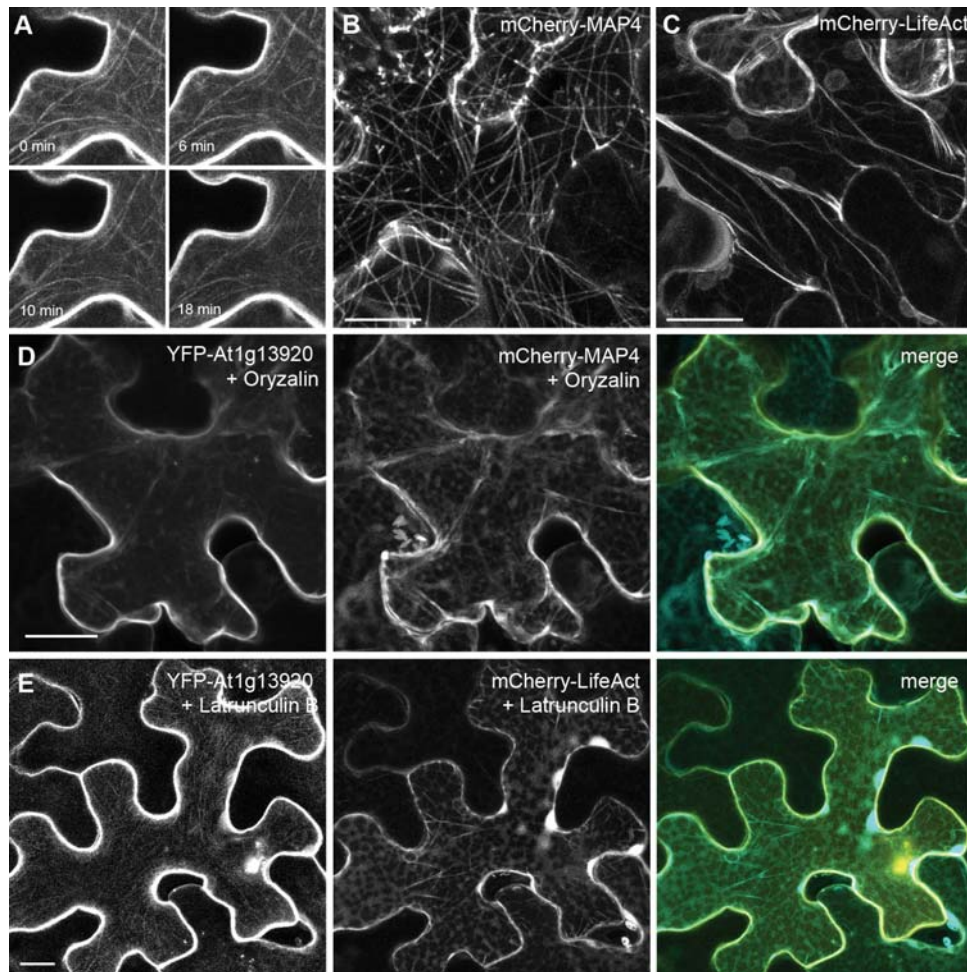
Eighteen different marker proteins were expressed in *N. benthamiana* leaf epidermal cells. Secant plant images are shown to demonstrate localization of the proteins to the plasma membrane. Arrowheads point towards partial nuclear and minor cytosolic localization of At1g69325, At1g53860, At1g13920 and At5g61280. Scale bar indicates 10 μ m.



Supplemental Figure 4 online.

Quantification of membrane domain parameters of all marker proteins.

Boxplots representing ten independent images of single protein expressing *N. benthamiana* leaf epidermal cells were used to quantify domain parameters as described in the Methods section. Letters indicate results of a one-way analysis of variance (ANOVA) followed by a Tukey HSD test.



Supplemental Figure 5 online.

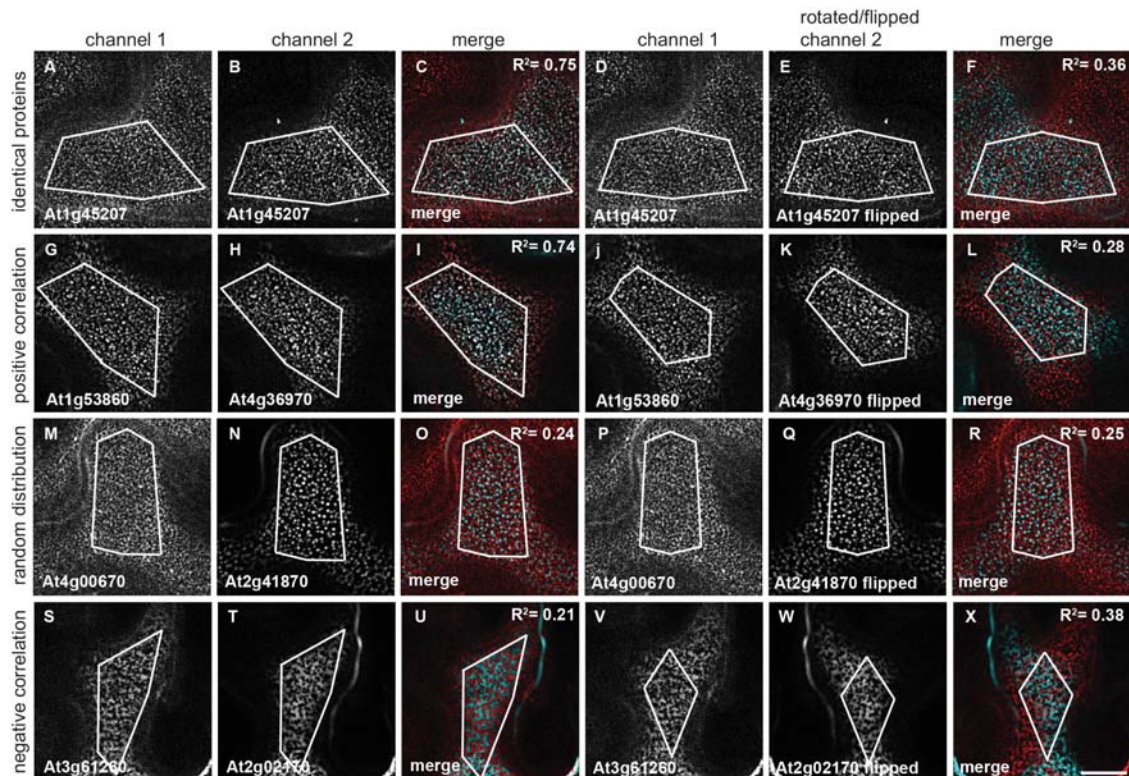
Filament-like localization of At1g13920 is dependent on microtubules.

(A) Time lapse experiments show that filament-like structures that are frequently labeled by At1g13920 are stable over an observation period of at least 20 minutes.

(B-C) Cells co-expressing the microtubule marker protein MAP4 (B) and the actin labeling peptide LifeAct (C) before treatment with oryzalin. Scale bars indicate 20 μm.

(D) Oryzalin treatment depolymerized microtubules and led to a loss of the At1g13920-labeled filaments and its predominant cytosolic localization. Scale bar indicates 20 μm.

(E) Depolymerization of the actin cytoskeleton by incubation in latrunculin B did not alter localization of At1g13920 but disrupted the majority of actin filaments. Scale bar indicates 20 μm.



Supplemental Figure 6 online.

Image processing and randomization for quantitative analysis of co-localizations.

To make any quantitative and robust statements on co-localization between two proteins, squared overlap coefficients (R^2) were calculated (C, I, O, U). For this, the channel 2 image was flipped or rotated (E, K, Q, W) to randomize the image. R^2 values were calculated for a new region of interest that contained image information of both channels (F, L, R, X). When mean R^2 values were significantly higher than the corresponding randomized values, pairs were ranked as positive correlations (co-localization). Pairs without any significant difference between these two values are randomly distributed and those where the randomized R^2 was significantly higher than the corresponding original R^2 value were ranked as negative correlation (mutual exclusion). Scale bars indicate 5 μm .

Supplemental Table 1 online.**Data from quantitative image analysis of co-localization experiments.**

Protein pairs were grouped as 'positive co-localization' when R^2 was significantly higher ($p < 0.05$) compared to R^2_{random} , as 'random co-localization' when R^2 was not significantly different compared to R^2_{random} and as 'exclusion' when R^2 was significantly lower ($p < 0.05$) compared to R^2_{random} . Significant levels were calculated by Student ttest. rd= random; std.err= standard error; n= number of independent images that were analyzed.

Protein pair	sq. Manders		Pearson			n	sq. Manders		Pearson		n	sq. Manders	Pearson
	R^2	std. err.	Rr	std. err.	rd R^2		rd std. err.	rd Rr	rd std. err.	ttest R^2			
At1g45207xAt1g45207	0,752	0,020	0,661	0,026	11	0,364	0,021	0,016	0,012	10	3,47E-11	6,20E-15	
At4g00670xAt4g00670	0,718	0,022	0,617	0,038	15	0,360	0,016	0,017	0,010	19	8,04E-14	1,30E-16	
At4g36970xAt4g36970	0,711	0,022	0,582	0,021	9	0,432	0,011	-0,003	0,006	11	6,46E-10	8,82E-17	
At1g30320xAt1g30320	0,687	0,018	0,607	0,021	17	0,365	0,013	0,054	0,015	11	9,02E-13	5,67E-17	
At2g02170xAt2g02170	0,653	0,007	0,524	0,015	13	0,352	0,008	0,002	0,008	15	1,67E-20	2,08E-22	
At2g41870xAt2g41870	0,635	0,009	0,332	0,012	8	0,476	0,005	-0,005	0,008	10	1,94E-11	2,93E-12	
At1g67590xAt1g67590	0,618	0,010	0,397	0,022	9	0,418	0,011	-0,015	0,010	11	1,28E-10	4,98E-13	
At3g57540xAt3g57540	0,609	0,006	0,303	0,012	8	0,459	0,005	-0,003	0,006	10	7,65E-13	5,32E-14	
At3g61260xAt3g61260	0,498	0,007	0,027	0,007	10	0,477	0,007	-0,017	0,004	11	3,66E-02	3,15E-05	

identical proteins

At4g36970xAt1g53860	0,737	0,024	0,698	0,032	12	0,282	0,016	0,012	0,007	12	1,52E-13	4,70E-16
At1g67590xAt2g02170	0,717	0,013	0,605	0,024	11	0,382	0,010	0,027	0,009	10	3,42E-14	5,11E-15
At4g36970xAt1g45207	0,633	0,029	0,435	0,054	11	0,412	0,015	0,030	0,008	11	1,33E-06	3,51E-07
At1g30320xAt2g02170	0,628	0,017	0,382	0,029	8	0,411	0,021	0,017	0,009	11	6,54E-07	1,37E-10
At1g67590xAt1g30320	0,572	0,025	0,487	0,036	13	0,238	0,014	-0,010	0,009	12	4,69E-11	6,11E-12
At2g41870xAt3g57540	0,569	0,007	0,217	0,014	10	0,465	0,005	-0,005	0,003	10	1,65E-10	1,21E-11
At1g53860xAt1g45207	0,513	0,012	0,222	0,014	15	0,408	0,012	-0,004	0,006	15	7,80E-07	7,68E-15
At1g67590xAt1g53860	0,492	0,013	0,217	0,016	10	0,385	0,011	-0,002	0,004	10	6,83E-06	8,75E-11
At1g53860xAt2g02170	0,446	0,008	0,251	0,010	12	0,302	0,009	-0,002	0,010	13	3,40E-11	9,97E-15
At2g02170xAt1g45207	0,434	0,009	0,286	0,009	11	0,275	0,009	0,001	0,005	11	5,84E-11	8,13E-18
At4g36970xAt3g57540	0,423	0,017	0,070	0,016	9	0,384	0,009	-0,007	0,004	21	3,70E-02	7,92E-07
At1g67590xAt3g57540	0,401	0,009	0,104	0,012	13	0,330	0,009	-0,004	0,008	9	3,44E-05	1,71E-06
At4g36970xAt1g30320	0,366	0,028	0,188	0,031	12	0,274	0,021	0,015	0,011	12	1,94E-02	5,43E-05
At1g53860xAt1g30320	0,298	0,010	0,139	0,016	10	0,238	0,014	-0,010	0,009	12	3,66E-03	3,36E-08

positive co-localization

Supplemental Table 1 online (continued)

Protein pair	sq. Manders		Pearson		n	sq. Manders		Pearson		n	sq. Manders		Pearson	
	R ²	std. err.	Rr	std. err.		rd R ²	rd std. err.	rd Rr	rd std. err.		ttest R ²	ttest Rr		
At2g02170xAt3g57540	0,424	0,009	-0,002	0,005	9	0,409	0,014	-0,007	0,007	9	4,00E-01	5,60E-01		
At1g45207xAt3g57540	0,417	0,009	0,039	0,006	19	0,396	0,008	-0,006	0,003	19	8,24E-02	3,84E-08		
At4g36970xAt2g02170	0,381	0,013	-0,002	0,010	10	0,366	0,011	-0,005	0,004	13	3,84E-01	7,88E-01		
At1g53860xAt2g41870	0,374	0,009	0,003	0,007	10	0,366	0,012	-0,005	0,006	12	5,87E-01	4,01E-01		
At1g67590xAt2g41870	0,361	0,019	0,087	0,010	13	0,312	0,022	-0,005	0,006	10	1,10E-01	4,88E-08		
At1g67590xAt1g45207	0,354	0,029	0,058	0,011	10	0,322	0,024	-0,011	0,003	10	3,90E-01	1,60E-05		
At2g41870xAt3g61260	0,353	0,007	-0,027	0,005	12	0,356	0,009	-0,018	0,007	12	8,37E-01	2,39E-01		
At1g45207xAt2g41870	0,353	0,010	0,045	0,021	12	0,333	0,010	0,012	0,008	12	3,33E-01	1,60E-01		
At1g45207xAt3g61260	0,318	0,011	-0,019	0,003	11	0,319	0,012	-0,020	0,004	11	9,54E-01	8,85E-01		
At2g41870xAt4g00670	0,239	0,021	-0,031	0,013	11	0,246	0,017	-0,007	0,005	11	7,88E-01	1,10E-01		
At1g30320xAt1g45207	0,133	0,008	0,050	0,007	18	0,116	0,009	0,002	0,005	17	1,53E-01	1,28E-06		
At1g30320xAt3g57540	0,132	0,005	0,014	0,007	12	0,122	0,005	-0,011	0,004	12	1,03E-01	5,25E-03		

random co-localization

At2g02170xAt2g41870	0,410	0,005	-0,042	0,009	10	0,436	0,006	-0,003	0,006	10	2,89E-03	2,79E-03
At1g53860xAt3g61260	0,373	0,011	-0,117	0,011	15	0,434	0,004	-0,005	0,006	14	2,52E-05	2,52E-09
At4g36970xAt3g61260	0,296	0,014	-0,128	0,026	11	0,353	0,006	0,010	0,008	12	9,82E-04	2,84E-05
At1g67590xAt4g36970	0,286	0,012	-0,009	0,012	13	0,385	0,011	-0,002	0,004	10	6,41E-06	6,29E-01
At1g67590xAt3g61260	0,208	0,013	-0,368	0,027	10	0,357	0,008	-0,019	0,009	11	5,12E-09	8,21E-11
At2g02170xAt3g61260	0,207	0,016	-0,432	0,047	15	0,383	0,012	-0,012	0,010	14	2,29E-09	4,98E-09
At4g00670xAt3g61260	0,193	0,014	-0,136	0,017	11	0,247	0,016	0,004	0,009	11	2,00E-02	4,04E-07
At1g30320xAt4g00670	0,191	0,023	-0,153	0,021	12	0,265	0,018	0,003	0,009	12	1,70E-02	6,06E-07
At1g30320xAt3g61260	0,153	0,006	-0,106	0,032	10	0,192	0,011	-0,017	0,010	10	5,61E-03	1,64E-02
At1g67590xAt4g00670	0,102	0,011	-0,291	0,019	13	0,217	0,015	0,004	0,008	13	1,60E-06	2,46E-13

exclusion

Supplemental Table 2 online.

List of primers used in this study.

cloning of overexpression constructs

gene ID	forward primer	reverse primer	vector
At3g61280	CACCATGCGGAGGAACAGAAGA	TTAGAAACATCCACAAGTTGCCTT	2
At2g45820	CACCATGCGGAGGAGCAAAAAGAC	TTAGAAACATCCACAAGTTGCCTT	2
At5g23750	GGGGACAAGTTTGTACAAAAAAGCAGGCTCCATGGCTGAAGAGGAACCG	GGGGACCACCTTTGTACAAAGAAAGCTGGGTTTTCATGCAATCCGAAAAGC	3
At1g69325	GGGGACAAGTTTGTACAAAAAAGCAGGCTCCATGAACGAAATCCACAGTGC	GGGGACCACCTTTGTACAAAGAAAGCTGGGTTTTCAGAGGCATGTAGAGGGTTTCC	3
At4g00670	GGCGGCCCTACCATGGAGCCAATATCCGATCC	CGTTTAAACC TTAGAAGCAGCTCAAAGATGA	1
At3g57540	GGCGGCCCTACCATGGACTTTGTACGGTCA	CGTTTAAACC TTAGAAGAAAGAGAAAGATGATC	1
At2g41870	GGCGGCCCTACCATGGCTGACTCTTTACCATCAAG	CGTTTAAACC TTAGGAGAAAGAGAAAGAGGAGC	1
At1g45207	GGCGGCCCTACCATGGCTCGGAGTCACTCGTAC	CGTTTAAACC TTAGAATACATGGCAGGTGAAGC	1
At2g02170	GGCGGCCCTACCATGGATTACGAACGAATCGG	GGCGGCCCTTAGAACAAGAAAGCTAAAGC	1
At1g30320	GGCGGCCCTACCATGGATTACGAGGAAATACAG	CGTTTAAACC TTAGAGAAACCAACCAACA	1
At1g53860	GGCGGCCCTACCATGGACTTCACAAGAAACAG	CGTTTAAACC TTAGACAAGTATATTGC	1
At4g36970	GGGGACAAGTTTGTACAAAAAAGCAGGCTCCATGAGAAAGACTTCTGTTTC	GGGGACCACCTTTGTACAAAGAAAGCTGGGTTTTCAGAGAGCAGAAAGAAATTTTC	3
At1g67590	CACCATGAGATCTAGTGTAGAAG	TATTGACACCAACAACGAG	2
At1g13920	GGGGACAAGTTTGTACAAAAAAGCAGGCTCCATGGATACCTTAATCAAGC	GGGGACCACCTTTGTACAAAGAAAGCTGGGTTTTCAGAAACAGCATGCATTTTC	3
At5g61280	GGGGACAAGTTTGTACAAAAAAGCAGGCTCCATGGATAAATTTGGTTAAGC	GGGGACCACCTTTGTACAAAGAAAGCTGGGTTTTCAGTAAACACCCGAAAGCAGAAA	3
KAT1	GGGGACAAGTTTGTACAAAAAAGCAGGCTTAATGTGATCTCTTGGACTCG	GGGGACCACCTTTGTACAAAGAAAGCTGGGTTTATTGATGAAAATACAAAATGATCACC	3
FLO11A	TTTGGTCTCTCACCATGTTCAAAAGTTGCAAGAGC	AAAGSTCTCACCCTGCTGCGAGTCACTTTC	4
FLO11B	TTTGGTCTCTCACCATGTTCAAAAGTTGCAAGAGC	AAAGSTCTCACCCTTCTGCTTAGAGTACCGATCC	4
SYMREM1	AGCGCGCCCTACCATGGAAGAATCGAAAACAAC	AGCGCGCCCTACTGAAAACCTTAAACC	1

cloning of Pro:YFP:ORF constructs

ProAt3g61260	TTTGGTCTCTCACCCTGGCCGTCGTTG	AAAGTCTCTTGTACAGTCGCCCTCTCAGCC	4
At3g61260	TTTGGTCTCGAATATGGCGGAGGAACAG	AAAGTCTCACCCTTTAGAAACATCCACAAGTTGC	4
ProAt2g45820	TTTGGTCTCTCACCCTGATTCCTATGCTCAAATC	AAAGTCTCTTGTCTGTCTCTCAGCCGAAAGAAAG	4
At2g45820	TTTGGTCTCAGAATATGGCGGAGGAGCAAAAAG	AAAGTCTCACCCTTTAGAAACATCCACAAGTTGC	4
ProAt4g36970	TTTGGTCTCTCACCCTGCGTTCGATCGTTCGTA	AAAGTCTCTTGTCTGTGTTGTTTCTCAAAGAAACAAAATC	4
At4g36970	TTTGGTCTCAGAATATGAGAAAGACTTCTGTTTC	AAAGTCTCACC TTAGAGAGCAGAAAGAAATTTTC	4
free YFP	TTTGGTCTCTGACAATGGTGAAGCAAGGGCGAGG	AAAGTCTCTATTCTTGTACAGCTCGTCCATGC	4

qPCR primers

At4g36970	GAACATGAACAACAAGGG	CGAGGAGCAAGCAAGTCTATG
-----------	--------------------	-----------------------

legend

- 1= for cloning into pksi
 - 2= for cloning into pENTR-D
 - 3= for cloning into pDONR207
 - 4= for cloning into pENTR-D Bsal
- START and STOP codons are depicted in red; Pro=promoter

Plasma Membranes Are Subcompartmentalized into a Plethora of Coexisting and Diverse Microdomains in *Arabidopsis* and *Nicotiana benthamiana*

Iris K. Jarsch, Sebastian S.A. Konrad, Thomas F. Stratil, Susan L. Urbanus, Witold Szymanski, Pascal Braun, Karl-Heinz Braun and Thomas Ott

Plant Cell 2014;26;1698-1711; originally published online April 8, 2014;
DOI 10.1105/tpc.114.124446

This information is current as of June 16, 2015

Supplemental Data	http://www.plantcell.org/content/suppl/2014/04/02/tpc.114.124446.DC1.html
References	This article cites 54 articles, 27 of which can be accessed free at: http://www.plantcell.org/content/26/4/1698.full.html#ref-list-1
Permissions	https://www.copyright.com/ccc/openurl.do?sid=pd_hw1532298X&iissn=1532298X&WT.mc_id=pd_hw1532298X
eTOCs	Sign up for eTOCs at: http://www.plantcell.org/cgi/alerts/ctmain
CiteTrack Alerts	Sign up for CiteTrack Alerts at: http://www.plantcell.org/cgi/alerts/ctmain
Subscription Information	Subscription Information for <i>The Plant Cell</i> and <i>Plant Physiology</i> is available at: http://www.aspb.org/publications/subscriptions.cfm

3.3 Publication II: S-Acylation anchors remorin proteins to the plasma membrane but does not primarily determine their localization in membrane microdomains

Sebastian S. A. Konrad*, Claudia Popp*, Thomas F. Stratil, Iris K. Jarsch, Veronika Thallmair, Jessica Folgmann, Macarena Marín and Thomas Ott

New Phytologist **203**, 758-769 (2014)

DOI: 10.1111/nph.12867

*These authors contributed equally to the work.

Ludwig-Maximilians-University (LMU) Munich, Institute of Genetics, 82152 Martinsried, Germany

Author contributions (Sebastian S.A. Konrad):

I predominantly contributed to the design of the study, as well as the analysis of data. Furthermore I was involved writing the manuscript. The following experiments were conducted by me:

- Cloning and mutagenesis of all *Arabidopsis thaliana* RemCA constructs and mutation variants thereof (Figure 4; Figure 5; Supplementary Figure S2; Supplementary Figure S4).
- Cloning of the C197A mutation of SYMREM1 and SYMREM1 RemCA (Figure 4).
- *In silico* S-acylation site prediction of *A. thaliana* Remorins (Table 1).
- Microscopical and biochemical RemCA-mediated PM binding analysis in *N. benthamiana* (Figure 4; Supplementary Figure S2).
- Co-localization studies for At4g36970, At4g36970 RemCA and At3g61260 (Supplementary Figure S4).
- Localization studies of SYMREM1, At4g36970, At4g36970 RemCA, At3g12360 and mutation variants of these in *N. benthamiana* (Figure 4).
- Establishment of the biotin switch protocol and experimental application of it on all Remorin and RemCA constructs presented in the study (Figure 5; Supplementary Figure S5).
- Cloning and expression of SYMREM1, SYMREM1⁷⁴⁻²⁰⁵, SYMREM1^{C197A} and SYMREM1 RemCA in *Saccharomyces cerevisiae* (Figure 6).
- Localization studies as well as microsomal fractionations of SYMREM1, SYMREM1⁷⁴⁻²⁰⁵, SYMREM1^{C197A} and SYMREM1 RemCA in *S. cerevisiae* (Figure 6; Supplementary Figure S6).

I hereby confirm the above mentioned statements:

.....

Prof. Dr. Thomas Ott

.....

Sebastian S. A. Konrad

Author contributions (Claudia Popp):

I initiated this project and contributed to conception of the study, as well as the analysis of data. Furthermore I was involved writing the manuscript. The following experiments were conducted by me:

- Cloning of SYMREM1 and SYMREM1 RemCA constructs as well as deletion constructs of SYMREM1 (Figure 1; Figure 2; Figure 6).
- Expression and localization studies of SYMREM1, SYMREM1 RemCA, SYMREM1¹⁻⁷³, SYMREM1¹⁷⁴⁻²⁰⁵, SYMREM1¹⁻¹⁷⁰, SYMREM1¹⁻¹⁹⁰ and SYMREM1¹⁷¹⁻²⁰⁵ in *Medicago truncatula* (Figure 2; Figure 6).
- Western Blots and microsomal fractionations of SYMREM1 and SYMREM1^{C197A} indicating band shift (Supplementary Figure S3).
- Cell viability experiments (Figure 1 d and e)

I hereby confirm the above mentioned statements:

.....

Prof. Dr. Thomas Ott

.....

Claudia Popp



S-acylation anchors remorin proteins to the plasma membrane but does not primarily determine their localization in membrane microdomains

Sebastian S. A. Konrad*, Claudia Popp*, Thomas F. Stratil, Iris K. Jarsch, Veronika Thallmair, Jessica Folgmann, Macarena Marín and Thomas Ott

Ludwig-Maximilians-University (LMU) Munich, Institute of Genetics, 82152 Martinsried, Germany

Author for correspondence:

Thomas Ott

Tel: +49 (0)89 2180 74704

Email: Thomas.Ott@biologie.

uni-muenchen.de

Received: 7 March 2014

Accepted: 22 April 2014

New Phytologist (2014) **203**: 758–769

doi: 10.1111/nph.12867

Key words: membrane domain, palmitoylation, protein–protein interaction, remorin, S-acylation.

Summary

- Remorins are well-established marker proteins for plasma membrane microdomains. They specifically localize to the inner membrane leaflet despite an overall hydrophilic amino acid composition. Here, we determined amino acids and post-translational lipidations that are required for membrane association of remorin proteins.
- We used a combination of cell biological and biochemical approaches to localize remorin proteins and truncated variants of those in living cells and determined S-acylation on defined residues in these proteins.
- S-acylation of cysteine residues in a C-terminal hydrophobic core contributes to membrane association of most remorin proteins. While S-acylation patterns differ between members of this multi-gene family, initial membrane association is mediated by protein–protein or protein–lipid interactions. However, S-acylation is not a key determinant for the localization of remorins in membrane microdomains.
- Although remorins bind via a conserved mechanism to the plasma membrane, other membrane-resident proteins may be involved in the recruitment of remorins into membrane domains. S-acylation probably occurs after an initial targeting of the proteins to the plasma membrane and locks remorins in this compartment. As S-acylation is a reversible post-translational modification, stimulus-dependent intracellular trafficking of these proteins can be envisioned.

Introduction

It has now been widely accepted that plasma membranes (PM) are functionally compartmentalized. These structures, called membrane micro-domains, are defined by a dynamic crosstalk between different lipids, membrane-resident proteins and probably the cortical cytoskeleton that results in the assembly of membrane subcompartments in the micrometer range (reviewed in Lingwood & Simons, 2010; Li *et al.*, 2013; Malinsky *et al.*, 2013). While live cell imaging of lipids revealed a heterogeneous distribution in cells and tissues (Vermeer *et al.*, 2009; Horn *et al.*, 2012), most work done in plants so far has focused on the roles of sterols. Such sterol-enriched sites can harbour a large number of signalling proteins and are important during plant-microbe interactions (reviewed in Zappel & Panstruga, 2008; Jarsch & Ott, 2011; Urbanus & Ott, 2012). Focal accumulation of membrane domain proteins during host cell infection indicates the existence of active cellular processes that specifically direct

signalling complexes to infection sites (Bhat *et al.*, 2005; Haney & Long, 2010; Lefebvre *et al.*, 2010; Underwood & Somerville, 2013). Increasing evidence suggests that a large number of PM-resident proteins do not freely diffuse inside the PM bilayer as single molecules but are preassembled into distinct subdomains (Kusumi *et al.*, 2012). However, not much is known about the mechanisms that target individual proteins to membrane domains in plant cells. Transmembrane proteins might not only assemble specific lipids in their vicinity and thereby directly contribute to the assembly of specific lipid shells, but also interact with other membrane-resident proteins and the actin cytoskeleton. Such interactions, among others, support the formation of larger domain clusters (Lingwood & Simons, 2010; van den Bogaart *et al.*, 2011). For extracellular proteins, the addition of glycosylphosphatidylinositol (GPI) moieties has been shown to contribute to their specific association with the apoplastic face of sterol-enriched membrane domains (Varma & Mayor, 1998). Accordingly, proteins carrying GPI-anchors are overrepresented in sterol-enriched detergent-resistant membranes (DRMs), indicating that addition of this lipid moiety directs

*These authors contributed equally to the work.

extracellular proteins into these fractions (Kierszniowska *et al.*, 2009). In plants, only few proteins have been identified that associate with membrane domains at the cytosolic face of the PM, among them flotillins and remorins (Raffaele *et al.*, 2009; Haney & Long, 2010; Li *et al.*, 2012; Jarsch *et al.*, 2014). Flotillins evolved in multicellular eukaryotes and form a small gene family with three members in *Arabidopsis thaliana*. They bind the inner leaflet via lipid modifications, called myristoylation and S-acylation (Neumann-Giesen *et al.*, 2004). Myristoylation is an irreversible modification of an N-terminal glycine residue while S-acylation (formerly called palmitoylation) of cysteine residues can occur throughout the entire protein (Blaskovic *et al.*, 2013). Importantly, S-acylation contributes not only to membrane association of proteins but also to the regulation of protein–protein interactions (Blaskovic *et al.*, 2013). The acylation reaction itself is either catalysed by membrane-resident protein acyl-transferases (PATs) or, rarely, occurs spontaneously (Bharadwaj & Bizzozero, 1995). In contrast to other lipid modifications that mediate PM association, S-acylation is reversible. This feature allows dynamic regulation of protein complexes. As such regulatory modes are required during signal transduction, it appears a natural consequence that a number of plant signalling proteins, such as small GTPases (Sorek *et al.*, 2007), calcium-dependent kinases (Martin & Busconi, 2000) and heteromeric G-proteins (Adjobo-Hermans *et al.*, 2006; Hemsley *et al.*, 2008), have been shown to be S-acylated. More globally, a recent proteomic study in *A. thaliana* reported the presence of 581 S-acylated proteins, among them two plant-specific remorins (Hemsley *et al.*, 2013). Remorins form a multigene family with 16 members in *A. thaliana* (Raffaele *et al.*, 2007). Plants that undergo root nodule symbiosis have evolved an additional subgroup that also comprises the SYMBIOTIC REMORIN 1 (SYMREM1) (Lefebvre *et al.*, 2010; Tóth *et al.*, 2012). The SYMREM1 protein interacts with symbiosis related receptor-like kinases and localizes in membrane microdomains along nodular infection threads (Lefebvre *et al.*, 2010; Tóth *et al.*, 2012). Knockout mutants in *Medicago truncatula* revealed that the protein controls rhizobial infections as these mutants developed more prematurely aborted nodules compared with wildtype plants (Lefebvre *et al.*, 2010; Tóth *et al.*, 2012). Remorins consist of a conserved C-terminal region that contains a canonical remorin signature. By contrast, their phosphorylated and intrinsically disordered N-terminal regions are highly variable in sequence composition and length and may serve regulatory functions during protein–protein interactions (Marín & Ott, 2012; Marín *et al.*, 2012; Tóth *et al.*, 2012). Remorins localize to distinct membrane domains at the cytosolic leaflet of the PM (Raffaele *et al.*, 2009; Lefebvre *et al.*, 2010; Perraki *et al.*, 2012; Demir *et al.*, 2013; Jarsch *et al.*, 2014) and serve as established marker proteins for PMs and membrane microdomains. Structurally these proteins lack a transmembrane domain and exhibit an overall hydrophilic amino acid profile (Reymond *et al.*, 1996; Raffaele *et al.*, 2009). Although they have been numerous found at the PM, their mode of association has not been fully understood. A recent study proposed that the potato remorin StREM1.3 physically inserts into the PM through a tight hairpin structure comprising amphipathic α -helices and that a

corresponding ‘remorin C-terminal anchor’ (RemCA) is required and sufficient for membrane binding of this remorin (Perraki *et al.*, 2012). Considering the fact that the homologous protein from *A. thaliana* is S-acylated (Hemsley *et al.*, 2013), the mode of membrane binding and localization to membrane microdomains remains to be fully elucidated.

In this study, we have finally unravelled the molecular mechanism that targets these membrane domain marker proteins to the PM and analysed the structural requirements for their specific localization.

Materials and Methods

Molecular cloning and sequence analyses

Remorin constructs were cloned from cDNA templates by Golden Gate cloning or standard Gateway (GW) technology using self-assembled level I and II plasmids or the pDONR207 entry vector, respectively (Binder *et al.*, 2014). In *Nicotiana benthamiana* Domin, all remorins were expressed using the pAM-PAT-YFP-GW vector. For expression in *Medicago truncatula* Gaertn. roots, the modified destination vector pUBi-YFP-GW-HYG was used, where the standard recombination site was replaced with an YFP-GW cassette via the sites KpnI and XbaI. Point mutations were introduced into the respective entry clones via inverted PCR.

Plant transformation and fluorescence microscopy

For analysis of SYMREM1, *M. truncatula* (ecotype A17) roots were transiently transformed as described previously (Boisson-Dernier *et al.*, 2001) with slight modifications. Plants were then grown on Fahraeus medium for 3 wk before imaging of the samples. For methyl- β -cyclodextrin (mbCD) treatments, roots expressing a genomic SYMREM1 construct with N-terminally fused yellow fluorescent protein (YFP) were incubated in 30 mM mbCD on the microscope slide and images were taken consecutively directly during immersion in the drug. Control experiments were performed in water. Images were taken 3 wk after transformation.

For heterologous expression, constructs were transformed into *Agrobacterium tumefaciens* strains GV3101 and AGL1. Transformation of *N. benthamiana* leaves was performed as previously described (Tóth *et al.*, 2012). All transformations were repeated at least three times independently. It should be noted that, in the case of *N. benthamiana* transformations, all cells represent independent transformation events.

Confocal laser scanning microscopy was performed using a Leica TCS SP5 confocal microscope equipped with $\times 63$ and $\times 20$ HCX PL APO water immersion lenses (Leica Microsystems, Mannheim, Germany). The YFP fluorophores were excited with the 514 nm argon laser line and emission was detected at 525–600 nm. FM4-64 fluorescence was excited using the argon laser line at 476 nm and emission was detected between 690 and 750 nm. In all cases, maximum projections of z-stacks are shown.

In silico analysis of SYMREM1

Ab initio modelling of SYMREM1 was performed using the I-TASSER server (Zhang, 2008; Roy *et al.*, 2010). Models for the N- and C-terminal regions were constructed independently and subsequently fused. Predictions of putative regions involved in protein interactions were performed using the PPI-Pred server (http://bioinformatics.leeds.ac.uk/ppi_pred/index.html) (Bradford & Westhead, 2005). Molecular graphics were produced using the UCSF Chimera package (<http://www.cgl.ucsf.edu/chimera>) (Pettersen *et al.*, 2004).

The hydrophobicity plot was generated on the basis of the SYMREM1 amino acid sequence (GenBank accession AEX20500) using the ExPASy Webserver (<http://web.expasy.org/cgi-bin/prot-scale/protscale.pl>).

Microsomal fractionation

Microsomal fractions were prepared by the addition of extraction buffer (230 mM sorbitol, 50 mM Tris/HCl (pH 7.5), 10 mM KCl, 3 mM ethylene glycol tetraacetic acid and protease inhibitors) to ground tissue of the microscopically examined material. Samples were spun at 20 000 *g* for 40 min before the extract was passed through two layers of Miracloth. The obtained supernatant was then spun down at 100 000 *g* for 1 h. The resulting pellets containing the microsomal fractions were resuspended in Tris-buffered saline (TBS) and used for western blot analysis. The supernatant contained all cytosolic proteins.

Biotin switch assays

Two *N. benthamiana* plants were independently infiltrated per construct, with *A. tumefaciens* carrying the respective plasmids. Before protein extraction, expression of the constructs was microscopically confirmed, using a Leica DMI 6000 epifluorescence microscope. Three fluorescent leaves per plant were harvested and samples were pooled for further processing. The biotin switch assay itself was conducted as described previously (Hemslley *et al.*, 2008). In brief, all free sulphhydryls were blocked by incubation in N-ethylmaleimide. Hydroxylamine-induced cleavage of the acylthioester bond resulted in removal of the fatty acid moiety and the generation of free sulphhydryls that were labelled using a sulphhydryl-reactive biotin, forming a biotinylated cysteine. S-acylated proteins were then purified using neutravidin-coupled agarose beads. Methanol/chloroform precipitations were carried out as described earlier (Wessel & Flugge, 1984). This experiment was repeated two to three times independently and always yielded the same result.

Quantification of bands on the Western blot was performed using ImageJ. Mean intensity values were obtained after subtraction of the background.

Western blot analysis

After sodium dodecyl sulfate–polyacrylamide gel electrophoresis (SDS-PAGE), proteins were transferred overnight at 4°C to

polyvinylidene fluoride membranes. Membranes were blocked in TBS containing 0.1% Tween 20 (TBS-T) and 5% milk for 10 h at 4°C. All constructs were detected using a polyclonal α -GFP antibody (Rockland Immunochemicals, Gilbertsville, PA, USA) at a 1 : 5000 dilution in TBS-T 5% milk overnight at 4°C. The membrane was washed three times with TBS-T before incubation with a horseradish peroxidase-conjugated α -rabbit antibody (GE Healthcare, Munich, Germany) at a 1 : 20 000 dilution in TBS-T 5% milk for 1 h at room temperature. Detection of chemiluminescence was carried out according to the ECL reagent manufacturer's instructions (Pierce; Thermo Fischer, Bonn, Germany).

Expression of SYMREM1 constructs in yeast

SYMREM1, SYMREM1^{C197A}, RemCA and truncated variants were cloned into the yeast expression vector pAG424GAL-EYFP-ccdB (Addgene, Cambridge, MA, USA) via Gateway technology. Yeast transformation in the NMY32 strain was performed as described earlier (Tóth *et al.*, 2012). Transformants were selected on synthetic dropout (SD) medium supplemented with 2% galactose to induce transgene expression. For microscopy, yeast cells were immobilized on glass slides with a 5% low melt agarose film.

For protein extractions, pellets from 12 ml cultures were washed with 1 mM ethylenediaminetetraacetic acid before disruption by glass beads in 50 mM Tris-HCl supplemented with protease inhibitors. Microsomal and cytosolic fractions were obtained by differential centrifugation as described earlier and subjected to western blot analysis.

Results

Sterol-dependent localization of SYMREM1 in membrane microdomains

In a first experiment, we assessed PM localization of SYMREM1 in detail. When ectopically expressing a SYMREM1 fusion protein in transgenic *M. truncatula* roots, we observed the expected labelling of PM microdomains (Fig. 1a). Interestingly, most observed membrane domains were immobile over the 30 min observation period (Fig. 1b, arrowheads). This is in agreement with previous localization studies of native SYMREM1 in root nodules (Lefebvre *et al.*, 2010) and other remorins (Raffaele *et al.*, 2009; Demir *et al.*, 2013; Jarsch *et al.*, 2014). Because formation of membrane domains has often been associated with the enrichment of sterols, we tested sterol-dependency of SYMREM1-labelled microdomains in living cells. For this, transgenic roots were incubated in the presence of 30 mM mbCD, a cyclic oligosaccharide that interacts with hydrophobic molecules, including sterols, and depletes them from membranes (Roche *et al.*, 2008). Indeed, most microdomains dissolved within the first 10 min upon mbCD application, indicating sterol-dependency of these membrane domains (Fig. 1c). Cell viability during mbCD treatment was confirmed by the persistent presence of cytoplasmic streaming in living root hair cells incubated in water (Fig. 1d) and 30 min after mbCD application (Fig. 1e).

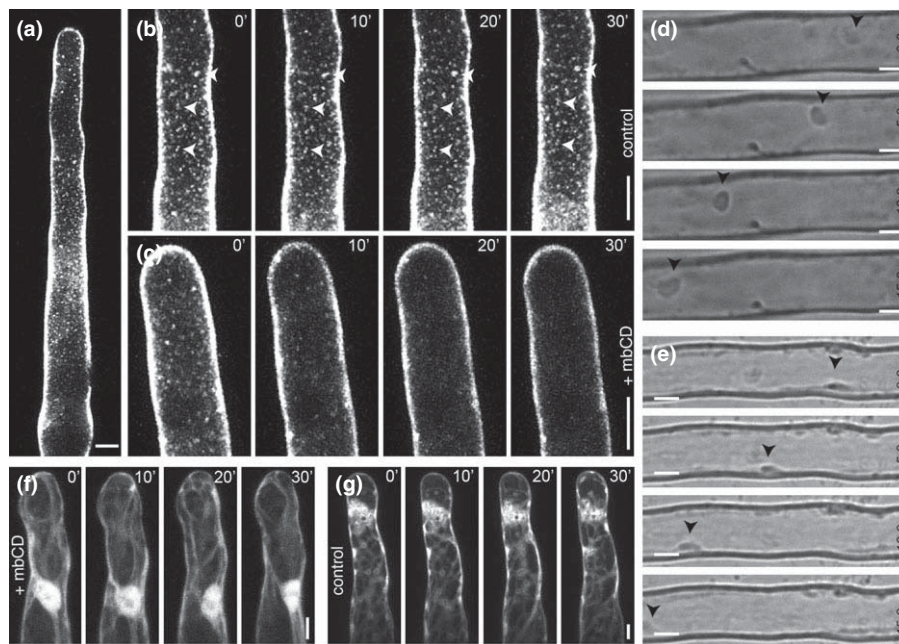


Fig. 1 SYMREM1 labels sterol-dependent membrane domains *in vivo*. (a) Image of a mature transgenic root hair from *Medicago truncatula* ectopically expressing a YFP-SYMREM1 fusion protein. (b) Membrane domain patterns did not change during imaging. Images were taken in 10 min intervals. Arrowheads mark laterally immobile membrane domains. (c) Application of 30 mM methyl- β -cyclodextrin (mbCD)-depleted membrane domains. Images were taken at 10 min intervals. (d, e) Cytoplasmic streaming was observed in 5 s intervals before (d) and after (e) incubation of roots in 30 mM mbCD for 30 min. Arrowheads point towards mobile cytosolic particles that allowed detection of cytoplasmic streaming. (f, g) Transgenic root hairs expressing free yellow fluorescent protein (YFP). No changes in fluorescence were observed when roots were treated with 30 mM mbCD for 30 min (f) or water as a control (g), indicating that the treatment did not affect the fluorophore alone. All images are z-projections. Bars: (a–c, f, g) 10 μ m; (d, e) 5 μ m.

Furthermore, we could exclude the possibility that the mbCD treatment affected the fluorophore itself, as application of the drug did not result in any difference from water-treated controls when we expressed free YFP protein in transgenic roots (Fig. 1f, g). These experiments demonstrate that SYMREM1 localizes to membrane domains in a sterol-dependent manner *in vivo*.

Identification of the membrane-binding site

As other remorins, the SYMREM1 protein shows an overall hydrophilic pattern (Fig. 2a). However, the C-terminal 35 residues may form a hydrophobic core out of which 19 residues are predicted to be intrinsically disordered and thus do not contain any secondary structure in solution. Using the PPI-Pred server, we found that 25 of these terminal residues are predicted to be involved in protein–protein interactions (indicated in red; Supporting Information, Fig. S1a). As hydrophobic sites are required for both direct membrane binding and protein–protein interactions, we generated a series of truncation variants of SYMREM1 N-terminally fused to a YFP fluorophore (YFP-SYMREM1), to investigate the role of its different protein regions in membrane binding. These constructs were expressed in transgenic *M. truncatula* roots, and secant (median) planes of root epidermal cells were analysed by confocal laser scanning microscopy. The results are shown in Fig. 2 as maximum intensity projections of z-stack images. As expected, the full-length protein entirely resided in the PM (Fig. 2b). The N-terminal region of SYMREM1 (residues 1–73; Fig. 2c) showed the same cytoplasmic localization pattern as the sole YFP fluorophore (Fig. S1b). By

contrast, the C-terminal region (residues 74–205) remained fully associated with the PM (Fig. 2d). Expression of C-terminally truncated proteins, where deletions were introduced in front of the predicted helical structure at position Cys171 (residues 1–170) or between the predicted intrinsically disordered C-terminal residues (residues 1–190), resulted in a predominantly cytosolic SYMREM1 protein (Fig. 2e,f). These results indicate that residues within the C-terminal region mediate PM localization. This was confirmed in a reciprocal experiment where a YFP fluorophore was found to be entirely associated with the PM when being fused to these 35 residues (SYMREM1^{171–205}) (Fig. 2g). In all cases, localization and integrity of the fusion proteins were biochemically confirmed by Western blot analyses after microsomal fractionation (Fig. 2, panels below images). Faint signals were still observed in the microsomal fractions of the truncated variants SYMREM1^{1–170} and SYMREM1^{1–190} (Fig. 2e,f), indicating that a proportion of the protein resided in the PM independently of the C-terminal 35 amino acid residues. In general, these data are in agreement with a recently published report, where the corresponding region in the remorin StREM1.3 from potato (RemCA) was shown to be required for membrane binding of this protein (Perraki *et al.*, 2012). For consistency we therefore used the term ‘RemCA’ throughout our study.

The presence of few C-terminal residues is indispensable for membrane localization of remorin proteins

Next we asked whether the C-terminal hydrophobic core is generally required for PM association of remorin proteins. To

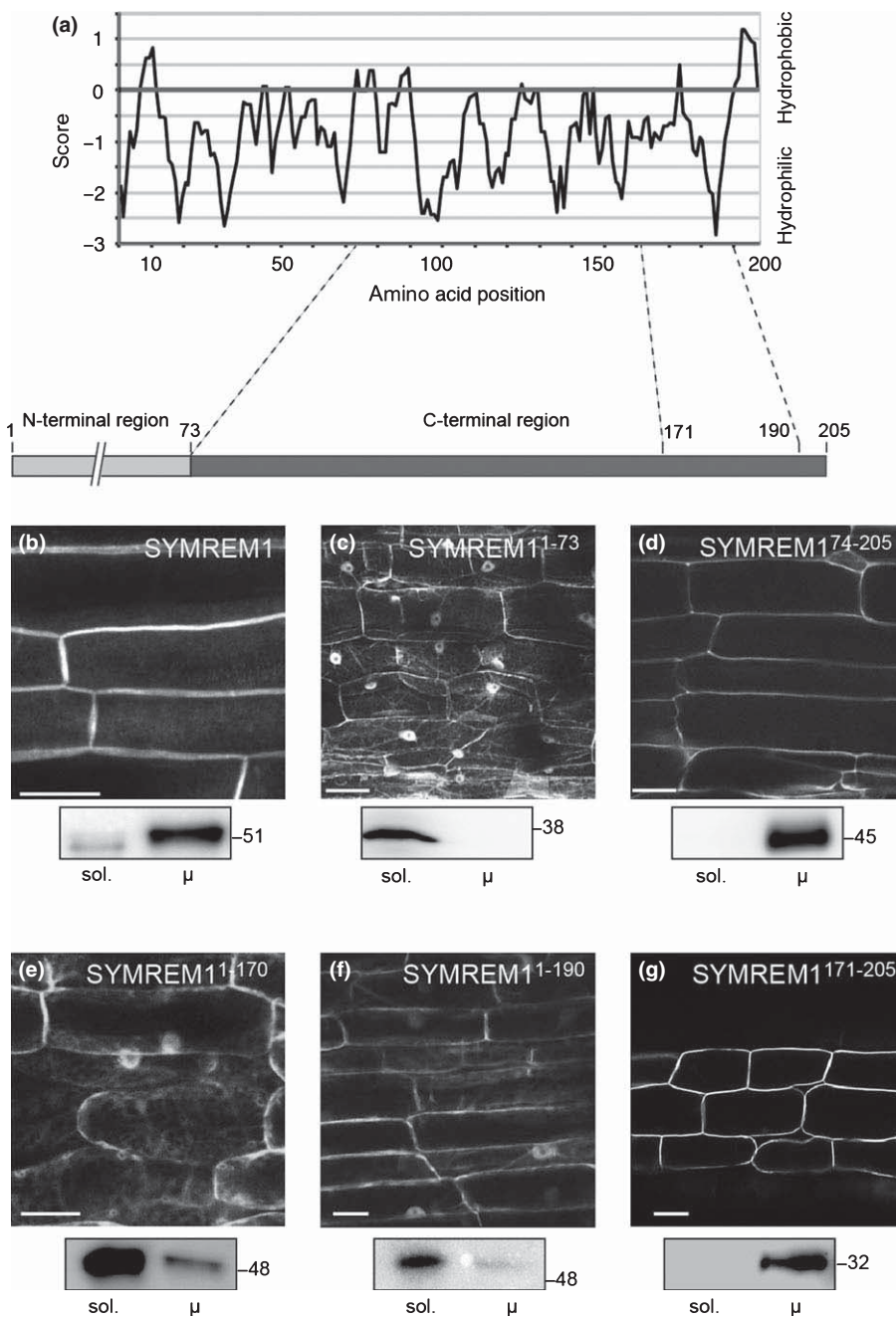


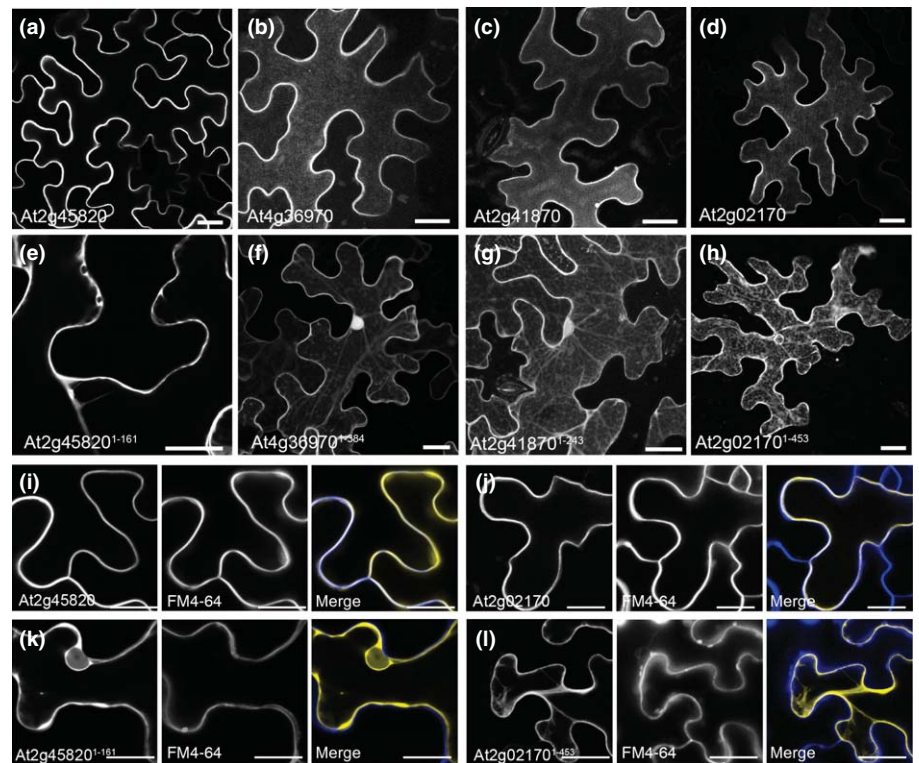
Fig. 2 The C-terminal residues mediate membrane anchoring of SYMREM1. (a) Hydrophobicity plot of SYMREM1. (b–g) Confocal images of transgenic *Medicago truncatula* roots expressing different full-length SYMREM1 (b) or truncated protein variants (c–g). The yellow fluorescent protein (YFP) fluorophore was always fused to the N-terminus of SYMREM1 protein variants. All images are z-projections of secant planes without the plasma membrane (PM) surface. Bars, 20 μ m. Western blot analysis shows the presence of intact fusion proteins (panels below images). sol., soluble protein fraction; μ , microsomal protein fraction.

investigate this, we cloned and expressed the coding regions of the closely related remorin At2g45820 (190 residues) and the three distantly related remorins, At2g41870 (274 residues), At4g36970 (427 residues) and At2g02170 (486 residues), from *A. thaliana*. As expected, all full-length proteins localized to the PM when being expressed in *N. benthamiana* leaf epidermal cells (Fig. 3a–d). Next, we truncated these proteins in front of the predicted terminal helix, as was done for SYMREM1. In analogy, expression of these truncated variants (At2g45820^{1–161}, At2g41870^{1–243}, At4g36970^{1–384}, At2g02170^{1–453}) resulted in an entire loss of PM binding of all proteins *in planta* (Fig. 3e–h). These data were verified for the shortest and the longest remorins by labelling PMs with the dye FM4-64. While full-length

At2g45820 and At2g02170 colocalized perfectly with FM4-64 (Fig. 3i,j), the truncated versions showed clear cytoplasmic localizations (Fig. 3k,l).

To reciprocally test if these regions were always sufficient to anchor YFP to the PM as shown for SYMREM1 (Fig. 2g), the C-terminal 35 amino acids (RemCAs) of all 16 *A. thaliana* remorins were fused to this fluorophore and expressed in *N. benthamiana* leaf epidermal cells. Surprisingly, only four of these RemCA peptides (At4g36970, At2g02170, At1g30320, At5g61280) were sufficient to fully anchor the YFP protein to the PM (Fig. S2a–d, Table 1). In all other cases, strong cytoplasmic localizations of the fusion proteins were observed (Fig. S2e–p). To test whether this cytosolic localization may (partially) derive

Fig. 3 The C-terminal residues determine membrane association throughout the remorin family. (a–h) All tested full-length proteins localized to the plasma membrane (PM) (a–d), while all mutant variants that were truncated by the respective remorin C-terminal anchor (RemCA) peptide were predominantly found in the cytosol when being expressed in *Nicotiana benthamiana* leaf epidermal cells (e–h). (i, j) PM counterstaining with the styryl dye FM4-64 showed colocalization with full-length At2g45820 and At2g02170. (k, l) No colocalization was observed between FM4-64 and the truncated variants At2g45820^{1–161} (k) and At2g02170^{1–453} (l). Yellow fluorescent protein (YFP) fluorescence is shown in yellow, and the FM4-64 stain is represented in blue. Bars, 20 μ m.



from fluorophore cleavage, proteins were extracted and compared with free YFP by Western blot analysis (Fig. S2q). Indeed, partial cleavage was detected for At1g69325, At4g00670, At3g57540, At2g41870, At1g45207, At4g36970 and At1g13290. Those proteins were therefore further subjected to microsomal fractionations to determine the degree of cytosolic and membrane localization. In all cases, the intact fusion protein localized predominantly to the cytosolic fraction (Fig. S2r). This implies that these RemCA peptides were not sufficient for strong immobilization of the fluorophore at the PM.

As all remorins contain a hydrophobic stretch at the C-terminus (Table 1), we excluded the possibility that the chemical properties of these residues alone are the sole determinants for PM localization of the proteins.

C-terminal cysteine residues contribute to PM localization of remorins

As stated earlier, post-translational lipid modifications often confer PM binding of proteins. Following a recent global approach in *A. thaliana*, where two remorins were found to be S-acylated (Hemsley *et al.*, 2013), we used the CSS-PALM 3.0 algorithm (<http://csspalm.biocuckoo.org/>) to predict putative S-acylation sites in all *A. thaliana* remorin proteins and SYMREM1. Except for At3G48940, At3G57540 and At2G41870, all remorins were found to harbour at least one C-terminal cysteine residue that may serve as putative sites of S-acylation (Table 1).

To test whether S-acylation is a key determinant for membrane association of RemCA peptides, we chose SYMREM1 and At4g36970, which have one and two predicted S-acylated

cysteines in their RemCA sequences, respectively. High-resolution imaging (*c.* $\times 10$ higher magnification than used here) recently revealed labelling of membrane microdomains by the full-length variants of these proteins (Jarsch *et al.*, 2014). The RemCA peptides of both remorins were sufficient to fully associate a fluorophore to the PM when expressed in *N. benthamiana* (Figs 4c, S2a). At3g61260 was used as a control. This *A. thaliana* remorin is the homolog of the well-studied StREM1.3 protein (Perraki *et al.*, 2012) and was found to be S-acylated (Hemsley *et al.*, 2013). It should be noted that the RemCA peptides of neither At3g61260 nor its closely related proteins At3g48940, At2g45820 and At5g23750 were sufficient to anchor soluble YFP to the PM (Table 1; Fig. S2).

To test the impact of point mutations at the predicted cysteine residues, we expressed a number of mutant variants in *N. benthamiana*. Introduction of a cysteine to alanine mutation at the predicted S-acylation site Cys197 in SYMREM1 did not lead to a significant decrease of PM localization of the full-length protein (Fig. 4b). Western blot analysis on microsomal fractions of protein extracts from *N. benthamiana* plants expressing wildtype SYMREM1 and mutated SYMREM1^{C197A} confirmed predominant PM association of both proteins (Fig. S3a). Interestingly, a small but reproducible band shift was observed in the SYMREM1^{C197A} mutant, indicating a possible modification on this residue (Fig. S3b). In contrast to the full-length protein, introduction of the same point mutation into the isolated membrane-binding domain of SYMREM1 (RemCA, SYMREM1^{171–205}) resulted in an entire loss of PM association of the fusion protein and labelling of mobile structures in the cytoplasm (Fig. 4d), while the wildtype peptide resided at the PM (Fig. 4c). These

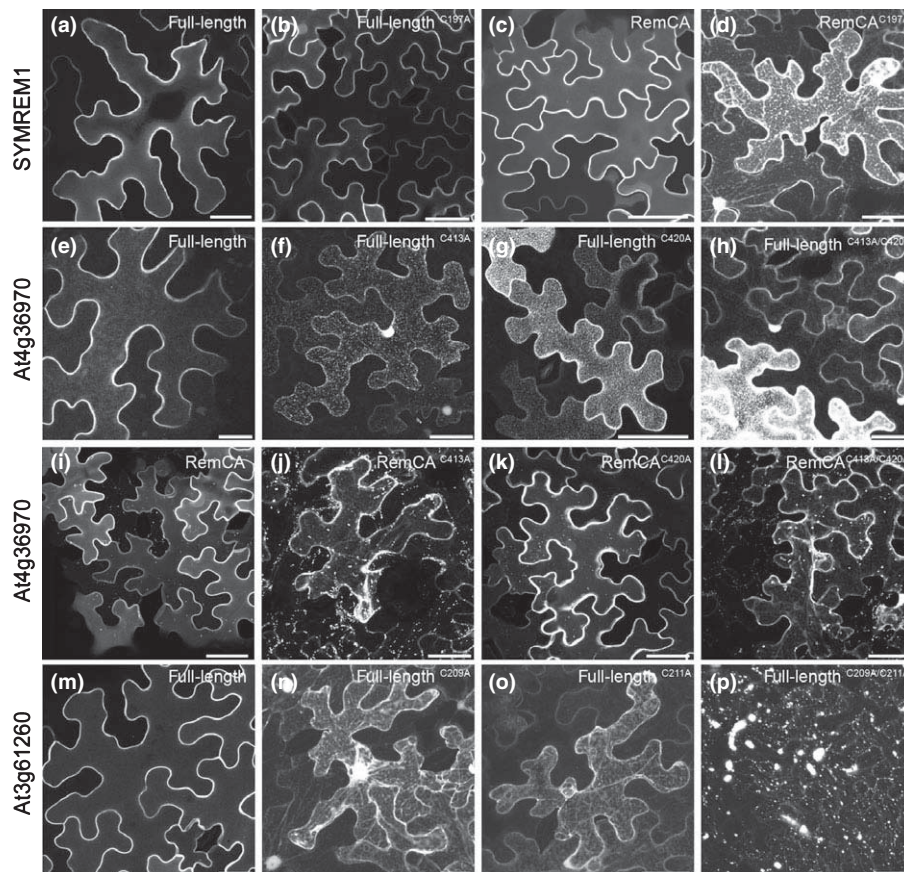


Fig. 4 Mutations in C-terminal cysteine residues alter localization patterns of remorin proteins when being expressed in *Nicotiana benthamiana* leaf epidermal cells. (a, b) Full-length SYMREM1 and the mutant variant SYMREM1^{C197A} remained plasma membrane (PM)-localized. (c, d) PM association of the remorin C-terminal anchor (RemCA) peptide of SYMREM1 is dependent on Cys197. Introduction of a C197A mutation in this residue resulted in an entire loss of membrane binding (d). (e–h) Mutations in the two predicted C-terminal S-acylation sites, Cys413 (f) and Cys420, of At4g36970 resulted in altered membrane domain patterning and partial cytosolic/nuclear localization of the C413A mutant (f). (h) The At4g36970 double cysteine mutant resembled both single mutations. (i) The yellow fluorescent protein (YFP)-RemCA peptide of At4g36970 is targeted to the PM and some mobile vesicles. PM localization is altered in the C413A (j) but not in the C420A (k) mutant of the At4g36970 RemCA peptide. (l) The At4g36970 RemCA double cysteine mutant resembled the C413A mutation. (m–p) Both C-terminal cysteines of At3g61260 are required for PM association of the protein. (p) The respective double mutant strongly aggregated in the cytoplasm. All images are z-projections. Bars, 50 μm.

(Fig. 4k), a mutation in Cys413 led to cytosolic and nuclear localization of the YFP fusion protein. In line with this, the C413A/C420A double mutant followed the same localization pattern as observed for the C413A single mutant (Fig. 4l). All results were confirmed in colocalization experiments with the lipophilic dye FM4-64 (Fig. S4a,b). These data are consistent with our results from *in planta* localization studies of mutated SYMREM1 and show that C-terminal cysteine residues are crucial for membrane attachment of the remorin membrane-anchoring motif.

Finally, we introduced mutations into the predicted S-acylation sites of At3g61260, a protein that has been shown to be S-acylated (Hemsley *et al.*, 2013). While the full-length protein was exclusively found at the PM (Fig. 4m), mutations of the C-terminal residues Cys209 and Cys211 resulted in both cytoplasmic and, for Cys209, additional nuclear localization (Fig. 4n, o). Interestingly, the double mutant (C209A/C211A) strongly aggregated in large, mobile clusters in the cytosol (Fig. 4p). Again, these data were confirmed by colocalization experiments with FM4-64 (Fig. S4c).

In all three cases, the mutation of *in silico* predicted S-acylation sites resulted in an altered localization pattern. The entire loss of PM attachment in mutant variants of the remorin membrane-binding domain from two different remorins and the alteration of localization of the full-length At3g61260 protein highlight the importance of these residues in PM targeting.

Interestingly, three *A. thaliana* remorins (At3g48940, At3g57540 and At2g41870) are entirely devoid of cysteine residues. Thus no putative S-acylation sites could be detected in these proteins when using the CSS PALM algorithm (Table 1). However, as shown for At2g41870, these proteins also require the C-terminal 35 residues to associate with the PM (Fig. 3c,g), indicating a possible alternative mode of membrane binding.

Remorins are S-acylated proteins

Next, we asked, whether the identified and mutated cysteine residues are indeed post-translationally modified. To verify the presence of S-acyl moieties, we performed a biotin switch assay, a

method that was successfully used to determine S-acylation of plant proteins (Hemsley *et al.*, 2008). We confirmed functionality of the assay on full-length At3g61260, where the presence of a band in the elution fraction of hydroxylamine-treated samples indicates S-acylation of the protein (Fig. S5a,b). Strong S-acylation signals were also observed for SYMREM1, and its RemCA peptide (Fig. 5a). By contrast, no S-acylation was detected in the C197A mutant of the full-length SYMREM1 protein and the isolated membrane-binding domain. This demonstrates that Cys197 is the only S-acylated residue in the SYMREM1 protein (Fig. 5a).

Accordingly, the At4g36970 RemCA peptide was also found to be S-acylated (Fig. 5b). A mutation in Cys413 of the At4g36970 RemCA was sufficient to abolish S-acylation of the peptide (Fig. 5b), demonstrating that this residue is an essential S-acylation site in the membrane-binding domain. These data are supported by the fact that no change in S-acylation was observed for the C420A mutation. Thus, this residue is not S-acylated (Fig. 5b). It should be noted that we were unfortunately unable to perform these experiments reliably on full-length At4g36970, because of the insolubility of the protein.

S-acylation is dispensable for SYMREM1 targeting to membrane microdomains

S-acylation has been suggested to contribute to microdomain localization of membrane-resident proteins (Blaskovic *et al.*, 2013). Therefore, we asked whether S-acylation is required for membrane domain localization of the SYMREM1 protein in

transgenic *M. truncatula* roots. Expression of full-length SYMREM1 or the C-terminal region (SYMREM1^{74–205}) resulted in clear labelling of membrane microdomains in root epidermal cells (Fig. 6a,b). Interestingly, this pattern was also observed when expressing the S-acylation mutant variant SYMREM1^{C197A}, albeit to weaker extent (Fig. 6c). By contrast, the YFP protein fused to the SYMREM1 membrane-binding domain (RemCA, SYMREM1^{171–205}) did not label such distinct sites in the majority of cells (Fig. 6d). These data imply that S-acylation and the presence of the hydrophobic core alone are not sufficient to target SYMREM1 into membrane domains. As remorins are able to form oligomers (Bariola *et al.*, 2004; Marin *et al.*, 2012; Tóth *et al.*, 2012), membrane localization of SYMREM1 could be mediated by interactions with other members of the remorin family. Therefore we expressed wildtype SYMREM1, SYMREM1^{74–205}, SYMREM1^{C197A} and SYMREM1^{170–205} in *Saccharomyces cerevisiae* (yeast), a biological system devoid of remorin proteins. Indeed, all fusion proteins that contained the full-length C-terminal region localized to the PM and clearly labelled distinct membrane domains in the PM independently of S-acylation at Cys197 (Fig. 6e–g). Reciprocally, expression of the PM binding domain alone was not sufficient to label membrane domains in yeast cells (Fig. 6h), although western blot analysis revealed the predominant presence of the fusion protein in the microsomal fraction (Fig. S6). These data clearly indicate that interaction with other remorins is not the basis for PM association of SYMREM1 and that other factors than S-acylation alone contribute to membrane domain targeting.

Discussion

Association of soluble proteins with the cytoplasmic leaflet of the PM can be mediated by interactions with other membrane-resident (e.g. transmembrane) proteins or post-translational lipidations. These lipid modifications, for example, S-acylation, can serve as key determinants for polar signalling, which enables cells to rapidly respond to extracellular stimuli and to efficiently organize proteins in a polar manner (Grunewald & Friml, 2010; Kleine-Vehn *et al.*, 2011). Prominent examples are small GTPases of the Rho of plants (ROP) family that laterally segregate in plant cells. ROP6, a type-I ROP that is involved in ABA signalling, is S-acylated upon activation and subsequently copurifies with DRM fractions (Sorek *et al.*, 2007). Furthermore, expression of deacylated ROP variants in transgenic plants resulted in nonpolar accumulation of reactive oxygen species (ROS), indicating that polar segregation of ROPs depends on S-acylation (Sorek *et al.*, 2010).

Plant-specific remorin proteins, for which putative roles during hormone responses, plant–microbe and plant–virus interactions have been suggested (Alliotte *et al.*, 1989; Raffaele *et al.*, 2009; Lefebvre *et al.*, 2010; Tóth *et al.*, 2012; Demir *et al.*, 2013), are canonical marker proteins for sterol-rich DRM fractions. More importantly, these proteins label membrane microdomains *in vivo* (Fig. 1) (Raffaele *et al.*, 2009; Lefebvre *et al.*, 2010; Peraki *et al.*, 2012; Demir *et al.*, 2013; Jarsch *et al.*, 2014). The mechanism that is used by remorin proteins to specifically target

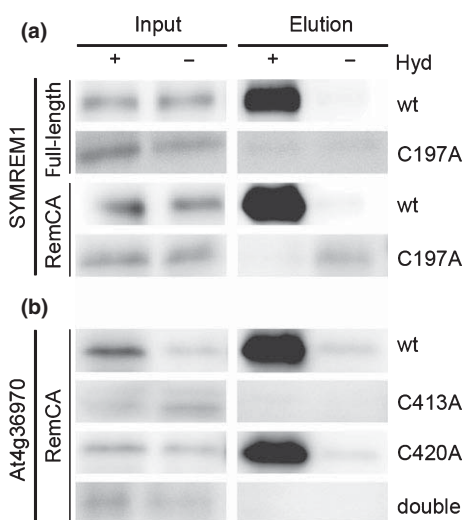


Fig. 5 Remorins are S-acylated proteins. S-acylated cysteine residues of remorin proteins purified from *Nicotiana benthamiana* were labelled by a biotin switch assay. (a) S-acylation of SYMREM1 and its corresponding membrane binding domain is indicated by the presence of a band in the elution fraction of the hydroxylamine (Hyd)-treated samples (+). Absence of this band in the C197A mutant variant revealed that Cys197 is the only S-acylated residue in this protein. wt, wildtype. (b) The remorin C-terminal anchor (RemCA) peptide of the remorin protein At4g36970 is S-acylated. Absence of a signal in the C413A mutant indicates S-acylation of this residue, while Cys420 is not S-acylated.

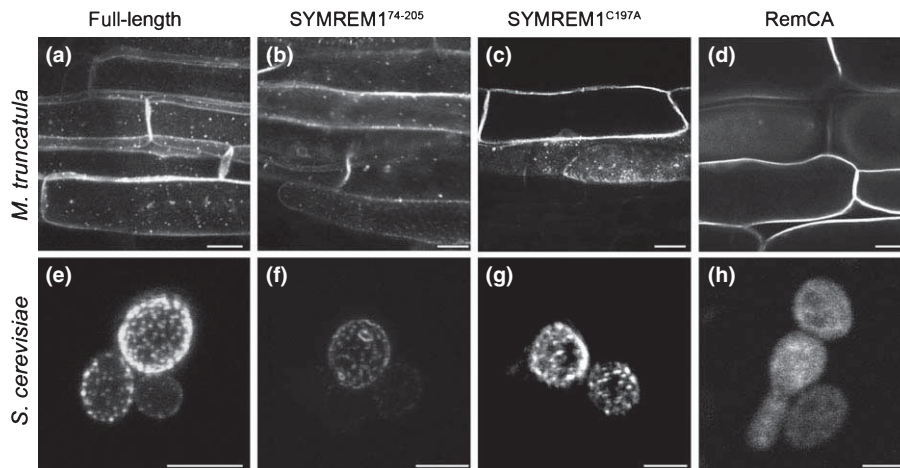


Fig. 6 Localization of remorins in membrane domains is not primarily determined by S-acylation. (a–d) Expression of different SYMREM1 constructs in transgenic *Medicago truncatula* roots revealed strong labelling of microdomains at the plasma membrane (PM) by the wildtype full-length construct (a) and the C-terminal region of SYMREM1 (b). Weaker labelling of membrane domains was also observed when expressing the deacylated mutant variant SYMREM1^{C197A} (c), while the membrane binding domain (remorin C-terminal anchor, RemCA) mostly showed uniform distribution on the PM (d). (e–h) Expression of different SYMREM1 constructs in yeast (*Saccharomyces cerevisiae*). Membrane domains were labelled by the wildtype full-length construct (e), the C-terminal region (f) and the deacylated mutant variant SYMREM1^{C197A} (g), while the membrane binding domain showed uniform distribution on the PM (h). All images are z-projections. Bars: (a–d) 10 μ m; (e–h) 5 μ m.

the inner leaflet of membrane domains remained controversial, especially as two different modes were proposed recently (Perraki *et al.*, 2012; Hemsley *et al.*, 2013). In this study, we have finally unravelled the binding mechanism of plant-specific remorin proteins on a molecular level. Our data clearly demonstrate that membrane binding of most remorins is mediated by S-acylation of cysteine residues in a C-terminal hydrophobic core, and is thus a combination of both models (Figs S1a, S7).

S-acylation is catalysed by transmembrane PATs (Roth *et al.*, 2002; Hemsley *et al.*, 2005). Therefore, remorins need to be initially directed to the PM to serve as S-acylation substrates. We propose that the C-terminal region with its terminal hydrophobic core mediates this initial affinity to the PM. This can occur via two routes: by direct protein–lipid interactions or by protein–protein interactions (Fig. S7). Indeed, recombinant StREM1.3 bound artificial, protein-free liposomes directly and showed a preferred interaction with phosphatidylinositol 3,4-bisphosphate (PI(3,4)P₂) *in vitro* (Perraki *et al.*, 2012). However, it remains to be tested whether the recombinant protein was post-translationally modified in bacteria before purification and whether this modification mediated membrane binding of StREM1.3. Our data support such a concern, as single point mutations in two C-terminal cysteine residues of the homologous remorin (At3g61260) from *A. thaliana* abolished membrane binding of the protein (Fig. 4n–p). Furthermore, none of the deacylated RemCA peptides remained associated with the PM (Figs 4, 5).

We demonstrated that despite only a few of the 35 C-terminal residues (RemCA) of different remorins are sufficient to confer membrane association of soluble fluorophores (Table 1), they are always indispensable for membrane binding of the full-length proteins (Fig. 3). It should be noted that *ab initio* modelling of SYMREM1 indicated that its RemCA peptide probably contributes to protein–protein

interactions (Fig. S1a). This prediction is experimentally supported as the C-terminal region of remorins was shown to be essential for oligomerization (Marin *et al.*, 2012; Tóth *et al.*, 2012) and interaction with other proteins (Marin *et al.*, 2012; Tóth *et al.*, 2012). In the case of SYMREM1, such interaction and membrane binding of its RemCA peptide are independent of other members of the remorin family, as PM association was also observed in yeast (Fig. 6e–h). As S-acylation may also control protein–protein interactions (Blaskovic *et al.*, 2013), the extent to which this feature also contributes to membrane association of remorin proteins remains to be studied.

Membrane domain localization of proteins in living cells can also be achieved by combinatorial lipidation, mainly myristoylation and S-acylation. In plants, double lipidation of *b*-type thiorodoxins (TRX) was shown to target these proteins to membrane microdomains *in planta* (Traverso *et al.*, 2013). By contrast, domain markers from *A. thaliana* and *M. truncatula* like flotillin and remorin proteins lack N-terminal glycine residues and are therefore not myristoylated. Thus, the possibility that membrane association of remorins *in vivo* is supported by protein–protein interactions independently of S-acylation could be especially essential for those remorins that are devoid of cysteine residues (At3g48940, At3g57540 and At2g41870) and that are therefore unlikely to be acylated. This hypothesis is further substantiated by the finding that an unacylated SYMREM1 protein remains in the PM (Fig. 4b).

We showed that S-acylation is not required for localization of remorins in immobile membrane domains *per se*, as the mutated SYMREM1^{C197A} protein still labelled these membrane compartments in plants and in yeast (Fig. 6), albeit to a lower extent. Interestingly, deacylation of At4g36970 even resulted in increased association of the protein with immobile membrane domains (Fig. 4f–h), indicating that S-acylation may eventually

restrict certain domain labelling patterns of some remorins. Therefore it is likely that another, as yet unknown factor contributes to their highly specific targeting of membrane domains.

Acknowledgements

This work was supported by the German Research Foundation (Deutsche Forschungsgemeinschaft, DFG) through an Emmy-Noether grant to T.O. (OT 423/2-1) and by two PhD fellowships from the Universität Bayern e.V. (S.S.A.K. and I.K.J.).

References

- Adjobo-Hermans MJ, Goedhart J, Gadella TW Jr. 2006. Plant G protein heterotrimers require dual lipidation motifs of Galpha and Ggamma and do not dissociate upon activation. *Journal of Cell Science* 119: 5087–5097.
- Alliotte S, Tire C, Engler G, Peleman J, Caplan A, Van Montagu M, Inze D. 1989. An auxin-regulated gene of *Arabidopsis thaliana* encodes a DNA-binding protein. *Plant Physiology* 89: 743–752.
- Bariola PA, Retelska D, Stasiak A, Kammerer RA, Fleming A, Hijri M, Frank S, Farmer EE. 2004. Remorins form a novel family of coiled coil-forming oligomeric and filamentous proteins associated with apical, vascular and embryonic tissues in plants. *Plant Molecular Biology* 55: 579–594.
- Bharadwaj M, Bizzozero OA. 1995. Myelin P0 glycoprotein and a synthetic peptide containing the palmitoylation site are both autoacylated. *Journal of Neurochemistry* 65: 1805–1815.
- Bhat RA, Miklis M, Schmelzer E, Schulze-Lefert P, Panstruga R. 2005. Recruitment and interaction dynamics of plant penetration resistance components in a plasma membrane microdomain. *Proceedings of the National Academy of Sciences, USA* 102: 3135–3140.
- Binder A, Lambert J, Morbitzer R, Popp C, Ott T, Lahaye T, Parniske M. 2014. A modular plasmid assembly kit for multigene expression, gene silencing and silencing rescue in plants. *PLoS ONE* 9: e88218.
- Blaskovic S, Blanc M, van der Goot FG. 2013. What does S-palmitoylation do to membrane proteins? *FEBS Journal* 280: 2766–2774.
- van den Bogaart G, Meyenberg K, Risselada HJ, Amin H, Willig KI, Hubrich BE, Dier M, Hell SW, Grubmüller H, Diederichsen U *et al.* 2011. Membrane protein sequestering by ionic protein–lipid interactions. *Nature* 479: 552–555.
- Boisson-Dernier A, Chabaud M, Garcia F, Becard G, Rosenberg C, Barker DG. 2001. *Agrobacterium rhizogenes*-transformed roots of *Medicago truncatula* for the study of nitrogen-fixing and endomycorrhizal symbiotic associations. *Molecular Plant-Microbe Interactions* 14: 695–700.
- Bradford JR, Westhead DR. 2005. Improved prediction of protein–protein binding sites using a support vector machines approach. *Bioinformatics* 21: 1487–1494.
- Demir F, Horntrich C, Blachutzik JO, Scherzer S, Reinders Y, Kierszniowska S, Schulze WX, Harms GS, Hedrich R, Geiger D *et al.* 2013. Arabidopsis nanodomain-delimited ABA signaling pathway regulates the anion channel SLAH3. *Proceedings of the National Academy of Sciences, USA* 110: 8296–8301.
- Grunewald W, Friml J. 2010. The march of the PINs: developmental plasticity by dynamic polar targeting in plant cells. *EMBO Journal* 29: 2700–2714.
- Haney CH, Long SR. 2010. Plant flotillins are required for infection by nitrogen-fixing bacteria. *Proceedings of the National Academy of Sciences, USA* 107: 478–483.
- Hemsley PA, Kemp AC, Grierson CS. 2005. The TIP GROWTH DEFECTIVE1 S-acyl transferase regulates plant cell growth in Arabidopsis. *Plant Cell* 17: 2554–2563.
- Hemsley PA, Taylor L, Grierson CS. 2008. Assaying protein palmitoylation in plants. *Plant Methods* 4: 2.
- Hemsley PA, Weimar T, Lilley KS, Dupree P, Grierson CS. 2013. A proteomic approach identifies many novel palmitoylated proteins in Arabidopsis. *New Phytologist* 197: 805–814.
- Horn PJ, Korte AR, Neogi PB, Love E, Fuchs J, Strupat K, Borisjuk L, Shulaev V, Lee YJ, Chapman KD. 2012. Spatial mapping of lipids at cellular resolution in embryos of cotton. *Plant Cell* 24: 622–636.
- Jarsch IK, Konrad SSA, Stratil TF, Urbanus SL, Szymanski W, Braun P, Braun KH, Ott T. 2014. Plasma membranes are subcompartmentalized into a plethora of coexisting and diverse microdomains in *Arabidopsis* and *Nicotiana benthamiana*. *Plant Cell* 26: 1698–1711.
- Jarsch IK, Ott T. 2011. Perspectives on remorin proteins, membrane rafts, and their role during plant-microbe interactions. *Molecular Plant-Microbe Interactions* 24: 7–12.
- Kierszniowska S, Seiwert B, Schulze WX. 2009. Definition of Arabidopsis sterol-rich membrane microdomains by differential treatment with methyl-beta-cyclodextrin and quantitative proteomics. *Molecular and Cellular Proteomics* 8: 612–623.
- Kleine-Vehn J, Wabnik K, Martiniere A, Langowski L, Willig K, Naramoto S, Leitner J, Tanaka H, Jakobs S, Robert S *et al.* 2011. Recycling, clustering, and endocytosis jointly maintain PIN auxin carrier polarity at the plasma membrane. *Molecular Systems Biology* 7: 540.
- Kusumi A, Fujiwara TK, Chadda R, Xie M, Tsunoyama TA, Kalay Z, Kasai RS, Suzuki KG. 2012. Dynamic organizing principles of the plasma membrane that regulate signal transduction: commemorating the fortieth anniversary of Singer and Nicolson's fluid-mosaic model. *Annual Review of Cell and Developmental Biology* 28: 215–250.
- Lefebvre B, Timmers T, Mbengue M, Moreau S, Herve C, Toth K, Bittencourt-Silvestre J, Klaus D, Deslandes L, Godiard L *et al.* 2010. A remorin protein interacts with symbiotic receptors and regulates bacterial infection. *Proceedings of the National Academy of Sciences, USA* 107: 2343–2348.
- Li R, Liu P, Wan Y, Chen T, Wang Q, Mettzbach U, Baluska F, Samaj J, Fang X, Lucas WJ *et al.* 2012. A membrane microdomain-associated protein, Arabidopsis Flot1, is involved in a clathrin-independent endocytic pathway and is required for seedling development. *Plant Cell* 24: 2105–2122.
- Li X, Luu DT, Maurel C, Lin J. 2013. Probing plasma membrane dynamics at the single-molecule level. *Trends in Plant Science* 18: 617–624.
- Lingwood D, Simons K. 2010. Lipid rafts as a membrane-organizing principle. *Science* 327: 46–50.
- Malinsky J, Opekarova M, Grossmann G, Tanner W. 2013. Membrane microdomains, rafts, and detergent-resistant membranes in plants and fungi. *Annual Review of Plant Biology* 64: 501–529.
- Marin M, Ott T. 2012. Phosphorylation of intrinsically disordered regions in remorin proteins. *Frontiers in Plant Science* 3: 86.
- Marin M, Thallmair V, Ott T. 2012. The intrinsically disordered N-terminal region of AtREM1.3 remorin protein mediates protein–protein interactions. *Journal of Biological Chemistry* 287: 39982–39991.
- Martin ML, Busconi L. 2000. Membrane localization of a rice calcium-dependent protein kinase (CDPK) is mediated by myristoylation and palmitoylation. *Plant Journal* 24: 429–435.
- Neumann-Giesen C, Falkenbach B, Beicht P, Claasen S, Luers G, Stuermer CA, Herzog V, Tikkanen R. 2004. Membrane and raft association of reggie-1/flotillin-2: role of myristoylation, palmitoylation and oligomerization and induction of filopodia by overexpression. *Biochemical Journal* 378: 509–518.
- Perraki A, Cacas JL, Crowet JM, Lins L, Castroviejo M, German-Retana S, Mongrand S, Raffaele S. 2012. Plasma membrane localization of *Solanum tuberosum* remorin from group 1, homolog 3 is mediated by conformational changes in a novel C-terminal anchor and required for the restriction of *Potato virus X* movement. *Plant Physiology* 160: 624–637.
- Petterson EF, Goddard TD, Huang CC, Couch GS, Greenblatt DM, Meng EC, Ferrin TE. 2004. UCSF Chimera – a visualization system for exploratory research and analysis. *Journal of Computational Chemistry* 25: 1605–1612.
- Raffaele S, Bayer E, Lafarge D, Cluzet S, German Retana S, Boubekeur T, Leborgne-Castel N, Carde JP, Lherminier J, Noirot E *et al.* 2009. Remorin, a *Solanaceae* protein resident in membrane rafts and plasmodesmata, impairs *Potato virus X* movement. *Plant Cell* 21: 1541–1555.

- Raffaële S, Mongrand S, Gamas P, Niebel A, Ott T. 2007. Genome-wide annotation of remorins, a plant-specific protein family: evolutionary and functional perspectives. *Plant Physiology* 145: 593–600.
- Reymond P, Kunz B, Paul-Pletzer K, Grimm R, Eckerskorn C, Farmer EE. 1996. Cloning of a cDNA encoding a plasma membrane-associated, uronide binding phosphoprotein with physical properties similar to viral movement proteins. *Plant Cell* 8: 2265–2276.
- Roche Y, Gerbeau-Pissot P, Buhot B, Thomas D, Bonneau L, Gresti J, Mongrand S, Perrier-Cornet JM, Simon-Plas F. 2008. Depletion of phytosterols from the plant plasma membrane provides evidence for disruption of lipid rafts. *FASEB Journal* 22: 3980–3991.
- Roth AF, Feng Y, Chen L, Davis NG. 2002. The yeast DHHC cysteine-rich domain protein Akr1p is a palmitoyl transferase. *Journal of Cell Biology* 159: 23–28.
- Roy A, Kucukural A, Zhang Y. 2010. I-TASSER: a unified platform for automated protein structure and function prediction. *Nature Protocols* 5: 725–738.
- Sorek N, Poraty L, Sternberg H, Bar E, Lewinsohn E, Yalovsky S. 2007. Activation status-coupled transient S acylation determines membrane partitioning of a plant Rho-related GTPase. *Molecular and Cellular Biology* 27: 2144–2154.
- Sorek N, Segev O, Gutman O, Bar E, Richter S, Poraty L, Hirsch JA, Henis YI, Lewinsohn E, Jurgens G *et al.* 2010. An S-acylation switch of conserved G domain cysteines is required for polarity signaling by ROP GTPases. *Current Biology* 20: 914–920.
- Tóth K, Stratil TF, Madsen EB, Ye J, Popp C, Antolin-Llovera M, Grossmann C, Jensen ON, Schussler A, Parniske M *et al.* 2012. Functional domain analysis of the remorin protein LjSYMREM1 in *Lotus japonicus*. *PLoS ONE* 7: e30817.
- Traverso JA, Micalella C, Martinez A, Brown SC, Satiat-Jeunemaitre B, Meinnel T, Giglione C. 2013. Roles of N-terminal fatty acid acylations in membrane compartment partitioning: Arabidopsis h-type thioredoxins as a case study. *Plant Cell* 25: 1056–1077.
- Underwood W, Somerville SC. 2013. Perception of conserved pathogen elicitors at the plasma membrane leads to relocalization of the Arabidopsis PEN3 transporter. *Proceedings of the National Academy of Sciences, USA* 110: 12492–12497.
- Urbanus SL, Ott T. 2012. Plasticity of plasma membrane compartmentalization during plant immune responses. *Frontiers in Plant Science* 3: 181.
- Varma R, Mayor S. 1998. GPI-anchored proteins are organized in submicron domains at the cell surface. *Nature* 394: 798–801.
- Vermeer JE, Thole JM, Goedhart J, Nielsen E, Munnik T, Gadella TW Jr. 2009. Imaging phosphatidylinositol 4-phosphate dynamics in living plant cells. *Plant Journal* 57: 356–372.
- Wessel D, Flugge UI. 1984. A method for the quantitative recovery of protein in dilute solution in the presence of detergents and lipids. *Analytical Biochemistry* 138: 141–143.
- Zappel NF, Panstruga R. 2008. Heterogeneity and lateral compartmentalization of plant plasma membranes. *Current Opinion in Plant Biology* 11: 632–640.
- Zhang Y. 2008. I-TASSER server for protein 3D structure prediction. *BMC Bioinformatics* 9: 40.

Supporting Information

Additional supporting information may be found in the online version of this article.

Fig. S1 Protein interaction scores within the SYMREM1 protein and free YFP in root epidermal cells.

Fig. S2 Analysis of RemCA-mediated PM binding throughout the remorin protein family.

Fig. S3 Western blots of microsomal fractionations of wildtype and mutated SYMREM1 fusion proteins.

Fig. S4 Colocalization studies for different mutant variants.

Fig. S5 Biotin switch assay and quantification.

Fig. S6 Western blot analysis of SYMREM1 constructs expressed in yeast.

Fig. S7 Proposed model for membrane-binding of remorin proteins.

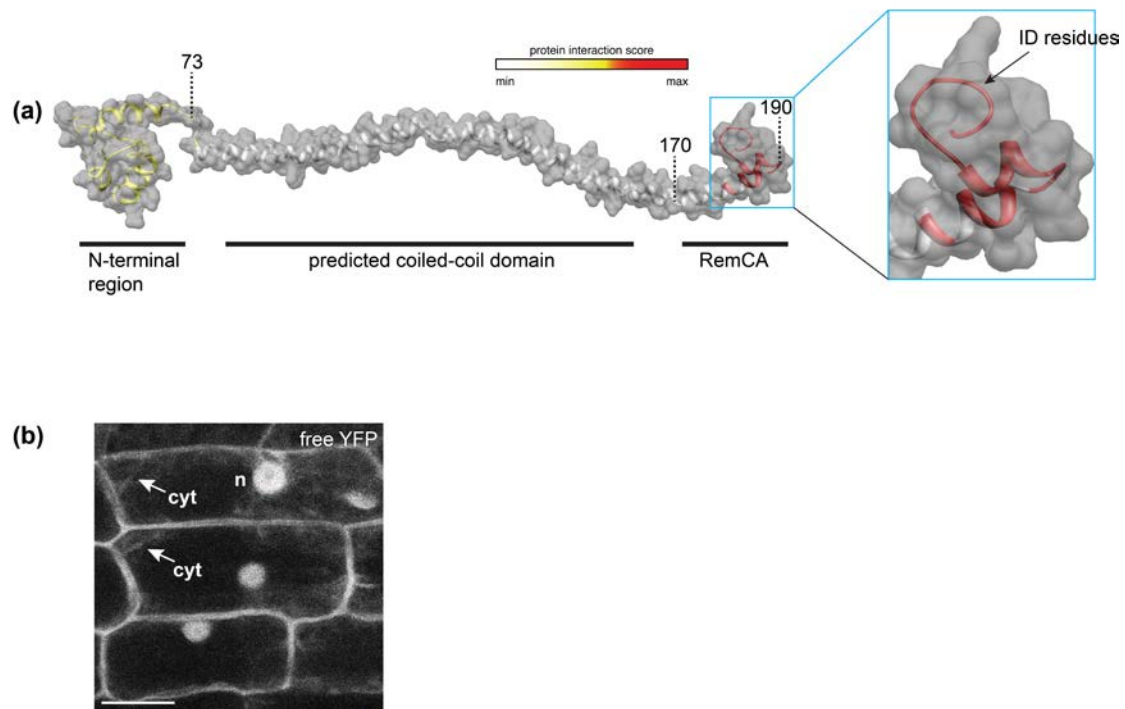
Please note: Wiley Blackwell are not responsible for the content or functionality of any supporting information supplied by the authors. Any queries (other than missing material) should be directed to the *New Phytologist* Central Office.

New Phytologist Supporting Information Figs S1–S7

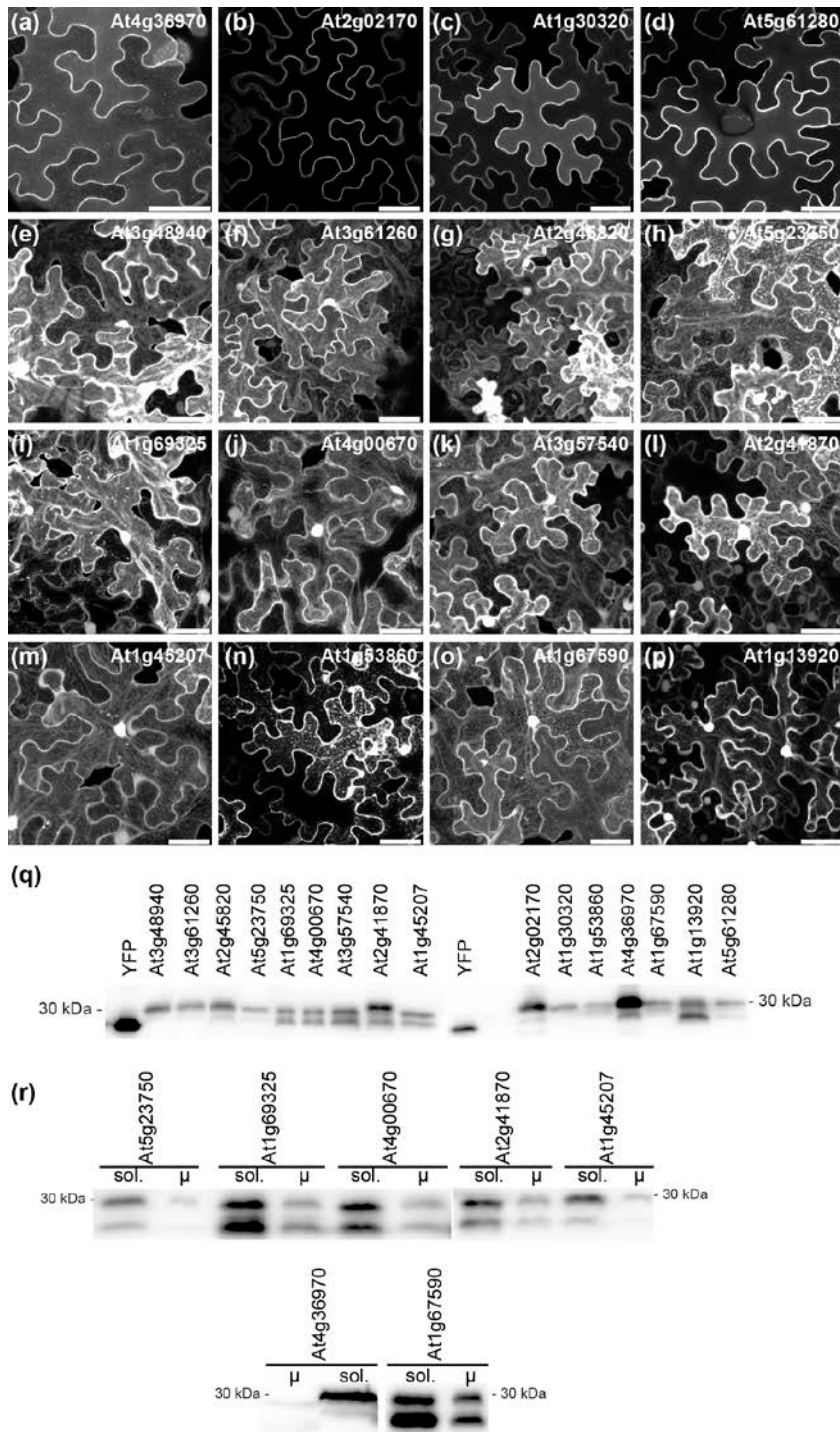
S-acylation anchors Remorin proteins to the plasma membrane but does not primarily determine their localization in membrane micro-domains

Sebastian S. A. Konrad, Claudia Popp, Thomas F. Stratil, Iris K. Jarsch, Veronika Thallmair, Jessica Folgmann, Macarena Marín and Thomas Ott

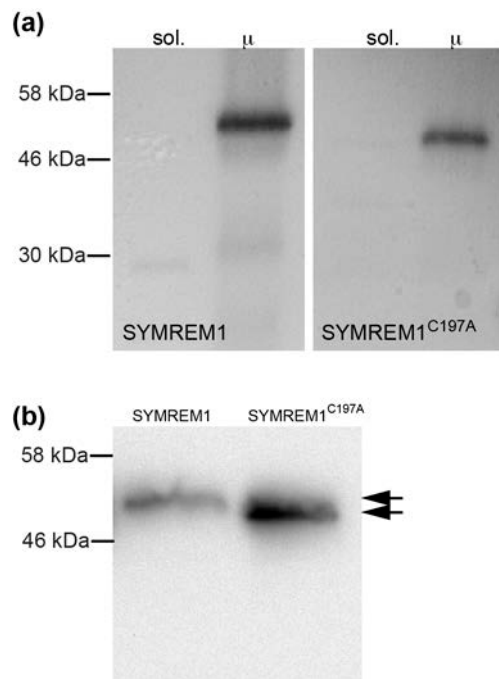
The following Supporting Information is available for this article:



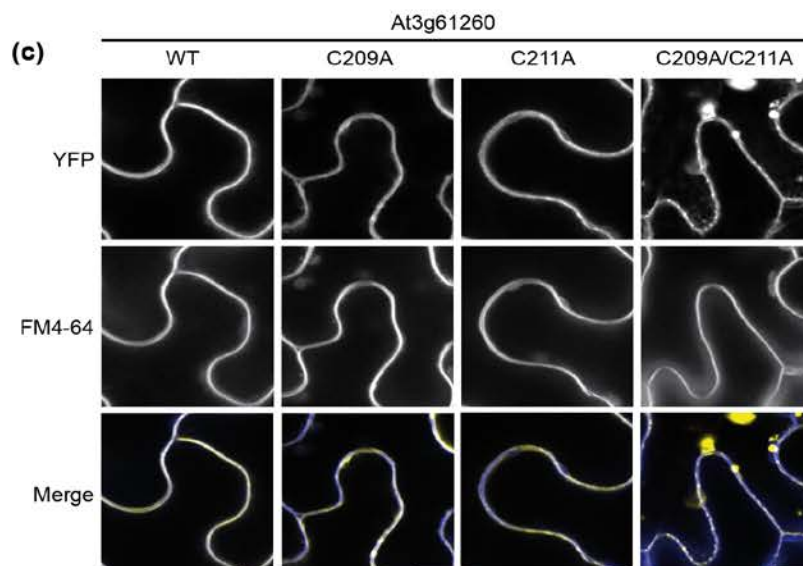
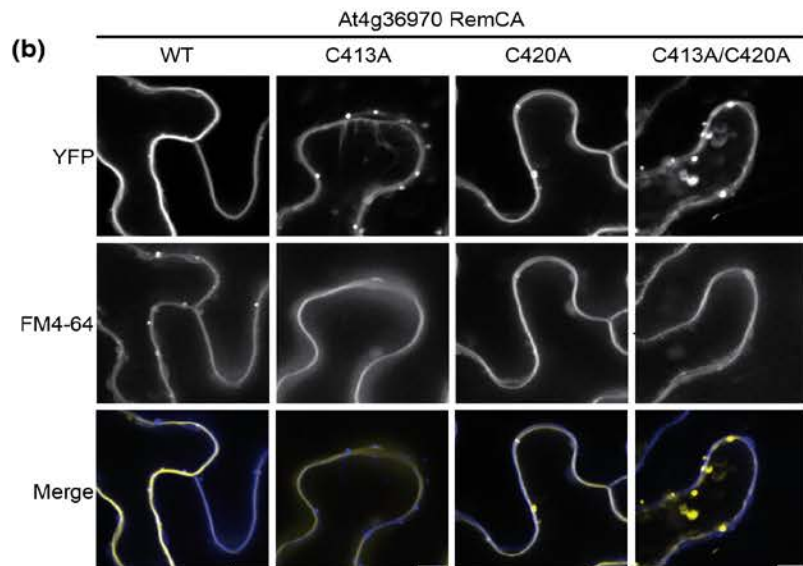
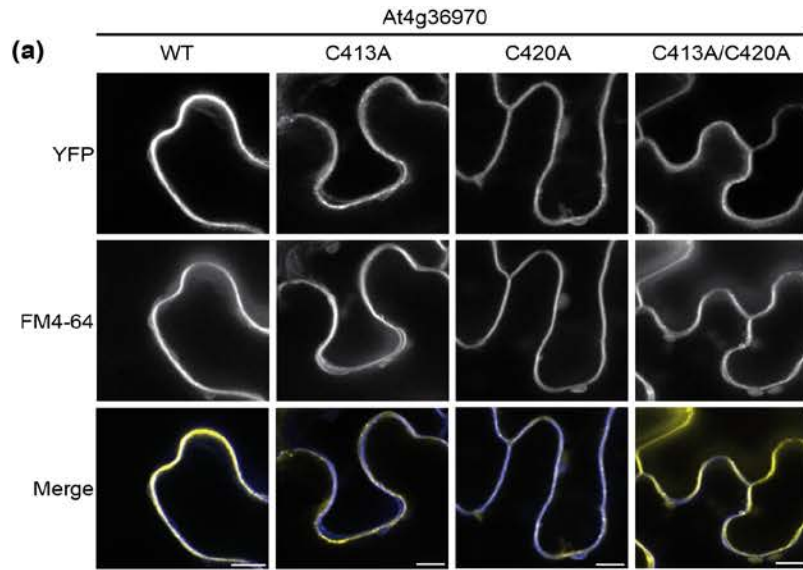
Supporting Information Fig. S1 Protein interaction scores within the SYMREM1 protein and free YFP in root epidermal cells. (a) *Ab initio* modelling of the SYMREM1 protein and colour-coded representation of putative regions that may contribute to protein interactions. Models for the N- and C-terminal regions were constructed independently and fused subsequently. Details can be found in the Materials and Methods section. ID, intrinsically disordered (b) *M. truncatula* root epidermal cell expressing a free YFP protein. The image shows a maximum intensity projection of a z-stack. n, nucleus; cyt, cytoplasmic strands. Bar, 5 μ m.



Supporting Information Fig. S2 Analysis of RemCA-mediated PM-binding throughout the Remorin protein family. (a–d) Four out of 16 RemCA peptides were sufficient to target the fluorophore almost exclusively to the plasma membrane of *N. benthamiana* root epidermal cells. (e–p) Representative images of the remaining twelve RemCA peptides show at least partial cytoplasmic and nuclear labelling. Bars, 20 μ m. (q) Western Blot on total protein extracts from *N. benthamiana* leaves expressing different RemCA peptides. Double bands indicate partial cleavage of the fusion protein. Samples were compared to free YFP. (r) Microsomal fractionations of total protein extracts were performed to assess partial cleavage of the respective constructs. sol., soluble protein fraction; μ , microsomal fraction.



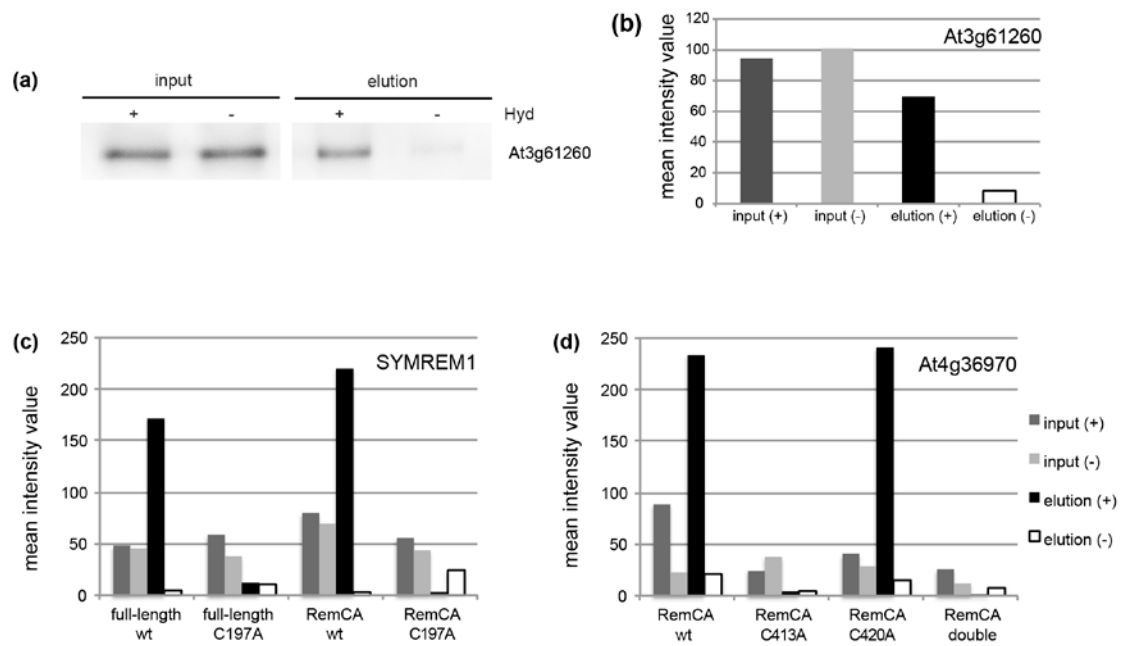
Supporting Information Fig. S3 Western Blots and microsomal fractionations of wild-type and mutated SYMREM1 fusion proteins. (a) Microsomal fractions were obtained from *N. benthamiana* leaves expressing YFP-SYMREM1 and YFP-SYMREM1^{C197A} fusion proteins. Both wild-type and the mutant variant were found in the microsomal fraction, indicating that they remained at the plasma membrane. (b) Microsomal fractions of wild-type and mutated SYMREM1 showed a band shift pattern. Western blots were probed with α -GFP antibodies.



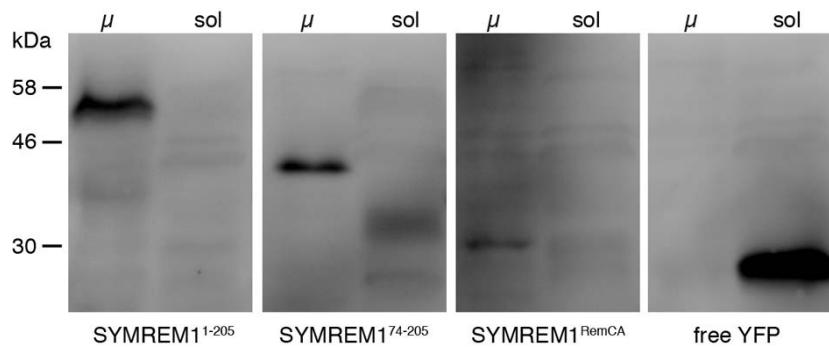
Supporting

Information Fig. S4

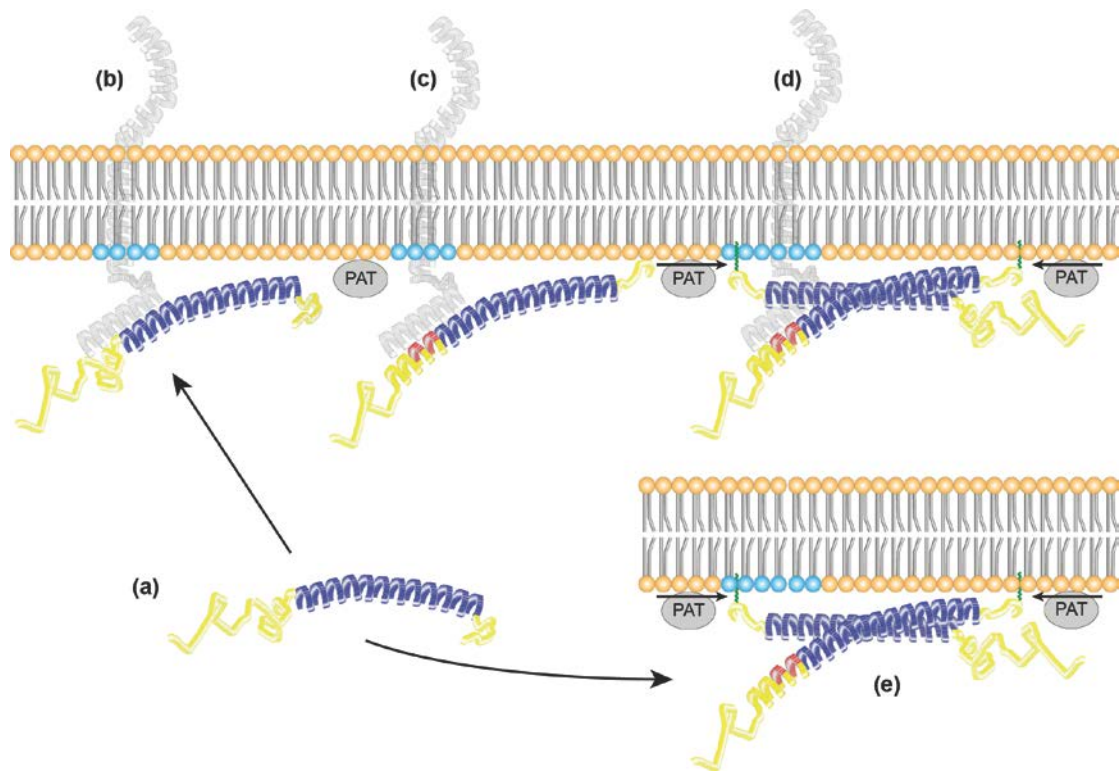
Co-localization studies for different mutant variants. YFP-tagged proteins were expressed in *N. benthamiana* leaf epidermal cells and counterstained with FM4-64. All images show maximum projections of z-stacks taken of secant planes. Bars, 5 μ m.



Supporting Information Fig. S5 Biotin switch assay and quantification. (a) Control experiment to prove functionality of the assay. Full-length At3g61260 is S-acylated as previously demonstrated in Hemsely *et al.* (2013). S-acylation of proteins is indicated by the presence of a band in the elution fraction of the hydroxylamine treated samples (+). (b) Quantification of the Western Blot in (a) using ImageJ. (c, d) Quantification of Western Blots shown in Fig. 5. Values were normalized to background levels. double, double mutant.



Supporting Information Fig. S6 Western blot analysis of YFP-SYMREM1 constructs expressed in yeast. Free YFP was expressed as a control for the fractionation procedure. Microsomal fractions were obtained and the corresponding SYMREM1 proteins were detected using a α -GFP antibody. μ , microsomal fraction; sol., soluble proteins.



Supporting Information Fig. S7 Proposed model for membrane-binding of Remorin proteins. Remorins are soluble proteins (a) that are initially immobilized at the PM via interactions with a membrane resident protein (b) or by direct protein-lipid interactions via their C-terminal hydrophobic core (e). (c) Interaction with a protein partner leads to partial disorder-to-order transition of the intrinsically disordered N-terminal region. This may involve protein phosphorylation (red). (d, e) A membrane-localized protein acyl transferase (PAT) S-acylates (green line) C-terminal cysteine residues of Remorins and possibly others throughout the protein. This lipidation tightly binds the protein to the PM and may confer some degree of specificity to sterol-rich sites (blue) in the PM. Oligomerization of Remorins contributes to the formation of larger domain platforms (hypothetical).

3.4 Publication III: Knockin' on pollen's Door: Live cell imaging of early polarization events in germinating *Arabidopsis* pollen

Frank Vogler ¹, Sebastian S.A. Konrad ² and Stefanie Sprunck^{1*}

Frontiers in Plant Science **6**, 246 (2015)

DOI: 10.3389/fpls.2015.00246

¹Cell Biology and Plant Biochemistry, Biochemie-Zentrum Regensburg, University of Regensburg, Regensburg Germany

²Faculty of Biology, Institute of Genetics, Ludwig-Maximilians-University of Munich, Martinsried, Germany

*Correspondence: Stefanie Sprunck, Department of Cell Biology and Plant Biochemistry, University of Regensburg, Universitaetsstrasse 31, 93053 Regensburg, Germany stefanie.sprunck@biologie.uni-regensburg.de

Author contributions:

TIRF microscopy of *A. thaliana* pollen tubes was done by me (Figure 3). Furthermore, I contributed to the publication by inventing the mounting technique for TIRF microscopy of *A. thaliana* pollen tubes and gave input to the written manuscript (Supplementary Figure S3).

I hereby confirm the above mentioned statements:

.....

Prof. Dr. Thomas Ott

(In agreement with corresponding author)

.....

Sebastian S. A. Konrad

Knockin' on pollen's door: live cell imaging of early polarization events in germinating *Arabidopsis* pollen

Frank Vogler¹, Sebastian S. A. Konrad² and Stefanie Sprunck^{1*}

¹ Cell Biology and Plant Biochemistry, Biochemie-Zentrum Regensburg, University of Regensburg, Regensburg Germany,

² Faculty of Biology, Institute of Genetics, Ludwig-Maximilians-University of Munich, Martinsried, Germany

OPEN ACCESS

Edited by:

Dazhong Dave Zhao,
University of Wisconsin-Milwaukee,
USA

Reviewed by:

Mark A. Johnson,
Brown University, USA
Yuan Qin,
Fujian Agriculture and Forestry
University, China

*Correspondence:

Stefanie Sprunck,
Department of Cell Biology and Plant
Biochemistry, University of
Regensburg, Universitaetsstrasse 31,
93053 Regensburg, Germany
stefanie.sprunck@
biologie.uni-regensburg.de

Specialty section:

This article was submitted to
Plant Evolution and Development,
a section of the journal
Frontiers in Plant Science

Received: 07 January 2015

Accepted: 27 March 2015

Published: 21 April 2015

Citation:

Vogler F, Konrad SSA and Sprunck S
(2015) Knockin' on pollen's door: live
cell imaging of early polarization
events in germinating *Arabidopsis*
pollen. *Front. Plant Sci.* 6:246.
doi: 10.3389/fpls.2015.00246

Pollen tubes are an excellent system for studying the cellular dynamics and complex signaling pathways that coordinate polarized tip growth. Although several signaling mechanisms acting in the tip-growing pollen tube have been described, our knowledge on the subcellular and molecular events during pollen germination and growth site selection at the pollen plasma membrane is rather scarce. To simultaneously track germinating pollen from up to 12 genetically different plants we developed an inexpensive and easy mounting technique, suitable for every standard microscope setup. We performed high magnification live-cell imaging during *Arabidopsis* pollen activation, germination, and the establishment of pollen tube tip growth by using fluorescent marker lines labeling either the pollen cytoplasm, vesicles, the actin cytoskeleton or the sperm cell nuclei and membranes. Our studies revealed distinctive vesicle and F-actin polarization during pollen activation and characteristic growth kinetics during pollen germination and pollen tube formation. Initially, the germinating *Arabidopsis* pollen tube grows slowly and forms a uniform roundish bulge, followed by a transition phase with vesicles heavily accumulating at the growth site before switching to rapid tip growth. Furthermore, we found the two sperm cells to be transported into the pollen tube after the phase of rapid tip growth has been initiated. The method presented here is suitable to quantitatively study subcellular events during *Arabidopsis* pollen germination and growth, and for the detailed analysis of pollen mutants with respect to pollen polarization, bulging, or growth site selection at the pollen plasma membrane.

Keywords: pollen activation, cell polarization, bulging, vesicular trafficking, ARO1, actin cytoskeleton, sperm cells

Introduction

The pollen tube (PT) of flowering plants is formed by the pollen grain vegetative cell and represents a cell of enormous specialization, responsible for the transport of the two male gametes through the female tissues of the pistil to the ovule. It is the fastest elongating plant cell (Sanati Nezhad et al., 2014) and can reach lengths of 30 cm, with growth rates up to 1 cm/h (Mascarenhas, 1993). PT growth is monotropic by expansion at an annular region

Abbreviations: ARO, Armadillo Repeat Only; epiBL, 24-epibrassinolide; F-actin, filamentous actin; GFP, green fluorescent protein; PGM, pollen germination medium; PT, pollen tube; RFP, red fluorescent protein; TIRE, total internal reflection fluorescence.

located at the tip in a process called polar tip growth (Taylor and Hepler, 1997; Geitmann, 2010).

Deeply embedded in the tissues of the pistil, *in vivo* PT growth is difficult to investigate with high temporal and spatial resolution and has been achieved so far only by using two-photon microscopy (Feijó and Moreno, 2004; Cheung et al., 2010). As an advantageous alternative, pollen can be germinated *in vitro* to study the cellular dynamics and complex signaling pathways that coordinate polar tip growth (Qin and Yang, 2011). From these studies we know that intensive exo- and endocytosis at the tip supported by regulated vesicle trafficking and cytoskeleton dynamics, as well as coordinated changes in cell wall properties are essential cellular activities of the growing PT (for review see Geitmann, 2010; Guan et al., 2013). Great advances have been made during the past years in identifying key signaling molecules for the proper elongation of the PT tip, such as Rho GTPases, calcium ions, and phosphoinositides (for review see Cheung and Wu, 2008; Qin and Yang, 2011; Steinhorst and Kudla, 2013). These key regulators are components of distinct signaling pathways forming a complex network that controls the cellular activities of tip-growing PTs (Guan et al., 2013). However, there are still significant gaps in our knowledge of PT growth regulation, especially with regard to the question when and how symmetry breaking in the apparently unpolar pollen vegetative cell occurs, and what the molecular mechanism for selecting the growth site is.

Polar tip growth of PTs is very similar to the polar elongation of root hairs on genetic and mechanistic levels (reviewed in Šamaj et al., 2006; Campanoni and Blatt, 2007; Kost, 2008; Lee and Yang, 2008). Root hair growth is known as a multi-phasic process, consisting of cell fate determination, the formation of a root hair bulge, and the initiation of tip growth in the root hair bulge, each of which is characterized by distinct physiological and mutant phenotypes in the model plant *Arabidopsis* (Schiefelbein and Somerville, 1990; Parker et al., 2000; Schiefelbein, 2000; Bibikova and Gilroy, 2003; Müller and Schmidt, 2004). Since pollen germination and the initiation of PT tip growth is rapid and much faster than root hair growth, it is technically more demanding to perform live cell imaging in order to study the cellular dynamics and the growth kinetics during pollen hydration, activation, germination and PT formation. Moreover, *in vitro* germination rates and growth dynamics of *Arabidopsis* pollen are known to be highly variable (Johnson-Brousseau and McCormick, 2004; Boavida and McCormick, 2007), complicating its use for cellular and molecular genetic studies of pollen germination and growth. However, methodological advances in germination techniques meanwhile facilitated the experimental use of *Arabidopsis* pollen (Bou Daher et al., 2009; Rodriguez-Enriquez et al., 2013; Vogler et al., 2014), offering possibilities to establish methods for larger-scale screening and quantitative phenotyping of wild type and mutant pollen.

To optimize high throughput time-lapse live imaging of germinating *Arabidopsis* pollen, we established an inexpensive and easy mounting technique suitable for every standard microscope, based on an improved pollen germination medium (Vogler et al., 2014). Using this setup for Spinning Disc confocal microscopy we investigated the growth kinetics and morphology changes of *Arabidopsis* PTs expressing GFP in the cytoplasm of the vegetative

pollen cell. We focused on early cell polarization events during pollen activation and germination by studying the spatiotemporal localization of GFP-labeled Armadillo Repeat Only 1 (ARO1), which is known to be essential for polar PT growth (Gebert et al., 2008). ARO1-GFP accumulates in the inverted cone-shaped region of growing PT tips in a brefeldin A and latrunculin B sensitive manner and TIRF microscopy, applied in this study, confirmed that ARO1-GFP localizes vesicle-associated at the PT tip.

We used *Arabidopsis* marker lines expressing ARO1-GFP and tagRFP-T-Lifeact in the pollen to study vesicle and filamentous actin (F-actin) dynamics before and during pollen germination. Furthermore, we used a pollen marker line with fluorescently labeled sperm cell nuclei and plasma membranes (Sprunck et al., 2012) to address the question when the two sperm cells, physically linked to the nucleus of the vegetative cell forming a male germ unit (MGU) (McCue et al., 2011; Zhou and Meier, 2014), are transported from the pollen grain into the germinated PT.

Our time-lapse live imaging of germinating *Arabidopsis* PTs revealed similarities between root hair formation and pollen germination as we observed successive phases of cell polarization, bulge formation, growth site selection, and the initiation of rapid tip growth. Prior to pollen germination, we observed a characteristic polarization of vesicle-associated ARO1-GFP and tagRFP-T-Lifeact labeled F-actin in the pollen grain. After bulging, a transition phase is observed where vesicle-associated ARO1-GFP heavily accumulates at the distal end of the bulge and adopts an inverted cone-like shape before the PT switches to rapid tip growth. At the same time, long F-actin cables appear, extending in parallel orientation from within the pollen grain into the PT, while the volume of the vacuole, arising opposite the germination site, increases. During the phase of rapid tip growth, F-actin bundles massively accumulate at the germination site and increasing vacuolization occurs, followed by sperm cell transport into the PT.

Materials and Methods

Plant Material

Arabidopsis thaliana (accession Col-0) plants were grown under long-day conditions (16 h light, 20°C, 70% humidity) in growth chambers after seeds were subjected to stratification 2 days at 4°C in the dark. Homozygous lines carrying the *P_{Lat52}:GFP* transgene were used to express cytoplasmic GFP in the vegetative PT cell (Twell et al., 1990). A C-terminal GFP fusion of the ARO1 protein under control of its endogenous promoter (Gebert et al., 2008) was used to investigate its subcellular localization in pollen and PTs. A double homozygous marker for *P_{HTR10}:HTR10-RFP* and *P_{HTR10}:TET9-GFP* line (Sprunck et al., 2012) was used to visualize sperm cell nuclei and sperm cell plasma membranes.

Molecular Cloning and Generation of Transgenic Lines

A double stranded DNA fragment encoding for a 17 aa actin binding domain termed Lifeact (Riedl et al., 2008) with additional 5' and 3' *Hind*III restriction sites was synthesized by proof-reading PCR on the partially overlapping template

oligonucleotides 5'-GGGGCCATGGAAGCTTTGGGACCAGC CGTAGGAATGGGTGTTGCTGATCTTATTAAGAAGTTTCGA GTCTATTTCTAAGGAGG-3' and 5'-GGGGAAGCTTATGCC ATGGCTCCAGCTACAGGTGCTCCCGCCCCTCCTTCCTCC TTAGAAATAGACTCGAACTTCTTAA-3' with the PCR primers Lifeact-fwd (5'-GGGGCCATGGAAGCTTTGG-3') and Lifeact-rev (5'-GGGGAAGCTTATGCCATGGC-3'). After *Hind*III digestion, the PCR product was ligated behind the fluorophore coding sequence into the modified Gateway destination vector pENTR-tagRFP-T (Denninger et al., 2014) to obtain pENTR-tagRFP-T-Lifeact. To achieve expression in pollen, 712 bp of the *ARO1* promoter with additional 5' *Sac*I and 3' *Spe*I sites were amplified from the 95P-Nos-ARO1p:ARO1-GFP plasmid (Gebert et al., 2008) with the primers pARO1-II-for (5'-TCGGGTACCGAGCTCAGATCTAAGCTG-3') and pARO1-II-rev (5'-TGTCGACGCGGCCGACTAGtCAGATC-3'). The 35S promoter of the binary gateway expression vector pB2GW7 (Karimi et al., 2002) was replaced by the *ARO1* promoter via *Sac*I/*Spe*I to obtain pB2GW7-ARO1p. Gateway LR reaction with pENTR-tagRFP-T-Lifeact and pB2GW7-ARO1p was performed according to the manufacturer's recommendations (Life Technologies) to obtain the expression vector pARO1:tagRFP-T-Lifeact that was used for *Agrobacterium*-mediated plant transformation by floral dip method (Clough and Bent, 1998).

Pollen Mounting and Live Cell Imaging

Micro-germination slides were prepared in either a single-well or a multi-well setup (Figures S1,S2). To prepare a single-well micro-germination slide, a 1–2 mm high planar plasticine layer was added on the margin of the ring of a slide with an attached glass ring (L4246, PLANO, Wetzlar, Germany). The well was filled with molten pollen germination medium (PGM) according to Vogler et al. (2014), containing 10 μ M 24-epibrassinolide (epiBL, Sigma-Aldrich E-1641) and solidified with 0.5% low melting point agarose. After solidification the center of the well was hand pollinated using single dehiscent anthers, manually removed from flowers at flower stage 13–14 (according to Smyth et al., 1990). The well was then sealed by gently pressing evenly a 24 \times 24 mm No. 1.5 cover slip onto the plasticine until it slightly touched the PGM. The illustrated instruction on how to prepare a single-well micro-germination slide is shown in Figure S1. Multi-well micro-germination slides were prepared by attaching a 12 well silicon profile (flexiPERM[®] micro12, SARSTEDT, Germany) to a standard microscope slide (26 \times 76 mm) and filling each well with 50–75 μ L molten PGM. After solidification, the silicon profile was removed and another 25 μ L of molten PGM were added on top of each agar pad to obtain convex shapes. After a frame of plasticine was modeled around the agar pads, they were hand pollinated and then sealed by gently pressing evenly a 24 \times 60 mm No. 1.5 cover slip on the plasticine frame. The scheme on how to prepare a multi-well micro-germination slide is shown in Figure S2. Immediately after pollen application, micro-germination slides were used for live-cell imaging. No obvious differences in germination or PT growth were observed between single-well or multi-well micro-germination setups. By contrast, much lower and highly variable germination rates as

well as slower PT growth rates were observed when PGM without 10 μ M epiBL was used to prepare the micro-germination slides, while the different phases of pollen germination and tube growth described in this work were unaffected.

Microscopy was performed on a ZEISS Cell Observer Spinning Disc confocal microscope (Yokogawa CSU-X1) equipped with a motorized stage using 20 \times /0.8 NA dry, 40 \times /1.30 NA DIC oil immersion or 63 \times /1.40 NA DIC oil immersion objectives. GFP fluorescence was excited with a 488 nm laser line and emission was detected from 505 to 545 nm. A 561 nm laser line was used to excite tagRFP-T and emission was detected from 570 to 640 nm. Free GFP in the pollen cytoplasm and ARO1-GFP fusion protein were imaged every 3 min, tagRFP-T-Lifeact every 10–15 min over 4–6 h in z-stacks of 11 optical slices at each of 10–20 positions representing individual pollen spots.

Morphological Modeling of Pollen Germination

We assumed two extreme morphological models describing cellular geometries of germinating PTs and simulated these models graphically with Illustrator CS4 software (Adobe). In the “protrusion model” we proposed linear growth at the tip of a protuberance, generating a constantly elongating cylinder with a dome-shaped tip that emerges from the germination site. In the “bulging model” a first phase of isodiametric inflation was assumed for the germinating PT, followed by a second phase in which isodiametric growth switches to polar growth at a dome-shaped tip. Thus, in the “protrusion model,” a tubular object constantly emerges out of an ellipse, representing the pollen grain. To generate the “bulging model” a circle, representing the PT, was placed below the upper margin of an ellipse, representing the pollen grain. The diameter of the circle was frame-wise and constantly increased, while keeping its position constant at the lowermost point. After 20 frames, we changed the distal region of the circle into a dome-shaped tip, which then constantly elongates in form of a cylinder like in the “protrusion model.” In both morphological models, the width of the dome-shaped tip was set identical and did not change during elongation. Furthermore, the net increase in PT area was set identical for both models. Modeled PTs were measured in ImageJ like described for microscopic images (Image Processing and Quantitative Analysis).

Pollen Staining and Microscopy

For membrane staining with FM4-64, pollen of ARO1-GFP expressing plants were germinated in 35 mm petri dishes on solidified PGM as described above. Three hours after pollination a small agar piece was excised and mounted upside down on a cover slip in a droplet of 8 μ M FM4-64 (Life Technologies) dissolved in liquid PGM. Images were taken with an inverted SP8 Confocal Laser Scanning Microscope (Leica Microsystems) with a 40 \times /1.3NA oil immersion objective and 1 airy unit pinhole opening. GFP and FM4-64 were excited simultaneously with a 488 nm laser line. GFP emission was detected from 495 to 550 nm and FM4-64 emission from 650 to 725 nm using HyD detectors. For DAPI staining, pollen of plants expressing *P_{ARO1}:tagRFP-T-Lifeact* were put in a droplet of DAPI staining solution (2.5 μ g/ml 4',6-diamidino-2-phenylindole (DAPI), 0.01% Tween-20, 5% DMSO, 50 mM PBS, pH 7.2). Confocal

z-stacks were acquired at the Spinning Disc system described above using a 100×/1.40 NA oil immersion objective. DAPI fluorescence was excited with a 365 nm LED illumination (COLIBRI, ZEISS) and emission light was filtered by the microscope stand built-in filter cube (emission filter: 447–507 nm) and channeled through an empty Spinning Disc position to display DAPI fluorescence on the same camera as for tagRFP-T and DIC channels.

TIRF Microscopy

For TIRF microscopy of PTs, a very planar gel pad was generated by laying two microscope slides orthogonal on the edges of three adjacent slides (Figure S3). 500 μ l of molten PGM containing 2% agarose was pipetted to the middle of the lower slides and immediately covered with another slide. After solidification, the uppermost slide and all flanking slides were removed and the PGM pad was hand pollinated as described above (Pollen Mounting and Live Cell Imaging). Pollinated slides were kept in a damp box for 3–5 h. Prior to microscopy, a droplet of double distilled water was pipetted onto the pad and a No. 1.5H cover slip was added. TIRF illumination was generated in a Delta Vision Elite (GE, Healthcare, Applied Precision) system with an Olympus IX-71 microscope, equipped with an Insight SSI(TM) solid state illumination system and an X4 laser module. Images were taken with an Olympus UAPON 100XOTIRF 1.49 NA oil immersion objective and recorded with a CoolSnap HQ2 CCD camera (Photometrics, Tucson, USA). GFP was excited with the 488 nm laser line and emission was detected between 501 and 549 nm. Image exposure time and TIRF angle were adjusted according to sample fluorescence intensity and specimen location.

Image Processing and Quantitative Analysis

All images were processed in ImageJ (<http://rsbweb.nih.gov/ij>, version 1.45). In time-lapse experiments, the frame before a PT emerged from the germination site was set to zero. Z-stacks of time lapse images of pollen expressing $P_{Lat52}:GFP$ were subjected to projection algorithms. Bright field images were sum slice, GFP images maximum intensity projected. Afterwards, for the GFP channel a threshold was applied to obtain binary images. The implemented WAND tool was used to determine the pollen area, which was then subtracted from all images for a given PT and subsequently the PT area was measured for each frame. The analysis of PTs was only carried out with those PTs where growth was not disturbed by any other object and which could be observed for at least 1 h. Of all PTs the shape descriptor “roundness” was measured, given by $4 \cdot \text{area} / (\pi \cdot (\text{major axis})^2)$ of a respective PT. To compare the frame wise PT area increase shortly after germination and in later PT growth phases, the mean frame wise increase of the first 10 and the last 10 frames was calculated and compared in a Friedman’s 2-way variance analysis. Z-stacks of time lapse images of pollen expressing $P_{ARO1}:ARO1-GFP$ were also subjected to maximum intensity projections first. For those pollen that were monitored at least half an hour before and after the time point of germination, images were cropped in a rectangular selection containing only the pollen and emerging PT. All frames of a PT were included in a stack histogram that was used for subsequently computing gray values for setting a 70% signal

threshold to determine the PT shape (false colored in red) and a 0.5% signal threshold (false colored in yellow) to determine the maximum intensity peaks for ARO1-GFP. Frame-wise PT area increase was measured by overlaying unbiased PT shape outlines that were obtained using the WAND tool, which was also used to determine the size of individual PT areas. ARO1-GFP maximum intensity peaks were quantified using a variable ROI selection and measuring its mean gray value that was subsequently multiplied by the ROI size. To compare multiple PTs in a mean value computation, ARO1-GFP maximum intensity was normalized for each PT to its maximum signal value. Z-stacks of images of pollen expressing tagRFP-T-Lifeact were maximum intensity projected and to better visualize the maximum signal intensities false colored using the “spectrum” LUT. Calculations were performed with Excel2010 (Microsoft) and statistical analyses were computed with SPSS22 (IBM).

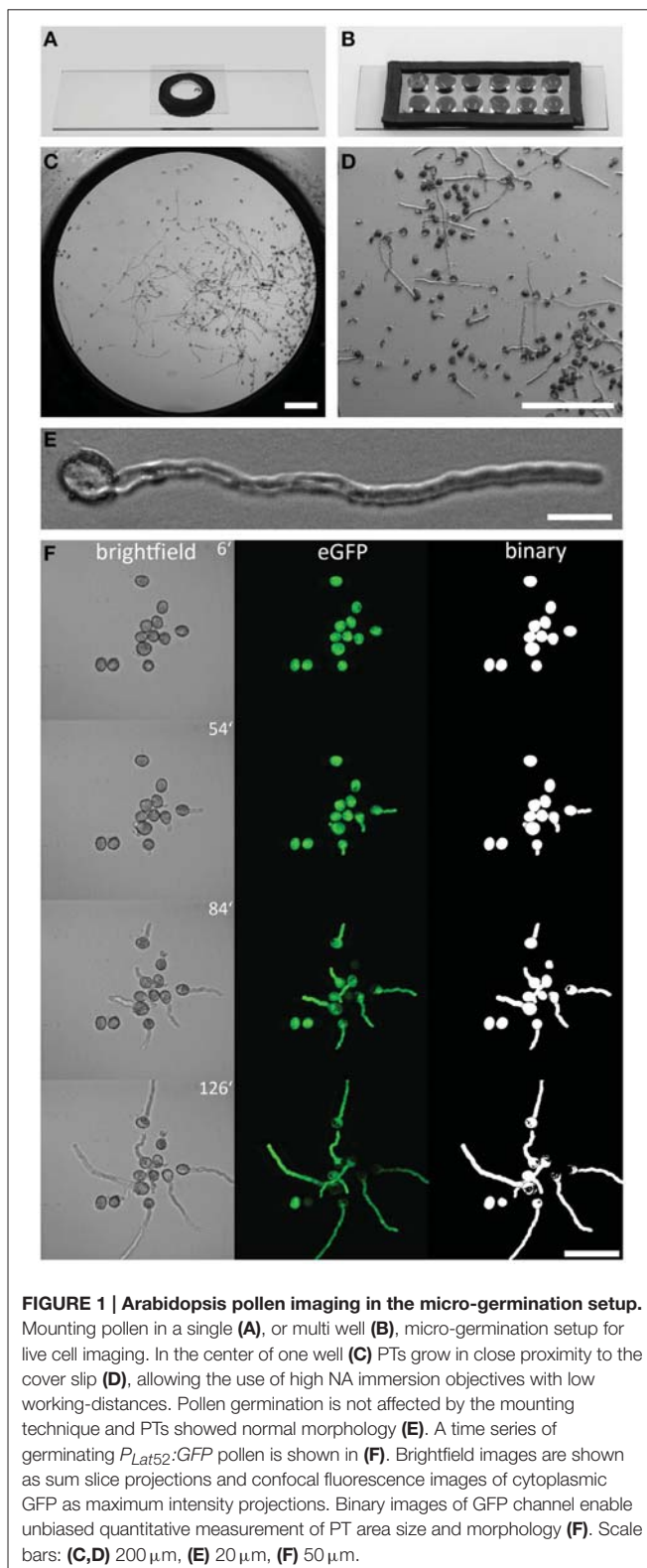
Results

Live Cell Imaging of Pollen Germination and PT Growth

To facilitate time lapse live cell imaging of Arabidopsis pollen germination and PT growth using high NA immersion objectives, we designed a single-well and a multi-well micro-germination setup as shown in **Figures 1A,B**. Both setups are fast and easy to prepare (see **Figures S1,S2**), based on inexpensive components. Pollen germination and PT growth of up to 12 genetically different plants can be simultaneously observed over many hours when using the 12-well micro-germination setup. Pollen germinates in the direct proximity to the cover slip in a film of PGM that is formed when the cover slip is gently pressed on the medium to seal the well (**Figure 1C**). Pollen germination rates within this film are very high (>80%) and homogeneous (**Figures 1D,F**), with normal PT morphology (**Figure 1E**). In an exemplary 10 well-setup, no temporal or morphological deviations in pollen germination or PT growth were observed (**Supplemental Movie 1**). This technique can be broadly used in every lab, adapted to many microscopic techniques and may be even up-scaled for the simultaneous imaging of pollen from more than 12 individuals.

Pollen Tube Growth Kinetics

We evaluated a total of 66 PTs expressing cytoplasmic GFP in the PT vegetative cell that fulfilled our quality criteria for quantitative PT analyses, that is the absence of any obstacle during germination and growth and the complete recording of at least 1 h after germination. As PTs represent 3-dimensional cylindrical objects, we did not determine PT length in μ m but measured the PT as area in μ m². Automatic size measurements using the WAND tool (ImageJ) were performed with thresholded binary images of maximum intensity projections (**Figure 2A**). The growth kinetics of this PT is depicted as frame-wise increase in PT area and as cumulative increase in PT area over time, respectively (**Figure 2B**). After germination, no marked increase in PT area can be observed during the first 21 min of PT growth. Twenty four minutes after germination, PT growth strongly increases and



rises even more after 42 min. Comparing the growth rate determined by PT area measurements with PT length as a measure of growth revealed similar growth kinetics (Figure S4). When

we estimated the ratio of PT length to PT area over time, we calculated an approximated conversion factor of $0.18 \mu\text{m}^{-1}$ for transferring PT area (μm^2) in PT length (μm).

When all 66 PTs were included into the quantification of growth kinetics, a high overall PT growth rate of $400.2 \mu\text{m}^2/\text{h}$ (mean cumulative PT area) was observed (Figure 2C). We observed no or only very low increase in the PT area during the first 12 min of PT formation, resembling a lag phase. To statistically test this, we compared the mean PT area increase rate for the first and the last 10 frames of PT growth (inset in Figure 2C). In almost all cases (59 of 66), the mean PT area increase during the first 30 min was lower than for the last 30 min. Friedman's 2-way variance analysis revealed that PT growth during the first 30 min is highly significantly slower ($p < 0.001$) than during the last 30 min.

From these results we conclude that PT growth in Arabidopsis starts with a first distinct phase of slow growth shortly after germination that is followed by a second phase of rapid PT growth. This is furthermore corroborated by the finding that in case of PT burst, also a short protuberance is first initiated but obviously does not pass over to the next phase of rapid elongation (Figure 2D). A later short phase of decelerated growth could be observed in about one third (21 of 66) of all PTs investigated (Figure 2B). This lag phase occurred when PTs reached a mean size of approximately $200 \mu\text{m}^2$ and it was more variable and less pronounced (Figure 2B; Figure S5).

Changes in PT Shape after Pollen Germination

We investigated the PT morphologies during germination and the transition to rapid tip growth in more detail and compared them with two extreme morphological models describing possible PT geometries. The "protrusion model" assumes that a PT would emerge from the pollen grain as an elongating cylinder with a dome-shaped tip that is maintained during germination and rapid tip growth (Figure 2E). As a result the diameter of the junction between the pollen grain and the PT, which is the site of germination, would remain rather constant in this model. By contrast the "bulging model" assumes that the PT initially exhibits isodiametric growth, leading to a round bulge emerging at the germination site (Figure 2F, red arrowhead). In a second phase, isodiametric growth would have to switch to polar tip growth by selecting a growth site and forming an elongating cylinder. A unique feature of the "bulging model" is that the isodiametric inflation of the bulge will increase the diameter of the germination site over time.

The differences between the two morphological models are highlighted in Figure 2G. For both models we determined a similar net increase in PT area and the same width of the dome-shaped tip. When we compared the increase in PT area over time it was indeed almost identical for both models (Figure 2H). We computed the course of "roundness" for both morphological models during germination and found the "roundness" to increase linearly to a sharp peak in the "protrusion model," followed by a rapid decrease when the PT continues to elongate (Figure 2I). In the "bulging model," by contrast, the course of roundness of a germinating PT forms a rather

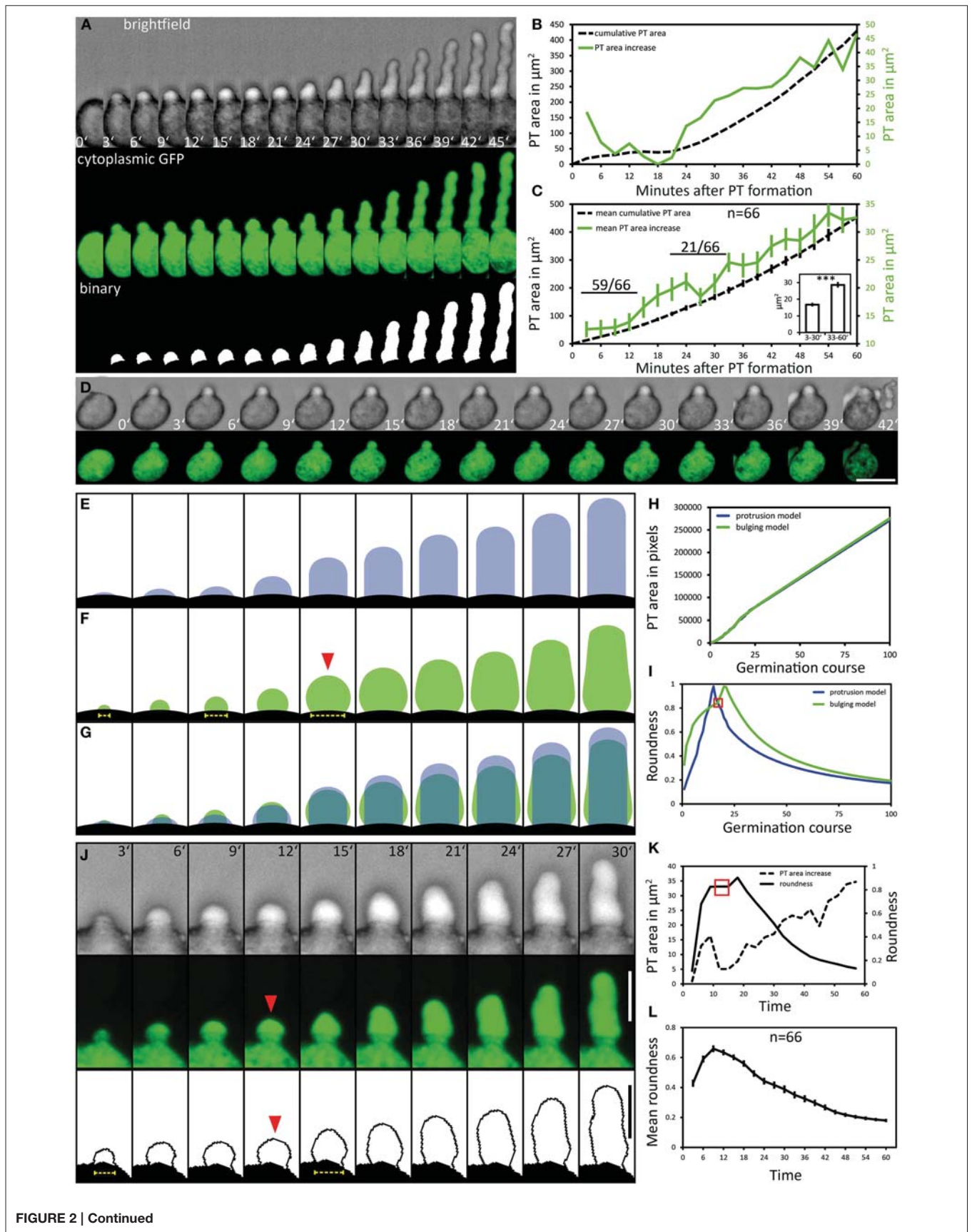


FIGURE 2 | Continued

FIGURE 2 | Pollen tube growth kinetics and morphology changes.

Pollen expressing GFP in the cytoplasm of the vegetative cell ($P_{Lat52}:GFP$) was used to quantitatively assess the kinetics of PT growth and PT morphology during germination. Brightfield and fluorescence channel, together with the binary image generated from the fluorescence channel, are shown in (A). Time point 0' indicates the last frame before germination. The quantification of the cumulative PT area and frame-wise increase in PT areas over time is given in (B). Mean values ± 1 SE of cumulative PT areas and the frame-wise increase in PT areas of 66 evaluated PTs are shown in (C). Numbers in (C) represent the frequency of an observed pattern. The mean frame-wise increase in PT areas for the first 10 frames of each pollen tube is significantly lower compared to the last 10 frames of each PT

[inset of (C); asterisks indicate statistically highly significant differences, $p < 0.001$]. A pollen that germinates but fails to burst after germination is shown in (D). "Protrusion" and "bulging" model for PT morphology changes during pollen germination and PT elongation are shown in (E,F). The overlay of both morphological models is shown in (G), their PT area increase over time is shown in (H). The course of "roundness" for both morphological models is shown in (I). Red solid arrowhead in (F) and red square in (I) highlights the transition from unpolar bulging to polar elongation in the "bulging model." A representative germinating PT is shown in (J) and its course of PT area increase and "roundness" is shown in (K). Mean values ± 1 SE of the "roundness" of 66 PTs are given in (L). Scale bars: (A,B) 25 μm , (J) 12.5 μm .

hyperbolic increasing curve with a broader maximum leading to an accentuated peak (Figure 2I).

Notably, live imaging of germinating pollen revealed considerable similarities to the "bulging model" (Figures 2J,K). During the first 12 min of germination the pollen vegetative cell forms a round bulge at the germination site that exhibits isodiametric growth. Afterwards, the uniformly expanding bulge undergoes the transition into a polar growing PT (Figure 2J; 15' to 18'). The changes in its shape are reflected by the course of "roundness" plotted for this PT (Figure 2K). A hyperbolic increase with a broad maximum (red box in Figure 2K) is characteristic for the phase of bulging. The following peak defines the transition phase, when the bulge starts to form a dome-shaped tip, followed by a switch to rapid tip growth (Figure 2K).

We found the same tendency when we plotted the mean course of "roundness" for all 66 PTs (Figure 2L). Furthermore, in 37 of 66 examined pollen the increasing diameter of the germination site during bulging was clearly visible (Figure 2J, yellow dotted line), which is in line with the unique feature predicted by the "bulging model" (Figure 2F, yellow dotted line).

ARO1-GFP is Associated to Vesicles

In the growing PT the GFP fusion of Armadillo Repeat Only 1 (ARO1) accumulates in the vesicle-rich "clear zone" (Figure 3A; Supplemental Movie 2). We observed partial co-localization of ARO1-GFP fluorescence with FM4-64 in the "clear zone," but almost no co-localization in the subapical part of the PT (Figure 3A). Spinning Disc confocal time-lapse imaging of growing PTs furthermore revealed that ARO1-GFP streams in a reverse fountain pattern (Supplemental Movie 2). The fact that ARO1-GFP accumulates in the PT tip in a brefeldin A-sensitive manner (Gebert et al., 2008) suggested that ARO1-GFP is associated to vesicles in the PT tip.

We performed TIRF microscopy to confirm the proposed vesicle-association of ARO1-GFP. By illuminating only a thin region of the PT tip, including the cytoplasmic zone immediately beneath the PT plasma membrane, we compared the fluorescent signals of ARO1-GFP with that of free GFP. As shown in Figure 3B, ARO1-GFP signals appeared as numerous dot-like structures with a size of approximately 200 nm in the PT tip. In contrast PTs expressing cytoplasmic GFP showed a homogenous fluorescence (Figure 3C).

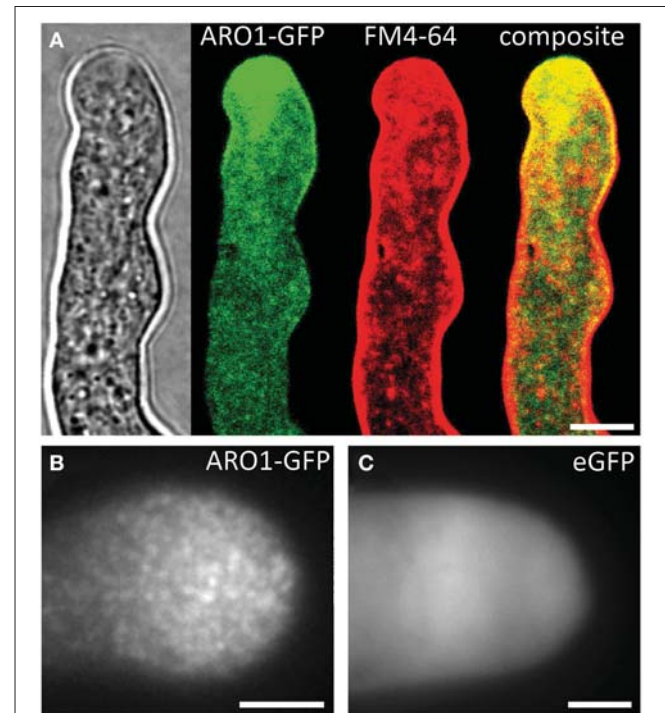
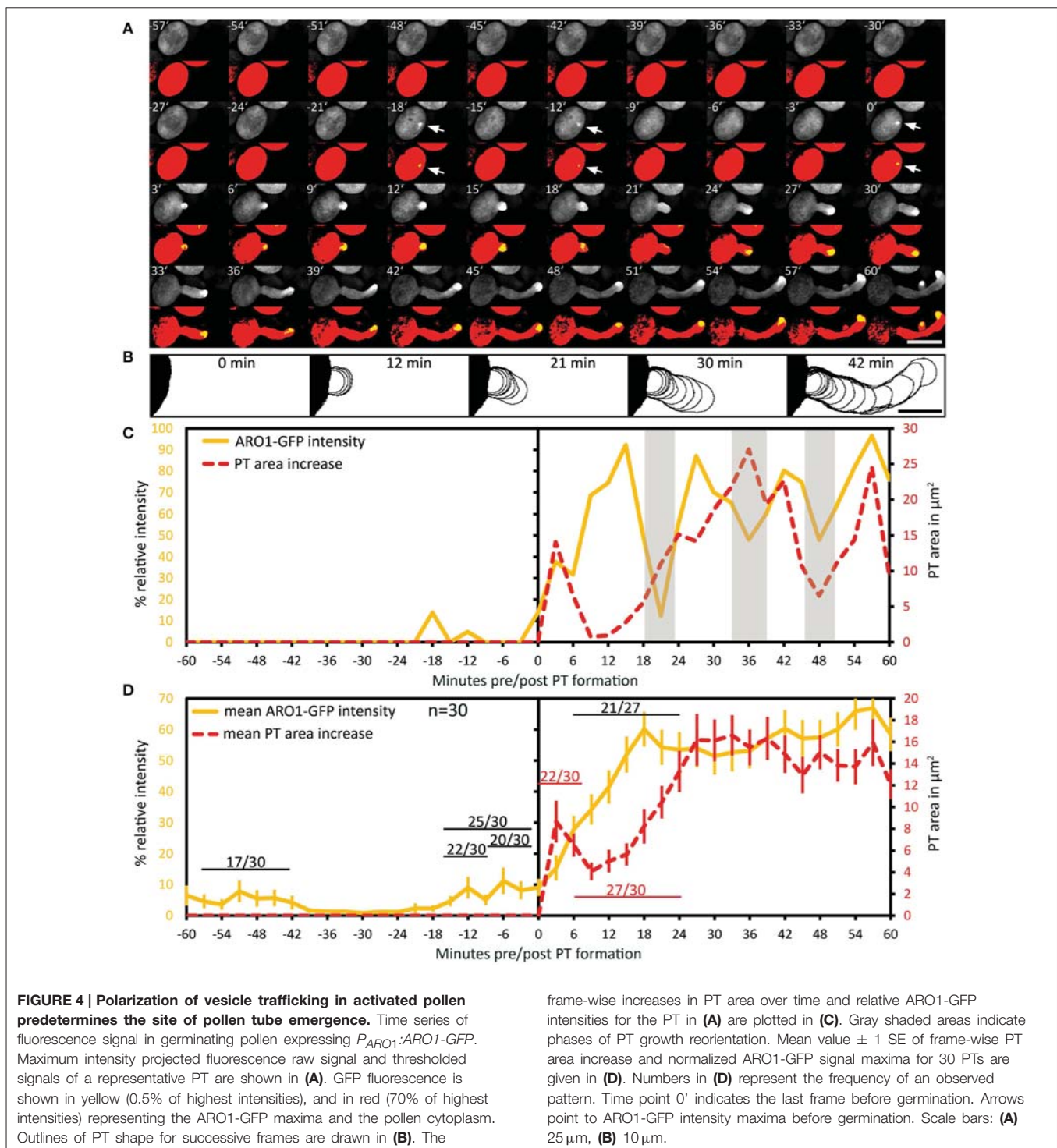


FIGURE 3 | ARO1-GFP localizes to vesicles at the pollen tube tip, accumulating in the inverted cone-shaped region. (A) At the PT tip, ARO1-GFP predominantly accumulates in the vesicle-rich inverted cone-shaped region and partially co-localizes with FM4-64. No co-localization of ARO1-GFP and FM4-64-stained membrane compartments is detected in the subapical region of the PT. **(B)** TIRF microscopy reveals that ARO1-GFP signals appear as discrete punctate structures of approximately 0.2 μm in the PT tip. These punctate structures are not observed in PTs that express cytoplasmic GFP **(C)**. Scale bars: 5 μm .

ARO1-GFP Decorated Vesicles Peak at the Future Germination Site During Pollen Activation

We then investigated the subcellular localization and signal intensity changes of vesicle-associated ARO1-GFP before and during pollen germination using Spinning Disc microscopy (Figure 4A; Supplemental Movie 3). The respective outlines of the frame wise increase in PT area are shown in Figure 4B. The quantification of ARO1-GFP signal intensity in relation to the increase in PT area is given in Figure 4C.



Notably, we observed 18 and 12 min before pollen germination high intensity peaks of ARO1-GFP subjacent to the future site of PT outgrowth (arrows in **Figure 4A**; peaks in **Figure 4C**), resembling two knocks on the door. During the following bulging phase (0–12 min), ARO1-GFP steadily accumulated at the distal pole of the bulge (**Figures 4A,C**). High fluorescence intensities at the PT tip, shaped as inverted cone, were observed when the PT

switched to rapid tip growth (24–60 min), with moderate downturns during short phases of tube growth re-orientation (30–36 min; 45–48 min), which also took place during the transition to rapid tip growth (18–24 min).

The quantitative analysis of 30 PTs is shown in **Figure 4D**. Sixty to thirty six minutes before germination, intensity peaks of ARO1-GFP appeared in 17 out of 30 pollen grains

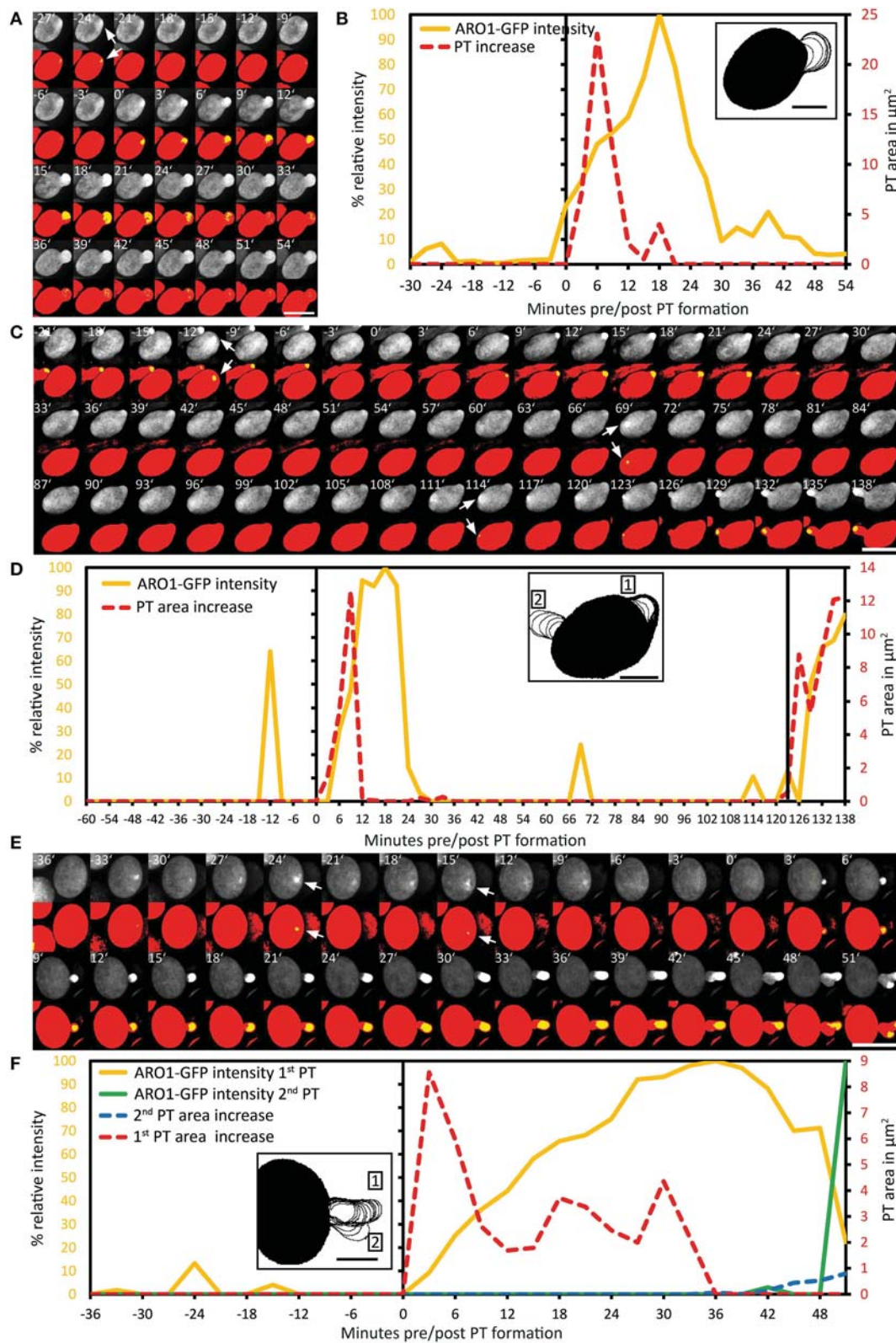


FIGURE 5 | Exceptional pollen germination events confirm the correlation between local vesicle accumulation and pollen tube emergence. The breakdown of vesicle accumulation in the pollen tube

bulge is accompanied with the failure to switch to rapid PT tip growth (A,B). After unsuccessful transition to rapid PT tip growth, the pollen cell may also (Continued)

FIGURE 5 | Continued

change the direction of polar vesicle trafficking, resulting in the establishment of a second germination site, as shown in (C,D). A branching pollen tube is shown in (E,F). After successful bulging the transition to rapid PT tip growth fails and a second growth site is selected, indicated by the accumulation of ARO1-GFP decorated vesicles in the tip of the PT branch. Maximum intensity projected fluorescence raw images and composite thresholded

images are shown in (A,C,E). GFP fluorescence is shown in yellow (0.5% of highest intensities) and in red (70% of highest intensities), representing the ARO1-GFP maxima and the pollen cytoplasm. Frame-wise PT area increase and relative ARO1-GFP intensity are shown in (B,D,F), where insets show frame-wise overlaid PT shape outlines. Time point 0' indicates the last frame before germination. Arrows point to ARO1-GFP intensity maxima before germination. Scale bars: (A,C,E) 25 μm , insets in (B,D,F) 10 μm .

(Supplemental Movie 3). These intensity peaks, indicating rapid and local vesicle accumulation, were often but not always located near the future site of PT outgrowth. However, shortly before germination in 25 out of 30 pollen at least one high-intensity peak was detected subjacent to the future site of PT outgrowth (Figure 4D). 22 of 30 pollen grains showed one peak 12 to 9 min before germination at the future germination site, and in two thirds of observed pollen the ARO1-GFP high-intensity peak was recorded 6 to 3 min before germination. In 50% of the pollen two high-intensity peaks were visible (Supplemental Movie 3), while one third of pollen showed a single peak before germination. Frequencies and statistics of ARO1-GFP intensity peaks in pollen subjacent to the future site of PT outgrowth are shown in Figure S6.

Taken together, the temporary polar accumulation of ARO1-GFP decorated vesicles in activated pollen precedes pollen germination and marks the future site of PT outgrowth. Furthermore, we observed a strong increase of ARO1-GFP signal intensity after bulging, indicating the transition to rapid PT elongation (Figure 4D). Like observed for PTs expressing cytoplasmic GFP, almost all (27 of 30) ARO1-GFP expressing PTs showed an initial lag phase of growth after germination. During this lag phase, including bulging and transition phase, ARO1-GFP signal intensity strongly increased at the distal end of the bulge/dome-shaped tip in 21 of 27 PTs. Nine minutes after ARO1-GFP reached its maximum signal intensity at the tip of the tube, PT elongation rates reached their maxima, recognized by the rapid increase in PT area over time (Figure 4D). By contrast, during the first 9 min of the bulging phase 22 of 30 bulges substantially expanded while the accumulation of ARO1-GFP decorated vesicles at the distal end of the bulge was delayed, suggesting that bulging does not depend on pronounced vesicle trafficking to the very tip of the bulge.

Patterns of Abnormal PT Growth Correlate with Deviating ARO1-GFP Signals

Using our multi-well micro-germination setup a high number of pollen germinated and thus we were able to observe very rare events (less than 3.3%) of abnormal PT growth, such as bulging without subsequent elongation (Figures 5A,B), the initiation of a second PT from one grain (Figures 5C,D) or the branching of a PT (Figures 5E,F).

In the first case of a PT that did not switch to the phase of rapid PT elongation, a high intensity peak of ARO1-GFP signals appeared 24 min before germination at the future site of PT outgrowth (Figures 5A,B). During germination a roundish PT bulge was formed showing isodiametric expansion and constant increase in ARO1-GFP fluorescence intensity with a maximum 18 min after germination. However, during the

following 12 min ARO1-GFP fluorescence rapidly decreased to only 10%, detected 30 min after germination. The decrease in ARO1-GFP signal intensity was accompanied with arrested PT growth (Figures 5A,B).

In one pollen grain a second tube was established during germination (Figures 5C,D). A sharp ARO1-GFP intensity maximum appeared subjacent to the future site of PT outgrowth, 12 min before pollen germination, the area of the bulge increased after pollen germination and ARO1-GFP accumulated in the bulge. However, 21 min after germination, ARO1-GFP fluorescence rapidly decreased and during the following 45 min neither the PT area increased, nor was any ARO1-GFP intensity maximum observed. Sixty nine minutes after first bulging, a new ARO1-GFP intensity maximum arose within the pollen grain, followed by another peak at the same site 45 min later. Nine minutes after the second ARO1-GFP fluorescence maximum the pollen grain started to germinate at this site. After bulging, ARO1-GFP steadily accumulated at the distal end of the second bulge and rapid PT elongation was successfully initiated (Figures 5C,D).

In the case of a branching PT (Figures 5E,F), two maxima of ARO1-GFP intensity occurred 24 and 15 min before pollen germination. During the following phase of bulging, ARO1-GFP signal intensity at the distal end of the bulge steadily increased and reached a maximum in the remarkable long transition phase, 36 min after germination. However, the switch to rapid PT growth did not occur at this site but a second growth site was selected, marked by ARO1-GFP signals appearing at the tip of the branching PT (Figure 5E; 42 min). During the following 6 min ARO1-GFP signal intensity at the first tube tip rapidly decreased while the PT branch expanded. Nine minutes after the PT initiated branching, another ARO1-GFP intensity maximum was detected in the new tip of the PT, while the signal in the old tip diminished (Figures 5E,F; 51 min).

The Actin Cytoskeleton Polarizes Prior to Germination and Undergoes Characteristic Changes during PT Growth

We used the ARO1 promoter to drive moderate expression of the tagRFP-T-Lifect fusion protein in pollen. DAPI staining was performed to visualize the nuclei of the vegetative cell and the sperm cells in pollen grains. Immediately after pollen mounting, the pollen actin cytoskeleton was not distributed with any polarity and showed homogenous accumulation in the cell periphery and pronounced fluorescent signals around the vegetative nucleus (Figures 6A,B), which has also been reported for mature *Brassica napus* pollen (Hause et al., 1992; Gervais et al., 1994).

We germinated tagRFP-T-Lifect expressing pollen in our micro-germination setup and observed that within half an hour

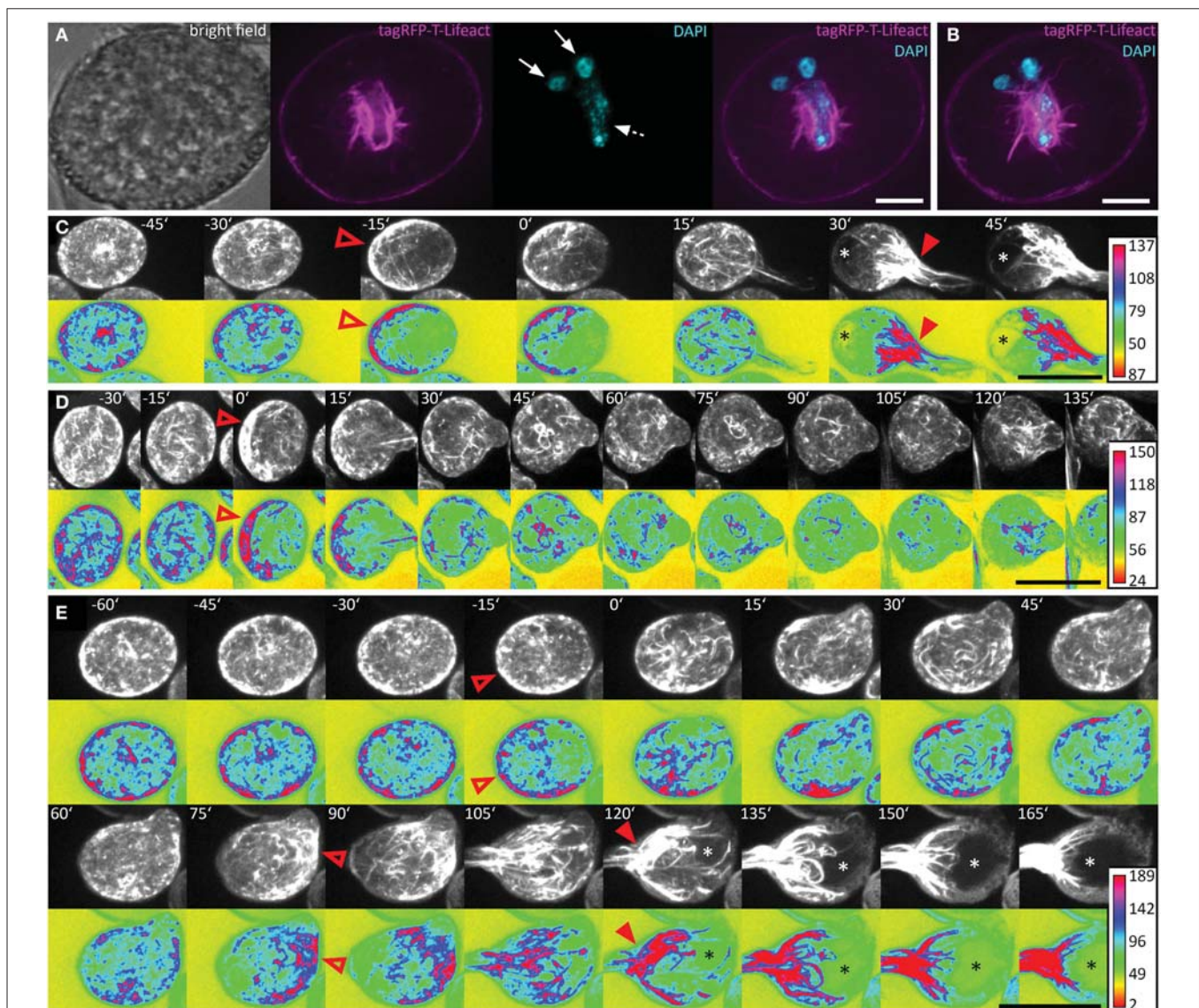


FIGURE 6 | The actin cytoskeleton undergoes characteristic changes during pollen germination. Pollen expressing tagRFP-T-Lifeact was used for live-cell imaging of F-actin architecture and dynamics during pollen germination and growth. A single optical slice through a representative DAPI stained pollen grain is shown in (A). Solid arrows mark the sperm cells and dashed arrows the vegetative nucleus. A composite maximum intensity projection of 19 optical slices is shown in (B), the typical pattern of actin dynamics during pollen germinating is presented in (C). A pronounced F-actin network accumulates at the periphery of the pollen vegetative cell, opposite to the future site of PT outgrowth (open arrowhead). Rapid PT tip growth is associated with

vacuole formation (asterisk) and the massive appearance of parallel F-actin bundles extending from within the pollen grain, into the pollen tube (solid arrowheads). In (D) a PT that failed to switch to rapid PT tip growth after bulging is shown. The germination of a second PT after first unsuccessful bulging is shown in (E). Maximum intensity projections of raw images and intensity based false-colored images are shown in (C–E) with respective calibration bars. Open red arrowheads indicate polar F-actin accumulation at the periphery of the pollen vegetative cell. Solid red arrowheads point at massively accumulating F-actin bundles that extend into the PT. Asterisks mark vacuoles. Time point 0' indicates the last frame before germination. Scale bars: (A) 10 μm , (B) 5 μm (C–E) 25 μm .

before germination F-actin accumulated at the periphery of the pollen vegetative cell, opposite to the future site of PT outgrowth (Figures 6C–E). Almost all (35 of 38) pollen grains showed this pattern of F-actin polarization before germination.

Within 15 min after pollen germination, we observed an increase in longitudinal actin cable formation pointing toward the PT axis and partially reaching into the tube (Figure 6C).

Very articulate actin reorganization appeared in all investigated PTs around 30 min after germination, when the PTs reached a mean size of $300 \pm 17 \mu\text{m}^2$. The actin cytoskeleton assembled at the site of PT outgrowth forming prominent longitudinal F-actin bundles that reached from the pollen grain into the PT. The formation of a large vacuole opposite to the germination site was observed simultaneously with the prominent F-actin assembly

near the site of PT outgrowth (**Figure 6C**). In later stages of PT growth, this dense assembly of F-actin cables was shifted into the PT (**Supplemental Movie 4**).

Again, we looked for exceptional germination scenarios and identified a PT that stopped growth after bulging (**Figure 6D**) and a PT that initiated a second tube from one pollen grain (**Figure 6E**). In the case of PT growth arrest after bulging, the F-actin polarized prior to germination at the pole opposite to the germination site and longitudinal actin cables reaching from the pollen grain into the PT bulge were present 15 min after germination. However after 30 min, the actin cytoskeleton started to depolarize and transition to rapid tip growth was not initiated (**Figure 6D**).

In the case of additional tube formation from one pollen grain, 15 min before germination the actin cytoskeleton accumulated at the periphery, opposite to the future site of PT outgrowth but after bulge formation, the F-actin almost completely depolarized until 60 min after the first germination (**Figure 6E**). F-actin repolarization was observed 75 min after the first germination event, opposing to the site where the second tube bulged later on. Fifteen to thirty minutes after the second F-actin polarization was observed at the periphery of the pollen vegetative cell, a second bulge was formed and underwent transition to rapid tip growth, showing all F-actin features of a normal growing PT.

Sperm Cell Transport Starts When the Switch to Rapid Tip Growth Has Taken Place

We used a marker line showing RFP fluorescence in the sperm cell nuclei and GFP fluorescence in the sperm cell plasma membranes to investigate whether the two sperm cells are relocated into the PT at a distinct growth phase (**Supplemental Movie 5**). The GFP-labeled sperm cell membranes show that the two sperm cells are closely interlinked and that one long membrane extension connects one of the sperm cells to the nucleus of the vegetative cell (**Figure 7**), thereby forming a transport unit known as the male germ unit (MGU). In *Arabidopsis*, the entrance of the three MGU components into the PT follows a regular order, both in planta (Lalanne and Twell, 2002) and in *in vitro* germinated

pollen (Zhou and Meier, 2014): the vegetative nucleus always precedes the sperm cells during entrance into the PT (Lalanne and Twell, 2002; own observations).

The tip of the GFP labeled long membrane extension of the leading sperm was used as a tracer for the position of the vegetative nucleus as it is hooked up to the vegetative nucleus. We defined the time point of MGU relocation into the PT when the tip of the sperm membrane extension became permanently visible outside the pollen grain (**Figure 7A**, green arrowhead). From 34 PTs we calculated a mean PT size of $350 \pm 13 \mu\text{m}^2$ at the time point of MGU translocation into the PT (**Figure 7B**), indicating that the sperm cell transport into the PT does not occur at random but when the PT has reached a certain length and growth phase. Two processes associated with rapid PT tip growth, the formation of a large vacuole within the pollen grain and the accumulation of prominent F-actin cables at the base of the growing PT (**Figure 7B**), have already taken place when we detected the sperm membrane extension in the PT.

Discussion

The PT is an attractive model for the analysis of tip growth mechanisms on the molecular and cellular level, especially in plant species amenable to forward genetic screens and with excellent genomic and bioinformatic resources such as *Arabidopsis thaliana*. Nevertheless, quantitative imaging of growing *Arabidopsis* PTs remained challenging, due to highly variable pollen germination rates in different experiments.

Here, we describe an inexpensive and easy mounting technique to simultaneously track germinating pollen from up to 12 genetically different plants. Our multi-well germination-slide with modified pollen germination medium yields high germination percentages and allows live cell imaging and subsequent quantitative image analysis of the whole process of *Arabidopsis* pollen activation, germination, and the establishment of polar tip growth.

By using our setup and pollen from different fluorescent marker lines we were able to precisely describe the kinetics of

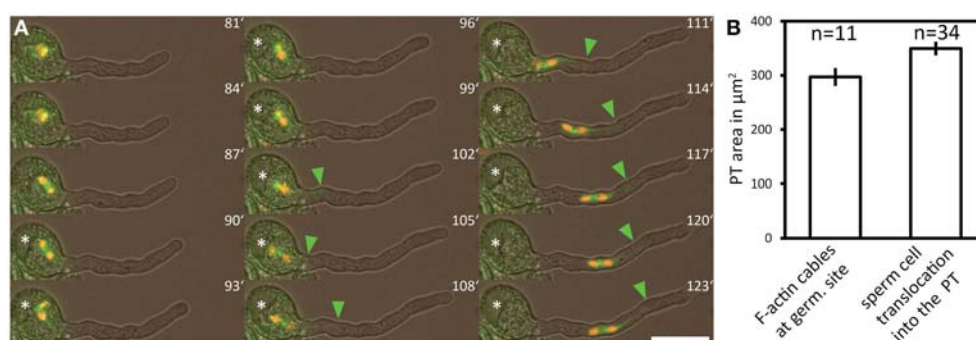


FIGURE 7 | The male germ unit is transported into the PT after the transition to rapid tip growth. A marker line labeling both sperm nuclei (red fluorescence) and the sperm plasma membrane (green fluorescence) was used for time lapse imaging of pollen germination. **(A)** Green arrowhead points to the tip of the long sperm cell membrane extension physically

associated to the vegetative cell nucleus, which has been transported into the pollen tube. Bar plots in **(B)** show average PT areas when F-actin bundles massively accumulate at the germination site (indication for rapid tip growth), compared to the mean PT area when the male germ unit is relocated into the PT. Scale bar in **(A)**: $25 \mu\text{m}$.

Arabidopsis pollen germination *in vitro*. We expressed tagRFP-T-Lifeact in pollen to investigate F-actin dynamics during pollen activation, germination and tube growth, as Lifeact has become the actin marker of choice in the PT (Qu et al., 2015). Vesicles within the pollen grain and the germinating PT were visualized by ARO1-GFP (Gebert et al., 2008). The accumulation of ARO1-GFP in the apical region of growing PTs and the rapid dissipation of this tip localization by brefeldin A treatment is reminiscent of YFP-RabA4d, an exocytotic vesicle marker of PTs (Lee et al., 2008; Szumlanski and Nielsen, 2009), and of GFP-Rab11b-tagged vesicles in tobacco PTs (de Graaf et al., 2005; Cheung and Wu, 2008). Transport vesicles in the tip of angiosperm PTs are known to follow a reverse fountain-streaming pattern (for review see Bove et al., 2008; Cheung and Wu, 2008; Chebli et al., 2013), as is the case for ARO1-GFP (**Supplemental Movie 2**). By TIRF microscopy, a method that has been successfully used to image secretory vesicles in *Picea meyeri* PTs (Wang et al., 2006), we were able to show that ARO1-GFP is associated to vesicles in the PT tip. The size of the punctate ARO1-GFP signals was approximately 200 nm in diameter, which is very close to the calculated size of 182 nm described for vesicles in Arabidopsis PTs (Ketelaar et al., 2008). Based on the vesicle-like appearance of ARO1-GFP in TIRF microscopy, its reverse fountain-streaming pattern and the BFA sensitive tip localization we conclude that ARO1-GFP shows a bona-fide vesicle association in the tip of growing PTs.

Germinating Arabidopsis Pollen Reveal Characteristic Tube Morphologies and Growth Kinetics, Accompanied with F-actin and Vesicle Polarization

Tip growing cells confine cellular expansion to a small area. The occurrence of a single growth site includes at least two distinct phases: the initiation of growth and the elongation phase (Geitmann, 2010). Our quantitative imaging of tube morphologies and growth kinetics enabled us to dissect the early events of germination and to define characteristic features associated with distinct phases (**Figure 8**). We observed successive phases of cell polarization before germination, bulge formation at the beginning of PT germination, the transition to polar growth and subsequent initiation of rapid tip growth.

The germination phase is characterized by an emerging PT that shows isodiametric expansion at the germination site. Some longer F-actin bundles become visible during that phase, extending from within the pollen grain into the bulge (**Figure 8B**). The growth rate of the expanding bulge, measured as increase in area over time, is rather slow during the first 15 min ($16.7 \pm 1.1 \mu\text{m}^2$), compared with later tube growth of $57.0 \pm 4.0 \mu\text{m}^2$ at 45–60 min after germination. In our experimental setup this slower growth phase persists on average 30 min and includes the transition phase (**Figure 8C**) in which the bulge slightly elongates and adopts a dome-shaped form before switching to the phase of rapid tip growth. Notably, we observed that the bulge expands while the accumulation of ARO1-GFP associated vesicles at the distal end of the bulge is slightly delayed. The fact that the Arabidopsis PT starts forming a uniformly expanding bulge before vesicles massively accumulate at the future site of polar

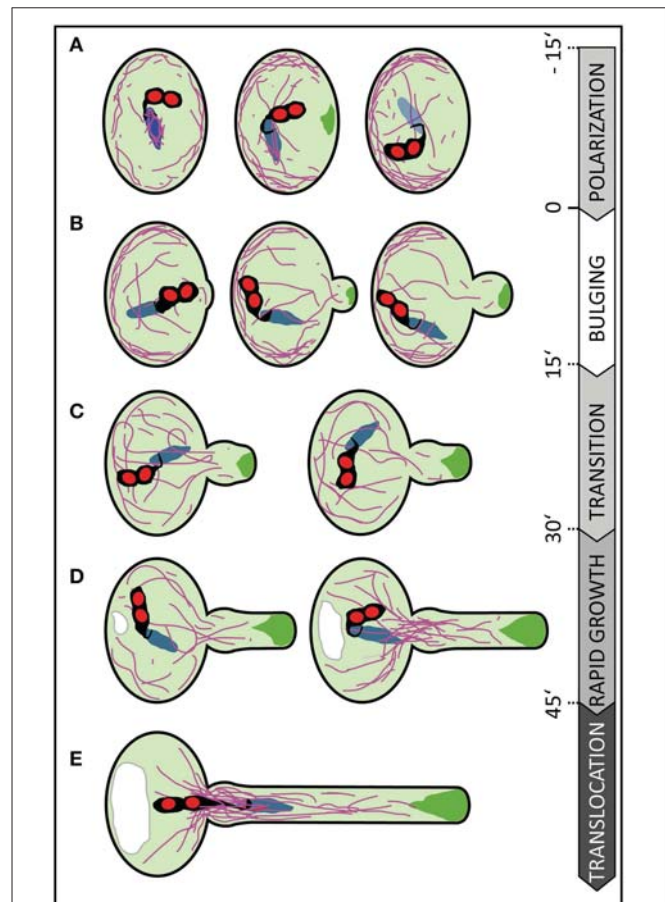


FIGURE 8 | Scheme summarizing subcellular changes observed during five different phases of pollen germination and tube growth.

At least five distinct phases were recognized in our live cell imaging studies on *in vitro* germinating Arabidopsis pollen. **(A)** In early rehydrating pollen F-actin is uniformly distributed at the pollen cell cortex and forms prominent bundles around the vegetative nucleus. Polarization of the pollen grain is indicated by ARO1-GFP decorated vesicles, transiently accumulating subjacent to the future germination site approximately 3–20 min prior germination, and by F-actin accumulating at the cell periphery, in the half of the pollen vegetative cell opposite to the later germination site. **(B)** During the following bulging phase a local protuberance becomes visible, showing isodiametric expansion. ARO1-GFP decorated vesicles start to accumulate in the bulge and first longitudinal F-actin bundles extend from the grain into the bulge. **(C)** The transition phase is indicated when the bulge becomes slightly tubular-shaped. Transition to tip growth is accompanied by a strong accumulation of ARO1-GFP decorated vesicles in the shape of an inverted cone and by the reorganization of the actin cytoskeleton. The polar dense F-actin at the cell periphery of the pollen grain dissipates and long actin bundles, often oriented toward the emerging PT, arise. **(D)** During the subsequent phase of rapid tip growth the PT area increases significantly. A vacuole is formed in the pollen grain, across from the germination site and F-actin bundles start to extend from within the pollen grain into the pollen tube. The accumulation of ARO1-GFP-decorated vesicles in the very tip of the growing pollen tube is most pronounced. **(E)** The translocation phase is initiated when the MGU becomes transported into the growing pollen tube. Sperm cell translocation is preceded by the formation of massive parallel F-actin bundles at the germination site. The vacuole in the pollen grain rapidly enlarges. Objects are not to scale. Color code: purple lines, F-actin; green areas, ARO1-GFP; red areas, sperm cell nuclei; black areas surrounding sperm cell nuclei, sperm cell membranes and cytoplasm; blue area, vegetative cell nucleus. Numbers indicate approximate time points for each phase before or after germination in minutes.

growth suggest that the bulging phase represents a rather turgor-driven deformation process, like assumed by Geitmann (2010). It furthermore indicates that the transition phase was preceded by the selection of a defined plasma membrane region for local exocytosis within the bulge. Thus, the burst of PTs soon after germination, especially observed in a number of pollen mutants such as *aro1-3* and *seth4* (Lalanne et al., 2004; Gebert et al., 2008), may be a turgor-driven event when the establishment of a local growth site was unsuccessful.

ARO1-GFP labeled vesicles heavily accumulate at the distal end of the bulge and finally adopt an inverted cone-like shape (Supplemental Movie 3). In elongating PTs the inverted cone-shaped zone at their apex is referred to as the “clear zone,” because this region is almost exclusively occupied by vesicles but lacks refracting starch containing amyloplasts (Hepler and Winship, 2015). The establishment of the vesicle-rich “clear zone” depends on acto-myosin-dependent long distance transport of vesicles toward the tip of the PT. This transport is mediated by F-actin cables, which are oriented parallel to the longitudinal axis of the PT and a cortical network of fine filaments located in the subapical region of the cell (Cai and Cresti, 2009; Chebli et al., 2013). Cortical actin filaments in the shank of angiosperm PTs are believed to be oriented with their barbed ends toward the apex, while the central actin bundles are thought to comprise filaments with the barbed ends pointing backwards (Chebli et al., 2013). The resulting reverse fountain-like cytoplasmic streaming observed in angiosperm PTs is likely to be involved in maintaining the “clear zone” by producing a constant shear between the anterograde and retrograde transport lanes, by which many of the vesicles, especially those near the surface of the inverted cone, will re-enter the tipward lanes and flow back to the apex (Hepler and Winship, 2015). Thus, the local accumulation and inverted cone-shaped appearance of ARO1-GFP labeled vesicles at the end of the bulging phase indicate that a distinct growth site has been selected, which also becomes apparent by the change in PT morphology and the increase in the median growth rate in the following transition phase (Figure 8C).

When rapid tip growth is initiated (Figure 8D), longitudinal actin cables extend from the pollen grain toward the apex of the PT and the volume of the vacuole opposite the germination site continuously increases. We observed the appearance of massive F-actin bundles near the germination site, extending from the pollen grain into the PT, when the PT area reached the average size of $300 \mu\text{m}^2$. Likewise, Rhodamine-phalloidin staining of *Pyrus communis* PTs showed articulate staining of actin at the PT base and of cables ranging into the tube (Tiwari and Polito, 1988). Notably, the male germ unit, comprising the two sperm cells associated to the vegetative cell nucleus, is transported from the pollen grain into the PT only when the PT completed its transition to rapid tip growth. In our experimental setup we detected the long membrane extension connecting the leading sperm cell to the vegetative nucleus in the PT when its area is $350 \pm 13 \mu\text{m}^2$ (Figure 8E), which equals to a PT length of $63 \pm 2.3 \mu\text{m}$. Zhou and Meier (2014) determined a PT length of approximately $35 \pm 10 \mu\text{m}$ when the vegetative cell nucleus permanently enters the PT. This difference may

be attributed to a different experimental setup but also to the fact that Zhou and Meier (2014) used a marker line with a mCherry-labeled vegetative nucleus rather than labeled sperm nuclei and membranes as we did. While sperm cell nuclei are spheres, the vegetative nucleus is elongated and irregularly shaped and can reach a remarkable length ($>20 \mu\text{m}$) in the growing PT.

New Insights into Arabidopsis Pollen Activation, Provided by Live Imaging of Vesicle Dynamics and F-actin

Most pollen grains are metabolically quiescent and highly desiccated (Edlund et al., 2004). They need to attain a certain degree of hydration before they germinate, which will increase the turgor and transform the unpolar pollen grain to a highly polarized cell, a process termed pollen activation. In the past many studies were performed on morphological and ultrastructural changes in activated pollen revealing that, inter alia, the grain starts to organize its cytoskeleton and endoplasmic reticulum, and forms secretory vesicles (Raghavan, 1997 and references cited therein). Depending on the species examined, PTs either grow out of preformed germinal pores (apertures) or break directly through the exine wall, as is the case with Arabidopsis pollen grains. The presence of cytoplasmic vesicles subjacent to the aperture was detected by ultrastructural studies on pollen from *Lycopersicon peruvianum*, *Nicotiana glauca* and *Narcissus pseudonarcissus* L. (Cresti et al., 1977, 1985; Heslop-Harrison and Heslop-Harrison, 1992). However, it is not yet clear how the pollen perceives external polarization signals and how they are transduced to select the site for tube emergence.

It was reported that the cytoplasmic Ca^{2+} concentration in Arabidopsis pollen increases at the potential germination site soon after hydration (Iwano et al., 2004) and that *in vitro* germination involves the formation of a “germination plaque” at the future site of tube emergence, containing cellulose, callose, pectin, and at least partly de-esterified pectin (Hoedemaekers et al., 2015). When we performed our live cell imaging on the dynamics of ARO-GFP1 labeled vesicles in hydrating pollen grains we observed the initial appearance of weak transient ARO1-GFP signals, arising at various areas of the pollen cell periphery. However, approximately 3–20 min before germination either one or two very strong fluorescent peaks of ARO1-GFP labeled vesicles appeared in the region where the PT protoplast will break through the exine, suggesting targeted vesicle secretion and probably local softening of the cell wall at this site. This would be in line with previous assumptions that vesicles filled with cell wall material and cell wall-modifying enzymes are directed toward the future emergence site to produce a local weak point at which the turgor-driven bulge formation is initiated afterwards (Krichevsky et al., 2007; Geitmann and Ortega, 2009; Cai et al., 2011).

The polarization of the actin cytoskeleton toward the site of tube emergence has been reported in activated *Pyrus communis* pollen (Tiwari and Polito, 1988) by using rhodamine-phalloidin labeling. Similar observations were made by TRITC-phalloidin staining for actin in hydrated *Narcissus pseudonarcissus* pollen (Heslop-Harrison and Heslop-Harrison, 1992). Notably, we

did not observe a similar pattern of polarization in our live imaging setup with hydrating *Arabidopsis* pollen grains expressing tagRFP-T-Lifeact: F-actin mainly accumulated at the cell periphery opposite to the future germination site and no conspicuous polarization toward the site of tube emergence was observed before PT bulging. We assume that the spatial configuration of actin arrays at the periphery of the other half of the activated *Arabidopsis* pollen grain may form a mechanical counter-bearing for the turgor-driven PT bulging.

Species-dependent variations in F-actin polarization during pollen grain activation would be conceivable, on the other hand previous reports using actin-binding proteins or their actin-binding domains have shown that each F-actin marker produces a different labeling pattern (Thomas et al., 2006; Wilsen et al., 2006; Cheung et al., 2008). However, the distribution of the actin cytoskeleton in hydrating *Arabidopsis* pollen grains by fluorescent phalloidin has, to our knowledge, not been investigated in detail and will be difficult to interpret without having any information about the cellular dynamics before and after the moment of fixation.

Conclusions

Our live imaging studies on germinating *Arabidopsis* PTs using the described mounting technique revealed characteristic growth phases and kinetics, together with specific spatiotemporal changes in vesicle transport and actin cytoskeletal organization. The method presented here allows the phenotypic assessment of larger numbers of *in vitro* germinating *Arabidopsis* pollen from wild type and mutant plants by live imaging. It facilitates the analyses of morphological alterations and growth kinetics, and the identification and subcellular localization of players contributing to cell polarity formation and growth site selection in germinating pollen.

Author Contributions

FV and SS designed the experiments, SS directed the project. Generation of constructs and transgenic plants, single- and multi-well micro-germination setup establishment, Spinning Disc microscopy, quantitative image analysis and statistics was carried out by FV. TIRF microscopy was performed by SK. FV wrote the manuscript with input from SK and SS.

References

- Bibikova, T., and Gilroy, S. (2003). Root hair development. *J. Plant Growth Regul.* 21, 383–415. doi: 10.1007/s00344-003-0007-x
- Boavida, L. C., and McCormick, S. (2007). Temperature as a determinant factor for increased and reproducible *in vitro* pollen germination in *Arabidopsis thaliana*. *Plant J.* 52, 570–582. doi: 10.1111/j.1365-313X.2007.03248.x

Acknowledgments

The authors thank David Twell for providing transgenic seeds for *P_{Lat52}:GFP*. Frank Sprenger kindly supported in Spinning Disc microscopy and Karin Koellen assisted in cloning. We thank Maria Enghart for assistance with morphological model and figure preparations and Thomas Dresselhaus and Maria Enghart for fruitful discussions. We are grateful to Thomas Ott for critically reading of the manuscript. This work was supported by grants from the German Research Council (SP686/1-2 to SS and SFB924).

Supplementary Material

The Supplementary Material for this article can be found online at: <http://journal.frontiersin.org/article/10.3389/fpls.2015.00246/abstract>

Supplemental Movie 1 | Time lapse imaging of pollen germinating in the multi-well micro-germination slide. Imaging of ARO1-GFP expressing pollen in an exemplary 10 well micro-germination setup was performed over 6 h. Note that position B1 was readjusted after 1 h PT growth. Time stamper shows hours and minutes. Scale bar: 50 μ m.

Supplemental Movie 2 | Vesicle-associated ARO1-GFP is enriched in the inverted cone-shaped “clear zone” of the pollen tube tip and shows reverse fountain streaming pattern. Time lapse Spinning Disc confocal imaging of ARO1-GFP at the PT tip. Royal LUT was used to highlight increasing signal intensities (low to high: blue to yellow to red to white). Time stamper shows minutes and seconds. Scale bar: 5 μ m.

Supplemental Movie 3 | Polar vesicle accumulation during pollen germination and PT tip growth, indicated by ARO1-GFP intensity changes. Time lapse imaging of a representative pollen expressing ARO1-GFP before germination, during bulging and PT growth. PT outlines are drawn in cyan, ARO1-GFP low-intensity threshold in red (70% highest intensities) and signal maxima in yellow (0.5% highest intensities). White arrowheads point to ARO1-GFP maxima in the ungerminated pollen grain, green arrows indicate ARO1-GFP maxima after germination. Time stamper shows minutes pre/post germination. Scale bar: 10 μ m.

Supplemental Movie 4 | F-actin dynamics during pollen germination and PT tip growth. Time lapse imaging of tagRFP-T-Lifeact expressing pollen before germination and during PT growth. Solid arrowheads highlight F-actin assembly at the periphery of the pollen cell, opposite to the later germination site. Empty arrowheads point at the massive accumulation of F-actin bundles at the PT base, during rapid PT growth. Time stamper shows minutes pre/post germination. Scale bar: 15 μ m.

Supplemental Movie 5 | Sperm cell translocation into the growing PT. Time lapse imaging of germinating pollen with fluorescently labeled sperm cell nuclei and plasma membranes. Solid arrowheads highlight the sperm plasma membrane protrusion that connects one sperm cell to the vegetative cell nucleus. Time stamper shows minutes pre/post germination. Scale bar: 15 μ m.

- Bou Daher, F., Chebli, Y., and Geitmann, A. (2009). Optimization of conditions for germination of cold-stored *Arabidopsis thaliana* pollen. *Plant Cell Rep.* 28, 347–357. doi: 10.1007/s00299-008-0647-1
- Bove, J., Vaillancourt, B., Kroeger, J., Hepler, P. K., Wiseman, P. W., and Geitmann, A. (2008). Magnitude and direction of vesicle dynamics in growing pollen tubes using spatiotemporal image correlation spectroscopy and fluorescence recovery after photobleaching. *Plant Physiol.* 147, 1646–1658. doi: 10.1104/pp.108.120212

- Cai, G., and Cresti, M. (2009). Organelle motility in the pollen tube: a tale of 20 years. *J. Exp. Bot.* 60, 495–508. doi: 10.1093/jxb/ern321
- Cai, G., Faleri, C., Del Casino, C., Emons, A. M., and Cresti, M. (2011). Distribution of callose synthase, cellulose synthase, and sucrose synthase in tobacco pollen tube is controlled in dissimilar ways by actin filaments and microtubules. *Plant Physiol.* 155, 1169–1190. doi: 10.1104/pp.110.171371
- Campanoni, P., and Blatt, M. R. (2007). Membrane trafficking and polar growth in root hairs and pollen tubes. *J. Exp. Bot.* 58, 65–74. doi: 10.1093/jxb/erl059
- Chebli, Y., Kroeger, J., and Geitmann, A. (2013). Transport logistics in pollen tubes. *Mol. Plant* 6, 1037–1052. doi: 10.1093/mp/ss073
- Cheung, A. Y., Boavida, L. C., Aggarwal, M., Wu, H. M., and Feijo, J. A. (2010). The pollen tube journey in the pistil and imaging the *in vivo* process by two-photon microscopy. *J. Exp. Bot.* 61, 1907–1915. doi: 10.1093/jxb/erq062
- Cheung, A. Y., Duan, Q. H., Costa, S. S., de Graaf, B. H., Di Stilio, V. S., Feijo, J., et al. (2008). The dynamic pollen tube cytoskeleton: live cell studies using actin-binding and microtubule-binding reporter proteins. *Mol. Plant* 1, 686–702. doi: 10.1093/mp/ssn026
- Cheung, A. Y., and Wu, H. M. (2008). Structural and signaling networks for the polar cell growth machinery in pollen tubes. *Annu. Rev. Plant Biol.* 59, 547–572. doi: 10.1146/annurev.arplant.59.032607.092921
- Clough, S. J., and Bent, A. F. (1998). Floral dip: a simplified method for Agrobacterium-mediated transformation of *Arabidopsis thaliana*. *Plant J.* 16, 735–743. doi: 10.1046/j.1365-313x.1998.00343.x
- Cresti, M., Ciampolini, F., Mulcahy, D. L. M., and Mulcahy, G. (1985). Ultrastructure of *Nicotiana glauca* pollen, its germination and early tube formation. *Am. J. Bot.* 72, 719–727. doi: 10.2307/2443685
- Cresti, M., Pacini, E., Ciampolini, F., and Sarfatti, G. (1977). Germination and early tube development *in vitro* of *Lycopersicon peruvianum* pollen: ultrastructural features. *Planta* 136, 239–247. doi: 10.1007/BF00385991
- de Graaf, B. H., Cheung, A. Y., Andreyeva, T., Levasseur, K., Kieliszewski, M., and Wu, H. M. (2005). Rab11 GTPase-regulated membrane trafficking is crucial for tip-focused pollen tube growth in tobacco. *Plant Cell* 17, 2564–2579. doi: 10.1105/tpc.105.033183
- Denninger, P., Bleckmann, A., Lausser, A., Vogler, F., Ott, T., Ehrhardt, D. W., et al. (2014). Male-female communication triggers calcium signatures during fertilization in *Arabidopsis*. *Nat. Commun.* 5, 4645. doi: 10.1038/ncomms5645
- Edlund, A. F., Swanson, R., and Preuss, D. (2004). Pollen and stigma structure and function: the role of diversity in pollination. *Plant Cell* 16, S84–S97. doi: 10.1105/tpc.015800
- Feijó, J. A., and Moreno, N. (2004). Imaging plant cells by two-photon excitation. *Protoplasma* 223, 1–32. doi: 10.1007/s00709-003-0026-2
- Gebert, M., Dresselhaus, T., and Sprunck, S. (2008). F-actin organization and pollen tube tip growth in *Arabidopsis* are dependent on the gametophyte-specific Armadillo repeat protein ARO1. *Plant Cell* 20, 2798–2814. doi: 10.1105/tpc.108.061028
- Geitmann, A. (2010). How to shape a cylinder: pollen tube as a model system for the generation of complex cellular geometry. *Sex. Plant Reprod.* 23, 63–71. doi: 10.1007/s00497-009-0121-4
- Geitmann, A., and Ortega, J. K. (2009). Mechanics and modeling of plant cell growth. *Trends Plant Sci.* 14, 467–478. doi: 10.1016/j.tplants.2009.07.006
- Gervais, C., Simmonds, D. H., and Newcomb, W. (1994). Actin microfilament organization during pollen development of *Brassica napus* cv. *Topas*. *Protoplasma* 183, 67–76. doi: 10.1007/BF01276814
- Guan, Y., Guo, J., Li, H., and Yang, Z. (2013). Signaling in pollen tube growth: crosstalk, feedback, and missing links. *Mol. Plant* 6, 1053–1064. doi: 10.1093/mp/ss070
- Hause, G., Hause, B., and Van Lammeren, A. A. M. (1992). Microtubular and actin-filament configurations during microspore and pollen development in *Brassica napus* L. cv. *Topas*. *Can. J. Bot.* 70, 1369–1376. doi: 10.1139/b92-172
- Hepler, P. K., and Winship, L. J. (2015). The pollen tube clear zone: clues to the mechanism of polarized growth. *J. Integr. Plant Biol.* 57, 79–92. doi: 10.1111/jipb.12315
- Heslop-Harrison, Y., and Heslop-Harrison, J. (1992). Germination of monocot angiosperm pollen: evolution of the actin cytoskeleton and wall during hydration, activation and tube emergence. *Annals Bot.* 69, 385–394.
- Hoedemaekers, K., Derksen, J., Hoogstrate, S. W., Wolters-Arts, M., Oh, S.-A., Twell, D., et al. (2015). BURSTING POLLEN is required to organize the pollen germination plaque and pollen tube tip in *Arabidopsis thaliana*. *New Phytol.* 206, 255–267. doi: 10.1111/nph.13200
- Iwano, M., Shiba, H., Miwa, T., Che, F.-S., Takayama, S., Nagai, T., et al. (2004). Ca²⁺ dynamics in a pollen grain and papilla cell during pollination of *Arabidopsis*. *Plant Physiol.* 136, 3562–3571. doi: 10.1104/pp.104.046961
- Johnson-Brousseau, S. A., and McCormick, S. (2004). A compendium of methods useful for characterizing *Arabidopsis* pollen mutants and gametophytically-expressed genes. *Plant J.* 39, 761–775. doi: 10.1111/j.1365-313X.2004.02147.x
- Karimi, M., Inzé, D., and Depicker, A. (2002). GATEWAY™ vectors for Agrobacterium-mediated plant transformation. *Trends Plant Sci.* 7, 193–195. doi: 10.1016/S1360-1385(02)02251-3
- Ketelaar, T., Galway, M. E., Mulder, B. M., and Emons, A. M. (2008). Rates of exocytosis and endocytosis in *Arabidopsis* root hairs and pollen tubes. *J. Microsc.* 231, 265–273. doi: 10.1111/j.1365-2818.2008.02031.x
- Kost, B. (2008). Spatial control of Rho (Rac-Rop) signaling in tip-growing plant cells. *Trends Cell Biol.* 18, 119–127. doi: 10.1016/j.tcb.2008.01.003
- Krichevsky, A., Kozlovsky, S. V., Tian, G. W., Chen, M. H., Zaltsman, A., and Citovsky, V. (2007). How pollen tubes grow. *Dev. Biol.* 303, 405–420. doi: 10.1016/j.ydbio.2006.12.003
- Lalanne, E., Michaelidis, C., Moore, J. M., Gagliano, W., Johnson, A., Patel, R., et al. (2004). Analysis of transposon insertion mutants highlights the diversity of mechanisms underlying male progamic development in *Arabidopsis*. *Genetics* 167, 1975–1986. doi: 10.1534/genetics.104.030270
- Lalanne, E., and Twell, D. (2002). Genetic control of male germ unit organization in *Arabidopsis*. *Plant Physiol.* 129, 865–875. doi: 10.1104/pp.003301
- Lee, Y. J., Szumlanski, A., Nielsen, E., and Yang, Z. (2008). Rho-GTPase-dependent filamentous actin dynamics coordinate vesicle targeting and exocytosis during tip growth. *J. Cell Biol.* 181, 1155–1168. doi: 10.1083/jcb.200801086
- Lee, Y. J., and Yang, Z. (2008). Tip growth: signaling in the apical dome. *Curr. Opin. Plant Biol.* 11, 662–671. doi: 10.1016/j.pbi.2008.10.002
- Mascarenhas, J. P. (1993). Molecular mechanisms of pollen tube growth and differentiation. *Plant Cell* 5, 1303–1314. doi: 10.1105/tpc.5.10.1303
- McCue, A. D., Cresti, M., Feijó, J. A., and Slotkin, R. K. (2011). Cytoplasmic connection of sperm cells to the pollen vegetative cell nucleus: potential roles of the male germ unit revisited. *J. Exp. Bot.* 62, 1621–1631. doi: 10.1093/jxb/err032
- Müller, M., and Schmidt, W. (2004). Environmentally induced plasticity of root hair development in *Arabidopsis*. *Plant Physiol.* 134, 409–419. doi: 10.1104/pp.103.029066
- Parker, J. S., Cavell, A. C., Dolan, L., Roberts, K., and Grierson, C. S. (2000). Genetic interactions during root hair morphogenesis in *Arabidopsis*. *Plant Cell* 12, 1961–1974. doi: 10.1105/tpc.12.10.1961
- Qin, Y., and Yang, Z. (2011). Rapid tip growth: insights from pollen tubes. *Semin. Cell Dev. Biol.* 22, 816–824. doi: 10.1016/j.semcdb.2011.06.004
- Qu, X., Jiang, Y., Chang, M., Liu, X., Zhang, R., and Huang, S. (2015). Organization and regulation of the actin cytoskeleton in the pollen tube. *Front. Plant Sci.* 5:786. doi: 10.3389/fpls.2014.00786
- Raghavan, V. (1997). *Molecular Embryology of Flowering Plants*. Cambridge: Cambridge University Press. doi: 10.1017/CBO9780511574528
- Riedl, J., Crevenna, A. H., Kessenbrock, K., Yu, J. H., Neukirchen, D., Bista, M., et al. (2008). Lifeact: a versatile marker to visualize F-actin. *Nat. Methods* 5, 605–607. doi: 10.1038/nmeth.1220
- Rodriguez-Enriquez, M. J., Mehdi, S., Dickinson, H. G., and Grant-Downton, R. T. (2013). A novel method for efficient *in vitro* germination and tube growth of *Arabidopsis thaliana* pollen. *New Phytol.* 197, 668–679. doi: 10.1111/nph.12037
- Šamaj, J., Müller, J., Beck, M., Böhm, N., and Menzel, D. (2006). Vesicular trafficking, cytoskeleton and signalling in root hairs and pollen tubes. *Trends Plant Sci.* 11, 594–600. doi: 10.1016/j.tplants.2006.10.002
- Sanati Nezhad, A., Packirisamy, M., and Geitmann, A. (2014). Dynamic, high precision targeting of growth modulating agents is able to trigger pollen tube growth reorientation. *Plant J.* 80, 185–195. doi: 10.1111/tpj.12613

- Schiefelbein, J. W. (2000). Constructing a plant cell. The genetic control of root hair development. *Plant Physiol.* 124, 1525–1531. doi: 10.1104/pp.124.4.1525
- Schiefelbein, J. W., and Somerville, C. (1990). Genetic control of root hair development in *Arabidopsis thaliana*. *Plant Cell* 2, 235–243. doi: 10.1105/tpc.2.3.235
- Smyth, D. R., Bowman, J. L., and Meyerowitz, E. M. (1990). Early flower development in *Arabidopsis*. *Plant Cell* 2, 755–767. doi: 10.1105/tpc.2.8.755
- Sprunck, S., Rademacher, S., Vogler, F., Gheyselinck, J., Grossniklaus, U., and Dresselhaus, T. (2012). Egg cell-secreted EC1 triggers sperm cell activation during double fertilization. *Science* 338, 1093–1097. doi: 10.1126/science.1223944
- Steinhorst, L., and Kudla, J. (2013). Calcium - a central regulator of pollen germination and tube growth. *Biochim. Biophys. Acta* 1833, 1573–1581. doi: 10.1016/j.bbamcr.2012.10.009
- Szumanski, A. L., and Nielsen, E. (2009). The Rab GTPase RabA4d regulates pollen tube tip growth in *Arabidopsis thaliana*. *Plant Cell* 21, 526–544. doi: 10.1105/tpc.108.060277
- Taylor, L. P., and Hepler, P. K. (1997). Pollen germination and tube growth. *Annu. Rev. Plant Phys.* 48, 461–491. doi: 10.1146/annurev.arplant.48.1.461
- Thomas, C., Hoffmann, C., Dieterle, M., Van Troys, M., Ampe, C., and Steinmetz, A. (2006). Tobacco WLIM1 is a novel F-actin binding protein involved in actin cytoskeleton remodeling. *Plant Cell* 18, 2194–2206. doi: 10.1105/tpc.106.040956
- Tiwari, S., and Polito, V. (1988). Organization of the cytoskeleton in pollen tubes of *Pyrus communis*: a study employing conventional and freeze-substitution electron microscopy, immunofluorescence, and rhodamine-phalloidin. *Protoplasma* 147, 100–112. doi: 10.1007/BF01403337
- Twell, D., Yamaguchi, J., and McCormick, S. (1990). Pollen-specific gene expression in transgenic plants: coordinate regulation of two different tomato gene promoters during microsporogenesis. *Development* 109, 705–713.
- Vogler, F., Schmalzl, C., Enghart, M., Bircheneder, M., and Sprunck, S. (2014). Brassinosteroids promote *Arabidopsis* pollen germination and growth. *Plant Reprod.* 27, 153–167. doi: 10.1007/s00497-014-0247-x
- Wang, X., Teng, Y., Wang, Q., Li, X., Sheng, X., Zheng, M., et al. (2006). Imaging of dynamic secretory vesicles in living pollen tubes of *Picea meyeri* using evanescent wave microscopy. *Plant Physiol.* 141, 1591–1603. doi: 10.1104/pp.106.080168
- Wilsen, K., Lovy-Wheeler, A., Voigt, B., Menzel, D., Kunkel, J., and Hepler, P. (2006). Imaging the actin cytoskeleton in growing pollen tubes. *Sex. Plant Reprod.* 19, 51–62. doi: 10.1007/s00497-006-0021-9
- Zhou, X., and Meier, I. (2014). Efficient plant male fertility depends on vegetative nuclear movement mediated by two families of plant outer nuclear membrane proteins. *Proc. Natl. Acad. Sci. U.S.A.* 111, 11900–11905. doi: 10.1073/pnas.1323104111

Conflict of Interest Statement: The authors declare that the research was conducted in the absence of any commercial or financial relationships that could be construed as a potential conflict of interest.

Copyright © 2015 Vogler, Konrad and Sprunck. This is an open-access article distributed under the terms of the Creative Commons Attribution License (CC BY). The use, distribution or reproduction in other forums is permitted, provided the original author(s) or licensor are credited and that the original publication in this journal is cited, in accordance with accepted academic practice. No use, distribution or reproduction is permitted which does not comply with these terms.

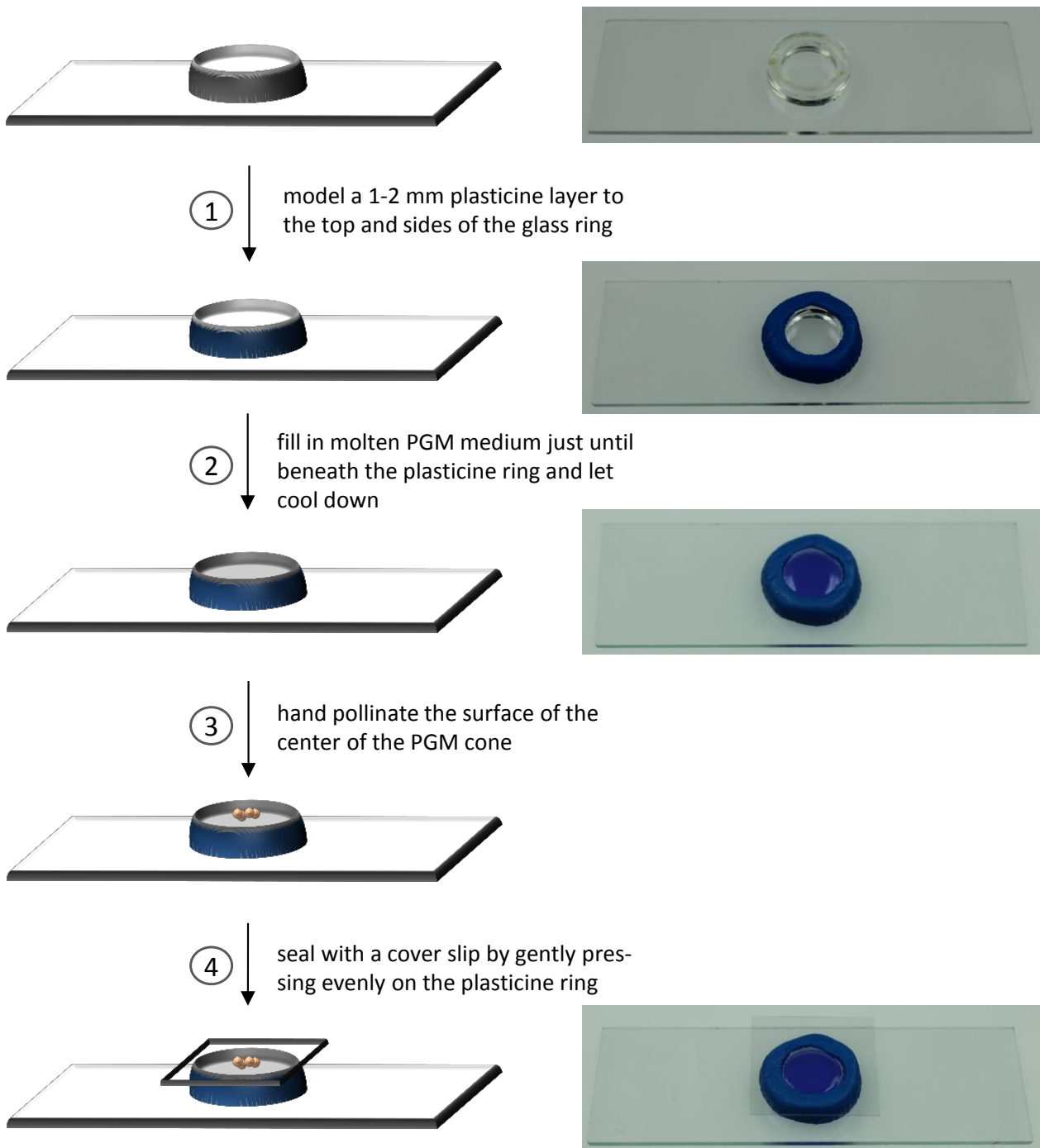


Figure S1: Preparing a single-well micro-germination slide

Mounting scheme as described in Material & Methods section. In the pictures on the right hand side Bromphenol blue was added to the PGM for a better visualization.

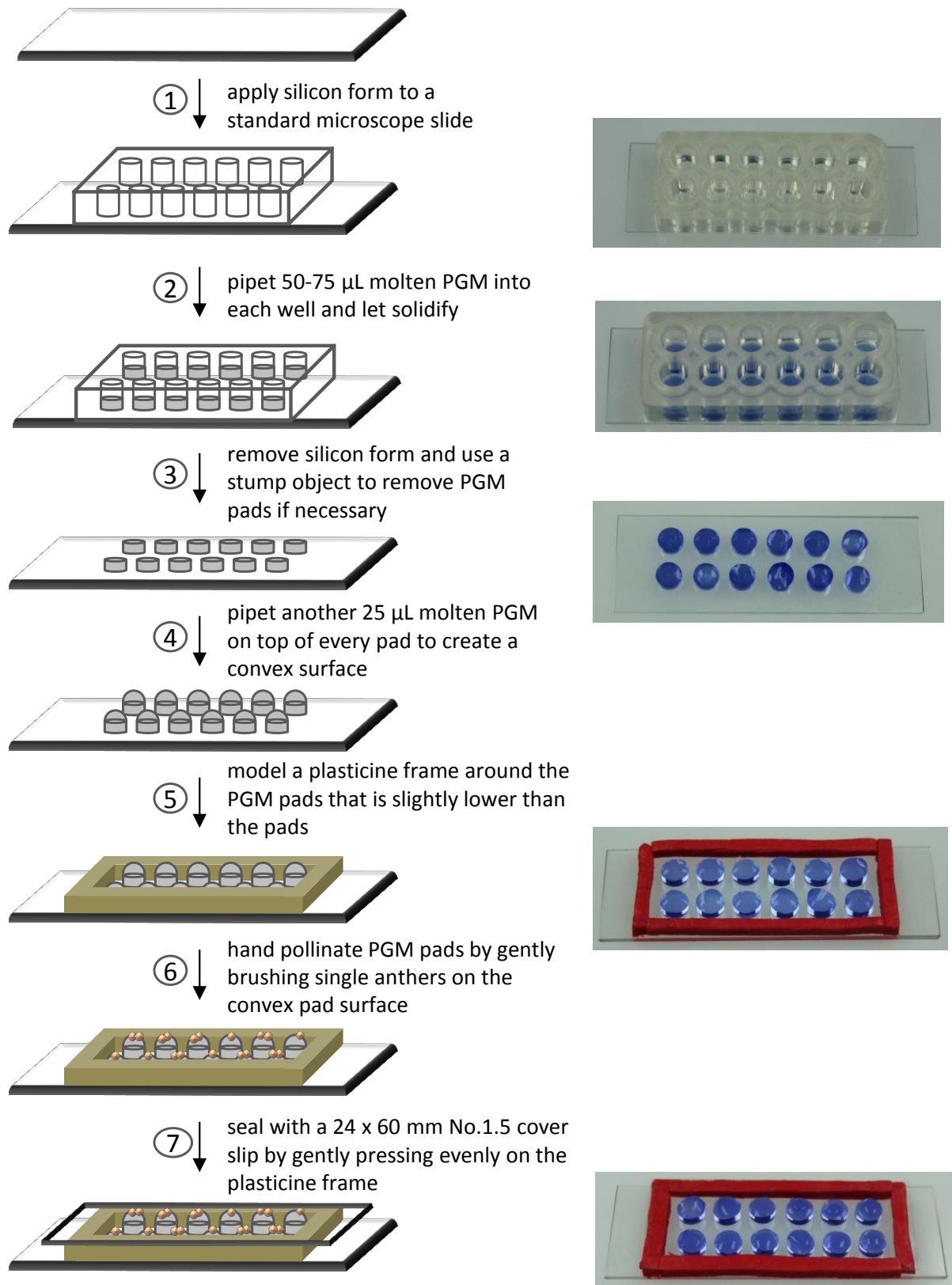


Figure S2: Preparing a multi-well germination slide

Mounting scheme as described in Material & Methods section. In the pictures on the right hand side Bromphenol blue was added to the PGM for a better visualization.

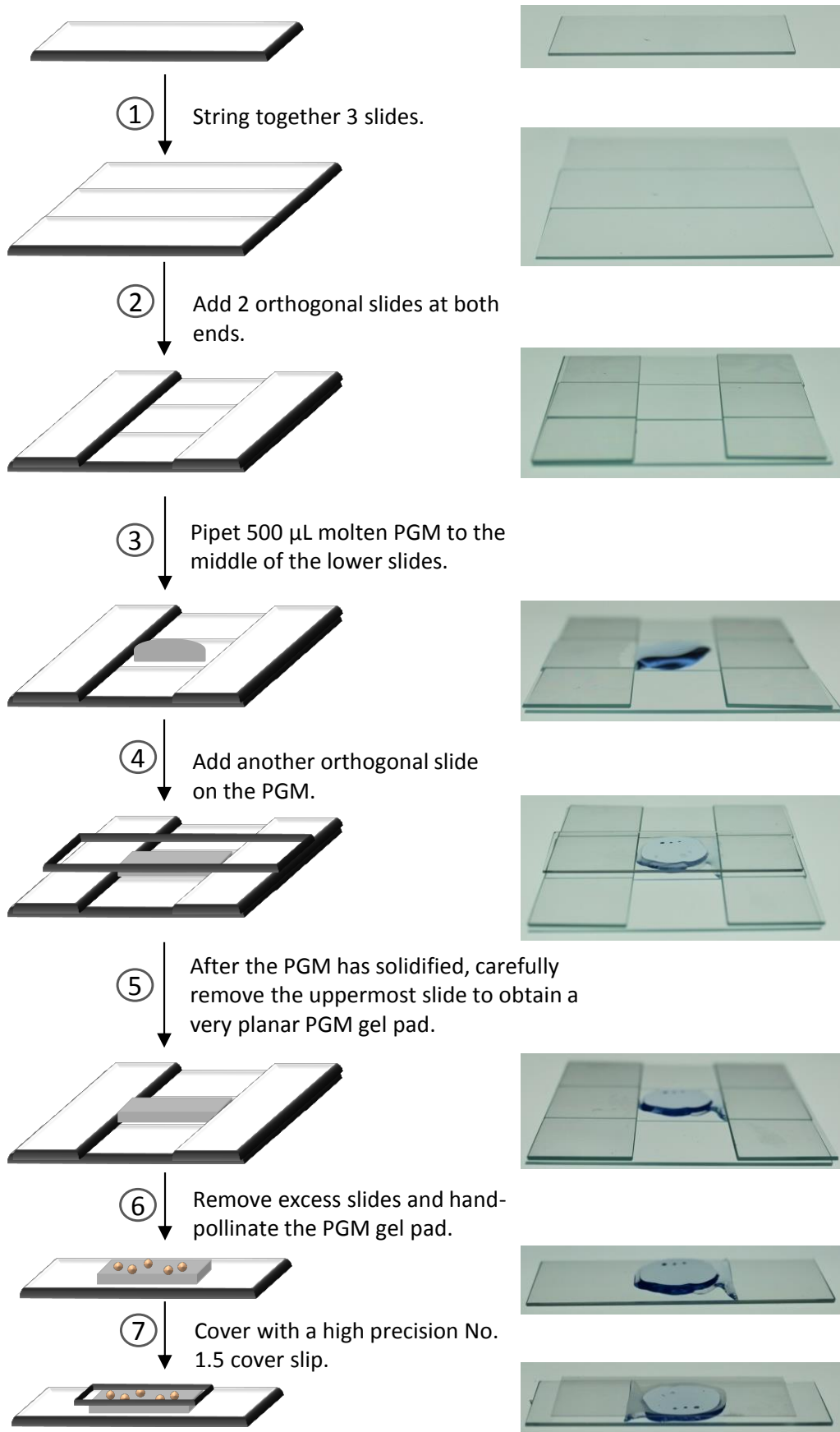


Figure S3: Preparing a germination slide for TIRF microscopy

Mounting scheme as described in Material & Methods section. In the pictures on the right hand side Bromphenol blue was added to the PGM for a better visualization.

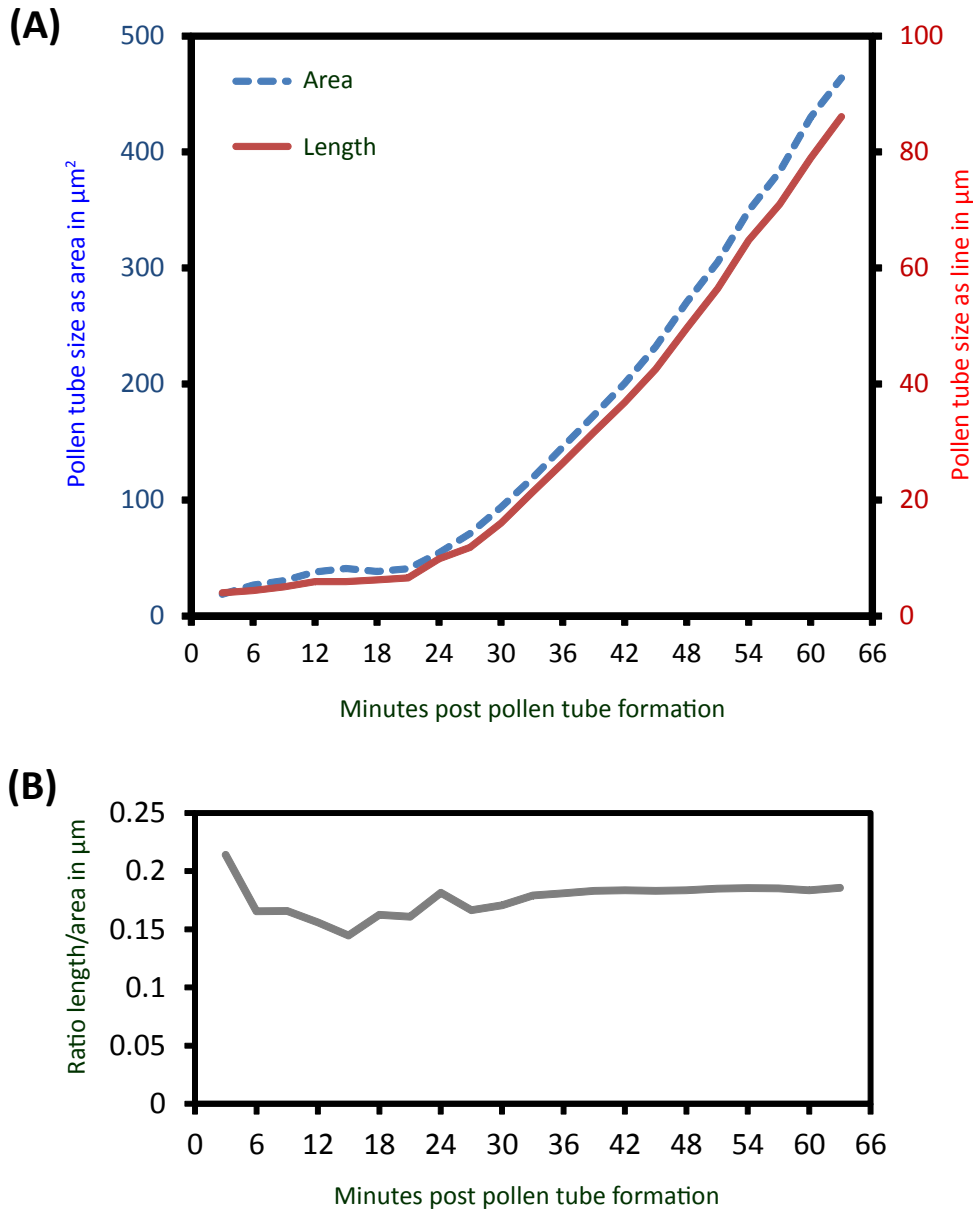


Figure S4: Pollen tube growth kinetics, measured as frame-wise increase in pollen tube area and in pollen tube length

The pollen tube shown in Figure 2A was used to compare its increase in area (μm^2) over time with increasing tube length (μm), measured along a segmented line from the germination site to the PT tip (**A**). The ratio of length and area over time for this PT is shown in (**B**). Note that especially during the first 30 minutes after pollen germination (bulging and transition phase), subtle differences are visible between the two methods, with a slightly better resolution in PT growth dynamics when measuring PT areas. The ratio length/area furthermore reveals that the PT area can be divided by $0.18 \mu\text{m}^{-1}$ which is the mean of all values shown in (**B**), to yield the approximate length of a PT in μm .

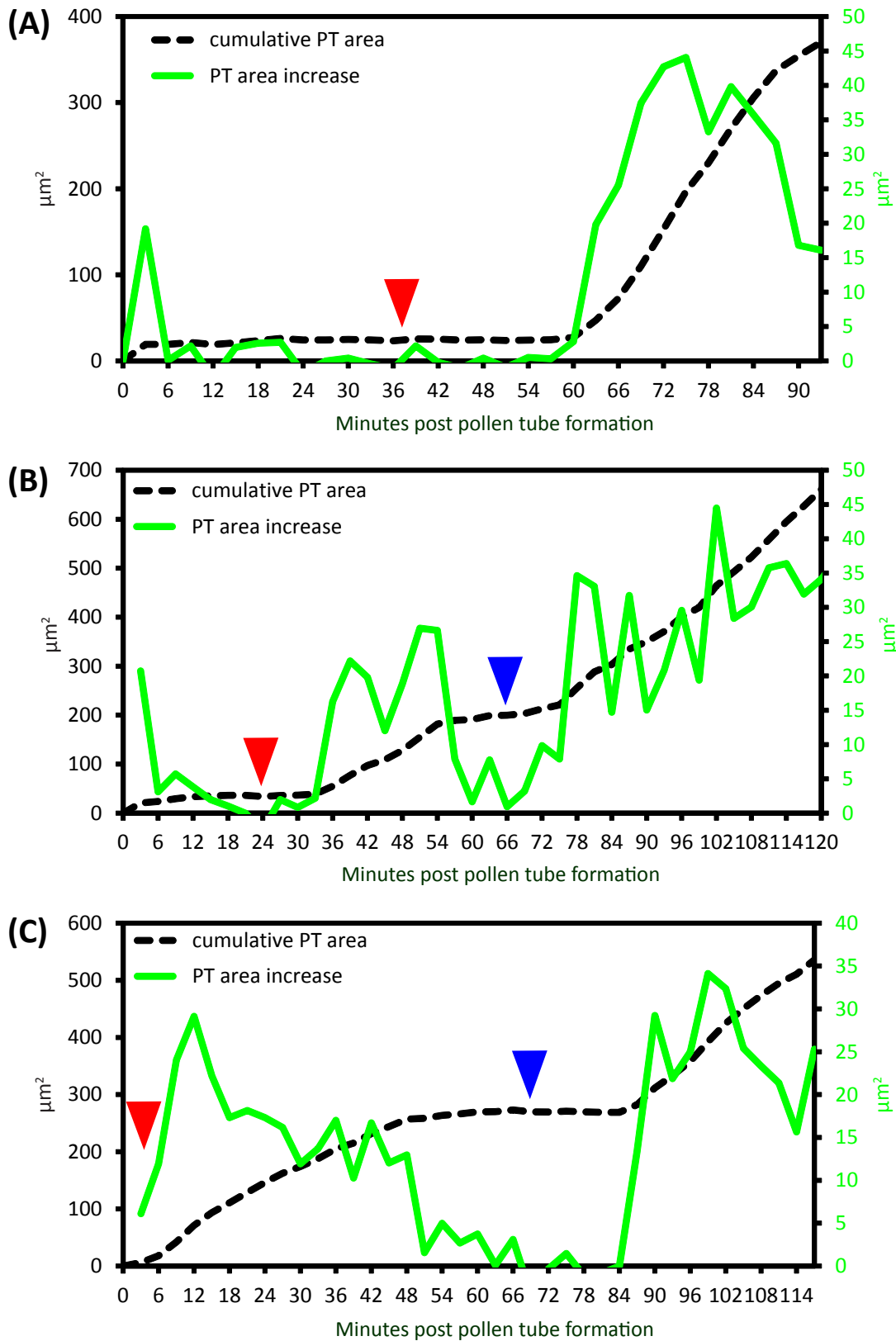


Figure S5: Deviating lag phases observed during in vitro pollen tube growth

PTs exhibiting varying lag phases. (A) PT with extended bulging phase. (B) and (C) show a second lag phase that can eventually be observed during rapid PT growth. Note that in (C) this second lag phase is very pronounced. Red arrowheads mark the first, blue arrowheads the second lag phase.

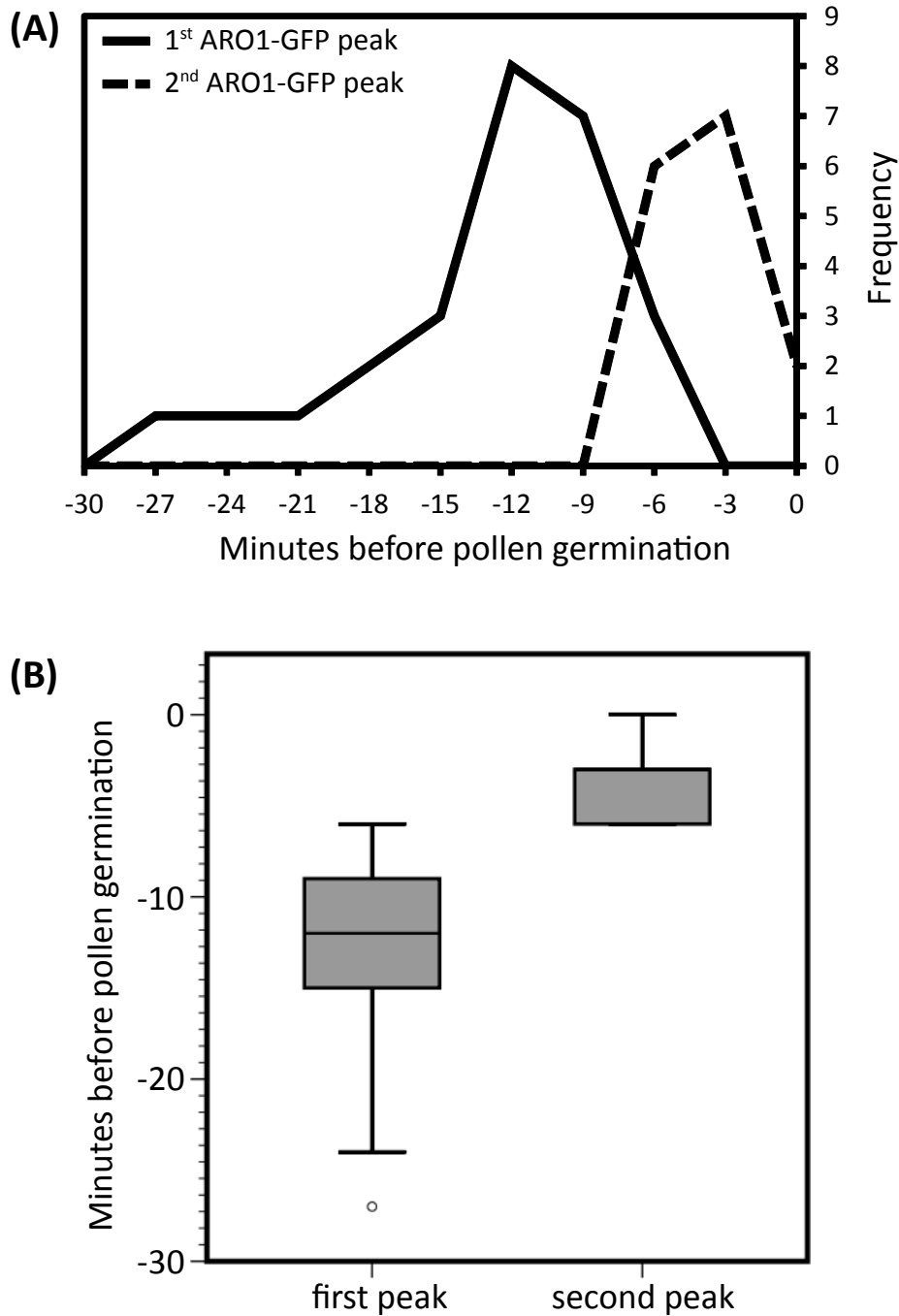


Figure S6: Frequencies and time points of ARO1-GFP intensity peaks in pollen grains before germination

In 25 of 30 pollen investigated, ARO1-GFP showed one to two signal intensity peaks within 30 minutes before germination, indicating rapid and local accumulation of ARO1-GFP decorated vesicles at the periphery of the pollen grain protoplast. The frequencies of observed intensity maxima are shown in **(A)** and corresponding boxplots in **(B)**.

3.5 Manuscript: Dissecting the multi-component assembly of a meso-scale membrane domain that controls host cell infection in *Medicago truncatula*

Thomas F. Stratil, Sebastian S.A. Konrad, Jessica Folgmann, Thomas Ott*

Institute of Genetics, Ludwig-Maximilians-Universität München, Großhaderner Str. 2-4, 82152 Planegg-Martinsried

* to whom correspondence should be addressed: Thomas.Ott@bio.lmu.de

Author contributions:

Design and conception of initial experiments of SYMREM1 and FLOT4 co-localization that were included in this manuscript were done by me (Basis for Figure 5; Figure 6 Supplementary 1). Furthermore, I contributed to this work by giving experimental assistance and helping Thomas F. Stratil with data evaluation.

I hereby confirm the above mentioned statements:

.....

Prof. Dr. Thomas Ott

.....

Sebastian S. A. Konrad

Dissecting the multi-component assembly of a meso-scale membrane domain that controls symbiotic infection

Thomas F. Stratil, Sebastian S.A. Konrad, Jessica Folgmann, Thomas Ott*

Institute of Genetics, Ludwig-Maximilians-Universität München, Großhaderner Str. 2-4,
82152 Planegg-Martinsried

* To whom correspondence should be addressed: Thomas.Ott@bio.lmu.de

ABSTRACT

Intracellular colonization of plant cells by symbiotic bacteria is a critical step for the host that requires stringent surveillance circuits at the plasma membrane to keep exclusive control over the infection process. Accumulating evidence suggests that such perception and signal transduction complexes are pre-formed in membrane compartments called microdomains (MDs). However, neither the existence of pathway-specific MDs nor their controlled assembly has been demonstrated. Here, we unravelled the sequential organization of membrane-resident signalling proteins that are indispensable for the intracellular infection of *Medicago truncatula* roots by symbiotic bacteria. We identified actin, the flotillin FLOT4, the remorin SYMREM1 and the entry receptor LYK3 as essential molecular building blocks that are required and sufficient for the assembly of an infection-related meso-scale membrane domain *in vivo*. Reciprocally, the combinatorial expression of these proteins in a heterologous cell system was sufficient to artificially reconstitute this specialized membrane domain *in vivo*.

1 **INTRODUCTION**

2

3 As is the case in other organisms plant plasma membranes (PMs) are highly
4 compartmentalized organelles where proteins and lipids segregate into distinct meso-
5 scale membrane domains (MDs) (for review see Konrad and Ott 2015, Malinsky *et al.*,
6 2013). Considering that cellular PMs are highly crowded spaces with a limited capacity
7 for free diffusion of proteins (Martiniere *et al.*, 2012, Ramadurai *et al.*, 2009), pre-
8 assembly of protein complexes would not only facilitate rapid signal transduction but also
9 maintain spatial separation of competing pathways. This hypothesis is strengthened by
10 recent evidence, which demonstrates the co-existence of a variety of different membrane
11 MDs in plants and yeast (Jarsch *et al.*, 2014, Spira *et al.*, 2012). Even though direct
12 evidence is still missing, it is tempting to speculate that a high degree of functional
13 specificity is maintained within these structures.

14 While plant proteins that have been identified to label MDs in vivo are functionally
15 scattered over a wide range of biological processes (reviewed in Konrad and Ott 2015),
16 several proteins that are involved in controlling the cellular infection of legume roots by
17 soil-born rhizobia during root-nodule symbiosis (RNS) have been shown to localize to
18 MDs (Haney and Long 2010, Haney *et al.*, 2011, Lefebvre *et al.*, 2010, Moling *et al.*,
19 2014). In model legumes such as *Medicago truncatula* RNS is characterized by the
20 colonization of roots via infection threads (ITs). They are initiated in a physical pocket
21 that is formed within tightly curled root hairs that entrap rhizobia in a micro-colony. ITs
22 are tip growing tunnel-like structures surrounded by a plasma membrane that encapsulate
23 these bacteria during the infection process and guide them in a tightly regulated manner
24 towards the inner root cortex, the site of intracellular release (reviewed in Popp and Ott

25 2011). Any of these morphological responses however is preceded and dependent on a
26 molecular dialog between the two partners. In *M. truncatula*, initial recognition of strain-
27 specific rhizobial signalling molecules, called Nod Factors (NFs), is mediated by the two
28 plasma membrane-resident LysM-type receptor-like kinases (RLKs) NOD FACTOR
29 PERCEPTION (NFP) and LYSIN MOTIF RECEPTOR KINASE 3 (LYK3) (Endre *et al.*,
30 2002, Limpens *et al.*, 2003, Smit *et al.*, 2007). These proteins form a heteromeric
31 complex in vivo that controls intracellular infection (Moling *et al.*, 2014, Pietraszewska-
32 Bogiel *et al.*, 2013). Interestingly, LYK3 was shown to label discrete MDs in root hairs
33 (Haney *et al.*, 2011) and in the L1 and L2 layers at the apex of root nodules (Moling *et al.*,
34 2014). The overall low protein levels of NFP do currently not allow the observation of
35 such patterns at high resolution (Moling *et al.*, 2014). While LYK3-labelled MDs are
36 laterally mobile in the absence of any symbiotic stimulus, the protein is laterally arrested
37 upon inoculation of root hairs with *Sinorhizobium meliloti* (Haney *et al.*, 2011). At this
38 stage, LYK3 co-localized with FLOTILLIN 4 (FLOT4), a legume-specific member of the
39 flotillin/reggie protein family. The fact that LYK3 gets dynamically recruited into these
40 static domains in a stimulus-dependent manner implies that this domain type provides a
41 central hub for symbiosis-related signal transduction and host cell infection. FLOT4 itself
42 is required for symbiotic infections since knock-down of the corresponding gene resulted
43 in an infection phenotype, where a large number of ITs were aborted in root hairs and
44 only a minority of them released bacteria into the host cell at the inner root cortex (Haney
45 and Long 2010). Data from other organisms suggest that flotillins might serve as
46 molecular scaffolds that are involved in the assembly of higher order complexes
47 (Amaddii *et al.*, 2012, Langhorst *et al.*, 2005). A similar function has been attributed to

48 plant-specific remorin proteins such as the SYMBIOTIC REMORIN 1 (SYMREM1), a
49 legume-specific member of this multi-gene family. This protein also controls rhizobial
50 infection and is able to physically interact with a number of RLKs including NFP and
51 LYK3 (Lefebvre *et al.*, 2010, Tóth *et al.*, 2012). Both, SYMREM1 and FLOT4 are
52 soluble proteins that anchor to laterally immobile MDs at the inner leaflet of the plasma
53 membrane (Konrad *et al.*, 2014). However, while *FLOT4* is constitutively expressed and
54 further induced upon rhizobial infection (Haney and Long 2010), expression of the
55 *SYMREM1* gene strictly depends on NF perception and rhizobial infection (Lefebvre *et*
56 *al.*, 2010, Tóth *et al.*, 2012).

57 Thus this PM-resident pathway may serve as a promising basis to unravel the spatio-
58 temporal assembly of a pathway specific membrane micro-domain.

59

60 **RESULTS**

61 **SYMREM1-labelled microdomains are actin-dependent**

62 We first aimed to identify the molecular building blocks that are genetically required for
63 the active recruitment of proteins into this MD, its maintenance and its lateral stability.
64 Due to the association of SYMREM1 with the cytosolic face of the PM we hypothesised
65 that cytoskeleton components contribute to this stability. To test this, we created a YFP-
66 SYMREM1 fusion protein and ectopically expressed this construct in transgenic *M.*
67 *truncatula* roots. As demonstrated earlier, SYMREM1 labelled distinct and immobile
68 MDs in root epidermal cells (as shown in Figure 1A). To monitor any alterations
69 precisely we first performed extensive quantitative image analysis. On average,
70 SYMREM1-labelled MDs occurred with a density of 0.057 domains/ μm^2 (standard error

71 (SE)=0.0051; n=47) (Figure 1A). Next, we verified our experimental conditions to
72 destabilize the microtubule (MT) and actin cytoskeleton. Therefore, we cloned and
73 expressed the MICROTUBULE ASSOCIATED PROTEIN 4 (MAP4) fused to the
74 mCherry fluorophore (mCherry-MAP4) in transgenic *M. truncatula* roots. MAP4 clearly
75 labelled MT tracks (Figure 1 - figure supplement 1A) that were efficiently distorted upon
76 application of the MT-depolymerising drug oryzalin (Figure 1 - figure supplement 1B).
77 Accordingly, we expressed the fluorescently-tagged 17 amino acid long peptide LifeAct
78 (Riedl et al., 2008) to label F-actin strands (Figure 1 - figure supplement 1C). The
79 majority of actin strands could be depolymerized using cytochalasin D (Figure 1 - figure
80 supplement 1D). To test a possible dependency of SYMREM1-labelled MDs on intact
81 microtubules we first treated *M. truncatula* roots expressing YFP-SYMREM1 with
82 oryzalin. While this treatment did not significantly affect SYMREM1 domain patterning
83 (MD density= 0.062 domains/ μm^2 ; SE= 0.0058; $p= 0.54$) (Figure 1B), the application of
84 cytochalasin D resulted in an almost entire loss of SYMREM1-labelled MDs (MD
85 density=0.018 domains/ μm^2 ; SE=0.0012; $p= 4.74\text{E}^{-10}$) (Figure 1C). These data indicate
86 that MDs labelled by SYMREM1 are strictly actin-dependent. To further verify this, we
87 performed extensive co-localization analysis of actin strands and SYMREM1-labelled
88 MDs (Figure 2). As illustrated, in root hairs that co-expressed Cerulean-LifeAct (Figure
89 2A) and mCherry-SYMREM1 (Figure 2B), the labelled MDs were always positioned
90 (Figure 2C) and stretched (arrowheads; Figure 2D-F) along actin filaments. Quantitative
91 pixel-based co-localization revealed an average Pearson Correlation Coefficient of $R_r=$
92 0.287 (SE= 0.022; n=10) indicating co-localization of actin and SYMREM1-labelled
93 MDs (Figure 2F). To verify this statistically and to test whether these co-localizations

94 appeared randomly, we applied a Costes Randomization procedure to all individual
95 images. For this, we randomized blocks of 10x10 pixels within one channel of an image
96 (mCherry-SYMREM1) and calculated the random Pearson Correlation Coefficient 'rd Rr'
97 between these artificially generated and the original images of the corresponding second
98 channel (Cerulean-LifeAct). In all cases we obtained significantly lower values (average
99 rd Rr=0.001; SE=0.0009; $p=3.76E^{-07}$) demonstrating a true co-localization and therefore
100 confirming that SYMREM1-labelled MDs are tightly linked to the actin cytoskeleton.

101

102 **The LYK3 mutant allele *hcl1* shows strong actin defects in transgenic roots**

103 As SYMREM1 interacts with the symbiotic RLKs NFP, LYK3 and DOES NOT MAKE
104 INFECTIONS 2 (DMI2) (Lefebvre *et al.*, 2010), we tested whether the localization of
105 SYMREM1 is qualitatively altered in any of the respective mutants. Expression of the
106 fluorescently tagged protein in transgenic *M. truncatula* roots (wild-type A17
107 background) resulted in the expected MD-labelling pattern in epidermal and outer cortical
108 cells (Figure 3A). Additionally, no differences to wild-type plants were observed upon
109 expression of the construct in the RLK mutants *nfp2* and *dmi2* (Figure 3B,C). Similarly,
110 expression of the SYMREM1 fusion protein in the LYK3 mutant allele *hcl4* (Smit *et al.*,
111 2007) yielded wild-type like patterns even though domain density appeared to be reduced
112 in this mutant (Figure 3D). In contrast, the *hcl1* allele showed strongly altered
113 SYMREM1 localization (Figure 3E). This mutant carries a glycine to glutamate mutation
114 in the conserved GxGxxG motif of the kinase domain (Smit *et al.*, 2007) that results in a
115 kinase-dead variant of the LYK3 receptor (Klaus-Heisen *et al.*, 2011). In this mutant
116 allele, root epidermal and outer cortical cells exhibited short parallel arrays of

117 SYMREM1 labelled MDs leading to a spike-like pattern (arrowheads; Figure 3E). Wild-
118 type like MD labelling patterns of SYMREM1 were restored in a complemented *hcll*
119 mutant (*hcll* comp.; Haney *et al.*, 2011) confirming *hcll* to be the causative mutation for
120 altered MD localization (Figure 3F).

121 As demonstrated above, lateral positioning of SYMREM1-labelled MDs is actin
122 dependent. Therefore, we asked whether the *hcll* mutant exhibits an altered actin
123 cytoskeleton. To test this, a YFP-LifeAct marker construct was expressed in the wild-
124 type A17, the *hcll* mutant and the complemented *hcll* background (Figure 4). First, we
125 analysed actin orientation in the wild-type A17 and the *hcll* mutant and categorized it
126 into three classes: longitudinal (0°-30° relative to the growth axis), oblique (30°-60°
127 relative to the growth axis) and transversal (60°-90° relative to the growth axis). In wild-
128 type roots the major proportion of actin in root epidermal and outer cortical cells was
129 orientated longitudinally (95%; Figure 4A). In contrast, actin orientation was
130 significantly altered with 47% being longitudinally, 21% oblique and 32% transversally
131 orientated in the *hcll* mutant (Figure 4B). Such changes were also observed in *hcll* root
132 hairs that were mostly round and less elongated (Figure 4C) compared to the wild-type
133 (Figure 2A) or the corresponding complemented mutant background (*hcll* comp.; Figure
134 4D).

135 To quantify actin patterns more globally, transects along the initial 1 cm from the root tip
136 were scored for the relative orientation of actin. Indeed, the same patterns as described
137 above were found along young parts of growing roots in both genotypes (Figure 4 - figure
138 supplement 1A, B). These data clearly demonstrate that transgenic roots of *hcll* show a
139 severe actin defect. Therefore, we hypothesised that altered MD patterning in *hcll* is

140 caused by its cytoskeleton phenotype. To test this, we co-expressed LifeAct (Figure 4E)
141 and SYMREM1 (Figure 4F) in the *hcl1* mutant. Indeed, actin and SYMREM1
142 significantly co-localized with each other (Figure 4G), demonstrating that the transversal
143 orientation of SYMREM1-labelled MDs in transgenic *hcl1* roots is caused by the altered
144 actin cytoskeleton. Interestingly, we found that the reported changes in actin orientation
145 were significantly more pronounced in transgenic hairy roots since staining of non-
146 transformed wild-type, *hcl4*, *hcl1* and complemented *hcl1* roots with Phalloidin 568
147 revealed only moderate alterations in actin orientation in root epidermal cells (Figure 4 -
148 figure supplement 2) although *hcl1* root hairs also exhibit the same bulky phenotype as
149 found on transgenic roots. These data indicate that the use of transgenic hairy roots as
150 obtained upon transformation with *Agrobacterium rhizogenes* may further pronounce
151 LYK3-related phenotypes and implies a functional connection between actin orientation
152 and LYK3 activity.

153

154 **SYMREM1 is targeted to a specific MD in a FLOT4-dependent manner**

155 Similar to the results described above, FLOT4 also showed an altered localization pattern
156 in *hcl1* root hairs (Haney and Long 2010). To verify this for epidermal and cortical cells
157 we co-expressed SYMREM1 and FLOT4 in transgenic *hcl1* roots. Indeed, both FLOT4
158 (Figure 4 - figure supplement 1C) and SYMREM1 (Figure 4 - figure supplement 1D)
159 followed the same transversal patterns (Figure 4 - figure supplement 1E), indicating that
160 both proteins may label the same membrane microdomain. To verify this more precisely,
161 we co-expressed both proteins in roots using the complemented *hcl1* mutant line (Haney
162 *et al.*, 2011). As expected, SYMREM1 (Fig 5A,D) and FLOT4 (Figure 5B,E) labelled

163 distinct MDs that greatly co-localized with a Pearson correlation coefficient of $R_r = 0.344$
164 ($SE = 0.027$; $p = 5.78E^{-09}$), which is significantly different to the values obtained by image
165 randomization (Figure 5C,F,G). These data clearly demonstrate that SYMREM1 and
166 FLOT4 are indeed targeted to the same MD. When quantifying domain density we
167 additionally observed an almost 7-fold increase in the number of SYMREM1 labelled
168 MDs during co-expression with FLOT4 (density = $0.395 \text{ domains}/\mu\text{m}^2$; $SE = 0.0581$)
169 compared to individual expression of SYMREM1 (density = $0.058 \text{ domains}/\mu\text{m}^2$;
170 $SE = 0.0058$) indicating that FLOT4 could be required for SYMREM1 recruitment. To test
171 this genetically, we created two RNA interference (RNAi) constructs. One was
172 previously shown to efficiently silence FLOT4 (Haney et al., 2010). The second RNAi
173 construct expanded from the 3'UTR to 114 bp into 5' direction of the *FLOT4* gene in
174 order to facilitate silencing in *Nicotiana benthamiana*, since the FLOT4-mCherry
175 constructs lack the 3'UTR. The co-expression of this construct together with a
176 fluorescently tagged FLOT4 variant in *N. benthamiana* leaf epidermal cells resulted in a
177 complete loss of fluorescence, indicating efficient silencing of the flotillin protein (Figure
178 5 - figure supplement 1). As FLOT4 is constitutively expressed in legume roots, we co-
179 expressed SYMREM1 alone or together with the FLOT4-RNAi construct in transgenic *M.*
180 *truncatula* (complemented *hcl1*) roots. While SYMREM1 labelled MDs with a density of
181 $0.077 \text{ MDs}/\mu\text{m}^2$ (Figure 5H) significantly less domains ($0.02 \text{ MDs}/\mu\text{m}^2$) were found in
182 FLOT4-silenced roots (Figure 5I). However, the presence of YFP-fluorescence and its
183 peripheral localization within these cells (Figure 5I) indicate successful expression and
184 membrane association of SYMREM1 under these conditions. These data demonstrate that

185 FLOT4 is essential for SYMREM1 accumulation in distinct membrane MDs but not for
186 PM localization of SYMREM1 *per se*.

187

188 **Artificial assembly of a root- and symbiosis-specific microdomain**

189 All three proteins (SYMREM1, FLOT4 and LYK3) are exclusively expressed in legume
190 roots and/or nodules, since rhizobial infection is limited to these organs. Results
191 presented above and in previous studies clearly indicate that all proteins are recruited into
192 MDs. If MDs indeed serve as hubs for specific signalling pathways, one would
193 hypothesize that all three components should be targeted to the same and symbiosis-
194 related microdomain (symMD). Therefore we tested, whether consecutive addition of
195 these constituents is sufficient to artificially reconstitute a symMD in a heterologous
196 system. We chose leaf epidermal cells of *Nicotiana benthamiana* as this cell type is
197 devoid of all three proteins but not actin. Interestingly, heterologous expression of
198 SYMREM1 alone in this system only resulted in low frequency labelling of MDs. Instead,
199 SYMREM1 was mostly homogenously distributed except for its exclusion from defined
200 tracks (Figure 6A). For other remorin proteins such structures have been previously
201 described to represent cortical MTs (Jarsch *et al.*, 2014). This indicates a lack of essential
202 components required for an efficient accumulation of SYMREM1 in MDs in these cells.
203 In contrast, FLOT4 (Figure 6B) and LYK3 (Figure 6C) labelled more distinct structures
204 when being expressed individually, even though these putative MDs did not resemble
205 those observed in the homologous system. Strikingly, co-expression of SYMREM1 and
206 FLOT4 in the same cell strongly induced compartmentalization of SYMREM1 (Figure
207 6D) while FLOT4 patterns only changed moderately (Figure 6E). Interestingly and in

208 striking contrast to SYMREM1/FLOT4 co-localizations observed in *M. truncatula* roots
209 (Figure 5A-G), these two proteins did not co-localize in *N. benthamiana* leaf epidermal
210 cells but mutually excluded each other (Figure 6F,G). Quantitative image analysis and
211 segmentation confirmed that both proteins remained in direct vicinity and tightly linked
212 but indeed failed to co-localize ($Rr = -0.395$, $SE = 0.030$; $rd Rr = -0.008$; $rd SE = 0.005$;
213 $p = 6.67E^{-13}$) (Figure 6G). This compartmentalized SYMREM1 localization was entirely
214 revertible upon additional expression of the FLOT4-RNAi construct (Figure 6 - figure
215 supplement 1). Since LYK3 is actively recruited into FLOT4-labelled domains and this
216 process coincides with induced expression of *SYMREM1* upon rhizobial infection (Haney
217 et al., 2011; Lefebvre et al., 2010), we tested whether additional expression of LYK3
218 altered SYMREM1 localization. To avoid spectral interference of three fluorophores we
219 created a T-DNA that allowed expression of FLOT4-mCherry, YFP-SYMREM1 and
220 LYK3-HA simultaneously. Indeed, transformation of this triple tandem construct into
221 leaf epidermal cells resulted in labelling of distinct and specific MDs by SYMREM1
222 (Figure 6H) and FLOT4 (Figure 6I). Quantitative image analysis now showed significant
223 co-localizations within the MDs labelled by both proteins ($Rr = 0.40$, $SE = 0.051$; rd
224 $Rr = 0.017$; $rd SE = 0.017$; $p = 3.03E^{-06}$) (Figure 6J,K). Additional Western Blot analysis
225 confirmed successful expression of the LYK3-HA construct (Figure 6 - figure
226 supplement 2A). We then verified whether these artificial MDs remain associated with
227 the actin cytoskeleton. For this we expressed fluorescently-labelled SYMREM1 and
228 LifeAct together with non-fluorescently tagged FLOT4. Indeed and as shown for the
229 homologous system (Figure 2), MDs were found in direct proximity of actin strands
230 (Figure 6 - figure supplement 2B-F), indicating that this feature was maintained in this

231 heterologous cell system. All together, these data demonstrate that LYK3 is essential for
232 the targeting of SYMREM1 into FLOT4-labelled MDs and that all three components in
233 addition to actin are required and sufficient to artificially reconstitute an essential
234 scaffolding core of this symMD in a heterologous system.

235 These data raised the reciprocal question: Is the lateral recruitment of LYK3 into the
236 FLOT4-labelled symMD SYMREM1-dependent? To test this we again used our
237 heterologous reconstitution assay and co-expressed FLOT4 and LYK3 (Figure 7). Under
238 these conditions, LYK3 failed to significantly co-localize with FLOT4, indicating that
239 FLOT4 alone is not sufficient to mediate LYK3 recruitment (Figure 7A-D). It should be
240 noted that image segmentation was not properly applicable to these images due to the
241 comparably low degree of compartmentalization. Therefore, values are only provided for
242 the shown dataset. In contrast, additional expression of a HA-SYMREM1 construct
243 resulted in significant compartmentalization and co-localization of the fluorophore-
244 tagged FLOT4 and LYK3 proteins (Rr=0.60, SE=0.046; rd Rr=0.021; rd SE=0.019;
245 $p=4.79E^{-08}$) (Figure 7E-H). In line with this, clear compartmentalization of LYK3 was
246 also observed in the presence of mCherry-SYMREM1 and FLOT4-HA (Figure 7I-L)
247 (Rr=0.39, SE=0.049; rd Rr=0.046; rd SE=0.030; $p=8.46E^{-04}$). These data clearly
248 demonstrate that the recruitment of LYK3 into FLOT4 labelled symMDs is SYMREM1-
249 dependent.

250 **DISCUSSION**

251 It has been a long-standing question how plant plasma membranes maintain
252 organizational platforms such as membrane microdomains (MDs). In plants, three main
253 structural elements may provide nucleation sites for MDs and immobilize these domains
254 at distinct positions at the PM. While lateral diffusion of a number proteins was
255 unaffected by cytoskeleton depolymerisation, degradation of the cell wall greatly
256 increased their diffusion rates (Martiniere *et al.*, 2012). Although this study did not aim to
257 resolve subcellular structures such as MDs, it can be assumed that the cell wall is an
258 essential factor for MD organization. Proteins like the plant-specific type-I formin AtFH1
259 from Arabidopsis which contains a transmembrane domain and interacts with both the
260 cell wall and the cytoskeleton (Martiniere *et al.*, 2011) are promising candidates to
261 function as anchor sites for MD assembly and thus represent a second group of core
262 elements. The third factor is the cell cytoskeleton, which has mostly been suggested in
263 non-plant species to be essential for MD formation (e.g. Dinic *et al.*, 2013, Gomez-
264 Llobregat *et al.*, 2013) although first evidence has also recently been provided in plants
265 (Hosy *et al.*, 2015). While previous work demonstrated that the presence of MDs labelled
266 by the Arabidopsis remorin At1g13920 is dependent on an intact microtubule
267 arrangement (Jarsch *et al.*, 2014), the symbiotic MD that is labelled by SYMREM1 and
268 FLOT4 (Figure 5) mainly depends on actin but not on microtubules (Figure 1). This
269 resembles patterns shown for the group 6 remorin GSD1 from rice that was identified in a
270 forward genetic screen for altered grain filling (Gui *et al.*, 2014). Thus, all three factors
271 should not be considered independently as emerging evidence suggests the existence of a

272 cell wall- plasma membrane- cytoskeleton continuum (Fujita *et al.*, 2012, Liu *et al.*, 2015,
273 McKenna *et al.*, 2014, Oda and Fukuda 2013).

274 In addition to structural components that allow a certain degree of protein immobilization,
275 molecular scaffolds are likely to recruit defined proteins into these structural sites to
276 facilitate larger and functional complex formation. Flotillins may represent primary
277 scaffolds that bind to core and more generic structural MD components such as actin
278 (Figure 8A,B). By this, they may pave the way for other process-specific MD
279 constituents. This could be either achieved by direct interaction with these proteins or by
280 creating specific lipid environments within the PM as a consequence of local protein
281 enrichment (Konrad and Ott 2015; Figure 8B). Such a model is supported by findings in
282 *Bacillus subtilis* where the loss of the bacterial flotillin YuaG resulted in increased areas
283 of lipid-ordered domains resulting in significantly less compartmentalized membrane
284 patches (Bach and Bramkamp 2013). Having established a specific local environment,
285 post-translationally modified FLOTs are required for subsequent recruitment of
286 additional proteins as demonstrated for the human dopamine transporter DAT (Cremona
287 *et al.*, 2011) and the epidermal growth factor receptor EGFR (Neumann-Giesen *et al.*,
288 2007). Interestingly, activation of EGFR directly signals to the actin cytoskeleton, a
289 process mediated by human FLOT2 (Neumann-Giesen *et al.*, 2007). These and other data
290 from human cell lines, where FLOTs were shown to be indirectly involved in regulating
291 cortical actin (Ludwig *et al.*, 2010), clearly indicate their involvement in cytoskeleton-
292 related processes. In plants the role of FLOTs has been less intensively studied but recent
293 data point towards their involvement in endocytotic events (Li *et al.*, 2012) and protein
294 compartmentalization at the plasma membrane (Wang *et al.*, 2015).

295 During root nodule symbiosis, FLOT4 enriched MDs are essential for the domain specific
296 accumulation of SYMREM1 (Figure 5) and the immobilization of the receptor-like
297 kinase LYK3 (Haney *et al.*, 2011). This probably represents a second and process-
298 specific wave of protein recruitment into this symbiosis specific MD. Considering the
299 actin phenotype observed in the *hcl1* mutant (Figure 4), we hypothesize that LYK3,
300 similar to the human EGFR, controls actin re-orientation during root hair curling and
301 infection thread progression. These data add to a reported microtubule defect of the *hcl1*
302 mutant (Catoira *et al.*, 2001).

303 It should however be noted that although FLOT4 is required for the specific targeting of
304 SYMREM1 into the symMD, it may not represent a primary structural component. Such
305 assumption is supported by Foerster Resonance Energy Transfer / Fluorescence Lifetime
306 Imaging Microscopy (FRET-FLIM) and Bi-molecular Fluorescence Complementation
307 (BiFC) experiments in *N. benthamiana* leaf epidermal cells that revealed spatially
308 confined physical interaction between *Lotus japonicus* SYMREM1 and NFR1 in distinct
309 MDs even in the absence of FLOT4 (Jarsch *et al.*, 2014). This indicates that SYMREM1
310 and LYK3 can interact but not specifically accumulate in MDs under these conditions. As
311 physical interaction between both proteins is confined to these domains even in the
312 absence of FLOT4, FLOT4 may mediate the spatial and efficient accumulation of
313 symbiosis-specific signalling proteins and thus controls the physical confinement of this
314 pathway.

315 Based on our and previously published data we propose the following model: FLOT4 and
316 LYK3 are constitutively expressed in *M. truncatula* root hairs (Figure 8B; Haney *et al.*,
317 2011). Under non-stimulated (non-symbiotic) conditions FLOT4 labels laterally

318 immobile MDs that are associated with the actin cytoskeleton while LYK3 is targeted to
319 mobile MDs (Figure 8B Haney, 2010; Haney *et al.*, 2011). In this situation, both proteins
320 label different types of domains. However, the fact that the NF receptors of *Lotus*
321 *japonicus* immuno-precipitate together in the absence of NFs (Ried *et al.*, 2014) indicates
322 the presence of a pre-formed receptor complex and consequently their co-localization in
323 the same MD. Upon rhizobial inoculation and perception of the secreted NFs by the
324 NFP/LYK complex, signal transduction is initiated (Figure 8C) leading to the induction
325 of gene expression (e.g. of *SYMREM1*; Lefebvre *et al.*, 2010). In legumes, root hairs
326 respond to NF perception by a typical deformation and re-orientation of the tip (Esseling
327 *et al.*, 2003), which is accompanied by local alterations of the actin and microtubule
328 cytoskeleton (de Ruijter *et al.*, 1999, Miller *et al.*, 1999, Sieberer *et al.*, 2005). Either
329 upon reaching a critical, local NF concentration or dependent on a second signal, LYK3
330 is actively recruited into FLOT4 labelled MDs (Figure 8D; Haney *et al.*, 2011). As LYK3
331 is already, even though moderately, compartmentalized when being heterologously
332 expressed in *N. benthamiana* leaf epidermal cells but fails to co-localize with FLOT4
333 (Figure 6) it is unlikely that this recruitment is directly mediated by this flotillin protein.
334 Since studies on FLOT4 targeting to MDs were performed on non-inoculated roots and in
335 *lyk3* mutant alleles, this process itself is independent of NFs or an activated LYK3 protein
336 (Haney and Long 2010), respectively. By contrast, it depends on the actin cytoskeleton
337 (Figure 4, figure supplement 1). As *SYMREM1* expression is induced upon NF
338 perception and rhizobial inoculation (Lefebvre *et al.*, 2010, Tóth *et al.*, 2012), we
339 hypothesize that the *SYMREM1* protein is subsequently recruited into the symMD in a
340 FLOT4- dependent manner (Figure 5H,I; Figure 6; Figure 8C). As *SYMREM1* can

341 physically interact with LYK3, we propose and demonstrate that SYMREM1 is essential
342 for the immobilization of LYK3 in FLOT4-labelled symMDs (Figure 7; Figure 8C-D).
343 However, although SYMREM1 can be phosphorylated by the NOD FACTOR
344 RECEPTOR 1 (NFR1; Tóth *et al.*, 2012), the putative ortholog of LYK3 from *L.*
345 *japonicus*, co-localization of SYMREM1 and FLOT4 is independent of an active LYK3
346 kinase as FLOT4 and SYMREM1 still co-localized in the *hcl1* mutant background
347 (Figure 4, supplement 1C-E). Continuous signalling would further trigger SYMREM1
348 oligomerization allowing the recruitment of additional and infection-related proteins into
349 the symMD (Figure 8E).

350 In summary we hypothesize that FLOT4 serves as a ‘forefront’ scaffold for SYMREM1
351 and presumably other early infection marker proteins. Later SYMREM1 may be required
352 for the second wave of recruitments into this MD. This could include proteins being
353 involved in local cell wall modifications that are required for the initial infection and
354 components that allow formation and maintenance of the infection thread membrane.

355

356

357 **MATERIALS AND METHODS**

358 Hairy Root Transformation

359 *Medicago truncatula* hairy root transformation was performed as previously described
360 using the *Agrobacterium rhizogenes* strain ARQUA1 (Boisson-Dernier *et al.*, 2001,
361 Konrad *et al.*, 2014) and transferred weekly to fresh plates containing Fahraeus medium
362 with a pH of 6.0.

363

364 *Nicotiana benthamiana* infiltration

365 *Nicotiana benthamiana* leaf infiltration was performed as previously described (Jarsch
366 *et al.*, 2014, Jarsch and Ott 2015, Tóth *et al.*, 2012). Agrobacteria were infiltrated at a
367 final OD 600nm of 0.4 for p35S::LYK3-GFP to 0.005 pUbi::HA-SYMREM1. Level 2
368 single expression vectors and Level 3 co-expression vectors obtained by Golden Gate
369 cloning (Binder *et al.*, 2014) were infiltrated with a final OD 600nm of 0.1 in presence of
370 the silencing suppressor P19. The infiltration with the FLOT4-RNAi silencing construct,
371 as well as the respective control was performed without P19. Microscopy was performed
372 2 and 3 days post infiltration. To obtain full PM localization of LYK3 and minimize
373 possible interference with the trafficking protein fraction, microscopy involving LYK3-
374 GFP or LYK3-HA constructs was conducted three days after leave infiltration.

375

376 Western blot analysis

377 *Nicotiana benthamiana* leaf disks were harvested 3 dpi and shock frozen with liquid
378 nitrogen. Proteins were extracted by grinding leaf disks in lysis buffer (150 mM NaCl, 10
379 mM TrisHCl pH 7.5, 1% Triton-X-100, 1 mM EDTA, 2 mM DTT, Pefabloc, protease
380 inhibitor cocktail (SIGMA p9599)). Samples were the spun down at 14000 rpm at 4°C
381 and the pellet was discarded. The samples were diluted with 5x SDS-sample buffer and
382 denatured at 70°C for 5 min. The protein samples were loaded onto 10% polyacrylamide
383 SDS-polyacrylamide gels and run at 150 Volts for 60 min. Afterwards proteins were
384 transferred onto a nitrocellulose membrane using a BIO-RAD Trans-Blot Turbo Transfer
385 System for 30 min at 25 V constant. For blocking and antibody incubation the SNAP
386 i.d.® 2.0 protein detection system (Merck Millipore) was used. The membrane was

387 blocked with 3% milk in 1xTBS-Tween (0.1%) and incubated with the α -HA-antibody
388 that was directly conjugated with horseradish peroxidase (1:3000, Roche). Detection of
389 proteins was performed with the SuperSignal™ West Pico Chemiluminescent Substrate
390 (Pierce).

391

392 Golden Gate and Gateway cloning/constructs

393 The coding sequence of *Medicago truncatula* SYMREM1 (Genbank accession
394 JQ061257) was recombined into the Gateway compatible pUBi::YFP-GW-HYG vector
395 (Konrad et al. 2014) via LR-reaction. All other constructs were cloned as Golden Gate
396 compatible constructs. Bpi and Bsa1 restriction sites were removed from SYMREM1,
397 LYK3 (Genbank accession AY372406), MAP4 (Genbank accession: M72414) cDNA
398 templates as well as the genomic FLOT4 (Genbank accession GU224281) sequence. A
399 double stranded Lifeact template with flanking Bsa1 restriction sites was directly inserted
400 into pUC-Bpi via blunt end StuI (NEB) cut-ligation for subsequent Golden Gate cloning.
401 Double stranded sequences for the FLOT4-RNAi constructs with flanking Bsa1 sites
402 were also cloned via blunt end StuI cut-ligation into pUC-Bpi. RNAi silencing vectors
403 were assembled as previously described (Binder *et al.*, 2014).

404 Level 2 single expression and Level 3 co-expression vectors for microscopy were
405 assembled in a Golden Gate compatible fashion (Binder *et al.*, 2014).

406

407 Confocal Laser-Scanning Microscopy

408 Confocal laser scanning microscopy was performed on a Leica TCS SP5 confocal
409 microscope equipped with 63x and 20x HCX PL APO water immersion lenses (Leica

410 Microsystems, Mannheim, Germany). GFP and Phalloidin 488 were excited with the
411 Argon laser (AR) line at 488 nm and the emission detected at 500-550 nm. YFP was
412 excited with the 514 nm AR laser line and detected at 520–555nm. mCherry fluorescence
413 and Phalloidin 568 were excited using the Diode Pumped Solid State (DPSS) laser at
414 561nm and emission was detected between 575-630 nm. Excitation of Cerulean was
415 performed at 860 nm with a picosecond rate pulsing Sapphire-Multi Photon Laser, and
416 emission was detected at 470-530 nm. Samples, co-expressing two fluorophores were
417 imaged in sequential mode between frames. Images were taken with a Leica DFC350FX
418 digital camera.

419

420 Quantitative Image Analysis

421 Image analysis was performed with the open source ImageJ/(Fiji) software (Schindelin *et*
422 *al.*, 2012). For illustration, images were background subtracted according to the rolling
423 ball algorithm, filtered with a Mean filter pixel radius of 1 and then maximum z-projected
424 ('create stack). Contrast was enhanced for visualization in figures but not for
425 quantification.

426 Pixel based co-localizations to determine Pearson Correlation Coefficient values were
427 performed using the Fiji Plugins 'Squassh' (Rizk *et al.*, 2014) and 'JACoP' (Bolte and
428 Cordelieres 2006). Image segmentation was performed with 'Squassh'.

429 Randomization was performed with the automatic Costes' Randomization method in
430 'JACoP' in which clusters of 10x10 pixels were randomly distributed in one channel and
431 correlated to the original values. Additionally, randomization was also performed on

432 maximum z-projections via horizontal flip of the mCherry channel as described
433 previously (Jarsch *et al.*, 2014, Jarsch and Ott 2015).

434

435 Fibril tool

436 The orientation of the actin cytoskeleton was analyzed in Fiji using the open source
437 plugin ‘Fibril Tool’ (Boudaoud *et al.*, 2014). For this, ROIs were drawn manually around
438 single cells from a z-stack, maximum z-projected of about 3-5 slices of 0.5 μm depth, and
439 analysed individually.

440

441 Membrane domain quantification

442 YFP-SYMREM1, LYK3-GFP or FLOT4-mCherry domain images were segmented to
443 differentiate background from domains. For this, the background was subtracted with the
444 rolling ball algorithm with a radius corresponding to the smallest structure of interest. I.e.,
445 the largest domain was encircled, and its dimension was used. A mean blur with radius 1
446 was then applied, and the slices (n=5-12 slices, with distances of 0.25 to 0.7 μm)
447 maximum projected along the z-axis. One additional background subtraction step was
448 performed. A threshold was applied to the images and the result saved as a binary mask.
449 The ‘create selection’ tool was used to mark the outlines and was overlaid onto the
450 original image to verify proper image segmentation. Domains were counted with the
451 ‘particle analyzer’ tool in Fiji.

452

453 Cytoskeleton depolymerisation

454 A 1mM Oryzalin (SIGMA-ALDRICH) stock solution in DMSO and a 10mM
455 Cytochalasin D (SIGMA ALDRICH) stock solution on EtOH were prepared. *Medicago*
456 *truncatula* root samples of 1 cm length were incubated in final concentrations of 10 μ M
457 Oryzalin or 10 μ M Cytochalasin D for 12 hours in water. The control samples were
458 incubated in water with the equal amount of solvent for the same amount of time. Actin
459 strands were stained with Phalloidin-ATTO 488 and Phalloidin ALEXA-FLUOR 568
460 (Life Technologies) as described previously (Yokota *et al.*, 2009).

461

462

463 **ACKNOWLEDGEMENTS**

464 We would like to thank all members of our team for their fruitful discussions throughout
465 the project and comments on the manuscript. Christina Bielmeier and Anne-Kathrin
466 Classen (LMU Munich) helped with different aspects during image analysis. Jana
467 Munstermann conducted the initial experiments on FLOT4. This work was funded by an
468 Emmy-Noether grant of the Deutsche Forschungsgemeinschaft (DFG; OT423/2-1) and
469 the Boehringer Ingelheim Foundation.

REFERENCES

- Amaddii, M., Meister, M., Banning, A., Tomasovic, A., Mooz, J., Rajalingam, K. and Tikkanen, R. 2012. Flotillin-1/reggie-2 protein plays dual role in activation of receptor-tyrosine kinase/mitogen-activated protein kinase signaling. *J Biol Chem*, **287**: 7265-7278. doi:10.1074/jbc.M111.287599.
- Bach, J.N. and Bramkamp, M. 2013. Flotillins functionally organize the bacterial membrane. *Mol Microbiol*, **88**: 1205-1217. doi:10.1111/mmi.12252.
- Binder, A., Lambert, J., Morbitzer, R., Popp, C., Ott, T., Lahaye, T. and Parniske, M. 2014. A modular plasmid assembly kit for multigene expression, gene silencing and silencing rescue in plants. *PLOS ONE*, **9**: e88218. doi:10.1371/journal.pone.0088218.
- Boisson-Dernier, A., Chabaud, M., Garcia, F., Becard, G., Rosenberg, C. and Barker, D.G. 2001. *Agrobacterium rhizogenes*-transformed roots of *Medicago truncatula* for the study of nitrogen-fixing and endomycorrhizal symbiotic associations. *Mol Plant Microbe Interact*, **14**: 695-700.
- Bolte, S. and Cordelieres, F.P. 2006. A guided tour into subcellular colocalization analysis in light microscopy. *J Microsc*, **224**: 213-232. doi:10.1111/j.1365-2818.2006.01706.x.
- Boudaoud, A., Burian, A., Borowska-Wykret, D., Uyttewaal, M., Wrzalik, R., Kwiatkowska, D. and Hamant, O. 2014. FibrilTool, an ImageJ plug-in to quantify fibrillar structures in raw microscopy images. *Nat Protoc*, **9**: 457-463. doi:10.1038/nprot.2014.024.
- Catoira, R., Timmers, A.C.J., Maillet, F., Galera, C., Penmetsa, R.V., Cook, D., Denarie, J. and Gough, C. 2001. The HCL gene of *Medicago truncatula* controls Rhizobium-induced root hair curling. *Development*, **128**: 1507-1518.
- Cremona, M.L., Matthies, H.J., Pau, K., Bowton, E., Speed, N., Lute, B.J., Anderson, M., Sen, N., Robertson, S.D., Vaughan, R.A., Rothman, J.E., Galli, A., Javitch, J.A. and Yamamoto, A. 2011. Flotillin-1 is essential for PKC-triggered endocytosis and membrane microdomain localization of DAT. *Nat Neurosci*, **14**: 469-477. doi:10.1038/nn.2781.
- de Ruijter, N., Bisseling, T. and Emons, A.M. 1999. Rhizobium Nod Factors Induce an Increase in Sub-apical Fine Bundles of Actin Filaments in *Vicia sativa* Root Hairs within Minutes. *Mol Plant Microbe Interact*, **12**: 829-832.
- Dinic, J., Ashrafzadeh, P. and Parmryd, I. 2013. Actin filaments attachment at the plasma membrane in live cells cause the formation of ordered lipid domains. *Biochim Biophys Acta*, **1828**: 1102-1111. doi:10.1016/j.bbamem.2012.12.004.
- Endre, G., Kereszt, A., Kevei, Z., Mihacea, S., Kalo, P. and Kiss, G.B. 2002. A receptor kinase gene regulating symbiotic nodule development. *Nature*, **417**: 962-966.
- Esseling, J.J., Lhuissier, F.G. and Emons, A.M. 2003. Nod factor-induced root hair curling: continuous polar growth towards the point of nod factor application. *Plant Physiol*, **132**: 1982-1988.
- Fujita, M., Lechner, B., Barton, D.A., Overall, R.L. and Wasteneys, G.O. 2012. The missing link: do cortical microtubules define plasma membrane nanodomains that

- modulate cellulose biosynthesis? *Protoplasma*, **249 Suppl 1**: S59-67. doi:10.1007/s00709-011-0332-z.
- Gomez-Llobregat, J., Buceta, J. and Reigada, R. 2013. Interplay of cytoskeletal activity and lipid phase stability in dynamic protein recruitment and clustering. *Sci Rep*, **3**: 2608. doi:10.1038/srep02608.
- Gui, J., Liu, C., Shen, J. and Li, L. 2014. Grain setting defect1, encoding a remorin protein, affects the grain setting in rice through regulating plasmodesmatal conductance. *Plant Physiol*, **166**: 1463-1478. doi:10.1104/pp.114.246769.
- Haney, C.H. and Long, S.R. 2010. Plant flotillins are required for infection by nitrogen-fixing bacteria. *Proc Natl Acad Sci U S A*, **107**: 478-483. doi:10.1073/pnas.0910081107.
- Haney, C.H., Riely, B.K., Tricoli, D.M., Cook, D.R., Ehrhardt, D.W. and Long, S.R. 2011. Symbiotic Rhizobia Bacteria Trigger a Change in Localization and Dynamics of the *Medicago truncatula* Receptor Kinase LYK3. *Plant Cell*, **23**: 2774-2787. doi:10.1105/tpc.111.086389.
- Hosy, E., Martiniere, A., Choquet, D., Maurel, C. and Luu, D.T. 2015. Super-resolved and dynamic imaging of membrane proteins in plant cells reveal contrasting kinetic profiles and multiple confinement mechanisms. *Mol Plant*, **8**: 339-342. doi:10.1016/j.molp.2014.10.006.
- Jarsch, I.K., Konrad, S.S., Stratil, T.F., Urbanus, S.L., Szymanski, W., Braun, P., Braun, K.H. and Ott, T. 2014. Plasma Membranes Are Subcompartmentalized into a Plethora of Coexisting and Diverse Microdomains in *Arabidopsis* and *Nicotiana benthamiana*. *Plant Cell*, **26**: 1698-1711. doi:10.1105/tpc.114.124446.
- Jarsch, I.K. and Ott, T. 2015. Quantitative Image Analysis of Membrane Microdomains Labelled by Fluorescently Tagged Proteins in *Arabidopsis thaliana* and *Nicotiana benthamiana*. *bio-protocol*, **5**: e1497.
- Klaus-Heisen, D., Nurisso, A., Pietraszewska-Bogiel, A., Mbengue, M., Camut, S., Timmers, T., Pichereaux, C., Rossignol, M., Gadella, T.W., Imberty, A., Lefebvre, B. and Cullimore, J.V. 2011. Structure-function similarities between a plant receptor-like kinase and the human interleukin-1 receptor-associated kinase-4. *J Biol Chem*. doi:10.1074/jbc.M110.186171.
- Konrad, S.S. and Ott, T. 2015. Molecular principles of membrane microdomain targeting in plants. *Trends Plant Sci*. doi:10.1016/j.tplants.2015.03.016.
- Konrad, S.S., Popp, C., Stratil, T.F., Jarsch, I.K., Thallmair, V., Folgmann, J., Marin, M. and Ott, T. 2014. S-acylation anchors remorin proteins to the plasma membrane but does not primarily determine their localization in membrane microdomains. *New Phytol*, **203**: 758-769. doi:10.1111/nph.12867.
- Langhorst, M.F., Reuter, A. and Stuermer, C.A. 2005. Scaffolding microdomains and beyond: the function of reggie/flotillin proteins. *Cell Mol Life Sci*, **62**: 2228-2240. doi:10.1007/s00018-005-5166-4.
- Lefebvre, B., Timmers, T., Mbengue, M., Moreau, S., Herve, C., Toth, K., Bittencourt-Silvestre, J., Klaus, D., Deslandes, L., Godiard, L., Murray, J.D., Udvardi, M.K., Raffaele, S., Mongrand, S., Cullimore, J., Gamas, P., Niebel, A. and Ott, T. 2010. A remorin protein interacts with symbiotic receptors and regulates bacterial infection. *Proc Natl Acad Sci U S A*, **107**: 2343-2348. doi:10.1073/pnas.0913320107.

- Li, R., Liu, P., Wan, Y., Chen, T., Wang, Q., Mettbach, U., Baluska, F., Samaj, J., Fang, X., Lucas, W.J. and Lin, J. 2012. A Membrane Microdomain-Associated Protein, *Arabidopsis* Flot1, Is Involved in a Clathrin-Independent Endocytic Pathway and Is Required for Seedling Development. *Plant Cell*, **24**: 2105-2122. doi:10.1105/tpc.112.095695
- Limpens, E., Franken, C., Smit, P., Willemse, J., Bisseling, T. and Geurts, R. 2003. LysM domain receptor kinases regulating rhizobial Nod factor-induced infection. *Science*, **302**: 630-633.
- Liu, Z., Persson, S. and Sanchez-Rodriguez, C. 2015. At the border: the plasma membrane-cell wall continuum. *J Exp Bot*, **66**: 1553-1563. doi:10.1093/jxb/erv019.
- Ludwig, A., Otto, G.P., Riento, K., Hams, E., Fallon, P.G. and Nichols, B.J. 2010. Flotillin microdomains interact with the cortical cytoskeleton to control uropod formation and neutrophil recruitment. *J Cell Biol*, **191**: 771-781. doi:10.1083/jcb.201005140.
- Malinsky, J., Opekarova, M., Grossmann, G. and Tanner, W. 2013. Membrane microdomains, rafts, and detergent-resistant membranes in plants and fungi. *Annu Rev Plant Biol*, **64**: 501-529. doi:10.1146/annurev-arplant-050312-120103.
- Martiniere, A., Gayral, P., Hawes, C. and Runions, J. 2011. Building bridges: formin1 of *Arabidopsis* forms a connection between the cell wall and the actin cytoskeleton. *Plant J*, **66**: 354-365. doi:10.1111/j.1365-313X.2011.04497.x.
- Martiniere, A., Lavagi, I., Nageswaran, G., Rolfe, D.J., Maneta-Peyret, L., Luu, D.T., Botchway, S.W., Webb, S.E., Mongrand, S., Maurel, C., Martin-Fernandez, M.L., Kleine-Vehn, J., Friml, J., Moreau, P. and Runions, J. 2012. Cell wall constrains lateral diffusion of plant plasma-membrane proteins. *Proc Natl Acad Sci U S A*, **109**: 12805-12810. doi:10.1073/pnas.1202040109.
- McKenna, J.F., Tolmie, A.F. and Runions, J. 2014. Across the great divide: the plant cell surface continuum. *Curr Opin Plant Biol*, **22**: 132-140. doi:10.1016/j.pbi.2014.11.004.
- Miller, D.D., de Ruijter, N.C.A., Bisseling, T. and Emons, A.M. 1999. The role of actin in root hair morphogenesis: studies with lipochito-oligosaccharide as a growth stimulator and cytochalasin as an actin perturbing drug. *Plant J*, **17**: 141-154.
- Moling, S., Pietraszewska-Bogiel, A., Postma, M., Fedorova, E., Hink, M.A., Limpens, E., Gadella, T.W. and Bisseling, T. 2014. Nod factor receptors form heteromeric complexes and are essential for intracellular infection in *Medicago* nodules. *Plant Cell*, **26**: 4188-4199. doi:10.1105/tpc.114.129502.
- Neumann-Giesen, C., Fernow, I., Amaddii, M. and Tikkanen, R. 2007. Role of EGF-induced tyrosine phosphorylation of reggie-1/flotillin-2 in cell spreading and signaling to the actin cytoskeleton. *J Cell Sci*, **120**: 395-406. doi:10.1242/jcs.03336.
- Oda, Y. and Fukuda, H. 2013. Spatial organization of xylem cell walls by ROP GTPases and microtubule-associated proteins. *Curr Opin Plant Biol*, **16**: 743-748. doi:10.1016/j.pbi.2013.10.010.
- Pietraszewska-Bogiel, A., Lefebvre, B., Koini, M.A., Klaus-Heisen, D., Takken, F.L., Geurts, R., Cullimore, J.V. and Gadella, T.W. 2013. Interaction of *Medicago truncatula* lysin motif receptor-like kinases, NFP and LYK3, produced in

- Nicotiana benthamiana induces defence-like responses. *PLOS ONE*, **8**: e65055. doi:10.1371/journal.pone.0065055.
- Popp, C. and Ott, T. 2011. Regulation of signal transduction and bacterial infection during root nodule symbiosis. *Curr Opin Plant Biol*, **14**: 458-467. doi:10.1016/j.pbi.2011.03.016.
- Ramadurai, S., Holt, A., Krasnikov, V., van den Bogaart, G., Killian, J.A. and Poolman, B. 2009. Lateral diffusion of membrane proteins. *J Am Chem Soc*, **131**: 12650-12656. doi:10.1021/ja902853g.
- Ried, M.K., Antolin-Llovera, M. and Parniske, M. 2014. Spontaneous symbiotic reprogramming of plant roots triggered by receptor-like kinases. *eLife*, **3**. doi:10.7554/eLife.03891.
- Rizk, A., Paul, G., Incardona, P., Bugarski, M., Mansouri, M., Niemann, A., Ziegler, U., Berger, P. and Sbalzarini, I.F. 2014. Segmentation and quantification of subcellular structures in fluorescence microscopy images using Squash. *Nat Protoc*, **9**: 586-596. doi:10.1038/nprot.2014.037.
- Schindelin, J., Arganda-Carreras, I., Frise, E., Kaynig, V., Longair, M., Pietzsch, T., Preibisch, S., Rueden, C., Saalfeld, S., Schmid, B., Tinevez, J.Y., White, D.J., Hartenstein, V., Eliceiri, K., Tomancak, P. and Cardona, A. 2012. Fiji: an open-source platform for biological-image analysis. *Nat Methods*, **9**: 676-682. doi:10.1038/nmeth.2019.
- Sieberer, B.J., Timmers, A.C. and Emons, A.M. 2005. Nod factors alter the microtubule cytoskeleton in *Medicago truncatula* root hairs to allow root hair reorientation. *Mol Plant Microbe Interact*, **18**: 1195-1204. doi:10.1094/MPMI-18-1195.
- Smit, P., Limpens, E., Geurts, R., Fedorova, E., Dolgikh, E., Gough, C. and Bisseling, T. 2007. *Medicago* LYK3, an entry receptor in rhizobial nodulation factor signaling. *Plant Physiol*, **145**: 183-191.
- Spira, F., Mueller, N.S., Beck, G., von Olshausen, P., Beig, J. and Wedlich-Soldner, R. 2012. Patchwork organization of the yeast plasma membrane into numerous coexisting domains. *Nat Cell Biol*, **14**: 640-648. doi:10.1038/ncb2487.
- Tóth, K., Stratil, T.F., Madsen, E.B., Ye, J., Popp, C., Antolin-Llovera, M., Grossmann, C., Jensen, O.N., Schussler, A., Parniske, M. and Ott, T. 2012. Functional Domain Analysis of the Remorin Protein LjSYMREM1 in *Lotus japonicus*. *PLOS ONE*, **7**: e30817. doi:10.1371/journal.pone.0030817.
- Wang, L., Li, H., Lv, X., Chen, T., Li, R., Xue, Y., Jiang, J., Jin, B., Baluska, F., Samaj, J., Wang, X. and Lin, J. 2015. Spatiotemporal Dynamics of BRI1 Receptor and Its Regulation by Membrane Microdomains in Living *Arabidopsis* Cells. *Mol Plant*. doi:10.1016/j.molp.2015.04.005.
- Yokota, K., Fukai, E., Madsen, L.H., Jurkiewicz, A., Rueda, P., Radutoiu, S., Held, M., Hossain, M.S., Szczyglowski, K., Morieri, G., Oldroyd, G.E., Downie, J.A., Nielsen, M.W., Rusek, A.M., Sato, S., Tabata, S., James, E.K., Oyaizu, H., Sandal, N. and Stougaard, J. 2009. Rearrangement of actin cytoskeleton mediates invasion of *Lotus japonicus* roots by *Mesorhizobium loti*. *Plant Cell*, **21**: 267-284. doi:10.1105/tpc.108.063693.

FIGURES AND LEGENDS

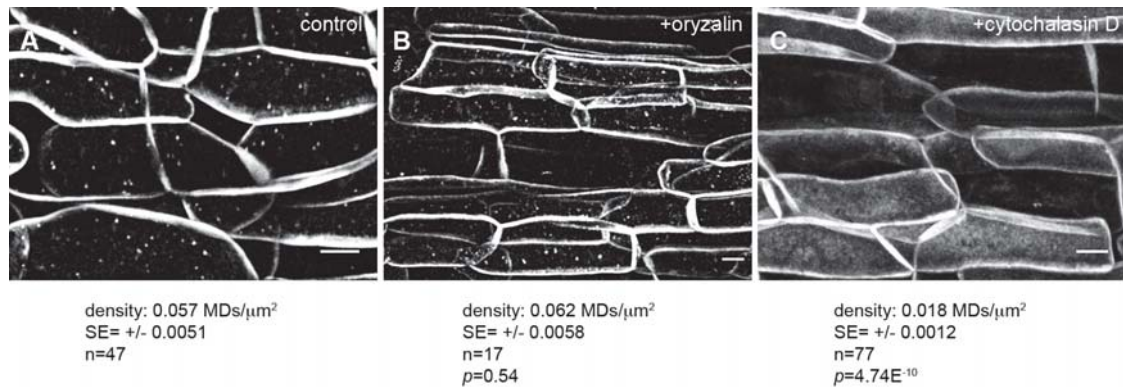


Figure 1. SYMREM1-labelled microdomains are actin-dependent. A YFP-SYMREM1 fusion protein was ectopically expressed in transgenic *M. truncatula* roots and imaged using confocal-laser scanning microscopy. (A) YFP-SYMREM1 labelled distinct membrane microdomains (MDs) in control roots. While treatment with the microtubule depolymerising drug oryzalin did not change YFP-SYMREM1 localization (B) disruption of the actin cytoskeleton by application of cytochalasin D abolish MD targeting of the protein (C). Quantitative image analysis was performed on all samples as indicated below the individual panels. SE= standard error; *p*-value= confidence interval obtained from a Student ttest. Scale bars indicate 10 μm.

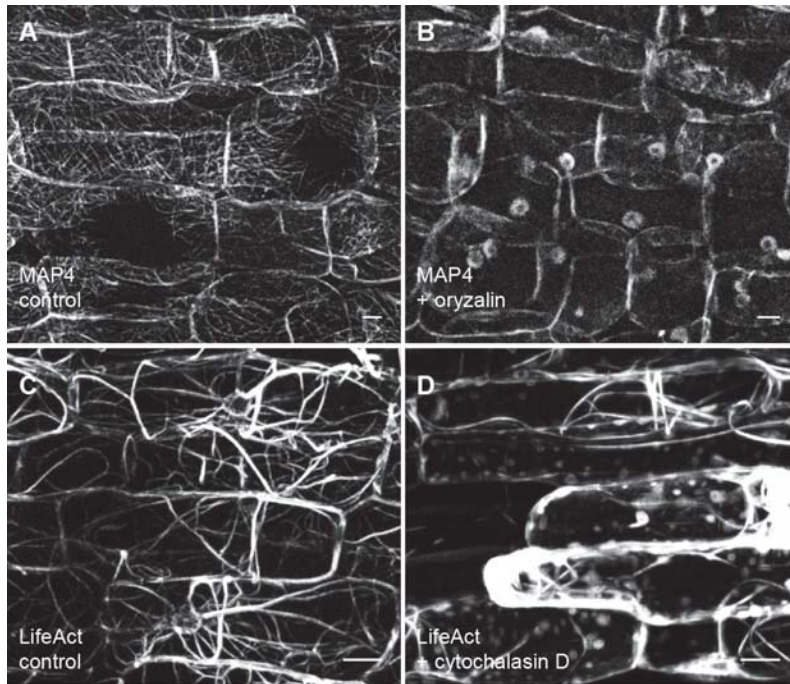


FIGURE 1- FIGURE SUPPLEMENT 1. Depolymerisation of microtubules and actin in *M. truncatula* roots. Expression of the microtubule (MT) associated protein MAP4-YFP clearly labelled the MT network (A) that was successfully depolymerised upon incubation with oryzalin (B). Similarly, actin strands were labelled by YFP-Lifeact (C) and their disruption monitored upon application of cytochalasin D (D). Scale bars indicate 10 μ m.

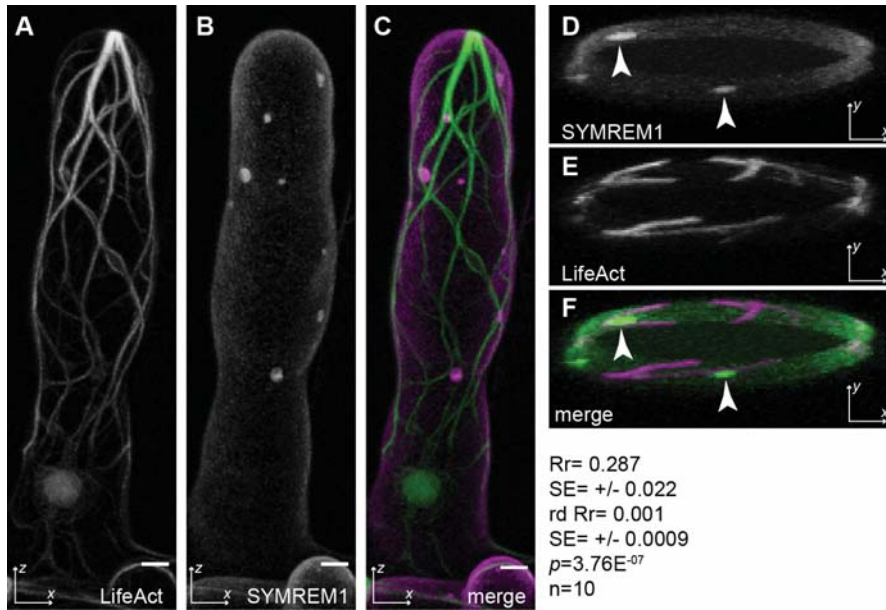


Figure 2. SYMREM1-labelled microdomains co-localize with actin filaments. Cerulean-Lifeact and mCherry-SYMREM1 were cloned in tandem and co-expressed from the same T-DNA in transgenic *M. truncatula* roots. Actin (A) and SYMREM1-labelled microdomains (B) were visualized in the same root hair and co-localized in this system (C). An optical cross-section of the same root hair revealed that SYMREM1-MDs were stretched along the x-axis (arrowheads; D) and actin filaments (E) leading to a significant co-localization (F). Quantitative image analysis was performed on all samples as indicated by the numbers given below panel F. Rr= Pearson correlation coefficient; rd Rr= Pearson correlation coefficient obtained after Costes randomization was applied to the Cerulean-Lifeact image. The respective standard errors (SE) are provided below the Pearson values. *p*-value= confidence interval obtained from a Student ttest comparing Rr and rd Rr. Scale bars indicate 5 μ m.

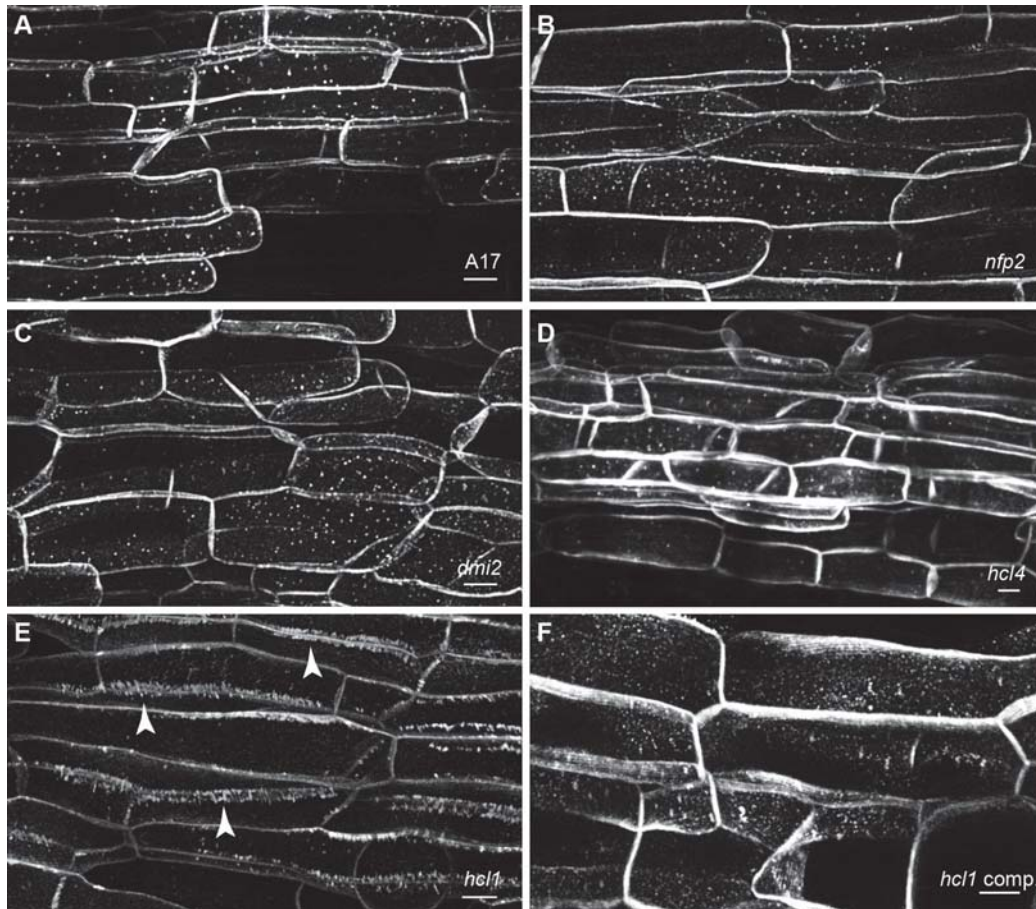


Figure 3. Patterns of SYMREM1-labelled microdomains are altered in the *hcl1* mutant allele. A YFP-SYMREM1 fusion protein was expressed in wild-type A17 roots (A). No qualitative differences were observed upon expression of this construct in the receptor mutant backgrounds *nfp2* (B), *dmi2* (C) and *hcl4* (D). In contrast SYMREM1 MD patterns were strongly altered in the *hcl1* mutant (E; arrowheads). Wild-type like patterns were restored in a complemented *hcl1* mutant line (Haney et al., 2011) (F). Scale bars indicate 10 μ m.

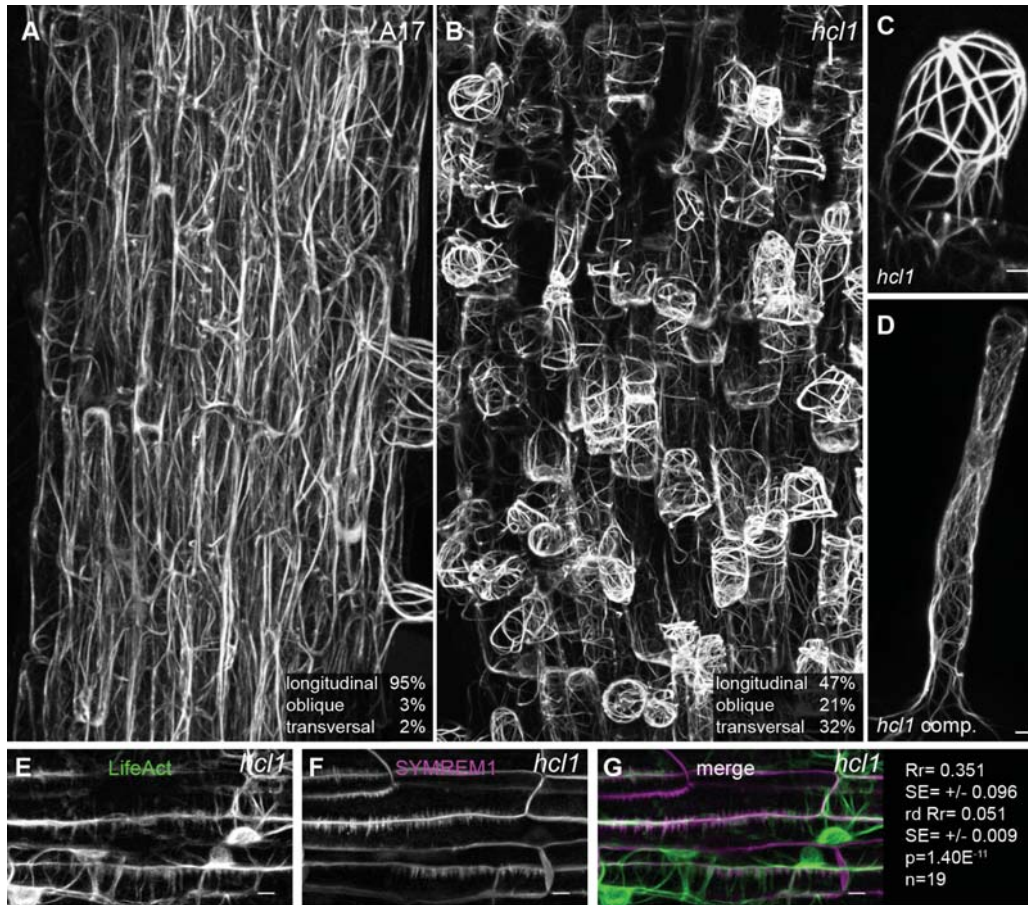


Figure 4. Transgenic roots of *hcl1* show a strongly altered actin pattern. YFP-Lifeact was expressed in wildtype A17 (A) and *hcl1* mutant roots (B) to visualize actin filaments. The orientation of actin strands relative to the root growth axis was scored in root epidermal cells and grouped into longitudinal (0-30°), oblique (30-60°) and transversal (60-90°). Actin filaments in oblique orientation were also found in *hcl1* root hairs (C) while they showed wild-type-like arrangements in the complemented *hcl1* mutant (D). Co-expression of Cerulean-Lifeact (E) and mCherry-SYMREM1 (F) in the *hcl1* mutant background resulted in a significant co-localization (G). Quantitative image analysis was performed on all samples as indicated by the numbers given beside panel G. Rr= Pearson correlation coefficient; rd Rr= Pearson correlation coefficient obtained after Costes randomization was applied to the Cerulean-Lifeact image. The respective standard errors (SE) are provided below the Pearson values. *p*-value= confidence interval obtained from a Student ttest comparing Rr and rd Rr. Scale bars indicate 10 μ m (A,B) and 5 μ m (C-G).

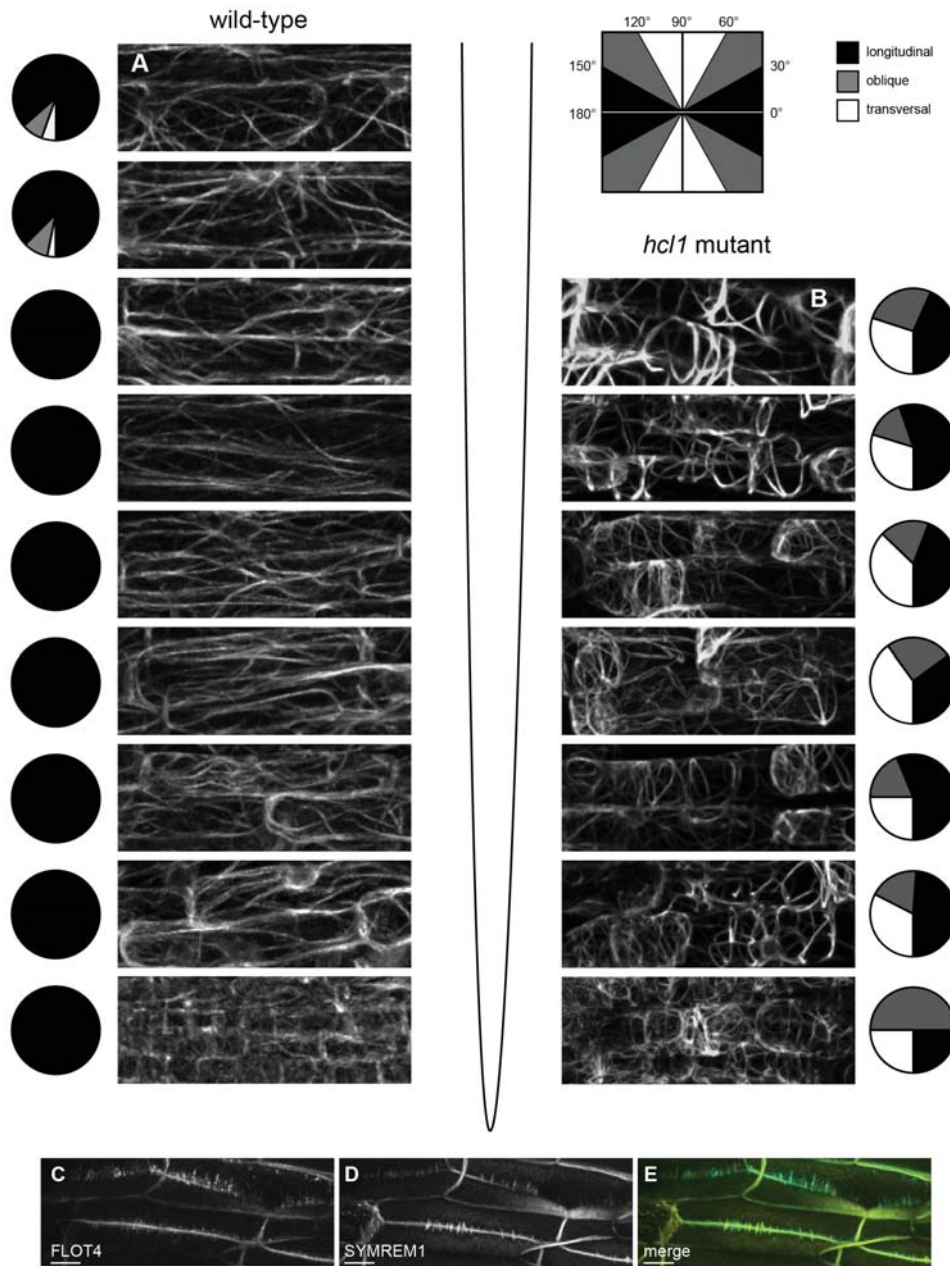


FIGURE 4- FIGURE SUPPLEMENT 1. Actin patterns are altered throughout *hcl1* roots and FLOT4 and SYMREM1 follow these patterns. Expressing the fluorescently-tagged Lifeact peptide in wild-type (A) and *hcl1* mutant roots (B) revealed and altered actin pattern in the mutant along the lower 1 cm of the root. As in Figure 4, actin orientation was categorized relative to the root growth axis and average values of each category are displayed as pie charts. Longitudinal, oblique and transversal patterns are represented by black, grey and white colouration, respectively. Co-expression of FLOT4-mCherry (C) and YFP-SYMREM1 (D) in *hcl1* roots revealed that both proteins followed the altered actin pattern described in Figure 4. Scale bars indicate 10 μ m.

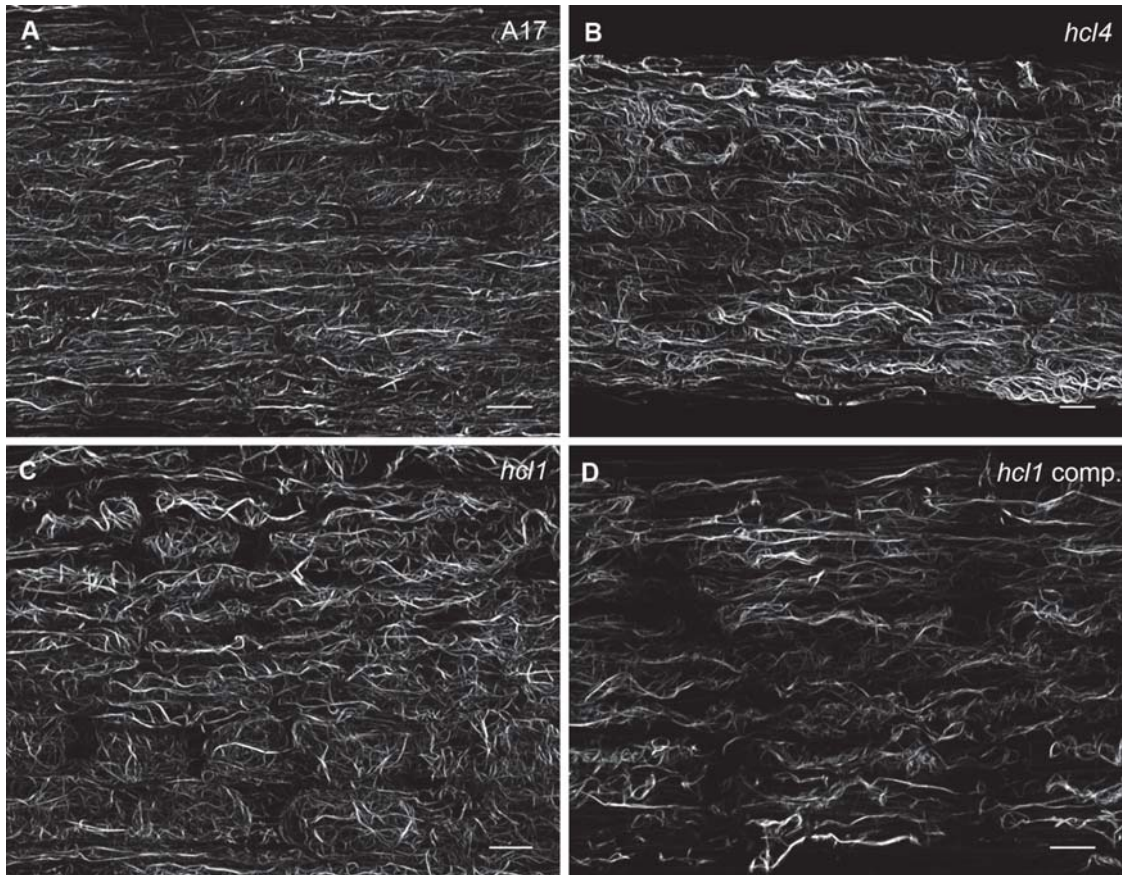


FIGURE 4- FIGURE SUPPLEMENT 2. Actin patterns are more similar in non-transformed roots. Instead of using hairy roots to express a transgene, actin was stained by Phalloidin 568 in wild-type A17 (A), the *hcl4* mutant (B), the *hcl1* mutant (C) and the complemented *hcl1* mutant allele (D). Under these conditions no obvious differences were found between the different genotypes. Scale bars indicate 20 μ m.

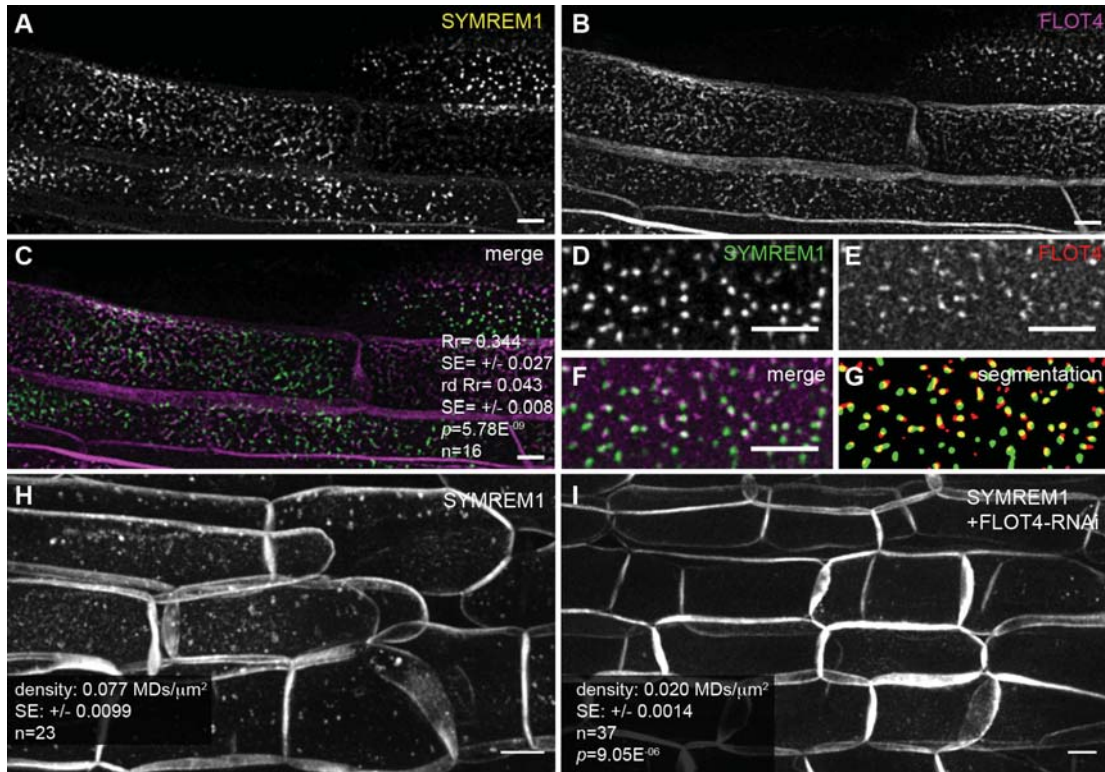


Figure 5. FLOT4 is an essential building block of SYMREM1-labelled microdomains. YFP-SYMREM1 (A) and FLOT4-mCherry (B) co-localized (C) in epidermal cells when being expressed in transgenic *M. truncatula* roots (complemented *hcl1* mutant background). Quantitative data are provided in panel C. Rr= Pearson correlation coefficient; rd Rr= Pearson correlation coefficient obtained after image randomization of the Cerulean-Lifeact image. The respective standard errors (SE) are provided below the Pearson values. *p*= confidence interval obtained from a Student ttest comparing Rr and rd Rr. Close-up of YFP-SYMREM1 (D) and FLOT4-Cherry (E) microdomains at the plasma membrane surface. Overlaying both channels (F) and image segmentation (G) better illustrate co-localization between the two proteins. While YFP-SYMREM1 labelled MDs in root epidermal cells (H), their density was greatly reduced upon co-expression with a FLOT4-RNAi construct (I). *p*-value= confidence interval obtained from a Student ttest comparing roots expressing endogenous FLOT4 (as in H) and those where FLOT4 was silenced (as in I). Scale bars indicate 5 μm (A-F) and 10 μm (H, I).

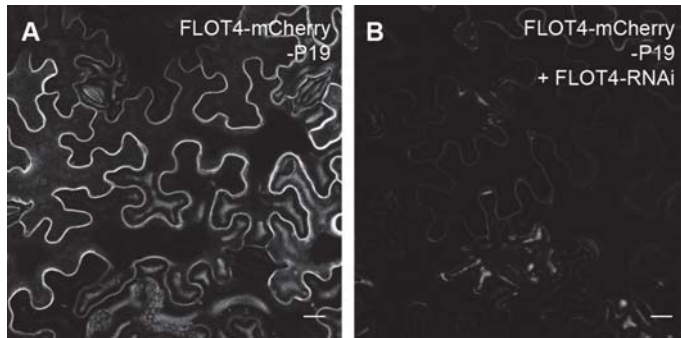


FIGURE 5- FIGURE SUPPLEMENT 1. A FLOT4-RNAi construct efficiently silences FLOT4. Based on published data (Haney 2010) we tested whether overexpressed FLOT4 can be efficiently silenced in *N. benthamiana* leaf epidermal cells. **(A)** Expression of FLOT4-mCherry resulted in clear localization of the fusion protein at the cell periphery. **(B)** In contrast, co-expression with a FLOT4-RNAi construct successfully abolished FLOT4-mCherry accumulation, indicating efficient silencing of the transgene. In both cases we resigned the use of the viral silencing suppressor P19 to not interfere with the cellular silencing machinery. Scale bars indicate 20 μ m.

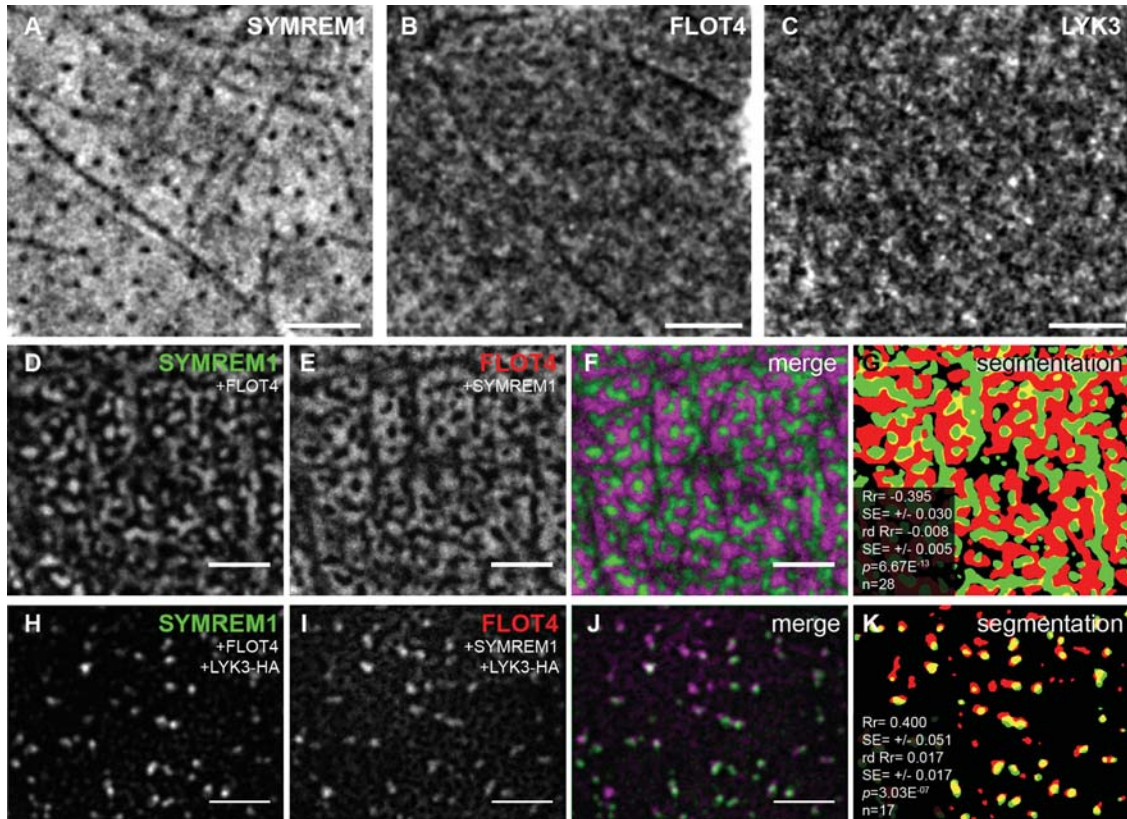


Figure 6. Artificial reconstitution of a symbiosis-related MD (symMD) in a heterologous system. *N. benthamiana* leaf epidermal cells individually expressing the legume-specific proteins YFP-SYMREM1, FLOT4-mCherry and LYK3-GFP revealed almost no MDs being labelled by SYMREM1 (A) while FLOT4 (B) and LYK3 (C) showed a low degree of protein compartmentalization. Co-expression of YFP-SYMREM1 and FLOT4-mCherry induced stronger compartmentalization of SYMREM1 (D) but not of FLOT4 (E). Overlaying the signals from both channels (F) and image segmentation (G) revealed a lack of co-localization and mutual exclusion of both proteins. In contrast triple expression of fluorophore-tagged YFP-SYMREM1 and FLOT4-mCherry together with hemagglutinin (HA) tagged LYK3 resulted in specific accumulations of SYMREM1 (H) and FLOT4 (I) in MDs that showed significant co-localization (J, K). Quantitative data are provided in panels G and K. Rr = Pearson correlation coefficient; $rd Rr$ = Pearson correlation coefficient obtained after image randomization. The respective standard errors (SE) are provided below the Pearson values. p = confidence interval obtained from a Student ttest comparing Rr and $rd Rr$. Scale bars indicate 5 μm .

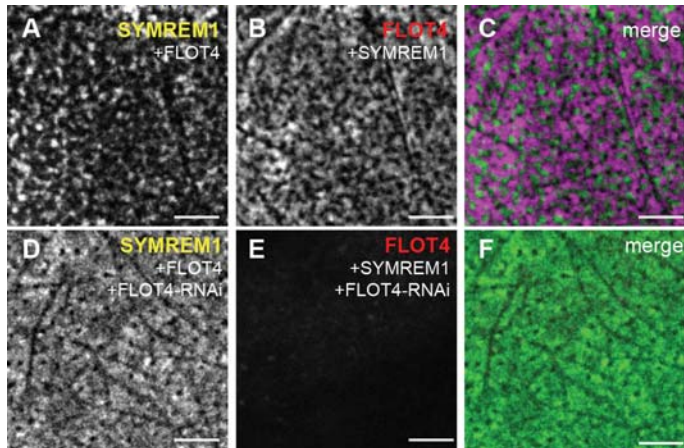


FIGURE 6- FIGURE SUPPLEMENT 1. Compartmentalization of SYMREM1 in leaf epidermal cells is FLOT4 dependent. Co expression of YFP-SYMREM1 (A) and FLOT4-mCherry (B) in *N. benthamiana* leaf epidermal cells resulted in compartmentalization of both proteins, although both proteins did not co-localize (C). Additional expression of a FLOT4-RNAi construct resulted in a loss of FLOT4-mCherry (E) and reverted the localization of SYMREM1 towards less compartmentalized patterns (D). Scale bars indicate 5 μ m.

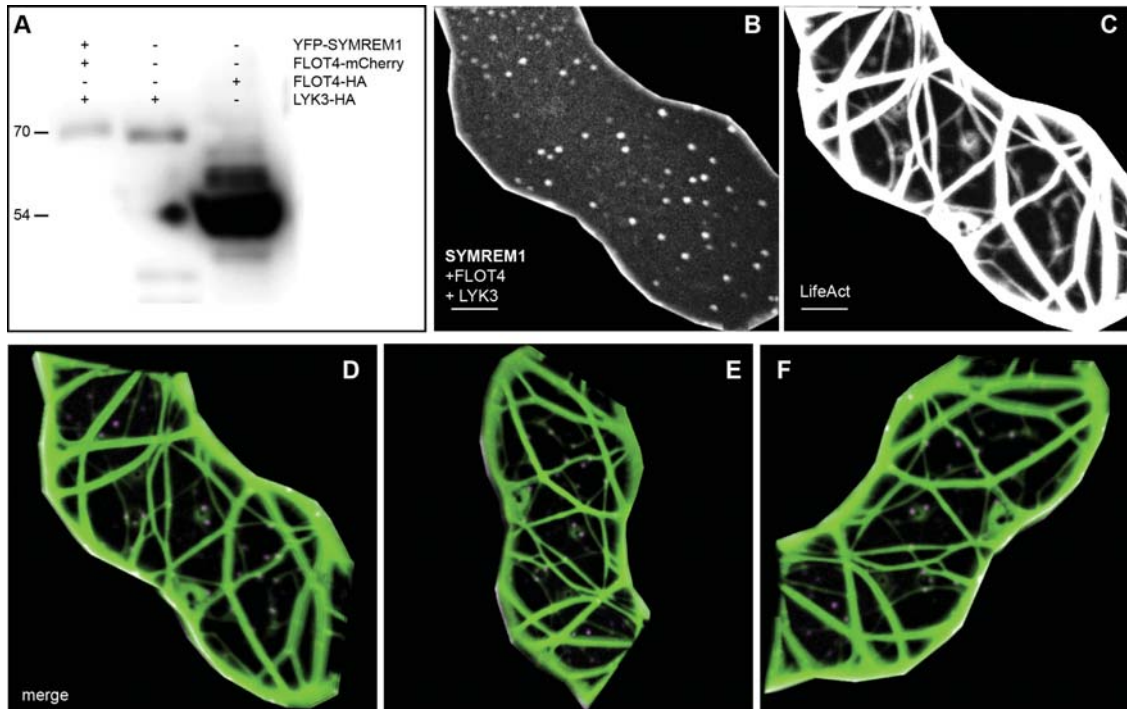


FIGURE 6- FIGURE SUPPLEMENT 2. The reconstituted MD co-localizes with actin. Western Blot analysis revealed the presence of all non-fluorescently tagged proteins shown in Figure 6 (A). Membrane domains labelled by YFP-SYMREM1 in *N. benthamiana* leaf epidermal cells (B) when being co-expressed with FLOT4-mCherry and Cerulean-Lifeact (C) clearly co-localized with actin strands (D-F) as also shown in the homologous system (Figure 2). Scale bars indicate 5 μ m.

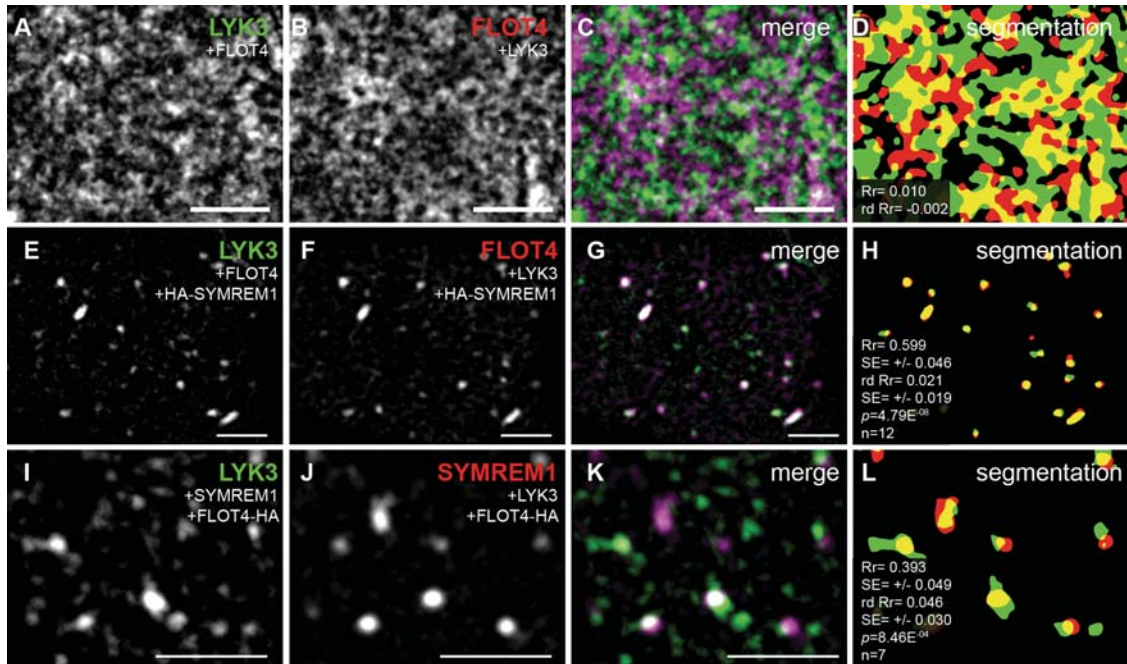


Figure 7. LYK3 is recruited into symMD in a SYMREM1-dependent manner. Combinatorial expression of LYK3, FLOT4 and SYMREM1 in *N. benthamiana* leaf epidermal cells. Co-expression of LYK3 (A) and FLOT4 (B) in the absence of SYMREM1 resulted in moderate compartmentalization of both proteins and the lack of significant co-localization (C, D). In contrast, additional expression of HA-SYMREM1 resulted in labelling of distinct MDs by LYK3 (E) and FLOT4 (F) that co-localized under these conditions (G, H). Similar patterns were observed during co-expression of LYK3-GFP (I) and mCherry-SYMREM1 (J) in the presence of FLOT4-HA where the fluorophore-tagged proteins co-localized (K, L). Proteins fused to GFP are indicated in green, those fused to mCherry in red. Rr= Pearson correlation coefficient; rd Rr= Pearson correlation coefficient obtained after Costes randomization was applied to the Cerulean-Lifeact image. The respective standard errors (SE) are provided below the Pearson values. p = confidence interval obtained from a Student ttest comparing Rr and rd Rr. Scale bars indicate 5 μ m.

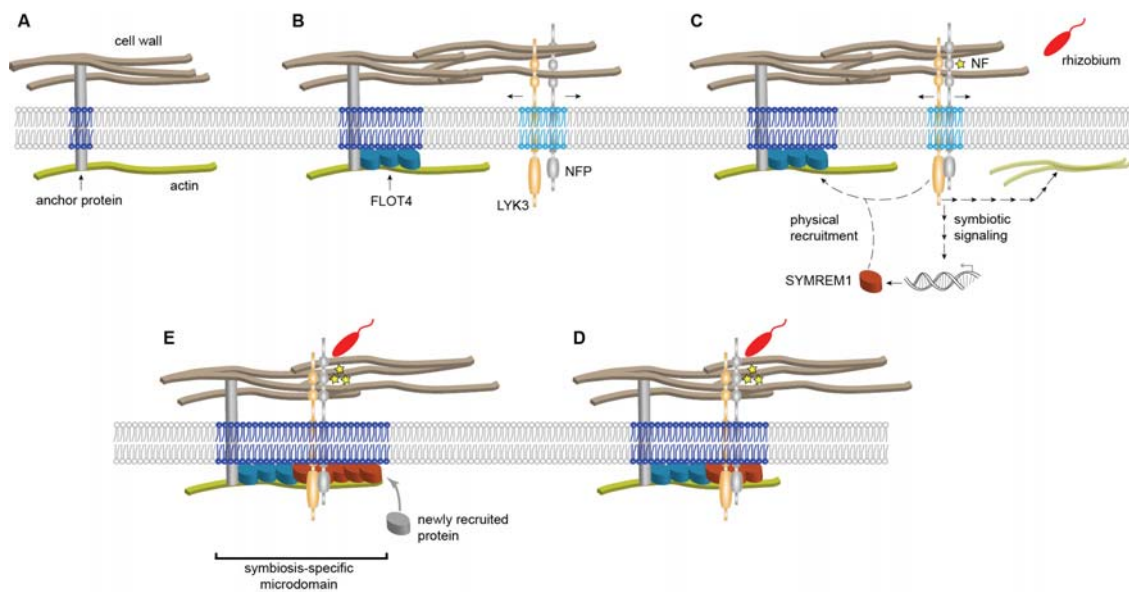


FIGURE 8. A model for the spatio-temporal assembly of a symbiosis-related MD. Lateral stability of a MD core is hypothetically mediated by the cell wall and the actin (or microtubule) cytoskeleton. Anchor proteins that physically connect the cell wall with the cytoskeleton serve as first nucleation points and confer lateral positioning of the MD (blue) (A). In legume roots FLOT4 and LYK3 are constitutively expressed. While LYK3 (orange) (and potentially NFP; grey) is mobile (indicated by arrows) and localizes to a distinct MD (light blue), FLOT4 (turquoise) associates with the MD core and generates initial specificity (B). Oligomerization or accumulation of FLOT4 monomers at the core MD potentially alters the local lipid environment and increases the MD size towards meso-scale dimensions (indicated in blue). Upon Perception of rhizobial Nod Factors (NF) LYK3 associates with NFP (in grey) and initiates downstream signalling that leads to transcriptional activation of *SYMREM1* (C). Furthermore LYK3 signals directly towards actin (indicated by multiple arrows) allowing morphological responses such as root hair deformation. SYMREM1 (red) functions as a secondary scaffold protein that allows recruitment of LYK3 into the FLOT4 labelled MD (D). Here, temporal induction might coincide with increased NF concentrations within a root hair curl. Finally SYMREM1 gets post-translationally modified (e.g. phosphorylated), oligomerises and subsequently recruits additional proteins into the newly formed symbiosis-related MD (E).

3.6 Current projects

3.6.1 Results

3.6.1.1 The receptor-like kinase FLS2 localizes to punctate membrane domains.

The introduction of hydrodynamic friction by transmembrane proteins is one hallmark of membrane sub-compartmentalization (Kusumi et al., 2012b). Hydrophobic mismatch effects and the specific miscibility characteristics of TMDs generate small areas of non-random membrane component distribution (see 2.1.1.4.1) (Marsh and Watts, 1982; Schwille et al., 1999; Lee, 2003; Soubias and Gawrisch, 2013). Sub-compartmentalization of transmembrane proteins has been demonstrated for LINKER FOR ACTIVATION OF T-CELLS (LAT), a scaffold protein important during T-CELL RECEPTOR (TCR) mediated T-cell immune responses (Zhang et al., 1999; Sommers; Connie et al., 2004). Their composition as well as their important role during surface signal perception makes plant RLKs important candidates to study membrane sub-organization.

RLKs often interact with multiple proteins upon signal perception thereby inducing another level of membrane sub-organization. The perception of the bacterial flagellum and its elicitor epitope flg22, is one of the best characterized perception systems of pathogen-associated molecular patterns (PAMPs) (Boller and Felix, 2009). The responsible RLK recognizing the flg22 epitope, FLAGELLIN SENSITIVE 2 (FLS2), undergoes a ligand-induced complex formation with its co-receptor BAK1, which is accompanied by trans- and autophosphorylation events and ultimately the endocytosis of FLS2 (Robatzek et al., 2006; Boller and Felix, 2009). Conditional localization to raft domains was suggested for FLS2, since it co-purified with DIM fractions in a comparative proteomic study between flg22 treated and untreated *A. thaliana* suspension cells (Keinath et al., 2010). As discussed above, DIM fractions are not a biochemical counterpart of any membrane structure present in living cells and claims of membrane raft localization based on DIM fractionations are insufficient (see 2.2.1). Nevertheless, FRAP experiments on *A. thaliana* protoplasts demonstrate that lateral mobility of FLS2 decreases in the presence of its ligand indicating that the lateral organization of the protein switches upon signal perception (Ali et al., 2007). Through a collaboration with the laboratory of Dr. Cyril Zipfel, the localization of FLS2 to membrane microdomains was demonstrated in *A. thaliana* using TIRF microscopy. To investigate, whether the same observations can be made with our experimental setup, the subcellular localization of this key immune receptor was investigated.

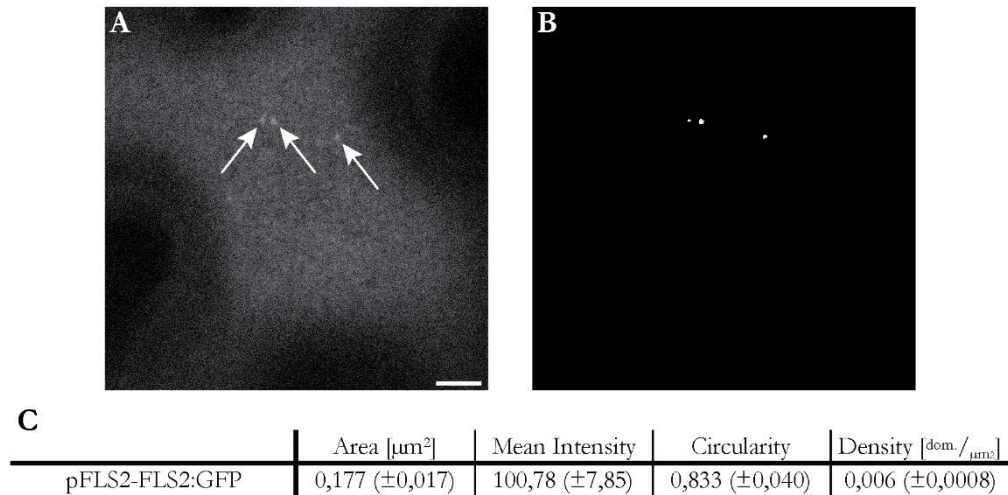


Figure 5: Membrane domain localization of FLS2-GFP in *N. benthamiana* leaf epidermal cells. (A) Confocal image of the upper PM plane of *N. benthamiana* leaf epidermal cell expressing FLS2:GFP under endogenous promoter control. Sparse but distinct bright accumulations of fluorescence signal indicate the proteins localize to membrane domains (arrows). (B) Segmentation of 'A' to quantify membrane domains labeled by FLS2:GFP. (C) A quantitative analysis of 21 different cells enabled us to describe the domains with the parameters given below. Scale bar indicates 5 μm

In order to investigate the putative compartmentalization of FLS2, we transiently expressed FLS2-GFP fusion constructs under expression control of the native FLS2 promoter sequence in *Nicotiana benthamiana* leaf epidermal cells and analysed the subcellular localization microscopically. Three days after infiltration, strong GFP fluorescence could be observed at the cell periphery confirming the PM localization of FLS2 as seen in other studies (Robatzek et al., 2006; Beck et al., 2012). Higher magnification of the upper cell plane revealed sparse but distinct domains of high fluorescence signal, surrounded by equally distributed weaker fluorescence (Figure 5). Since FLS2 undergoes endocytosis, it may be possible that the observed FLS2 membrane domains represent initiation sites of endocytosis (Robatzek et al., 2006; Beck et al., 2012). However, these structures are known to be laterally stable, whereas the observed structures in this experiments displayed a notable lateral mobility. To further describe the FLS2 labelled membrane domains, a quantitative analysis of 21 different cell surface views was conducted. FLS2 labelled membrane domains covered a mean area of $0.177 \mu\text{m}^2 (\pm 0.017 \mu\text{m}^2)$, displayed a mean intensity value of $100 (\pm 7)$ and a circularity value of $0.8 (\pm 0.04)$ in which 1 equals a perfect circle (Figure 5). FLS2 membrane domains exhibited a domain density of $0.06 \text{ domains}/\mu\text{m}^2 (\pm 0.001 \text{ domains}/\mu\text{m}^2)$ making them significantly less abundant than any Remorin labelled membrane domain, or the membrane domains of FLOT1A and FLOT1B (Jarsch et al., 2014).

3.6.1.2 Relocalization of membrane proteins to non-native membrane domains

One way to show the biological role of punctate membrane domains would be by altering a protein's membrane domain localization, without the removal of the protein from the PM. Mislocalization could be achieved via mutation of known membrane localization motifs or by forced interactions with proteins that localize to different membrane domains. Forced interaction can be conferred by antibodies derived from members of the *Camelidae* family. They differ from conventional mammalian antibodies because they lack light chain subunits. Therefore, these “nanobodies” are structurally less complex than conventional antibodies, facilitating their heterologous expression in diverse cell types. A special GFP-binding nanobody (GBP), suitable for expression and localization experiments *in vivo* has been developed (Rothbauer et al., 2006) that enables these antibodies to be used in a variety of biotechnological approaches (Muyldermans, 2001; Conrad and Sonnewald, 2003).

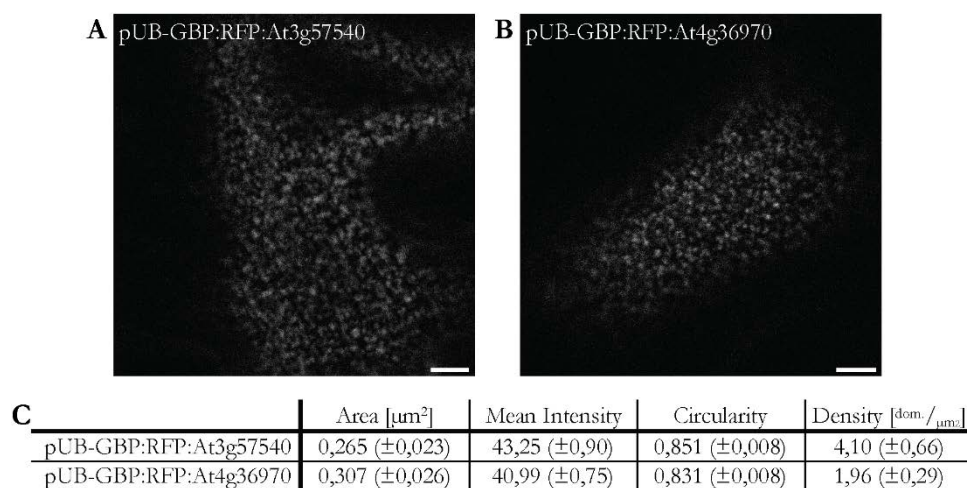


Figure 6: Localization of GBP:RFP labelled Remorins At3g57540 and At4g36970.

Confocal microscopy of GBP:RFP labelled Remorins At3g57540 and At4g36970 expressed under constitutive expression in *N. benthamiana*. At3g57540 (A) as well as At4g36970 (B) labelled distinct membrane domains in the upper PM plane of leaf epidermal cells. Images of at least 17 individual cells were used to quantitatively describe these domains (C). Scale bars indicate 5 μm

To investigate the effects of membrane domain mislocalization, FLS2 was chosen as a target protein.

We generated GBP:RFP fusions of Remorin proteins At3g57540 and At4g36970 and transiently expressed these constructs in *N. benthamiana* leaf epidermal cells. Overall cells varied in expression strength. In highly expressing cells domain localization was not clear. This observation is due to the reported accumulation of protein that is not bound to a domain within the inter-domain space (Otto and Nichols, 2011; Jarsch et al., 2014). For this reason, only weak expressing cells were considered. In those cells, fluorescence signals derived from the two GBP:RFP:Remorin constructs

Results

were observed in distinct membrane domains (Figure 6 A & B). The domains displayed no notable lateral mobility, but were stable over 1 h.

Even though the added GBP tag is small compared to conventional antibodies, it adds a considerable size to the fusion protein. Moreover, the binding capacity of GBP might interfere with native localization to membrane domains of Remorin proteins. Therefore, 17 cells expressing GBP:RFP:At3g57540 and 19 cells expressing GBP:RFP:At4g36970 were used for quantification of the domain parameters size, intensity, circularity and density. As Figure 6 C shows, for both constructs, all values except for the mean intensity value differed significantly from the published domain parameters. The increase of domain size to $0.265 \mu\text{m}^2$ ($\pm 0.023 \mu\text{m}^2$) for At3g57540 and $0.307 \mu\text{m}^2$ ($\pm 0.026 \mu\text{m}^2$) for AtRem 6.4 as well as the increase of domain density to 4.10 domains/ μm^2 (± 0.66 domains/ μm^2) for At3g57540 and 1.96 domains/ μm^2 (± 0.29 domains/ μm^2)

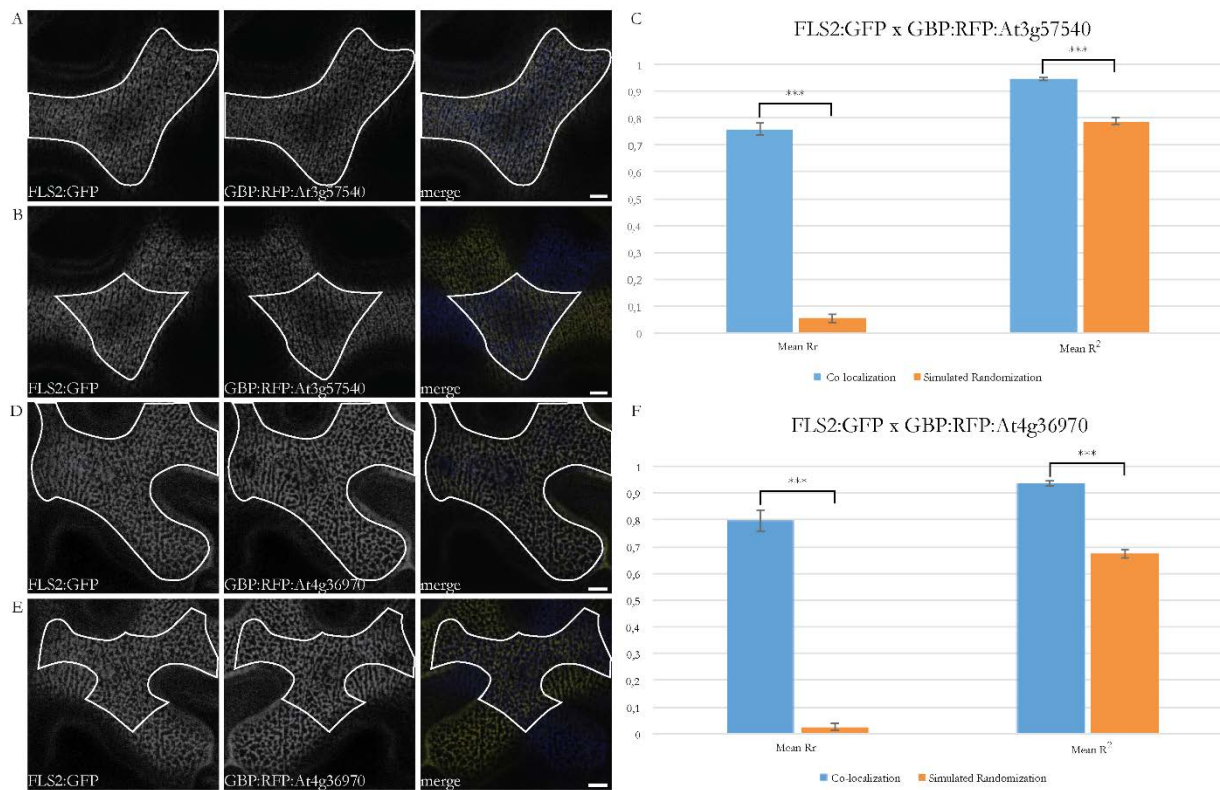


Figure 7: Relocalization of FLS2:GFP due to co-expression with GBP:RFP labelled Remorins.

Co-localization analysis of cells co-expressing FLS2:GFP and either GBP:RFP:At3g57540 (A) or GBP:RFP:At4g36970 (D). Of every image, only areas showing signal (indicated by white masks) were considered for the calculation of Pearson's correlation coefficient (Rr) and the squared overlap coefficient (R²). Likewise, the correlation coefficients were calculated on a simulated randomized image samples that were generated by flipping the image of RFP fluorescence horizontally (B & D). The correlation coefficients are indicated in C and F. Scale bars indicate 5 μm . ***= students t-test p-value > 0.001.

for At4g36970 suggest that the protein abundance is higher and domain localization might be altered due to overexpression of the protein.

To test whether the GBP:RFP:Remorin constructs are able to successfully bind and mislocalize FLS2:GFP, we co-expressed FLS2:GFP either with GBPRFP:At3g57540 or GBP:RFP:At4g36970 in *N. benthamiana* leaf epidermal cells. The localization pattern was investigated microscopically (Figure 7A and D). To quantify the co-localization coefficients, at least 8 images were acquired. Similar to Jarsch et al. 2014, the Pearson correlation coefficient R_r (Manders et al., 1993) and the squared overlap coefficient R^2 (Manders et al., 1993) were calculated (Figure 7 C and F). The strength of calculating correlations using the Pearson correlation coefficient is its insensitivity to background noise (Adler and Parmryd, 2014). Its values theoretically range from -1 to 1 where 1 describes perfect co-localization and -1 exclusion of signal (Manders et al., 1993). However, negative and low R_r values are difficult to interpret and often vary significantly because of intensity differences in the two observed channels (Zinchuk et al., 2007). The squared overlap coefficient R^2 varies between 0 and 1, where 1 is defined as a perfect co-localization event. It is less prone to calculation artifacts due to intensity variations, but therefore also considerably error prone to image noise (Adler and Parmryd, 2014). Since R^2 is also strongly influenced by the amount of pixels considered in both channels, the pixel ratio from both channels was calculated ($N_{\text{channel 1}}/N_{\text{channel 2}}$). Only images with a ratio, close to 1 were considered. To simulate a random distribution of proteins, one channel of each image pair was flipped horizontally and the co-localization of signal containing regions of interest in this new “simulated randomized” image pair was calculated (Figure 7 B and E). In case of the co-expression of FLS2-GFP and GBP:RFP:At3g57540, fluorescence signal of both fluorophores showed a dense, irregular distribution over the whole membrane that was interrupted by filamentous structures (Figure 7 A). The high Pearson correlation coefficient of 0.757 and equally high Manders correlation coefficient of 0.943 (Figure 7 C) demonstrate the almost perfect co-localization of the two fluorescence signals. The fluorescence pattern of the co-localization of FLS2:GFP and GBP:RFP:At4g36970 exhibited a more scattered, network-like structure, that was disrupted by filamentous structures (Figure 7 D). Again, the Pearson and Manders correlation coefficients yield high values of 0.796 and 0.936 respectively, demonstrating that the GBP binding tag is able to actively alter the localization of FLS2-GFP in *N. benthamiana*.

To summarize, these experiments show that co-expression of GBP:RFP tagged Remorins and FLS2:GFP induces significant alterations of both proteins lateral distribution within the PM. With further improvement of experimental conditions, the introduced system is a promising tool to investigate the role of FLS2 localization to membrane domains.

3.6.2 Material and Methods

3.6.2.1 Methods

3.6.2.1.1 Recombinant DNA methods

3.6.2.1.1.1 DNA Amplification using polymerase chain reaction (PCR)

3.6.2.1.1.1.1 Analytical PCR

Analytical polymerase chain reactions (PCR) were carried out to verify the insertion of fragments after cloning steps or the successful transformation of *A. tumefaciens*. For these purposes, the NEB *Taq*-polymerase was used. PCR reaction mixtures were prepared according to the polymerase manufacturers recommendations. 20 µl of the PCR mix (see 3.6.2.4.4) were incubated in a thermocycler set to the following cycling conditions.

Table 1 Cycle conditions for analytical PCR reactions

Cycle step	Temperature	Time	Cycles
Initial Denaturation	94 °C	2 min	1
Denaturation	94 °C	30 sec	7
Annealing	48-60 °C *	30 sec	36
Elongation	72 °C	30 sec/kb	1
Final Extension	72 °C	8 min	1
Hold	4 °C	∞	

*temperature varies according to the melting temperature of used primers

Difficult PCR reactions were carried out with a touch-down PCR protocol that differs in a decreasing annealing temperature of – 0,5 °C per cycle.

3.6.2.1.1.1.2 Preparative PCR

Preparative polymerase chain reactions were used to amplify DNA fragments for cloning purposes. Therefore, the Phusion© High-Fidelity Polymerase was used as its proofreading ability and high processivity ensure error free, long amplicons. PCR reaction mixtures were prepared according to the polymerase manufacturers recommendations. 20 µl of the PCR mix (see 3.6.2.4.4) were incubated in a thermocycler set to the following cycling conditions

Results

Table 2 Cycle conditions for preparative PCR reactions

Cycle step	Temperature	Time	Cycles
Initial Denaturation	98 °C	2 min	1
Denaturation	98 °C	20 sec	7
Annealing	55-60 °C *	20 sec	36
Elongation	72 °C	15 sec/kb	1
Final Extension	72 °C	5 min	1
Hold	4 °C	∞	

*temperature varies according to the melting temperature of used primers

Difficult PCR reactions were carried out with a touch-down PCR protocol that differs in a decreasing annealing temperature of – 0,5 °C per cycle.

3.6.2.1.1.2 Restriction digest of plasmid DNA

To verify the insertion of DNA fragments into plasmid backbones, analytical restriction digestions were performed using appropriate restriction enzymes. Digestion reactions were assembled on ice and incubation temperature as well as time were chosen according to manufacturers recommendation.

3.6.2.1.1.3 Multi-fragment cloning with the Golden Gate Cloning Toolbox

Constructs were cloned using the Golden Gate cloning toolkit described in (Binder et al., 2014). Mutagenesis of BsaI and BpiI free inserts was conducted by insertion of silent point mutations (see 3.6.2.1.1.4)

3.6.2.1.1.4 Site directed mutagenesis during amplification

In order to mutate single nucleotide residues within a DNA sequence, oligonucleotides were generated that included a BpiI restriction site that generated an overlap including the site of mutagenesis. After DNA amplification, individual fragments were combined into a LI vector by cut-ligation (see 3.6.2.1.1.3), thereby reconstituting the DNA sequence of interest.

3.6.2.1.1.5 Sequencing of DNA

Sequencing of DNA was conducted by the Genetics Sequencing service at the LMU. Reactions were prepared as stated by the protocols provided by the service.

3.6.2.2 Methods for plant work

3.6.2.2.1 Plant growth conditions

Prior to transformation, *N. benthamiana* plants were grown 4-6 weeks at 22 °C/ 60 % humidity long-day (16 h light/ 8h dark) conditions in a walk-in growth cabinet.

3.6.2.2.2 Transient protein expression in *N. benthamiana* leaf epidermal cells

Agrobacterium tumefaciens mediated transient transformation of *N. benthamiana* was performed as described in (Tóth et al., 2012) using OD=0.01 for infiltration. After infiltration, plants were incubated for 2-3 days at growth conditions before expression was checked microscopically

3.6.2.3 Microscopy methods

3.6.2.3.1 Confocal microscopy

Using a biopsy puncher (4mm diameter), leaf discs from transformed *N. benthamiana* plants were prepared and mounted on a glass slide, using a No. 1.5 cover slip glass.

Confocal microscopy was performed on a Leica TCS SP5 CLSM using a 20x/0.7 water immersion lens. GFP was excited using the 488 nm laser line of a 100 mW Lasos LGK 7872 ML05 SP5 argon laser and fluorescence was recorded from 495 nm to 550 nm. Excitation of RFP was accomplished with a 10 mW Lasos YLK6110T Diode Pumped Solid State-Laser with a 561 nm output. Fluorescence was recorded between 570 nm and 650 nm. To reduce background noise, 2 line and 2 frame averages were performed per image. For co-localization analysis, images were captured using sequential scans between frames.

3.6.2.3.2 Particle analysis

All image analysis was performed using Fiji (Schindelin et al., 2012). Segmentation of up to 17 to 21 images was done using manual thresholds on background-subtracted images with a rolling ball radius of 80 pixels. Using the particle analysis tool, shape descriptors were determined. Average values for domain area, intensity, circularity and were calculated and evaluated using Microsoft Excel.

3.6.2.3.3 Co-localization analysis

All image analysis was performed using Fiji (Schindelin et al., 2012). Calculation of Pearson correlation coefficients and R^2 , was done with the Wright Cell Imaging Facility Colocalisation Analysis Tool (Li et al., 2004). Prior to calculation, the images were subjected to a background subtraction of 80 pixels in order to avoid influence of image noise. The calculation was restricted to regions of interest that excluded signal-free areas of the image, auto-fluorescence or cell-wall reflections.

3.6.2.4 Buffers and solutions

3.6.2.4.1 Antibiotic stock solutions

Antibiotic	Stock concentration
Ampicillin	100 mg/ml
Carbenicilin	50 mg/ml
Chloramphenicol	34 mg/ml
Gentamicin	25 mg/ml
Kanamycin	50 mg/ml
Rifampicin	50 mg/ml
Spectinomycin	100 mg/ml
Streptomycin	200 mg/ml

3.6.2.4.2 Infiltration medium for *Agrobacterium tumefaciens* mediated transformation of *N. benthamiana*.

Component	[Final]
MgCl ₂	10 mM
MES KOH pH 5.6	10 mM
Acetosyringone	150 μM
Agrobacteria	Appropriate OD

3.6.2.4.3 Buffers and solutions for recombinant DNA techniques**3.6.2.4.4 Reaction mix for analytical PCR**

Component	Amount
dNTPs (10 mM each)	0,2 μ l
MgCl ₂ (50 mM)	0.2 μ l
10X Standard Taq-polymerase buffer	2 μ l
Fwd Primer (10 pmol/ μ l)	0.2 μ l
Rev Primer (10 pmol/ μ l)	0.2 μ l
<i>Taq</i> -Polymerase	0.05 μ l
Template (colony dipped in H ₂ O)	1,5 μ l
H ₂ O	16,65 μ l

3.6.2.4.5 Reaction mix for preparative PCR

Component	Amount
dNTPs (10 mM each)	0,2 μ l
5X Phusion HF-Buffer	4 μ l
Fwd Primer (10 pmol/ μ l)	0.2 μ l
Rev Primer (10 pmol/ μ l)	0.2 μ l
Phu-Polymerase	0.2 μ l
Template	5-50 ng
H ₂ O	ad 20 μ l

3.6.2.4.6 Cut-ligation reaction mix to generate LI constructs

Component	Amount
LI vector	100 ng
PCR fragment	200 ng
BpI	1 μ l
T4 DNA Ligase	2 μ l
10X T4 DNA Ligase Buffer	1,5 μ l
H ₂ O	ad 15 μ l

3.6.2.4.7 Cut-ligation reaction mix to generate LII constructs

Component	Amount
LII vector	100 ng
Fragment A-B	100 ng
Fragment B-C	100 ng
Fragment C-D	100 ng
Fragment D-E	100 ng
Fragment E-F	100 ng
Fragment F-G	100 ng
BsaI	1 μ l
T4 DNA Ligase	2 μ l
10X T4 DNA Ligase Buffer	1,5 μ l
H ₂ O	ad 15 μ l

3.6.2.4.8 Reaction mix for analytical restriction digestions

Component	Amount
Vector	200 ng
Restriction enzyme	0,3 μ l
10X NEB buffer	1,5 μ l
H ₂ O	ad 15 μ l

4 Discussion

4.1 Membrane domains represent a new layer of compartmentalization

4.1.1 The role of Remorin lipidation

Although Remorin proteins were initially identified as PM resident proteins over 20 years ago, the mechanism of how Remorins actually bind to the PM remained unclear. Since sequence predictions were unable to identify any known membrane attachment mechanism with high accuracy, the mode used by these proteins to associate with the PM was unclear (Raffaele et al., 2009). Recent work demonstrated that the C-terminal 35 amino-acids of StRem1.3, termed the RemCA, are indispensable for the PM localization of this protein (Perraki et al., 2012). Moreover it has been illustrated that the RemCA peptide confers a tight PM association that is comparable to transmembrane proteins. Circular dichroism experiments suggest the peptides folding into two α -helical structures in nonpolar environments. *In silico* predictions of RemCA fold into a α -helix suggested that the peptide forms two amphipathic helices, one large comprised of amino acids 172-186 and a shorter one from amino-acids 190-195 (Perraki et al., 2012).

Based upon these data it was hypothesized that StRem1.3 binds the PM via two stages of RemCA folding. The whole process is initiated by the folding of the large 172-186 helix in the proximity of the membrane. Through this mechanism, positively charged residues become concentrated at one plane of the helix, attracting the protein to the negatively charged surface of the PM via electrostatic interactions. Here, it should destabilize the lipid packing to open a gap where the hydrophobic section of the large amphipathic helix can insert into the PM. The hydrophobicity within the membrane core is supposed to induce folding of the second helix, including the formation of a hairpin that creates a hydrophobic pocket. Functional implication of this hydrophobic pocket would be a deepening and strengthening of the Remorin insertion into the membrane. Based on the peptides binding to PtdSer, phosphatidic acid (PA), PtdIns P3,5, PtdIns P3,4 and sphingosine 1-phosphate on lipid strips, it was further hypothesized that RemCA confers direct lipid binding specificity and thereby controls the proteins localization to membrane domains (Perraki et al., 2012).

As appealing as this model is, it is questionable if this is really the universal mode of Remorin proteins PM attachment. Even though these peptides are important for binding, they are obviously not sufficient for it, as the RemCA peptides of all *Arabidopsis* Remorins except for At2g02170, At1g30320, At4g36970 and At5g61280 were unable to localize to the PM (Konrad et al., 2014). Moreover, other mechanisms have been proposed (Hemsley et al., 2013). My work ultimately

Discussion

showed that S-acylation, known to confer strong attachment to membranes, is a predominant post-translational modification of *Arabidopsis* Remorins, including the StRem1.3 homologue AtRem1.2 (shown in Hemsley et al. (2013)), and the symbiotic Remorin SYMREM1 from *Medicago truncatula*. In contrast to other S-acylated proteins, for example Flotillins (Li et al., 2012; Trusov et al., 2012) which are S-acylated at N-terminal protein regions, lipidation of Remorin proteins is restricted to the C-terminal RemCA region (Konrad et al., 2014). Point mutations of cysteine residues prohibited S-acylation and led to a loss of PM localization in several RemCA peptides as well as strongly interfered with full-length protein localizations. The same principle has been demonstrated using the calcium sensor CBL2. This *A. thaliana* protein localizes to the vacuolar membrane and is S-acylated. However, mutations of S-acylated cysteine residues abolished the protein's membrane localization (Batistič et al., 2012). This illustrates the functional relevance of S-acylation as a membrane attachment mechanism and elevates this post-translational modification as the major membrane binding mechanism of Remorin proteins (Konrad et al., 2014).

In mammalian systems, S-acylation is commonly perceived to be associated with protein localization to membrane domains (Levental et al., 2010). At least for Remorin proteins, membrane domain localization seems to be more diverse, since the S-acylation mutant SYMREM1C197A still localizes to distinct membrane domains within the PM of yeast cells and *M. truncatula* root epidermal cells. Deacylation of At4g36970 resulted in an increased association with immobile membrane domains (Konrad et al., 2014). This argues that S-acylation may in some cases restrict membrane domain localization and that Remorins are targeted to these sites by another, so far undescribed mechanism.

Whereas deacylation of PM localized RemCA peptides of At4g36970 and SYMREM1 resulted in a loss of PM localization, the corresponding deacylated full-length proteins remained at the PM. This observation indicates that other mechanisms influence the PM localization of Remorin proteins. The presence of the coiled-coil domain, correlated with this localization pattern, suggesting that in addition to S-acylation, protein-protein interactions are also important for PM localization of Remorins (Konrad et al., 2014).

Weak membrane association is a feature, often observed to be required prior to S-acylation (Lavy and Yalovsky, 2006; Sorek et al., 2007; Batistič et al., 2008). The reason for this is the inherent property of PAT enzymes (S-acylation conferring enzymes, see 2.1.1.3) acting as transmembrane proteins (Roth et al., 2002; Hemsley et al., 2005; Batistič, 2012). In order to interact with PAT enzymes, proteins that are subsequently S-acylated must exhibit at least a weak intrinsic affinity to the membrane hosting target specific PATs (Batistič, 2012). Whether or not this is mediated by the predicted long α -helical stretch, hypothesized by Perraki et al., 2012 to form in the vicinity of membranes, remains to be shown.

Prediction of S-acylated residues within Remorins At3g48940, At3g57540 and At2g41870 of *Arabidopsis* yielded no putative S-acylation sites (Konrad et al., 2014). It may be that these proteins undergo rare acylation reactions such as O- or N-acylation, but the experimental procedure used in this study does not allow identification of these modifications. Since Remorins are devoid of other lipidation motifs, protein-protein interactions might also be crucial for membrane attachment of Remorins lacking S-acylated Cysteines in their C-terminal region (Konrad et al., 2014).

Since Remorin proteins have been established as universal markers for *Arabidopsis* microdomains, it is important to understand the mechanism of how these proteins actually bind to the PM. Even though S-acylation of Remorin proteins strongly increases their affinity to the PM, it is not the primary determinant of their sub-compartmentalization within the lipid environment. This is astonishing, since our knowledge about lipid-lipid interactions and the resulting phase behaviours of membrane lipids (see 2.1.1.1) would suggest, that S-acylated proteins associate with densely packed areas within the membrane due to the saturation status of their lipid anchor. However, neither S-acylation nor any other lipidation has so far been shown to be sufficient for targeting to plant membrane domains *in vivo* (Hemsley, 2014). Moreover, the loss of S-acylation does not impair protein localization to PM compartments of caveolins (Dietzen et al., 1995). For this reason, it may be appropriate to change the point of view on membrane sub-organization away from being lipid-centric and to include additional factors beyond lipid-lipid interactions to predominantly drive membrane organization.

The most prominent factor would be membrane-associated proteins (see 2.1.1.2). It has been suggested that local protein crowding promotes the segregation of proteins into membrane domains and that membrane domain formation is driven by proteins (Levental et al., 2010; Drücker et al., 2013). This is supported by the finding that the sequence of TMDs influence their localization pattern in yeast cells and that proteins, whose TMDs share a higher sequence similarity are more likely to co-localize (Spira et al., 2012). However, membrane domains labelled by different proteins never show perfect co-localizations (Spira et al., 2012; Jarsch et al., 2014). It should therefore be considered that membrane domains are gradual transitions of differentially organized structures. As a consequence the lipid environment may be dictated by the protein composition via their specific lipid interaction properties. Considering Remorin proteins, the essential interactions would mainly involve lipid headgroups and amino-acid residues in the vicinity of the S-acylation site. Based on these physiochemical properties, other proteins could be recruited into these domains. Changing lipidation states of proteins within these domains would then allow dynamic changes in the proteolipid environment in order to remove old or recruit new components to the membrane domain (Hemsley, 2014).

4.1.2 The diversity of Remorin labelled membrane domains opens new possibilities to investigate PM sub-compartmentalization

The preparation of DIMs was considered the biochemical method of choice to study membrane domains throughout different biological systems including plants (Brown and Rose, 1992; Simons and Ikonen, 1997; Ayllón et al., 2002; Fittipaldi et al., 2003; Mongrand et al., 2004). Co-purification of sphingolipids, cholesterol and GPI-anchored proteins in DIM fractions led to the assumption that DIMs represent a *bona fide* membrane domain. It should however be kept in mind that DIMs are artificial structures that are not present in living cells and thus cannot represent the real heterogeneity of co-existing membrane domains *in vivo* (Zurzolo et al., 2003; Kierszniowska et al., 2009; Simons and Gerl, 2010; Tanner et al., 2011). Even though DIMs may be used as a biochemical method to enrich certain proteins and lipids, accumulation of two proteins in these fractions does not provide any evidence, whether these proteins co-localize within an intact plasma membrane. Conversely, the absence of a protein from DIMs cannot be equalized with a lack of its sub-compartmentation in cells (Malinsky et al., 2013). Therefore, live cell imaging currently represents the most direct way to describe membrane domains *in vivo*.

Membrane domains have been visualized in the prokaryotic organisms *Bacillus subtilis* and *Paramecium tetraurelia* (Bach and Bramkamp, 2013; Reuter et al., 2013) and various eukaryotic biological systems (Harder, 2003; Ghossoub et al., 2011; Spira et al., 2012; Tóth et al., 2012; Jarsch et al., 2014). This widespread appearance suggests that membrane sub-compartmentalization is an ancient organizational principle, whose biological reasoning is far from understood. Most investigations on non-random protein distribution were restricted to individual or a very small subset of proteins. Only recently an astonishingly high degree of PM sub-organization in yeast was shown. Using TIRF microscopy on a representative subset of 46 proteins covering main functional categories, Spira et al. 2012 revealed the PM sub-organization of *S. cerevisiae*. Even though the vast majority of proteins bound the PM via one or more TMDs, all proteins investigated displayed non-homogeneous lateral distributions ranging from distinct patches to network-like structures (Spira et al., 2012).

Plant PMs are also sub-compartmentalized into distinct microdomains (Sutter et al., 2006; Törnroth-Horsefield et al., 2006; Homann et al., 2007; Krügel et al., 2008; Raffaele et al., 2009; Gutierrez et al., 2010; Li et al., 2011; Tóth et al., 2012; Demir et al., 2013; Hao et al., 2014; Klymchenko and Kreder, 2014). The conditional co-localization of *M. truncatula* FLOT4 together with LYK3 elegantly showed the co-existence of different domains within plant PMs (Haney et al., 2011). The detailed investigation of microdomains, in *A. thaliana* and *N. benthamiana* labelled by 20 different proteins, including Remorins and Flotillins proteins provides the first insight into the variety of different membrane microdomains in plants. Extensive co-localization analysis revealed

the disparity in localization among these proteins and revealed that phylogenetically close proteins were more likely to co-localize than phylogenetically distinct protein pairs. Using quantitative imaging, these distinct membrane domains could be characterized using several parameters such as size, shape or density (Jarsch et al., 2014).

The physical limitation of light microscopy defined by to the diffraction limits of light (Abbe, 1873; Rayleigh, 1903) is a major obstacle for microscopy approaches. Membrane domains labelled by StRem1.3 in *A. thaliana* have been observed to have a size of 97 nm large membrane domains labelled by StRem1.3 in *Arabidopsis*, using stimulated emission depletion (STED) microscopy (Demir et al., 2013). The same domains, visualized with CLSM could only be resolved to a mean domain size of 250 nm. Moreover, electron microscopy of immunolabelled *N. benthamiana* PM vesicles predicted StRem1.3 marked membrane domains to be ~75 nm wide (Raffaele et al., 2009). Therefore, the actual size of Remorin labelled membrane domains determined by this study may be an overestimation.

With a mean domain size of 0.25 μm^2 Remorin labelled membrane domains so far seem to be significantly larger than postulated “raft domains” of mammalian cells (Anderson and Jacobson, 2002; Edidin, 2003; Simons and Gerl, 2010). The large size of plant membrane domains suggests that they are clusters of single rafts that are interconnected via protein and lipid interactions (Lingwood and Simons, 2010; Tanner et al., 2011). These clusters are hypothesized to host specific subsets of proteins that are required for certain cellular processes (Demir et al., 2013; Hemsley, 2014). Characterization of these mini-proteomes will be challenging but could provide valuable information about the mechanisms and regulation of cellular functions. This work establishes a protein marker set for a large number of membrane domains in plants, providing a first step to help tackle these questions (Jarsch et al., 2014).

4.1.3 The influence of the cytoskeleton and cell-wall on membrane dynamics

While membrane domains in mammalian systems and artificial membranes are highly dynamic, this does not seem to be different in plants. Observation of membrane domains over 20 minutes showed that large structures labelled by Remorin proteins can be rather immobile. FRAP half-life recovery times ranging from 20 to 50 seconds further support this view (Jarsch et al., 2014). Slow diffusion rates of PM proteins are a frequently observed phenomenon in plants. Proteins such as KAT1, PIN2, KNOLLE, BOR1 and NIP5;1 also exhibit very low lateral mobility, with only a subfraction of these proteins displaying mobile behaviour (Sutter et al., 2006; Men et al., 2008; Takano et al., 2010; Roppolo et al., 2011; Martinière et al., 2012; Boutté and Moreau, 2014). In animal systems, diffusion of proteins is also restricted – a phenomenon that is most likely caused

Discussion

by membrane adjacent cytoskeletal structures that form diffusion barriers for membrane components (Kusumi et al., 2005; Goswami et al., 2008; Gowrishankar et al., 2012; Kusumi et al., 2012a; Gomez-Llobregat et al., 2013; Umemura and Nakano, 2013). Even though there are examples of plant membrane proteins that are involved in or dependent on cytoskeleton dynamics like actin nucleation inducing FORMIN1 or the microtubule binding protein MIDD1, the majority of membrane proteins diffuses independently from cytoskeletal structures (Martinière et al., 2011; Oda and Fukuda, 2012). One Remorin protein, At1g13920, localized to filamentous structures at the PM that were dissolved with the microtubule depolymerizing drug oryzalin, leading to the assumption that microtubules may be involved in the localization of At1g13920 (Jarsch et al., 2014). Accumulating evidence suggests that the major component restricting diffusion of proteins in plants is the cell-wall (Martinière et al., 2012).

Similar to the PM, cell-wall composition is heterogeneous and depends on the developmental program of the cell as well as environmental conditions (Burton et al., 2010). Composed primarily of cellulose, the cell wall is synthesized by the cellulose synthase complex. This multimeric protein complex moves through the PM along microtubules, depositing cellulose into the apoplastic space (Paredez et al., 2006; McFarlane et al., 2014). Besides cellulose, hemicelluloses, pectins, proteins and lignins also contribute to cell-wall composition (Scheller and Ulvskov, 2010; Vanholme et al., 2010; Albenne et al., 2013; Atmodjo et al., 2013).

Since the cell-wall represents the skeleton of plants, it is often perceived as being a stiff structure. Surprisingly, it has been found to be a dynamic network that undergoes constant reconstruction (Wolf et al., 2012). Deformations of cell wall components, for example the Ca²⁺-mediated formation of so-called egg-box pectin, influence cell growth and play an important role during the perception of abiotic as well as biotic stresses (Cabrera et al., 2008; Cabrera et al., 2010). Therefore plants maintain a sophisticated signalling system to monitor cell wall integrity, including a multitude of PM RLKs, mechanosensitive ion-channels and downstream signalling molecules (Hématy et al., 2007; Nakagawa et al., 2007; Xu et al., 2008). WAK1 is one of these cell surface RLKs that has been found to bind oligagalacturonides (OGAs), cell wall derived signalling molecules (Brutus et al., 2010). OGAs are pectin-derived molecules that can cause extensive effects on cells, including changes in gene expression, stomatal closure, ethylene production, cell wall reinforcement and ROS production (Hahn et al., 1981; Nothnagel et al., 1983; Simpson et al., 1998; Ridley et al., 2001; Moscatiello et al., 2006). Since pectin is a prominent target of pathogenic cell wall-degrading enzymes, OGAs are also thought to play an important role during plant immunity (Osorio et al., 2008).

Other WAK proteins and WAK-like proteins have been associated with cell elongation processes, coordination of solute concentration during growth and salt stress (He et al., 1996; Lally et al.,

2001; Wagner and Kohorn, 2001; Kohorn et al., 2006; Kohorn et al., 2009). Several Remorins including the group 1 Remorin At3g61260 have been found to interact with WAKs (Jones et al., 2014). This connection is especially interesting since several Remorins are implicated to play important roles during salt or abiotic stresses – conditions that are accompanied by extensive cell wall reconstructions (Nohzadeh Malakshah et al., 2007; Wolf et al., 2012; Checker and Khurana, 2013; Yue et al., 2014).

Tissue-specific labelling of membrane domains by the group 1 Remorins At1g61260 and At2g45820 emphasizes that Remorins might play a role in cell wall derived PM organization. In contrast to their rather uniform localization pattern in leaf and root epidermal cells, both proteins label distinct membrane domains in the hypocotyl of 5 day old seedlings and may also do so in different environmental conditions (Jarsch et al., 2014). Cells within the hypocotyl are known to undergo rapid cell expansion and growth that is largely dependent on cell wall reconstruction (Wolf et al., 2012). Even though it is unclear what role Remorins play in this environment, the signs for cell wall dependent localization of some Remorin proteins are obvious. Therefore, besides their use as a biotechnological tool to breed salt tolerant plants, Remorins could also be useful tools to investigate abiotic stress and cell wall related signalling pathways (Yue et al., 2014).

4.1.4 Investigating the biological function of punctate membrane domains by active mislocalization of the immune receptor FLS2 within the PM

In contrast to polar and equatorial membrane domains, where localizations can be directly linked to tasks such as directional solute transport or hindrance of diffusion, the functional implication of punctate membrane domain localization has remained elusive. One exception is the *A. thaliana* Flotillin FLOT1A. Using confocal and transmission electron microscopy, it was shown that this Flotillin localizes to distinct patches along the PM of *A. thaliana* root epidermis cells as well as at PM invaginations and endosomal structures (Li et al., 2012; Jarsch et al., 2014). Since FLOT1A has been observed to label vesicles budding from the PM it was assumed, that it plays a role in endocytotic processes (Li et al., 2012). Therefore, membrane domains labelled by FLOT1A are most possibly formation sites of endocytic vesicles (Li et al., 2012). Another example are the proteins LYK3 and FLOT4 that conditionally localize to a symbiotic membrane domain ((Haney et al., 2011); see 2.2.3.3) and indirectly hint at the involvement of membrane domains in signalling processes.

Investigating the functional role of membrane domains is very difficult due to their inherent nature as diverse, multi-component systems. Attempts to delete single components from these systems, for example depletion of sterols with methyl- β cyclodextrin, often has pleiotropic effects on the

whole cell, including the distribution of PtdIns and organization of the actin cytoskeleton (Kwik et al., 2003; Valitova et al., 2014). Therefore, assumptions made based on these methods need further experimental backup. The approach of forced relocation of FLS2 into a different membrane sub-compartment has been introduced here to circumvent these issues (see 3.6.1.2). *Camelidae* nanobodies have been used in a variety of biotechnological applications as conductors of forced interactions. In plants, these nanobodies have been successfully used to inhibit the function of starch-branching enzymes, resulting in a significantly increased starch content of potato tubers (Jobling et al., 2003). Promising experiments also showed that nanobodies can be used to confer resistance against viruses in crop plants (Ghannam et al., 2015). GFP-binding nanobodies were shown to be able to redirect proteins and whole organelles in living bacteria, thereby altering vital processes such as locomotion along oxygen gradients (Borg et al., 2015). In *N. benthamiana*, transiently expressed GFP binding nanobodies have been used to mislocalize proteins. To do this a GFP-binding nanobody was translationally fused to RFP to create a traceable GFP binding reporter, which was also used in this work. Co-expression of this reporter protein with plastid or mitochondrial localized GFP-fusion proteins gave rise to additional GFP fluorescence in the cell cytosol. The nuclear localized bZIP transcription factor TGA5 and the SNARE protein VAMP722 that are usually found at the endomembrane, were forced to the cytoplasm by co-expression with GBP:RFP (Schornack et al., 2009).

GFP-binding nanobodies are an especially versatile tool because of the widespread use of GFP as a fluorescent protein tag. This is particularly important in plant systems where the creation of stable plant lines consumes a considerable amount of time. Moreover, it enables us to utilize published plant lines with documented phenotypes. We chose the LRR-RLK FLS2 as model to study the role of PM sub-compartmentalization for several reasons. Most importantly, the molecular function of FLS2 is well documented and the molecular output of FLS2 activation can be measured on several layers (Boller and Felix, 2009). These include outputs such as stomatal closure, impaired seedling growth, callose depositions within the cell-wall, production of ROS, early phosphorylation of the RLK, activation of the MITOGEN ACTIVATED PROTEIN KINASE (MAPK) cascade, and transcriptional upregulation of early defence genes (Gomez-Gomez et al., 1999; Gómez-Gómez and Boller, 2000; Asai et al., 2002; Melotto et al., 2006; Miller et al., 2009; Schulze et al., 2010). All of these reactions are phenotypically accessible and allow us to quantify the efficiency of FLS2 signalling. Some of these responses are temporally and/or qualitatively confined. Activation of MAPK via phosphorylation for example, happens within 10 min after signal perception and decreases after 26 min (Asai et al., 2002). Accordingly, the production of ROS leading to an acidification of the extracellular space, starts within 5 min and reaches its peak 10 min after signal perception (Felix et al., 1999). This allows the detection of even subtle changes in FLS2 signalling

efficiency, such as delayed activation of signal transduction or a decrease in ROS production.

However, before data can be acquired, several technical obstacles have to be overcome. Though the initial experiments shown here were done in the transient *N. benthamiana* expression system, this is not an option to perform FLS2 activation assays, since endogenous FLS2 protein would mask the results (Chakravarthy et al., 2010). Transient expression directly in *A. thaliana* is not possible, since the innate immune system prevents *Agrobacterium* mediated gene transfer in wildtype plants and the inducible AvrPto expression plant line, engineered to overcome these issues degrades key plant immune receptors, including FLS2 (Hauck et al., 2003; Xiang et al., 2008). Therefore, GBP:RFP tagged Remorin expression in the stable transformed proFLS2-FLS2:GFP plant line is necessary.

The transformation of *Arabidopsis* with constitutive expressing Remorin constructs has an embryolethal phenotype (Jarsch et al., 2014). Therefore, GBP:RFP tagged Remorin constructs have to be introduced into the *Ws-0* proFLS2-FLS2:GFP line using an inducible promoter system. The dexamethasone (DEX) inducible promoter system is based on the constitutive expression of a chimeric transcription factor, that consists of the hormone-binding domain of the glucocorticoid receptor that is translationally fused to the DNA-binding and trans-activating domains from the yeast transcription factor GAL4 and the viral VP16 protein (Aoyama and Chua, 1997).

The observation that the GBP:RFP tagged Remorins At3g57540 and At4g36970 almost perfectly co-localized with GFP:FLS2 in transient *N. benthamiana* expression suggests that this system indeed works perfectly to reorganize the FLS2 distribution within the PM (Figure 7 C & F). However, the distribution pattern of proteins did not resemble the normal dotted Remorin localization, nor the localization pattern of FLS2 (Figure 7A & D). It is therefore unclear, whether forced interaction between these proteins happens in artificial membrane domains or the interaction interferes with the structure of one of the proteins native domain. The observation that the GBP:RFP tagged proteins already label larger domains than previously described (Jarsch et al., 2014) (Figure 6), also suggests that expression levels in these experiments were too high and may therefore alter protein localization (Jarsch et al., 2014). Furthermore, it has to be verified that both components are indeed PM resident and forced interaction does not inhibit transport of FLS2 to the PM.

Experimental data on the functional relevance of membrane domains are still incomplete. In yeast, localization of TMD containing proteins is primarily determined by sequence composition of the TMD segment. This is illustrated by the co-localization of the isolated TMD segment of Pmp1 with the full-length protein. Further proof was given through experiments with Pmp1 and the ferro-O₂-oxidoreductase Fer3. The low sequence similarity between the TMDs of Pmp1 and Fer3 predicted that, both proteins should only randomly overlap in co-localization experiments.

Discussion

Astonishingly, a chimeric protein in which the TMD segment of Fer3 was swapped with that of Pmp1, resulted in co-localization of this Fer3Pmp1 named protein with Pmp1. This chimeric protein was also used to assess the functionality of Fer3 in its non-native domain as it usually complements the growth deficiency of a *Δfer3* mutant in low-iron growth media. Most surprisingly, Fer3Pmp1 was not able to rescue this phenotype, arguing that localization of Fer3 to the PM is not sufficient for Fer3 function (Spira et al., 2012). Since it cannot be ruled out that the TMD segment of Fer3 contained important regulatory or functional components, this study took a second approach also using the GBP nanobody: The arginine permease Can1, one of the first membrane domain localized proteins identified, is enriched in the “membrane complex marked by Can1” (MCC) that also harbours a protein of unknown function, Sur7. Wild-type yeast cells are sensitive to the toxic arginine analogue canavanine. This toxicity is conferred by the function of Can1 (Opekarova et al., 1993). Redirecting Can1-GFP fusion proteins localization to Pmp1 domains, enabled cells to grow in the presence of canavanine comparably as well as *Δcan1*, indicating that the function of Can1 is lost when it is not present in the MCC (Spira et al., 2012). In contrast, immobilization of Can1-GFP within the MCC by co-expression of Sur7-GBP fusions retained canavanine sensitivity (Spira et al., 2012). Likewise, disruption of the MCC by deletion of important components such as Pil1 or NCE102, that both impaired, but did not completely prevent MCC formation resulted in reduced but significant growth in presence of canavanine (Spira et al., 2012).

These results demonstrate that correct sub-compartmentalization is indeed important for protein function of different transporter proteins in yeast. The establishment of a comparable system using Remorin proteins and the immune receptor FLS2 is therefore a promising approach to demonstrate the importance of membrane sub-organization for efficient signal transduction and the impact of perturbations of this system in multicellular organisms.

5 Abbreviations

APT	Acyl-protein thioesterase
BAK1	BRI1-ASSOCIATED KINASE 1
BRI1	BRASSINOSTEROID INSENSITIVE 1
C-	Carboxy-
CASP	CASPARIAN STRIP MEMBRANE PROTEIN
CBL	Calcineurin B-like
CPK	Calcium dependent protein kinase
CSC	Cell wall synthesising complex
CSD	Casparian strip domain
DEX	Dexamethasone
DIM	Detergent insoluble membranes
DANN	Desoxyribonucleic acid
EFR	EF-TU Receptor
ER	Endoplasmic reticulum
F2PK	6-phosphofructo-2-kinase/fructose-2,6-bisphosphate 2-phosphatase
FLOT	Flotillin
FLS2	FLAGELLIN SENSING 2
Ftase	Farnesyltransferase
GBP	GFP-binding protein
GFP	Green fluorescent protein
GGTase	Geranylgeranyltransferase
GPI	Glycosylphosphatidylinositol
GPMV	giant plasmamembrane vesicles
ID	Intrinsically disordered
LAT	LINKER FOR ACTIVATION OF T-CELLS
LPD	Lipid-binding domain
LRR	Leucine rich repeat
MAPK	MITOGEN ACTIVATED PROTEIN KINASE
MIDD1	MICROTUBULE DEPLETION DOMAIN 1
N-	Amino-
NADPH	Nicotinamide adenine dinucleotide phosphate
NFR	NOD FACTOR RECEPTOR
NMT	N-myristoyl transferase
MCC	Membrane complex marked by Can1
OGA	Oligalacuronic acid
PAMP	Pathogen associated molecular pattern
PAT	Protein-acyl transferase
PI	Phosphoinositide
PIN	PIN-FORMED
PM	Plasma membrane
PPT	Palmitoyl protein thioesterase
PtdCho	Phosphatidylcholine
PtdEtn	Phosphatidylethanolamine

Abbreviations

PtdIns	Phosphatidylinositol
PtdSer	Phosphatidylserine
RBOHD	RESPIRATORY BURST OXIDASE HOMOLOGUE
RFP	Red fluorescent protein
RIN4	RPM1 INTERACTING PROTEIN 4
RLK	Receptor like kinase
RNA	Ribonucleicacid
RNS	Root nodule symbiosis
ROP	Rho of plant
ROS	Reactive oxygen species
SLAC1	SLOW ANION CHANNEL 1
SLAH3	SLOW ANION CHANNEL 1 HOMOLOGUE 3
SM	Sphingomyelin
STED	Stimulated emission depletion
SWEET	SUGARS WILL EVENTUALLY BE EXPORTED
SYMREM1	SYMBIOTIC REMORIN 1
SYMRK	SYMBIOTIC RECEPTOR KINASE
TMD	Transmembrane domain
TRX	Thioredoxin
VSG	Variable surface glycoproteins
WAK	WALL ASSOCIATED KINASE

6 Danksagung

Für mich war die Erkenntnis der unzähligen ungeklärten Fragen über die Welt, welche uns unmittelbar umgibt, die wertvollste meiner Zeit am Institut für Genetik. Den vielen Personen, die mir geholfen haben, dieses Wissen als Ansporn wahrzunehmen und damit einen nicht unwesentlichen Teil zur Entstehung dieser Arbeit beigetragen haben, möchte ich hiermit danken:

Zu aller erst gebührt mein Dank Prof. Dr. Thomas Ott, der mir ermöglicht hat, diese Arbeit in seiner Arbeitsgruppe anzufertigen und mich schon zu Studienzeiten durch überdurchschnittlichen Betreuungsaufwand unterstützte. Vielen Dank Thomas, für das Vertrauen, dass du mir in den letzten vier Jahren entgegengebracht hast und das Löschen unzähliger ‚h’s‘. Vor allem aber möchte ich mich für den ab und zu fälligen Schubs aus meiner Comfort-Zone bedanken, denn Vieles lernt man nur außerhalb dieser.

Herrn Prof. Dr. Marc Bramkamp möchte ich für die Erstellung des Zweitgutachtens danken, sowie allen weiteren Mitgliedern der Prüfungskommission.

Meinen großartigen Kollegen der AG Ott, die mir durch wertvolle Diskussionen, kritische Fragen, hilfreiche Tipps und viel Teamarbeit zur Seite standen. Danke, Corinna, Macarena, Iris, Claudia, Jessica und Karl-Heinz, für die gute Zeit und die Späße, die ihr ausgehalten habt. Ganz besonders möchte ich mich bei Thomas Stratil bedanken, dem hilfreichsten Menschen, der mir je begegnet ist. Danke für die ehrlichen wissenschaftlichen sowie persönlichen Gespräche, aber vor allem auch die starke Zeit außerhalb des Labors.

Bei den vielen Studenten, die ich während meiner Zeit hier betreuen durfte, für die Lektionen in Wissensvermittlung und Gruppendynamik. Vor allem meiner Masterstudentin Jana „Uschi“ Munstermann, welche mich mit ihrer bodenständigen Art nach wie vor begeistert. Ich hoffe, du hast deine langen Stunden mit Dichtegradienten schichten und Mikroskopieren in guter Erinnerung. Außerdem möchte ich mich bei der besten Bachelorstudentin aller Zeiten, Sandy Niesik bedanken. Die AG Ott hat noch nie eine Studentin gesehen, die vom ersten Tag an so emsig und strukturiert ihr Projekt bearbeitet hat wie du. Ich suche immer noch nach einer passenden Präsentationsform für deinen Holotyp des Laborbuchs.

Bei den Kollegen aus den Arbeitsgruppen der Genetik möchte ich mich für die freundliche Atmosphäre, und die wissenschaftlichen Diskussionen bedanken. Besonderer Dank geht an Verena, für an gscheidn Ratsch und blaues Mitgefühl, und Gisela weil sequenzieren doch immer noch möglich ist.

Danksagung

Bei meinen Freunden ob in Uni oder an der Kletterwand möchte ich mich für die moralische Unterstützung und die vielen tollen Unternehmungen abseits der Forschung bedanken.

Thomas, Iris und Addie möchte ich für das kritische Lesen dieser Arbeit danken.

Meiner Freundin Veronica möchte ich dafür danken, dass sie mich mit ihrer Motivationsarbeit und konstanten Unterstützung angetrieben hat und zur rechten Zeit mit schönen Momenten mir gezeigt hat, sich auf das Wesentliche zu beschränken.

Am wichtigsten ist es mir, meiner Familie zu danken. Für den Rückhalt und Unterstützung, die ich von meinen Eltern Ingrid und Günther sowie meinen Brüdern Matthias und Maximilian bekomme und ohne die diese Arbeit nicht entstanden wäre.

7 References

- Abbe, E.** (1873). Beiträge zur Theorie des Mikroskops und der mikroskopischen Wahrnehmung. *Archiv für Mikroskopische Anatomie* **9**, 413-418.
- Adler, J., and Parmryd, I.** (2014). Quantifying colocalization: thresholding, void voxels and the H(coef). *PloS ONE* **9**.
- Alassimone, J., Naseer, S., and Geldner, N.** (2010). A developmental framework for endodermal differentiation and polarity. *Proceedings of the National Academy of Sciences* **107**, 5214-5219.
- Albenne, C., Canut, H., and Jamet, E.** (2013). Plant cell wall proteomics: the leadership of *Arabidopsis thaliana*. *Frontiers in Plant Science* **4**.
- Alberts, B., Johnson, A., Walter, P., Lewis, J., Raff, M., and Roberts, K.** (2007). *Molecular Biology of the Cell*. (New York: Garland Science).
- Ali, G., Prasad, K., Day, I., and Reddy, A.S.N.** (2007). Ligand-Dependent Reduction in the Membrane Mobility of FLAGELLIN SENSITIVE2, an *Arabidopsis* Receptor-Like Kinase. *Plant and Cell Physiology* **48**, 1601-1611.
- Almén, M.S., Nordström, K.J., Fredriksson, R., and Schiöth, H.B.** (2009). Mapping the human membrane proteome: a majority of the human membrane proteins can be classified according to function and evolutionary origin. *BMC Biology* **7**, 50.
- Anderson, R.G., and Jacobson, K.** (2002). A role for lipid shells in targeting proteins to caveolae, rafts, and other lipid domains. *Science* **296**, 1821-1825.
- Antonny, B., Beraud-Dufour, S., Chardin, P., and Chabre, M.** (1997). N-Terminal Hydrophobic Residues of the G-Protein ADP-Ribosylation Factor-1 Insert into Membrane Phospholipids upon GDP to GTP Exchange. *Biochemistry* **36**, 4675-4684.
- Antonny, B., Madden, D., Hamamoto, S., Orci, L., and Schekman, R.** (2001). Dynamics of the COPII coat with GTP and stable analogues. *Nature Cell Biology* **3**, 531-537.
- Aoyama, T., and Chua, N.-H.** (1997). A glucocorticoid-mediated transcriptional induction system in transgenic plants. *The Plant Journal* **11**, 605-612.
- Asai, T., Tena, G., Plotnikova, J., Willmann, M., R., Chiu, W.-L., Gomez-Gomez, L., Boller, T., Ausubel, F., M., and Sheen, J.** (2002). MAP kinase signalling cascade in *Arabidopsis* innate immunity. *Nature* **415**, 977-983.
- Atmodjo, M.A., Hao, Z., and Mohnen, D.** (2013). Evolving views of pectin biosynthesis. *Annual Review of Plant Biology* **64**, 747-779.
- Ayllón, V., Fleischer, A., Cayla, X., García, A., and Rebollo, A.** (2002). Segregation of Bad from lipid rafts is implicated in the induction of apoptosis. *Journal of Immunology* **168**.
- Bach, J.N., and Bramkamp, M.** (2013). Flotillins functionally organize the bacterial membrane. *Molecular Microbiology* **88**, 1205-1217.
- Bagatolli, L.A., Ipsen, J.H., Simonsen, A.C., and Mouritsen, O.G.** (2010). An outlook on organization of lipids in membranes: searching for a realistic connection with the organization of biological membranes. *Progress in Lipid Research* **49**, 378-389.
- Balla, T.** (2006). Phosphoinositide-derived messengers in endocrine signaling. *Journal of Endocrinology* **188**, 135-153.
- Barberon, M., Dubeaux, G., Kolb, C., Isono, E., Zelazny, E., and Vert, G.** (2014). Polarization of IRON-REGULATED TRANSPORTER 1 (IRT1) to the plant-soil

- interface plays crucial role in metal homeostasis. *Proceedings of the National Academy of Sciences* **111**, 8293-8298.
- Barbez, E., and Kleine-Vehn, J.** (2013). Divide Et Impera--cellular auxin compartmentalization. *Current Opinion in Plant Biology* **16**, 78-84.
- Barbosa, I.C., Zourelidou, M., Willige, B.C., Weller, B., and Schwechheimer, C.** (2014). D6 PROTEIN KINASE activates auxin transport-dependent growth and PIN-FORMED phosphorylation at the plasma membrane. *Developmental Cell* **29**, 674-685.
- Batistič, O.** (2012). Genomics and localization of the Arabidopsis DHHC-cysteine-rich domain S-acyltransferase protein family. *Plant Physiology* **160**, 1597-1612.
- Batistič, O., Sorek, N., Schültke, S., Yalovsky, S., and Kudla, J.** (2008). Dual fatty acyl modification determines the localization and plasma membrane targeting of CBL/CIPK Ca²⁺ signaling complexes in Arabidopsis. *The Plant Cell* **20**, 1346-1362.
- Batistič, O., Rehers, M., Akerman, A., Schlücking, K., Steinhorst, L., Yalovsky, S., and Kudla, J.** (2012). S-acylation-dependent association of the calcium sensor CBL2 with the vacuolar membrane is essential for proper abscisic acid responses. *Cell Research* **22**, 1155-1168.
- Beck, M., Ji, Z., Faulkner, C., MacLean, D., and Robatzek, S.** (2012). Spatio-Temporal Cellular Dynamics of the Arabidopsis Flagellin Receptor Reveal Activation Status-Dependent Endosomal Sorting. *The Plant Cell Online* **24**, 4205-4219.
- Benschop, J.J., Mohammed, S., O'Flaherty, M., Heck, A.J., Slijper, M., and Menke, F.L.** (2007). Quantitative phosphoproteomics of early elicitor signaling in Arabidopsis. *Mol Cell Proteomics* **6**, 1198-1214.
- Bhat, R.A., Miklis, M., Schmelzer, E., Schulze-Lefert, P., and Panstruga, R.** (2005). Recruitment and interaction dynamics of plant penetration resistance components in a plasma membrane microdomain. *Proceedings of the National Academy of Sciences* **102**, 3135-3140.
- Binder, A., Lambert, J., Morbitzer, R., Popp, C., Ott, T., Lahaye, T., and Parniske, M.** (2014). A modular plasmid assembly kit for multigene expression, gene silencing and silencing rescue in plants. *PLoS ONE* **9**.
- Blonder, J., Martha, L.H., David, A.L., Carl, F.S., Li-Rong, Y., Thomas, P.C., Haleem, J.I., Bradley, G.S., and Timothy, D.V.** (2004). Proteomic analysis of detergent-resistant membrane rafts. *Electrophoresis* **25**, 1307-1318.
- Boisson, B., Giglione, C., and Meinel, T.** (2003). Unexpected protein families including cell defense components feature in the N-myristoylome of a higher eukaryote. *The Journal of Biological Chemistry* **278**, 43418-43429.
- Boller, T., and Felix, G.** (2009). A Renaissance of Elicitors: Perception of Microbe-Associated Molecular Patterns and Danger Signals by Pattern-Recognition Receptors. *Annual Review of Plant Biology* **60**, 379-406.
- Bonnett, H.T.** (1968). The root endodermis: fine structure and function. *The Journal of Cell Biology* **37**, 199.
- Borg, S., Popp, F., Hofmann, J., Leonhardt, H., Rothbauer, U., and Schüler, D.** (2015). An Intracellular Nanotrap Redirects Proteins and Organelles in Live Bacteria. *mBio* **6**.
- Borner, G., H. H., Lilley, K., S., Stevens, T., J., and Dupree, P.** (2003). Identification of Glycosylphosphatidylinositol-Anchored Proteins in Arabidopsis. A Proteomic and Genomic Analysis. *Plant Physiology* **132**, 568-577.
- Boutté, Y., and Moreau, P.** (2014). Plasma membrane partitioning: from macro-domains to new views on plasmodesmata. In *Frontiers in Plant Science*, pp. 128.
- Bozkurt, T., Schornack, S., Banfield, M., and Kamoun, S.** (2012). Oomycetes, effectors, and all that jazz. *Current Opinion in Plant Biology*.
- Bozkurt, T.O., Richardson, A., Dagdas, Y.F., Mongrand, S., Kamoun, S., and Raffaele, S.** (2014). The plant membrane-associated REM1.3 remorin accumulates in discrete

- perihaustral domains and enhances susceptibility to *Phytophthora infestans*. *Plant Physiology* **165**, 1005-1018.
- Bretscher, M.S.** (1983). Distribution of receptors for transferrin and low density lipoprotein on the surface of giant HeLa cells. *Proceedings of the National Academy of Sciences* **80**, 454-458.
- Brown, D.A., and Rose, J.K.** (1992). Sorting of GPI-anchored proteins to glycolipid-enriched membrane subdomains during transport to the apical cell surface. *Cell* **68**, 533-544.
- Brutus, A., Sicilia, F., Macone, A., Cervone, F., and De Lorenzo, G.** (2010). A domain swap approach reveals a role of the plant wall-associated kinase 1 (WAK1) as a receptor of oligogalacturonides. *Proceedings of the National Academy of Sciences* **107**, 9452-9457.
- Burkhard, P., Stetefeld, J., and Strelkov, S.V.** (2001). Coiled coils: a highly versatile protein folding motif. *Trends in Cell Biology* **11**, 82-88.
- Burton, R.A., Gidley, M.J., and Fincher, G.B.** (2010). Heterogeneity in the chemistry, structure and function of plant cell walls. *Nature Chemical Biology* **6**, 724-732.
- Cabrera, J.C., Boland, A., Messiaen, J., Cambier, P., and Van Cutsem, P.** (2008). Egg box conformation of oligogalacturonides: the time-dependent stabilization of the elicitor-active conformation increases its biological activity. *Glycobiology* **18**, 473-482.
- Cabrera, J.C., Boland, A., Cambier, P., Frettinger, P., and Cutsem, P.V.** (2010). Chitosan oligosaccharides modulate the supramolecular conformation and the biological activity of oligogalacturonides in *Arabidopsis*. *Glycobiology* **20**, 775-786.
- Camp, L.A., and Hofmann, S.L.** (1993). Purification and properties of a palmitoyl-protein thioesterase that cleaves palmitate from H-Ras. *The Journal of Biological Chemistry* **268**, 22566-22574.
- Chakravarthy, S., Velásquez, A.C., Ekengren, S.K., Collmer, A., and Martin, G.B.** (2010). Identification of *Nicotiana benthamiana* Genes Involved in Pathogen-Associated Molecular Pattern-Triggered Immunity. *Molecular Plant-Microbe Interactions* **23**, 715-726.
- Checker, V.G., and Khurana, P.** (2013). Molecular and functional characterization of mulberry EST encoding remorin (MiREM) involved in abiotic stress. *Plant Cell Reports* **32**, 1729-1741.
- Chen, L.-Q., Hou, B.-H., Lalonde, S., Takanaga, H., Hartung, M.L., Qu, X.-Q., Guo, W.-J., Kim, J.-G., Underwood, W., Chaudhuri, B., Chermak, D., Antony, G., White, F.F., Somerville, S.C., Mudgett, M.B., and Frommer, W.B.** (2010). Sugar transporters for intercellular exchange and nutrition of pathogens. *Nature* **468**, 527-532.
- Chinchilla, D., Shan, L., He, P., de Vries, S., and Kemmerling, B.** (2009). One for all: the receptor-associated kinase BAK1. *Trends in Plant Science* **14**, 535-541.
- Chinchilla, D., Zipfel, C., Robatzek, S., Kemmerling, B., Nürnberger, T., Jones, J.D., Felix, G., and Boller, T.** (2007). A flagellin-induced complex of the receptor FLS2 and BAK1 initiates plant defence. *Nature* **448**, 497-500.
- Conrad, U., and Sonnewald, U.** (2003). Antibody jabs for plant enzymes. *Nature Biotechnology* **21**, 35-36.
- Contreras, F.X.X., Ernst, A.M., Haberkant, P., Björkholm, P., Lindahl, E., Gönen, B., Tischer, C., Elofsson, A., von Heijne, G., Thiele, C., Pepperkok, R., Wieland, F., and Brügger, B.** (2012). Molecular recognition of a single sphingolipid species by a protein's transmembrane domain. *Nature* **481**, 525-529.
- Cornelius, F.** (2001). Modulation of Na,K-ATPase and Na-ATPase Activity by Phospholipids and Cholesterol. I. Steady-State Kinetics. *Biochemistry* **40**, 8842-8851.
- Cosson, P., Perrin, J., and Bonifacino, J.S.** (2013). Anchors aweigh: protein localization and transport mediated by transmembrane domains. *Trends in Cell Biology* **23**, 511-517.
- Daviet, L., Malvoisin, E., and Wild, T.F.** (1997). Thrombospondin induces dimerization of membrane-bound, but not soluble CD36. *Thrombosis and Haemostasis* **78**, 897-901.

- Demir, F., Horntrich, C., Blachutzik, J.O., Scherzer, S., Reinders, Y., Kierszniowska, S., Schulze, W.X., Harms, G.S., Hedrich, R., Geiger, D., and Kreuzer, I.** (2013). Arabidopsis nanodomain-delimited ABA signaling pathway regulates the anion channel SLAH3. *Proceedings of the National Academy of Sciences* **110**, 8296-8301.
- Di Paolo, G., and De Camilli, P.** (2006). Phosphoinositides in cell regulation and membrane dynamics. *Nature* **443**, 651-657.
- Diaz-Rohrer, B.B., Levental, K.R., Simons, K., and Levental, I.** (2014). Membrane raft association is a determinant of plasma membrane localization. *Proceedings of the National Academy of Sciences* **111**, 8500-8505.
- Dietzen, D.J., Hastings, W.R., and Lublin, D.M.** (1995). Caveolin Is Palmitoylated on Multiple Cysteine Residues: PALMITOYLATION IS NOT NECESSARY FOR LOCALIZATION OF CAVEOLIN TO CAVEOLAE. *Journal of Biological Chemistry* **270**, 6838-6842.
- Dörmann, P., Kim, H., Ott, T., Schulze-Lefert, P., Trujillo, M., Wewer, V., and Hüchelhoven, R.** (2014). Cell-autonomous defense, re-organization and trafficking of membranes in plant-microbe interactions. *The New Phytologist* **204**, 815-822.
- Downes, B.P., Saracco, S.A., Lee, S., Crowell, D.N., and Vierstra, R.D.** (2006). MUBs, a Family of Ubiquitin-fold Proteins That Are Plasma Membrane-anchored by Prenylation. *Journal of Biological Chemistry* **281**, 27145-27157.
- Drücker, P., Pejic, M., Galla, H.-J., and Gerke, V.** (2013). Lipid Segregation and Membrane Budding Induced by the Peripheral Membrane Binding Protein Annexin A2. *The Journal of Biological Chemistry* **288**, 24764-24776.
- Dupuy, A., D., and Engelman, D., M.** (2008). Protein area occupancy at the center of the red blood cell membrane. *Proceedings of the National Academy of Sciences* **105**, 2848-2852.
- Edidin, M.** (2003). Lipids on the frontier: a century of cell-membrane bilayers. *Nature Reviews* **4**, 414-418.
- Elortza, F., Mohammed, S., Bunkenborg, J., Foster, L.J., Nühse, T.S., Brodbeck, U., Peck, S.C., and Jensen, O.N.** (2006). Modification-Specific Proteomics of Plasma Membrane Proteins: Identification and Characterization of Glycosylphosphatidylinositol-Anchored Proteins Released upon Phospholipase D Treatment. *Journal of Proteome Research* **5**, 935-943.
- Enstone, D., E., Peterson, C., A., and Ma, F.** (2003). Root Endodermis and Exodermis: Structure, Function, and Responses to the Environment. *Journal of Plant Growth Regulation* **21**, 335-351.
- Ernst, A., M., Contreras, F.X., Brügger, B., and Wieland, F.** (2010). Determinants of specificity at the protein-lipid interface in membranes. *FEBS letters* **584**, 1713-1720.
- Fahy, E., Subramaniam, S., Brown, A.H., Glass, C., K., Merrill, A., H., Murphy, R., C., Raetz, C., R. H., Russell, D., W., Seyama, Y., Shaw, W., Shimizu, T., Spener, F., van Meer, G., Van Nieuwenhze, M., S., White, S., H., Witztum, J., L., and Dennis, E., A.** (2005). A comprehensive classification system for lipids. *Journal of Lipid Research* **46**, 839-861.
- Farmer, E.E., and Pearce, G.** (1989). In vitro phosphorylation of plant plasma membrane proteins in response to the proteinase inhibitor inducing factor. *Proceedings of the National Academy of Sciences* **86**, 1539-1542.
- Febbraio, M., Hajjar, D., P., and Silverstein, R., L.** (2001). CD36: a class B scavenger receptor involved in angiogenesis, atherosclerosis, inflammation, and lipid metabolism. *Journal of Clinical Investigation* **108**, 785.
- Feigenson, G., W., and Buboltz, J., T.** (2008). Ternary Phase Diagram of Dipalmitoyl-PC/Dilauroyl-PC/Cholesterol: Nanoscopic Domain Formation Driven by Cholesterol. *Biophysical journal* **80**, 2775-2788.
- Felix, G., Duran, J.D., Volko, S., and Boller, T.** (1999). Plants have a sensitive perception system for the most conserved domain of bacterial flagellin. *Plant Journal* **18**, 265-276.

- Fidorra, M., Duelund, L., Leidy, C., Simonsen, A.C., and Bagatolli, L.A.** (2006). Absence of fluid-ordered/fluid-disordered phase coexistence in ceramide/POPC mixtures containing cholesterol. *Biophysical journal* **90**, 4437-4451.
- Finet, C., and Jaillais, Y.** (2012). Auxology: when auxin meets plant evo-devo. *Developmental Biology* **369**, 19-31.
- Fittipaldi, A., Ferrari, A., Zoppé, M., Arcangeli, C., Pellegrini, V., Beltram, F., and Giacca, M.** (2003). Cell membrane lipid rafts mediate caveolar endocytosis of HIV-1 Tat fusion proteins. *Cell membrane lipid rafts mediate caveolar endocytosis of HIV-1 Tat fusion proteins* **278**.
- Ford, M., Pearse, B., Higgins, M., Vallis, Y., Owen, D., Gibson, A., Hopkins, C., Evans, P., and McMahon, H.** (2001). Simultaneous Binding of PtdIns(4,5)P₂ and Clathrin by AP180 in the Nucleation of Clathrin Lattices on Membranes. *Science* **291**, 1051-1055.
- Fredriksson, R., Lagerström, M.C., Lundin, L.-G., and Schiöth, H.B.** (2003). The G-Protein-Coupled Receptors in the Human Genome Form Five Main Families. Phylogenetic Analysis, Paralogon Groups, and Fingerprints. *Molecular Pharmacology* **63**, 1256-1272.
- Fromme, J., Orci, L., and Schekman, R.** (2008). Coordination of COPII vesicle trafficking by Sec23. *Trends in Cell Biology* **18**, 330-336.
- Frye, L.D., and Edidin, M.** (1970). The rapid intermixing of cell surface antigens after formation of mouse-human heterokaryons. *Journal of Cell Science* **7**, 319-335.
- Fujiwara, T., Ritchie, K., Murakoshi, H., Jacobson, K., and Kusumi, A.** (2002). Phospholipids undergo hop diffusion in compartmentalized cell membrane. *The Journal of Cell Biology* **157**, 1071-1081.
- Gawrisch, K., Barry, J.A., Holte, L.L., Sinnwell, T., Bergelson, L.D., and Ferretti, J.A.** (1995). Role of interactions at the lipid-water interface for domain formation. *Molecular Membrane Biology* **12**, 83-88.
- Ghannam, A., Kumari, S., Muyltermans, S., and Abbady, A.** (2015). Camelid nanobodies with high affinity for broad bean mottle virus: a possible promising tool to immunomodulate plant resistance against viruses. *Plant Molecular Biology* **87**, 355-369.
- Ghossoub, R., Molla-Herman, A., Bastin, P., and Benmerah, A.** (2011). The ciliary pocket: a once forgotten membrane domain at the base of cilia. *Biology of the Cell* **103**, 131-144.
- Gish, L.A., and Clark, S.E.** (2011). The RLK/Pelle family of kinases. *The Plant Journal* **66**, 117-127.
- Goldberg, J.** (1998). Structural basis for activation of ARF GTPase: mechanisms of guanine nucleotide exchange and GTP-myristoyl switching. *Cell* **95**, 237-248.
- Goldenberg, N.M., and Steinberg, B.E.** (2010). Surface Charge: A Key Determinant of Protein Localization and Function. *Cancer Research* **70**, 1277-1280.
- Gomez-Gomez, L., Felix, G., and Boller, T.** (1999). A single locus determines sensitivity to bacterial flagellin in *Arabidopsis thaliana*. *The Plant Journal* **18**, 277-284.
- Gómez-Gómez, L., and Boller, T.** (2000). FLS2: An LRR Receptor-like Kinase Involved in the Perception of the Bacterial Elicitor Flagellin in *Arabidopsis*. *Molecular Cell* **5**, 1003-1011.
- Gomez-Llobregat, J., Buceta, J., and Reigada, R.** (2013). Interplay of cytoskeletal activity and lipid phase stability in dynamic protein recruitment and clustering. *Scientific Reports* **3**.
- Gonen, T., Sliz, P., Kistler, J., Cheng, Y., and Walz, T.** (2004). Aquaporin-0 membrane junctions reveal the structure of a closed water pore. *Nature* **429**, 193-197.
- Goswami, D., Gowrishankar, K., Bilgrami, S., Ghosh, S., Raghupathy, R., Chadda, R., Vishwakarma, R., Rao, M., and Mayor, S.** (2008). Nanoclusters of GPI-anchored proteins are formed by cortical actin-driven activity. *Cell* **135**, 1085-1097.
- Gowrishankar, K., Subhasri, G., Suvrajit, S., Rumamol, C., Satyajit, M., and Madan, R.** (2012). Active Remodeling of Cortical Actin Regulates Spatiotemporal Organization of Cell Surface Molecules. *Cell* **149**, 1353-1367.
- Grimsrud, P.A., den Os, D., Wenger, C.D., Swaney, D.L., Schwartz, D., Sussman, M.R., Ané, J.-M., and Coon, J.J.** (2010). Large-Scale Phosphoprotein Analysis in *Medicago*

- truncatula Roots Provides Insight into in Vivo Kinase Activity in Legumes. *Plant Physiology* **152**, 19-28.
- Grunewald, W., and Friml, J.** (2010). The march of the PINs: developmental plasticity by dynamic polar targeting in plant cells. *The EMBO Journal* **29**, 2700-2714.
- Gutierrez, R., Grossmann, G., Frommer, W.B., and Ehrhardt, D.W.** (2010). Opportunities to explore plant membrane organization with super-resolution microscopy. *Plant Physiology* **154**, 463-466.
- Hahn, M.G., Darvill, A.G., and Albersheim, P.** (1981). Host-Pathogen Interactions : XIX. The endogenous elicitor, a fragment of a plant cell wall polysaccharid that elicits phytoalexin accumulation in soybeans. *Plant Physiology* **68**, 1161-1169.
- Haney, C.H., and Long, S.R.** (2010). Plant flotillins are required for infection by nitrogen-fixing bacteria. *Proceedings of the National Academy of Sciences* **107**, 478-483.
- Haney, C.H., Riely, B.K., Tricoli, D.M., Cook, D.R., Ehrhardt, D.W., and Long, S.R.** (2011). Symbiotic rhizobia bacteria trigger a change in localization and dynamics of the *Medicago truncatula* receptor kinase LYK3. *The Plant Cell* **23**, 2774-2787.
- Hansen, S.B., Tao, X., and MacKinnon, R.** (2011). Structural basis of PIP2 activation of the classical inward rectifier K⁺ channel Kir2.2. *Nature* **477**, 495-498.
- Hao, H., Fan, L., Chen, T., Li, R., Li, X., He, Q., Botella, M.A., and Lin, J.** (2014). Clathrin and Membrane Microdomains Cooperatively Regulate RbohD Dynamics and Activity in *Arabidopsis*. *The Plant Cell* **26**, 1729-1745.
- Harder, T.** (2003). Formation of functional cell membrane domains: the interplay of lipid- and protein-mediated interactions. *Philosophical Transactions of the Royal Society B: Biological Sciences* **358**, 863-868.
- Hauck, P., Thilmony, R., and He, S.Y.** (2003). A *Pseudomonas syringae* type III effector suppresses cell wall-based extracellular defense in susceptible *Arabidopsis* plants. *Proceedings of the National Academy of Sciences* **100**, 8577-8582.
- He, Z., Wang, Z.Y., Li, J., Zhu, Q., Lamb, C., Ronald, P., and Chory, J.** (2000). Perception of brassinosteroids by the extracellular domain of the receptor kinase BRI1. *Science* **288**, 2360-2363.
- He, Z.H., Fujiki, M., and Kohorn, B.D.** (1996). A cell wall-associated, receptor-like protein kinase. *The Journal of Biological Chemistry* **271**, 19789-19793.
- Heese, A., Hann, D.R., Gimenez-Ibanez, S., Jones, A.M., He, K., Li, J., Schroeder, J.I., Peck, S.C., and Rathjen, J.P.** (2007). The receptor-like kinase SERK3/BAK1 is a central regulator of innate immunity in plants. *Proceedings of the National Academy of Sciences* **104**, 12217-12222.
- Hématy, K., Sado, P.-E., Tuinen, A.V., Rochange, S., Desnos, T., Balzergue, S., Pelletier, S., Renou, J.-P., and Höfte, H.** (2007). A Receptor-like Kinase Mediates the Response of *Arabidopsis* Cells to the Inhibition of Cellulose Synthesis. *Current Biology* **17**, 922-931.
- Hemsley, P.A.** (2014). The importance of lipid modified proteins in plants. *The New Phytologist* **205**, 476-489.
- Hemsley, P.A., and Grierson, C.S.** (2008). Multiple roles for protein palmitoylation in plants. *Trends in Plant Science* **13**, 295-302.
- Hemsley, P.A., Kemp, A.C., and Grierson, C.S.** (2005). The TIP GROWTH DEFECTIVE1 S-acyl transferase regulates plant cell growth in *Arabidopsis*. *The Plant Cell* **17**, 2554-2563.
- Hemsley, P.A., Weimar, T., Lilley, K.S., Dupree, P., and Grierson, C.S.** (2013). A proteomic approach identifies many novel palmitoylated proteins in *Arabidopsis*. *The New Phytologist* **197**, 805-814.
- Homann, U., Meckel, T., Hewing, J., Hütt, M.-T.T., and Hurst, A.C.** (2007). Distinct fluorescent pattern of KAT1::GFP in the plasma membrane of *Vicia faba* guard cells. *European Journal of Cell Biology* **86**, 489-500.

- Honerkamp-Smith, A.R., Veatch, S.L., and Keller, S.L. (2009). An introduction to critical points for biophysicists; observations of compositional heterogeneity in lipid membranes. *Biochimica et biophysica acta* **1788**, 53-63.
- Huang, K., Yanai, A., Kang, R., Arstikaitis, P., Singaraja, R.R., Metzler, M., Mullard, A., Haigh, B., Gauthier-Campbell, C., Gutekunst, C.-A.A., Hayden, M.R., and El-Husseini, A. (2004). Huntingtin-interacting protein HIP14 is a palmitoyl transferase involved in palmitoylation and trafficking of multiple neuronal proteins. *Neuron* **44**, 977-986.
- Hurst, C., H., and Hemsley, P.A. (2015). Current perspective on protein S-acylation in plants: more than just a fatty anchor? *Journal of Experimental Botany* **66**, 1599-1606.
- Illya, G., Lipowsky, R., and Shillcock, J.C. (2006). Two-component membrane material properties and domain formation from dissipative particle dynamics. *The Journal of Chemical Physics* **125**, 114710.
- Ipsen, H., Karlström, Mourtisen, Wennerström, and Zuckermann. (1987). Phase equilibria in the phosphatidylcholine-cholesterol system. *Biochimica et biophysica acta* **905**, 162-172.
- Jacinto, T., Farmer, E.E., and Ryan, C.A. (1993). Purification of potato leaf plasma membrane protein pp34, a protein phosphorylated in response to oligogalacturonide signals for defense and development. *Plant Physiology* **103**, 1393-1397.
- Jack, E.R., Madine, J., Lian, L.Y., and Middleton, D.A. (2008). Membrane interactions of peptides representing the polybasic regions of three Rho GTPases are sensitive to the distribution of arginine and lysine residues. *Mol Membr Biol* **25**, 14-22.
- Jain, M.K. (1989). Biomembranes: Molecular structure and function. *Cell* **58**, 813-814.
- Janmey, P.A., and Lindberg, U. (2004). Cytoskeletal regulation: rich in lipids. *Nature Reviews* **5**, 658-666.
- Jaqaman, K., Kuwata, H., Touret, N., Collins, R., Trimble, W., S., Danuser, G., and Grinstein, S. (2010). Cytoskeletal Control of CD36 Diffusion Promotes Its Receptor and Signaling Function. *Cell* **146**, 593-606.
- Jarsch, I.K., and Ott, T. (2011). Perspectives on remorin proteins, membrane rafts, and their role during plant-microbe interactions. *Molecular plant-microbe interactions : MPMI* **24**, 7-12.
- Jarsch, I.K., Konrad, S.S.A., Stratil, T.F., Urbanus, S.L., Szymanski, W., Braun, P., Braun, K.-H.H., and Ott, T. (2014). Plasma Membranes Are Subcompartmentalized into a Plethora of Coexisting and Diverse Microdomains in *Arabidopsis* and *Nicotiana benthamiana*. *The Plant Cell* **26**, 1698-1711.
- Jensen, R.B., Cour, T.L., Albrethsen, J., Nielsen, M., and Skriver, K. (2001). FYVE zinc-finger proteins in the plant model *Arabidopsis thaliana*: identification of PtdIns3P-binding residues by comparison of classic and variant FYVE domains. *The Biochemical Journal* **359**, 165-173.
- Jeong, S., Volny, M., and Lukowitz, W. (2012). Axis formation in *Arabidopsis* - transcription factors tell their side of the story. *Current Opinion in Plant Biology* **15**, 4-9.
- Jobling, S.A., Jarman, C., Teh, M.-M., Holmberg, N., Blake, C., and Verhoeven, M.E. (2003). Immunomodulation of enzyme function in plants by single-domain antibody fragments. *Nature Biotech* **21**, 77-80.
- Jones, A.M., Xuan, Y., Xu, M., Wang, R.-S.S., Ho, C.-H.H., Lalonde, S., You, C.H., Sardi, M.I., Parsa, S.A., Smith-Valle, E., Su, T., Frazer, K.A., Pilot, G., Pratelli, R., Grossmann, G., Acharya, B.R., Hu, H.-C.C., Engineer, C., Villiers, F., Ju, C., Takeda, K., Su, Z., Dong, Q., Assmann, S.M., Chen, J., Kwak, J.M., Schroeder, J.I., Albert, R., Rhee, S.Y., and Frommer, W.B. (2014). Border control--a membrane-linked interactome of *Arabidopsis*. *Science* **344**, 711-716.
- Kaiser, H.-J., Orłowski, A., Róg, T., Nyholm, T.K.M., Chai, W., Feizi, T., Lingwood, D., Vattulainen, I., and Simons, K. (2011). Lateral sorting in model membranes by cholesterol-mediated hydrophobic matching. *Proceedings of the National Academy of Sciences* **108**, 16628-16633.

- Kania, U., Fendrych, M., and Friml, J.** (2014). Polar delivery in plants; commonalities and differences to animal epithelial cells. In *Open Biology*, pp. 140017.
- Kawano, Y., Fujiwara, T., Yao, A., Housen, Y., Hayashi, K., and Shimamoto, K.** (2014). Palmitoylation-Dependent Membrane Localization of the Rice R protein Pit Is Critical for the Activation of the Small GTPase OsRac1. *The Journal of Biological Chemistry* **289**, 19079-19088.
- Keinath, N.F., Kierszniowska, S., Lorek, J., Bourdais, G., Kessler, S.A., Shimosato-Asano, H., Grossniklaus, U., Schulze, W.X., Robatzek, S., and Panstruga, R.** (2010). PAMP (pathogen-associated molecular pattern)-induced changes in plasma membrane compartmentalization reveal novel components of plant immunity. *The Journal of Biological Chemistry* **285**, 39140-39149.
- Kierszniowska, S., Seiwert, B., and Schulze, W.X.** (2009). Definition of Arabidopsis sterol-rich membrane microdomains by differential treatment with methyl-beta-cyclodextrin and quantitative proteomics. *Molecular & Cellular Proteomics* **8**, 612-623.
- Killian, J.A., and von Heijne, G.** (2000). How proteins adapt to a membrane-water interface. *Trends in Biochemical Sciences* **25**, 429-434.
- Kim, H.-S.S., Desveaux, D., Singer, A.U., Patel, P., Sondek, J., and Dangl, J.L.** (2005). The *Pseudomonas syringae* effector AvrRpt2 cleaves its C-terminally acylated target, RIN4, from Arabidopsis membranes to block RPM1 activation. *Proceedings of the National Academy of Sciences* **102**, 6496-6501.
- Kim, H., O'Connell, R., Maekawa-Yoshikawa, M., Uemura, T., Neumann, U., and Schulze-Lefert, P.** (2014). The powdery mildew resistance protein RPW8.2 is carried on VAMP721/722 vesicles to the extrahaustorial membrane of haustorial complexes. *The Plant Journal* **79**, 835-847.
- Kinoshita, T., Cano-Delgado, A., Seto, H., Hiranuma, S., Fujioka, S., Yoshida, S., and Chory, J.** (2005). Binding of brassinosteroids to the extracellular domain of plant receptor kinase BRI1. *Nature* **433**, 167-171.
- Kleine-Vehn, J., and Friml, J.** (2008). Polar targeting and endocytic recycling in auxin-dependent plant development. *Annual Review of Cell and Developmental Biology* **24**, 447-473.
- Kleine-Vehn, J., Wabnik, K., Martinière, A., Langowski, Ł., Willig, K., Naramoto, Leitner, J., Tanaka, H., Jakobs, S., Robert, S., Luschnig, C., Govaerts, W., Hell, S., W., Runions, J., and Friml, J.** (2011). Recycling, clustering, and endocytosis jointly maintain PIN auxin carrier polarity at the plasma membrane. In *Molecular Systems Biology*.
- Klymchenko, A.S., and Kreder, R.** (2014). Fluorescent probes for lipid rafts: from model membranes to living cells. *Chemistry & Biology* **21**, 97-113.
- Kohorn, B.D., Johansen, S., Shishido, A., Todorova, T., Martinez, R., Defeo, E., and Obregon, P.** (2009). Pectin activation of MAP kinase and gene expression is WAK2 dependent. *The Plant Journal* **60**, 974-982.
- Kohorn, B.D., Kobayashi, M., Johansen, S., Riese, J., Huang, L.-F., Koch, K., Fu, S., Dotson, A., and Byers, N.** (2006). An Arabidopsis cell wall-associated kinase required for invertase activity and cell growth. *The Plant Journal* **46**, 307-316.
- Komatsu, S.** (2008). Plasma membrane proteome in Arabidopsis and rice. *Proteomics* **8**, 4137-4145.
- Konrad, S.S., Popp, C., Stratil, T.F., Jarsch, I.K., Thallmair, V., Folgmann, J., Marín, M., and Ott, T.** (2014). S-acylation anchors remorin proteins to the plasma membrane but does not primarily determine their localization in membrane microdomains. *The New Phytologist* **203**, 758-769.
- Konrad, S.S.A., and Ott, T.** (2015). Molecular principles of membrane microdomain targeting in plants. *Trends in Plant Science* **20**, 351-361.
- Kraft, M.L.** (2013). Plasma membrane organization and function: moving past lipid rafts. *Molecular Biology of the Cell* **24**, 2765-2768.

- Krauß, M., and Haucke, V.** (2007). Phosphoinositide-metabolizing enzymes at the interface between membrane traffic and cell signalling. *EMBO Reports* **8**, 241-246.
- Krügel, U., Veenhoff, L.M., Langbein, J., Wiederhold, E., Liesche, J., Friedrich, T., Grimm, B., Mertinoia, E., Poolman, B., and Kühn, C.** (2008). Transport and sorting of the solanum tuberosum sucrose transporter SUT1 is affected by posttranslational modification. *The Plant Cell* **20**, 2497-2513.
- Kusumi, A., Suzuki, K.G., Kasai, R.S., Ritchie, K., and Fujiwara, T.K.** (2011). Hierarchical mesoscale domain organization of the plasma membrane. *Trends in Biochemical Sciences* **36**, 604-615.
- Kusumi, A., Fujiwara, T.K., Chadda, R., Xie, M., Tsunoyama, T.A., Kalay, Z., Kasai, R.S., and Suzuki, K.G.** (2012a). Dynamic organizing principles of the plasma membrane that regulate signal transduction: commemorating the fortieth anniversary of Singer and Nicolson's fluid-mosaic model. *Annual Review of Cell and Developmental Biology* **28**, 215-250.
- Kusumi, A., Fujiwara, T.K., Morone, N., Yoshida, K.J., Chadda, R., Xie, M., Kasai, R.S., and Suzuki, K.G.** (2012b). Membrane mechanisms for signal transduction: the coupling of the meso-scale raft domains to membrane-skeleton-induced compartments and dynamic protein complexes. *Seminars in Cell & Developmental Biology* **23**, 126-144.
- Kusumi, A., Nakada, C., Ritchie, K., Murase, K., Suzuki, K., Murakoshi, H., Kasai, R.S., Kondo, J., and Fujiwara, T.** (2005). Paradigm shift of the plasma membrane concept from the two-dimensional continuum fluid to the partitioned fluid: high-speed single-molecule tracking of membrane molecules. *Annual Review of Biophysics and Biomolecular Structure* **34**, 351-378.
- Kwik, J., Boyle, S., Fooksman, D., Margolis, L., Sheetz, M.P., and Edidin, M.** (2003). Membrane cholesterol, lateral mobility, and the phosphatidylinositol 4,5-bisphosphate-dependent organization of cell actin. *Proceedings of the National Academy of Sciences* **100**, 13964-13969.
- Lalanne, E., Honys, D., and Johnson, A.** (2004). SETH1 and SETH2, Two Components of the Glycosylphosphatidylinositol Anchor Biosynthetic Pathway, Are Required for Pollen Germination and Tube Growth in Arabidopsis. *The Plant Cell* **16**, 229-240.
- Lally, D., Ingmire, P., Tong, H.Y., and He, Z.H.** (2001). Antisense expression of a cell wall-associated protein kinase, WAK4, inhibits cell elongation and alters morphology. *The Plant Cell* **13**, 1317-1331.
- Lang, D.M., Lommel, S., Jung, M., Ankerhold, R., Petrusch, B., Laessing, U., Wiechers, M.F., Plattner, H., and Stuermer, C.A.** (1998). Identification of reggie-1 and reggie-2 as plasmamembrane-associated proteins which cocluster with activated GPI-anchored cell adhesion molecules in non-caveolar micropatches in neurons. *Journal of Neurobiology* **37**, 502-523.
- Lau, S., Slane, D., Herud, O., Kong, J., and Jürgens, G.** (2012). Early embryogenesis in flowering plants: setting up the basic body pattern. *Annual Review of Plant Biology* **63**, 483-506.
- Lavy, M., and Yalovsky, S.** (2006). Association of Arabidopsis type-II ROPs with the plasma membrane requires a conserved C-terminal sequence motif and a proximal polybasic domain. *The Plant Journal* **46**, 934-947.
- Lee, A.G.** (2003). Lipid-protein interactions in biological membranes: a structural perspective. *Biochimica et biophysica acta* **1612**, 1-40.
- Lee, I.-H.H., Saha, S., Polley, A., Huang, H., Mayor, S., Rao, M., and Groves, J.T.** (2015). Live Cell Plasma Membranes Do Not Exhibit a Miscibility Phase Transition over a Wide Range of Temperatures. *The journal of physical chemistry. B*.
- Lefebvre, B., Furt, F., Hartmann, M.-A.A., Michaelson, L.V., Carde, J.-P.P., Sargueil-Boiron, F., Rossignol, M., Napier, J.A., Cullimore, J., Bessoule, J.-J.J., and Mongrand, S.** (2007). Characterization of lipid rafts from *Medicago truncatula* root plasma

- membranes: a proteomic study reveals the presence of a raft-associated redox system. *Plant Physiology* **144**, 402-418.
- Lefebvre, B., Timmers, T., Mbengue, M., Moreau, S., Hervé, C., Tóth, K., Bittencourt-Silvestre, J., Klaus, D., Deslandes, L., Godiard, L., Murray, J.D., Udvardi, M.K., Raffaele, S., Mongrand, S., Cullimore, J., Gamas, P., Niebel, A., and Ott, T.** (2010). A remorin protein interacts with symbiotic receptors and regulates bacterial infection. *Proceedings of the National Academy of Sciences* **107**, 2343-2348.
- Levental, I., Lingwood, D., Grzybek, M., Coskun, U., and Simons, K.** (2010). Palmitoylation regulates raft affinity for the majority of integral raft proteins. *Proceedings of the National Academy of Sciences* **107**, 22050-22054.
- Li, J., and Chory, J.** (1997). A putative leucine-rich repeat receptor kinase involved in brassinosteroid signal transduction. *Cell* **90**, 929-938.
- Li, J., Wen, J., Lease, K.A., Doke, J.T., Tax, F.E., and Walker, J.C.** (2002). BAK1, an Arabidopsis LRR receptor-like protein kinase, interacts with BRI1 and modulates brassinosteroid signaling. *Cell* **110**, 213-222.
- Li, Q., Lau, A., Morris, T.J., Guo, L., Fordyce, C.B., and Stanley, E.F.** (2004). A Syntaxin 1, G α , and N-Type Calcium Channel Complex at a Presynaptic Nerve Terminal: Analysis by Quantitative Immunocolocalization. *The Journal of Neuroscience* **24**, 4070-4081.
- Li, R., Liu, P., Wan, Y., Chen, T., Wang, Q., Mettbach, U., Baluska, F., Samaj, J., Fang, X., Lucas, W.J., and Lin, J.** (2012). A membrane microdomain-associated protein, Arabidopsis Flot1, is involved in a clathrin-independent endocytic pathway and is required for seedling development. *The Plant Cell* **24**, 2105-2122.
- Li, X., Wang, X., Yang, Y., Ruili, L., Qihua, H., Fang, X., Luu, D.-T., Maurel, C., and Jinxing, L.** (2011). Single-molecule analysis of PIP2;1 dynamics and partitioning reveals multiple modes of Arabidopsis plasma membrane aquaporin regulation. *The Plant Cell* **23**, 3780-3797.
- Lingwood, D., and Simons, K.** (2010). Lipid rafts as a membrane-organizing principle. *Science* **327**, 46-50.
- Lucas, W.J., and Smith, F.A.** (1973). The Formation of Alkaline and Acid Regions at the Surface of *Chara corallina* Cells. *Journal of Experimental Botany* **24**, 1-14.
- Luna, E., Pastor, V., Robert, J., Flors, V., Mauch-Mani, B., and Ton, J.** (2011). Callose deposition: a multifaceted plant defense response. *Molecular Plant-Microbe Interactions* **24**, 183-193.
- Luschnig, C., and Vert, G.** (2014). The dynamics of plant plasma membrane proteins: PINs and beyond. *Development* **141**, 2924-2938.
- Malinsky, J., Opekarová, M., Grossmann, G., and Tanner, W.** (2013). Membrane microdomains, rafts, and detergent-resistant membranes in plants and fungi. *Annual Review of Plant Biology* **64**, 501-529.
- Manders, E.M., Verbeek, F.J., and Aten, J.A.** (1993). Measurement of co-localization of objects in dual-colour confocal images. *Journal of Microscopy* **169**, 375-382.
- Marín, M., and Ott, T.** (2014). Intrinsic Disorder in Plant Proteins and Phytopathogenic Bacterial Effectors. *Chemical Reviews* **114**, 6912-6932.
- Marín, M., Thallmair, V., and Ott, T.** (2012). The intrinsically disordered N-terminal region of AtREM1.3 remorin protein mediates protein-protein interactions. *The Journal of Biological Chemistry* **287**, 39982-39991.
- Marín, M., Uversky, V.N., and Ott, T.** (2013). Intrinsic Disorder in Pathogen Effectors: Protein Flexibility as an Evolutionary Hallmark in a Molecular Arms Race. *The Plant Cell* **25**, 3153-3157.
- Markmann, K., and Parniske, M.** (2009). Evolution of root endosymbiosis with bacteria: How novel are nodules? *Trends in Plant Science* **14**, 77-86.
- Marmagne, A., Ferro, M., Meinel, T., Bruley, C., Kuhn, L., Garin, J., Barbier-Brygoo, H., and Ephritikhine, G.** (2007). A high content in lipid-modified peripheral proteins and

- integral receptor kinases features in the arabidopsis plasma membrane proteome. *Molecular & Cellular Proteomics* **6**, 1980-1996.
- Marmagne, A., Rouet, M.-A.A., Ferro, M., Rolland, N., Alcon, C., Joyard, J., Garin, J., Barbier-Brygoo, H., and Ephritikhine, G.** (2004). Identification of new intrinsic proteins in Arabidopsis plasma membrane proteome. *Molecular & Cellular Proteomics* **3**, 675-691.
- Marsh, D., and Watts, A.** (1982). Spin-labelling and lipid-protein interactions in membranes. In *Lipid-protein Interactions in Membranes* (Wiley), pp. 53-126.
- Martin, B., Eryang, L., Arun, S., Tomas, K., Marie-Theres, H., and Staffan, P.** (2012). POM-POM2/CELLULOSE SYNTHASE INTERACTING1 Is Essential for the Functional Association of Cellulose Synthase and Microtubules in Arabidopsis. *The Plant Cell*.
- Martín, M.L., and Busconi, L.** (2000). Membrane localization of a rice calcium-dependent protein kinase (CDPK) is mediated by myristoylation and palmitoylation. *The Plant Journal* **24**, 429-435.
- Martinière, A., Gayral, P., Hawes, C., and Runions, J.** (2011). Building bridges: formin1 of Arabidopsis forms a connection between the cell wall and the actin cytoskeleton. *The Plant Journal* **66**, 354-365.
- Martinière, A., Lavagi, I., Nageswaran, G., Rolfe, D.J., Maneta-Peyret, L., Luu, D.-T.T., Botchway, S.W., Webb, S.E., Mongrand, S., Maurel, C., Martin-Fernandez, M.L., Kleine-Vehn, J., Friml, J., Moreau, P., and Runions, J.** (2012). Cell wall constrains lateral diffusion of plant plasma-membrane proteins. *Proceedings of the National Academy of Sciences* **109**, 12805-12810.
- Maurel, C., Santoni, V., Luu, D.-T.T., Wudick, M.M., and Verdoucq, L.** (2009). The cellular dynamics of plant aquaporin expression and functions. *Current Opinion in Plant Biology* **12**, 690-698.
- Maurer-Stroh, S., Washietl, S., and Eisenhaber, F.** (2003). Protein prenyltransferases. *Genome Biology* **4**, 212.
- Maures, T.J., Su, H.-W., Argetsinger, L.S., Grinstein, S., and Carter-Su, C.** (2011). Phosphorylation controls a dual-function polybasic nuclear localization sequence in the adapter protein SH2B1 to regulate its cellular function and distribution. *Journal of Cell Science* **124**.
- McFarlane, H.E., Döring, A., and Persson, S.** (2014). The Cell Biology of Cellulose Synthesis. *Annual Review of Plant Biology* **65**, 69-94.
- McGilvray, I.D., Serghides, L., Kapus, A., and Rotstein, O.D.** (2000). Nonopsonic monocyte/macrophage phagocytosis of Plasmodium falciparum-parasitized erythrocytes: a role for CD36 in malarial clearance. *Blood* **96**, 3231-3240.
- McIntosh, T., J., Vidal, A., and Simon, S., A.** (2008). Sorting of Lipids and Transmembrane Peptides Between Detergent-Soluble Bilayers and Detergent-Resistant Rafts. *Biophysical journal* **85**, 1656-1666.
- McKenna, J.F., Tolmie, A.F., and Runions, J.** (2014). Across the great divide: the plant cell surface continuum. *Current Opinion in Plant Biology* **22**, 132-140.
- McMahon, H.T., and Boucrot, E.** (2011). Molecular mechanism and physiological functions of clathrin-mediated endocytosis. *Nature Reviews* **12**, 517-533.
- McTaggart, S.J.** (2006). Isoprenylated proteins. *Cellular and Molecular Life Sciences* **63**, 255-267.
- Meijer, H.J., and Munnik, T.** (2003). Phospholipid-based signaling in plants. *Annual Review of Plant Biology* **54**, 265-306.
- Melotto, M., Underwood, W., Koczan, J., Nomura, K., and He, S.Y.** (2006). Plant stomata function in innate immunity against bacterial invasion. *Cell* **126**, 969-980.
- Men, S., Boutté, Y., Ikeda, Y., Li, X., Palme, K., Stierhof, Y.-D.D., Hartmann, M.-A.A., Moritz, T., and Grebe, M.** (2008). Sterol-dependent endocytosis mediates post-cytokinetic acquisition of PIN2 auxin efflux carrier polarity. *Nature Cell Biology* **10**, 237-244.

- Michniewicz, M., Zago, M.K., Abas, L., Weijers, D., Schweighofer, A., Meskiene, I., Heisler, M.G., Ohno, C., Zhang, J., Huang, F., Schwab, R., Weigel, D., Meyerowitz, E.M., Luschnig, C., Offringa, R., and Friml, J. (2007). Antagonistic regulation of PIN phosphorylation by PP2A and PINOID directs auxin flux. *Cell* **130**, 1044-1056.
- Miller, G., Schlauch, K., Tam, R., Cortes, D., Torres, M.A., Shulaev, V., Dangel, J.L., and Mittler, R. (2009). The plant NADPH oxidase RBOHD mediates rapid systemic signaling in response to diverse stimuli. *Science Signaling* **2**, ra45.
- Moling, S., Pietraszewska-Bogiel, A., Postma, M., Fedorova, E., Hink, M.A., Limpens, E., Gadella, T.W., and Bisseling, T. (2014). Nod Factor Receptors Form Heteromeric Complexes and Are Essential for Intracellular Infection in Medicago Nodules. *The Plant Cell* **26**, 4188-4199.
- Mongrand, S., Morel, J., Laroche, J., Claverol, S., Carde, J.-P.P., Hartmann, M.-A.A., Bonneau, M., Simon-Plas, F., Lessire, R., and Bessoule, J.-J.J. (2004). Lipid rafts in higher plant cells: purification and characterization of Triton X-100-insoluble microdomains from tobacco plasma membrane. *The Journal of Biological Chemistry* **279**, 36277-36286.
- Moon, G.J., Clough, B.F., Peterson, C.A., and Allaway, W.G. (1986). Apoplastic and symplastic pathways in *Avicennia marina* (Forsk.) Vierh. roots revealed by fluorescent tracer dyes. *Functional Plant Biology* **13**, 637-648.
- Morrow, I.C., Rea, S., Martin, S., Prior, I.A., Prohaska, R., Hancock, J.F., James, D.E., and Parton, R.G. (2002). Flotillin-1/reggie-2 traffics to surface raft domains via a novel golgi-independent pathway. Identification of a novel membrane targeting domain and a role for palmitoylation. *The Journal of Biological Chemistry* **277**, 48834-48841.
- Moscatiello, R., Mariani, P., Sanders, D., and Maathuis, F., J. M. (2006). Transcriptional analysis of calcium-dependent and calcium-independent signalling pathways induced by oligogalacturonides. *Journal of Experimental Botany* **57**, 2847-2865.
- Mouritsen, O.G. (2011). Model answers to lipid membrane questions. In *Cold Spring Harbor Perspectives in Biology*.
- Mouritsen, O.G., and Bloom. (1984). Mattress model of lipid-protein interactions in membranes. *Biophysical Journal* **46**, 141-153.
- Mueller-Roeber, B., and Pical, C. (2002). Inositol phospholipid metabolism in Arabidopsis. Characterized and putative isoforms of inositol phospholipid kinase and phosphoinositide-specific phospholipase C. *Plant Physiology* **130**, 22-46.
- Muyldermans, S. (2001). Single domain camel antibodies: current status. *Journal of Biotechnology* **74**, 277-302.
- Nable, R.O., Bañuelos, G.S., and Paull, J.G. (1997). Boron toxicity. *Plant and Soil* **193**, 181-198.
- Nakada, C., Ritchie, K., Oba, Y., Nakamura, M., Hotta, Y., Iino, R., Kasai, R.S., Yamaguchi, K., Fujiwara, T., and Kusumi, A. (2003). Accumulation of anchored proteins forms membrane diffusion barriers during neuronal polarization. *Nature Cell Biology* **5**, 626-632.
- Nakagami, H., Sugiyama, N., Mochida, K., Daudi, A., Yoshida, Y., Toyoda, T., Tomita, M., Ishihama, Y., and Shirasu, K. (2010). Large-Scale Comparative Phosphoproteomics Identifies Conserved Phosphorylation Sites in Plants. *Plant Physiology* **153**, 1161-1174.
- Nakagawa, Y., Katagiri, T., Shinozaki, K., Qi, Z., Tatsumi, H., Furuichi, T., Kishigami, A., Sokabe, M., Kojima, I., Sato, S., Kato, T., Tabata, S., Iida, K., Terashima, A., Nakano, M., Ikeda, M., Yamanaka, T., and Iida, H. (2007). Arabidopsis plasma membrane protein crucial for Ca²⁺ influx and touch sensing in roots. *Proceedings of the National Academy of Sciences* **104**, 3639-3644.
- Nam, K.H., and Li, J. (2002). BRI1/BAK1, a receptor kinase pair mediating brassinosteroid signaling. *Cell* **110**, 203-212.

- Nelson, C.J., Hegeman, A.D., and Harms, A.C.** (2006). A quantitative analysis of Arabidopsis plasma membrane using trypsin-catalyzed 18O labeling. *Molecular & Cellular Proteomics* **5**, 1382-1395.
- Neumann-Giesen, C., Falkenbach, B., Beicht, P., Claasen, S., Lüers, G., Stuermer, C.A., Herzog, V., and Tikkanen, R.** (2004). Membrane and raft association of reggie-1/flotillin-2: role of myristoylation, palmitoylation and oligomerization and induction of filopodia by overexpression. *The Biochemical Journal* **378**, 509-518.
- Nimchuk, Z., Marois, E., Kjemtrup, S., Leister, R.T., Katagiri, F., and Dangel, J.L.** (2000). Eukaryotic fatty acylation drives plasma membrane targeting and enhances function of several type III effector proteins from *Pseudomonas syringae*. *Cell* **101**, 353-363.
- Nixon, B., Mitchell, L.A., Anderson, A.L., McLaughlin, E.A., O'Bryan, M.K., and Aitken, R.J.** (2011). Proteomic and functional analysis of human sperm detergent resistant membranes. *Journal of Cellular Physiology* **226**, 2651-2665.
- Nohzadeh Malakshah, S., Habibi Rezaei, M., Heidari, M., and Salekdeh, G.H.** (2007). Proteomics reveals new salt responsive proteins associated with rice plasma membrane. *Bioscience, Biotechnology, and Biochemistry* **71**, 2144-2154.
- Nothnagel, E.A., McNeil, M., Albersheim, P., and Dell, A.** (1983). Host-Pathogen Interactions : XXII. A Galacturonic Acid Oligosaccharide from Plant Cell Walls Elicits Phytoalexins. *Plant Physiology* **71**, 916-926.
- Nühse, T.S., Bottrill, A.R., Jones, A.M.E., and Peck, S.C.** (2007). Quantitative phosphoproteomic analysis of plasma membrane proteins reveals regulatory mechanisms of plant innate immune responses. *The Plant Journal* **51**, 931-940.
- Oda, Y., and Fukuda, H.** (2012). Initiation of Cell Wall Pattern by a Rho- and Microtubule-Driven Symmetry Breaking. *Science* **337**, 1333-1336.
- Oldroyd, G.E.D., and Downie, J.A.** (2004). Calcium, kinases and nodulation signalling in legumes. *Nat Rev Mol Cell Biol* **5**, 566-576.
- Opekarova, M., Caspari, T., and Tanner, W.** (1993). Unidirectional arginine transport in reconstituted plasma-membrane vesicles from yeast overexpressing CAN1. *European Journal of Biochemistry* **211**, 683-688.
- Oriol, G., Matthew, J.B., Jelena, G.J., Kenji, M., Christian, M., Carmen, A.G., Pedro, B.A., Stefan, B., Carlos, F.T., Lars Juhl, J., Michael, K., Jamie, T., Vladimir, R., Christoph, W.M., Peer, B., Marko, K., Robert, B.R., and Anne-Claude, G.** (2010). A systematic screen for protein-lipid interactions in *Saccharomyces cerevisiae*. *Molecular Systems Biology* **6**.
- Osorio, S., Castillejo, C., Quesada, M., A., Medina-Escobar, N., Brownsey, G., J. , Suau, R., Heredia, A., Botella, M., A, and Valpuesta, V.** (2008). Partial demethylation of oligogalacturonides by pectin methyl esterase1 is required for eliciting defence responses in wild strawberry (*Fragaria vesca*). *The Plant Journal* **54**, 43-55.
- Otto, G.P., and Nichols, B.J.** (2011). The roles of flotillin microdomains--endocytosis and beyond. *Journal of Cell Science* **124**, 3933-3940.
- Paredez, A.R., Somerville, C.R., and Ehrhardt, D.W.** (2006). Visualization of cellulose synthase demonstrates functional association with microtubules. *Science* **312**, 1491-1495.
- Park, S., Szumlanski, A., L. , Gu, F., Guo, F., and Nielsen, E.** (2011). A role for CSLD3 during cell-wall synthesis in apical plasma membranes of tip-growing root-hair cells. *Nature Cell Biology* **13**, 973-980.
- Parton, R.G.** (1996). Caveolae and caveolins. *Current Opinion in Cell Biology* **8**, 542-548.
- Perraki, A., Cacas, J.-L.L., Crowet, J.-M.M., Lins, L., Castroviejo, M., German-Retana, S., Mongrand, S., and Raffaele, S.** (2012). Plasma membrane localization of *Solanum tuberosum* remorin from group 1, homolog 3 is mediated by conformational changes in a novel C-terminal anchor and required for the restriction of potato virus X movement]. *Plant Physiology* **160**, 624-637.

- Peterson, C., A.** (1987). The Exodermal Casparian Band of Onion Roots Blocks the Apoplastic Movement of Sulphate Ions. *Journal of Experimental Botany* **38**, 2068-2081.
- Pfister, A., Barberon, M., Alassimone, J., Kalmbach, L., Lee, Y., Vermeer, J., E. M., Yamazaki, M., Li, G., Maurel, C., Takano, J., Kamiya, T., Salt, D., E., Roppolo, D., and Geldner, N.** (2014). A receptor-like kinase mutant with absent endodermal diffusion barrier displays selective nutrient homeostasis defects. In *eLife*.
- Pierre-Jerome, E., Moss, B.L., and Nemhauser, J.L.** (2013). Tuning the auxin transcriptional response. *Journal of Experimental Botany* **64**, 2557-2563.
- Pierre, M., Traverso, J.A., Boisson, B., Domenichini, S., Bouchez, D., Giglione, C., and Meinel, T.** (2007). N-myristoylation regulates the SnRK1 pathway in Arabidopsis. *The Plant Cell* **19**, 2804-2821.
- Pink, D.A., Chapman, D., Laidlaw, D.J., and Wiedmer, T.** (1984). Electron spin resonance and steady-state fluorescence polarization studies of lipid bilayers containing integral proteins. *Biochemistry* **23**, 4051-4058.
- Podell, S., and Gribskov, M.** (2004). Predicting N-terminal myristoylation sites in plant proteins. *BMC Genomics* **5**, 37.
- Popp, C., and Ott, T.** (2011). Regulation of signal transduction and bacterial infection during root nodule symbiosis. *Current Opinion in Plant Biology* **14**, 458-467.
- Postel, S., Küfner, I., Beuter, C., Mazzotta, S., Schwedt, A., Borlotti, A., Halter, T., Kemmerling, B., and Nürnberger, T.** (2010). The multifunctional leucine-rich repeat receptor kinase BAK1 is implicated in Arabidopsis development and immunity. *European Journal of Cell Biology* **89**, 169-174.
- Pumplin, N., Zhang, X., Noar, R.D., and Harrison, M.J.** (2012). Polar localization of a symbiosis-specific phosphate transporter is mediated by a transient reorientation of secretion. *Proceedings of the National Academy of Sciences* **109**, E665-E672.
- Raffaele, S., Mongrand, S., Gamas, P., Niebel, A., and Ott, T.** (2007). Genome-wide annotation of remorins, a plant-specific protein family: evolutionary and functional perspectives. *Plant Physiology* **145**, 593-600.
- Raffaele, S., Bayer, E., Lafarge, D., Cluzet, S., German Retana, S., Boubekeur, T., Leborgne-Castel, N., Carde, J.-P.P., Lherminier, J., Noirot, E., Satiat-Jeunemaître, B., Laroche-Traineau, J., Moreau, P., Ott, T., Maule, A.J., Reymond, P., Simon-Plas, F., Farmer, E.E., Bessoule, J.-J.J., and Mongrand, S.** (2009). Remorin, a solanaceae protein resident in membrane rafts and plasmodesmata, impairs potato virus X movement. *The Plant Cell* **21**, 1541-1555.
- Rayleigh, L.** (1903). On the theory of optical images, with special reference to the microscope. *Philosophical Magazine* **23**, 474-482.
- Reiland, S., Messerli, G., Baerenfaller, K., Gerrits, B., Endler, A., Grossmann, J., Gruissem, W., and Baginsky, S.** (2009). Large-Scale Arabidopsis Phosphoproteome Profiling Reveals Novel Chloroplast Kinase Substrates and Phosphorylation Networks. *Plant Physiology* **150**, 889-903.
- Resh, M.D.** (2006). Trafficking and signaling by fatty-acylated and prenylated proteins. *Nature Chemical Biology* **2**, 584-590.
- Reuter, A.T., Stuermer, C.A., and Plattner, H.** (2013). Identification, Localization, and Functional Implications of the Microdomain-Forming Stomatins Family in the Ciliated Protozoan *Paramecium tetraurelia*. *Eukaryotic Cell* **12**, 529-544.
- Reymond, P., Kunz, B., Paul-Pletzer, K., Grimm, R., Eckerskorn, C., and Farmer, E.E.** (1996). Cloning of a cDNA encoding a plasma membrane-associated, uronide binding phosphoprotein with physical properties similar to viral movement proteins. *The Plant Cell* **8**, 2265-2276.
- Ridge, R.W., and Rolfe, B.G.** (1985). *Rhizobium* sp. Degradation of Legume Root Hair Cell Wall at the Site of Infection Thread Origin. *Applied and Environmental Microbiology* **50**, 717-720.

- Ridley, B.L., O' Neill, M.A., and Mohnen, D. (2001). Pectins: structure, biosynthesis, and oligogalacturonide-related signaling. *Phytochemistry* **57**, 929-967.
- Rivera-Milla, E., Stuermer, C.A., and Málaga-Trillo, E. (2006). Ancient origin of reggie (flotillin), reggie-like, and other lipid-raft proteins: convergent evolution of the SPFH domain. *Cellular and Molecular Life Sciences* **63**, 343-357.
- Robatzek, S., Chinchilla, D., and Boller, T. (2006). Ligand-induced endocytosis of the pattern recognition receptor FLS2 in Arabidopsis. *Genes & Development* **20**, 537-542.
- Rocks, O., Gerauer, M., Vartak, N., Koch, S., Huang, Z.-P.P., Pechlivanis, M., Kuhlmann, J., Brunsveld, L., Chandra, A., Ellinger, B., Waldmann, H., and Bastiaens, P.I. (2010). The palmitoylation machinery is a spatially organizing system for peripheral membrane proteins. *Cell* **141**, 458-471.
- Roppolo, D., Rybel, B.D., Tendon, V.D., Pfister, A., Alassimone, J., Vermeer, J., E. M., Yamazaki, M., Stierhof, Y.-D., Beeckman, T., and Geldner, N. (2011). A novel protein family mediates Casparian strip formation in the endodermis. *Nature* **473**, 180-U564.
- Roth, A.F., Feng, Y., Chen, L., and Davis, N.G. (2002). The yeast DHHC cysteine-rich domain protein Akr1p is a palmitoyl transferase. *The Journal of Cell Biology* **159**, 23-28.
- Rothbauer, U., Zolghadr, K., Tillib, S., Nowak, D., Schermelleh, L., Gahl, A., Backmann, N., Conrath, K., Muyldermans, S., Cardoso, M.C., and Leonhardt, H. (2006). Targeting and tracing antigens in live cells with fluorescent nanobodies. *Nature Methods* **3**, 887-889.
- Rothberg, K.G., Ying, Y.S., Kamen, B.A., and Anderson, R.G. (1990). Cholesterol controls the clustering of the glycopospholipid-anchored membrane receptor for 5-methyltetrahydrofolate. *The Journal of Cell Biology* **111**, 2931-2938.
- Rothman, J., and Lenard, J. (1977). Membrane asymmetry. *Science* **195**, 743-753.
- Roy, S., Plowman, S., Rotblat, B., Prior, I.A., Muncke, C., Grainger, S., Parton, R.G., Henis, Y.I., Kloog, Y., and Hancock, J.F. (2005). Individual palmitoyl residues serve distinct roles in H-ras trafficking, microlocalization, and signaling. *Molecular & Cellular Proteomics* **25**, 6722-6733.
- Running, M.P. (2014). The role of lipid post-translational modification in plant developmental processes. In *Frontiers in Plant Science*.
- Ryan, E., Grierson, C.S., Cavell, A., Steer, M., and Dolan, L. (1998). TIP1 is required for both tip growth and non-tip growth in Arabidopsis. *The New Phytologist* **138**, 49-58.
- Sazuka, T., Keta, S., Shiratake, K., Yamaki, S., and Shibata, D. (2004). A proteomic approach to identification of transmembrane proteins and membrane-anchored proteins of Arabidopsis thaliana by peptide sequencing. *DNA Research* **11**, 101-113.
- Scheller, H.V., and Ulvskov, P. (2010). Hemicelluloses. *Annual Review of Plant Biology* **61**, 263-289.
- Schiefelbein, J., Galway, M., Masucci, J., and Ford, S. (1993). Pollen tube and root-hair tip growth is disrupted in a mutant of Arabidopsis thaliana. *Plant Physiology* **103**, 979-985.
- Schindelin, J., Arganda-Carreras, I., Frise, E., Kaynig, V., Longair, M., Pietzsch, T., Preibisch, S., Rueden, C., Saalfeld, S., Schmid, B., Tinevez, J.-Y.Y., White, D.J., Hartenstein, V., Eliceiri, K., Tomancak, P., and Cardona, A. (2012). Fiji: an open-source platform for biological-image analysis. *Nature Methods* **9**, 676-682.
- Schornack, S., Fuchs, R., Huitema, E., Rothbauer, U., Lipka, V., and Kamoun, S. (2009). Protein mislocalization in plant cells using a GFP-binding chromobody. *The Plant Journal* **60**, 744-754.
- Schrack, K., Fujioka, S., Takatsuto, S., Stierhof, Y.-D.D., Stransky, H., Yoshida, S., and Jürgens, G. (2004). A link between sterol biosynthesis, the cell wall, and cellulose in Arabidopsis. *The Plant Journal* **38**, 227-243.
- Schulze, B., Mentzel, T., Jehle, A.K., Mueller, K., Beeler, S., Boller, T., Felix, G., and Chinchilla, D. (2010). Rapid heteromerization and phosphorylation of ligand-activated

References

- plant transmembrane receptors and their associated kinase BAK1. *Journal of Biological Chemistry* **285**, 9444-9451.
- Schwacke, R., Schneider, A., van der Graaff, E., Fischer, K., Catoni, E., Desimone, M., Frommer, W.B., Flügge, U.-I., and Kunze, R.** (2003). ARAMEMNON, a Novel Database for Arabidopsis Integral Membrane Proteins. *Plant Physiology* **131**, 16-26.
- Schwille, P., Korlach, J., and Webb, W., W.** (1999). Fluorescence correlation spectroscopy with single-molecule sensitivity on cell and model membranes. *Cytometry* **36**, 176-182.
- Sergent, O., Djoudi-Aliche, F., and Lagadic-Gossmann, D.** (2012). Up-to-Date Insight About Membrane Remodeling as a Mechanism of Action for Ethanol-Induced Liver Toxicity.
- Shahinian, S., and Silvius, J.R.** (1995). Doubly-lipid-modified protein sequence motifs exhibit long-lived anchorage to lipid bilayer membranes. *Biochemistry* **34**, 3813-3822.
- Sharpe, H.J., Stevens, T.J., and Munro, S.** (2010). A comprehensive comparison of transmembrane domains reveals organelle-specific properties. *Cell* **142**, 158-169.
- Shisheva, A.** (2008). PIKfyve: Partners, significance, debates and paradoxes. *Cell Biology International* **32**, 591-604.
- Shiu, S.-H., and Bleecker.** (2001a). Plant Receptor-Like Kinase Gene Family: Diversity, Function, and Signaling. *Science Signaling* **2001**, re22.
- Shiu, S.-H., and Bleecker, A., B.** (2001b). Receptor-like kinases from Arabidopsis form a monophyletic gene family related to animal receptor kinases. *Proceedings of the National Academy of Sciences* **98**, 10763-10768.
- Silvius, J., R., and l'Heureux, F.** (1994). Fluorometric Evaluation of the Affinities of Isoprenylated Peptides for Lipid Bilayers. *Biochemistry* **33**, 3014-3022.
- Simons, K., and van Meer, G.** (1988). Lipid sorting in epithelial cells. *Biochemistry* **27**, 6197-6202.
- Simons, K., and Ikonen, E.** (1997). Functional rafts in cell membranes. *Nature* **387**, 569-572.
- Simons, K., and Gerl, M.J.** (2010). Revitalizing membrane rafts: new tools and insights. *Nature Reviews* **11**, 688-699.
- Simpson, S.D., Ashford, D.A., Harvey, D.J., and Bowles, D.J.** (1998). Short chain oligogalacturonides induce ethylene production and expression of the gene encoding aminocyclopropane 1-carboxylic acid oxidase in tomato plants. *Glycobiology* **8**, 579-583.
- Singer, S.J., and Nicolson, G.L.** (1972). The Fluid Mosaic Model of the Structure of Cell Membranes. *Science* **175**, 720-731.
- Sommers; Connie, L., Samelson; Lawrence, E., and Love; Paul, E.** (2004). LAT: a T lymphocyte adapter protein that couples the antigen receptor to downstream signaling pathways. *BioEssays : news and reviews in molecular, cellular and developmental biology* **26**, 61-67.
- Sorek, N., Poraty, L., Sternberg, H., Bar, E., Lewinsohn, E., and Yalovsky, S.** (2007). Activation status-coupled transient S acylation determines membrane partitioning of a plant Rho-related GTPase. *Molecular and Cellular Biology* **27**, 2144-2154.
- Soubias, O., and Gawrisch, K.** (2013). Rhodopsin-lipid interactions studied by NMR. *Methods in Enzymology* **522**, 209-227.
- Spang, A.** (2008). Membrane traffic in the secretory pathway. *Cellular and Molecular Life Sciences* **65**, 2781-2789.
- Sperling, P., Warnecke, D., and Heinz, E.** (2004). Plant Sphingolipids. In *Lipid Metabolism and Membrane Biogenesis*, G. Daum, ed, pp. 337-381.
- Spira, F., Mueller, N.S., Beck, G., von Olshausen, P., Beig, J., and Wedlich-Söldner, R.** (2012). Patchwork organization of the yeast plasma membrane into numerous coexisting domains. *Nature Cell Biology* **14**, 640-648.
- Sprent, J.I.** (2007). Evolving ideas of legume evolution and diversity: a taxonomic perspective on the occurrence of nodulation. *The New Phytologist* **174**, 11-25.
- Steinwand, B.J., and Kieber, J.J.** (2010). The Role of Receptor-Like Kinases in Regulating Cell Wall Function. *Plant Physiology* **153**, 479-484.

- Subczynski, W.K., Wisniewska, A., Hyde, J.S., and Kusumi, A. (2007). Three-dimensional dynamic structure of the liquid-ordered domain in lipid membranes as examined by pulse-EPR oxygen probing. *Biophysical journal* **92**, 1573-1584.
- Sugiyama, N., Nakagami, H., Mochida, K., Daudi, A., Tomita, M., Shirasu, K., and Ishihama, Y. (2008). Large-scale phosphorylation mapping reveals the extent of tyrosine phosphorylation in Arabidopsis.
- Sutter, J.-U.U., Campanoni, P., Tyrrell, M., and Blatt, M.R. (2006). Selective mobility and sensitivity to SNAREs is exhibited by the Arabidopsis KAT1 K⁺ channel at the plasma membrane. *The Plant Cell* **18**, 935-954.
- Takamori, S., Holt, M., Stenius, K., Lemke, E.A., Grønborg, M., Riedel, D., Urlaub, H., Schenck, S., Brügger, B., Ringler, P., Müller, S.A., Rammner, B., Gräter, F., Hub, J.S., De Groot, B.L., Mieskes, G., Moriyama, Y., Klingauf, J., Grubmüller, H., Heuser, J., Wieland, F., and Jahn, R. (2006). Molecular Anatomy of a Trafficking Organelle. *Cell* **127**, 831-846.
- Takano, J., Wada, M., Ludewig, U., and Schaaf, G. (2006). The Arabidopsis major intrinsic protein NIP5; 1 is essential for efficient boron uptake and plant development under boron limitation. *The Plant Cell* **18**, 1498-1509.
- Takano, J., Noguchi, K., Yasumori, M., Kobayashi, M., Gajdos, Z., Miwa, K., Hayashi, H., Yoneyama, T., and Fujiwara, T. (2002). Arabidopsis boron transporter for xylem loading. *Nature* **420**, 337-340.
- Takano, J., Tanaka, M., Toyoda, A., Miwa, K., Kasai, K., Fuji, K., Onouchi, H., Naito, S., and Fujiwara, T. (2010). Polar localization and degradation of Arabidopsis boron transporters through distinct trafficking pathways. *Proceedings of the National Academy of Sciences* **107**, 5220-5225.
- Tanner, W., Malinsky, J., and Opekarová, M. (2011). In plant and animal cells, detergent-resistant membranes do not define functional membrane rafts. *The Plant Cell* **23**, 1191-1193.
- Tejos, R., Sauer, M., Vanneste, S., Palacios-Gomez, M., Li, H., Heilmann, M., van Wijk, R., Vermeer, J.E., Heilmann, I., Munnik, T., and Friml, J. (2014). Bipolar Plasma Membrane Distribution of Phosphoinositides and Their Requirement for Auxin-Mediated Cell Polarity and Patterning in Arabidopsis. *The Plant Cell* **26**, 2114-2128.
- Törnroth-Horsefield, S., Wang, Y., Hedfalk, K., Johanson, U., Karlsson, M., Tajkhorshid, E., Neutze, R., and Kjellbom, P. (2006). Structural mechanism of plant aquaporin gating. *Nature* **439**, 688-694.
- Torres, M.A., Onouchi, H., Hamada, S., Machida, C., Hammond-Kosack, K.E., and Jones, J.D.G. (1998). Six Arabidopsis thaliana homologues of the human respiratory burst oxidase (gp91phox). *The Plant Journal* **14**, 365-370.
- Tóth, K., Stratil, T.F., Madsen, E.B., Ye, J., Popp, C., Antolín-Llovera, M., Grossmann, C., Jensen, O.N., Schüssler, A., Parniske, M., and Ott, T. (2012). Functional domain analysis of the Remorin protein LjSYMREM1 in Lotus japonicus. In *PLoS ONE*.
- Traverso, J.A., Micallella, C., Martinez, A., Brown, S.C., Satiat-Jeunemaître, B., Meinel, T., and Giglione, C. (2013). Roles of N-terminal fatty acid acylations in membrane compartment partitioning: Arabidopsis h-type thioredoxins as a case study. *The Plant Cell* **25**, 1056-1077.
- Trusov, Y., Chakravorty, D., and Botella, J. (2012). Diversity of heterotrimeric G-protein gamma subunits in plants. *BMC Research Notes* **5**, 608.
- Umemura, T., and Nakano, A. (2013). Plant TGNs: dynamics and physiological functions. *Histochemistry and Cell Biology* **140**, 341-345.
- Vain, T., Crowell, E.F., Timpano, H., Biot, E., Desprez, T., Mansoori, N., Trindade, L.M., Pagant, S., Robert, S., Hofte, H., Gonneau, M., and Vernhettes, S. (2014). The Cellulase KORRIGAN Is Part of the Cellulose Synthase Complex. *Plant Physiology* **165**.

- Valitova, J., Sulkarnayeva, A., Kotlova, E., Ponomareva, A., Mukhitova, F.K., Murtazina, L., Ryzhkina, I., Beckett, R., and Minibayeva, F. (2014). Sterol binding by methyl- β -cyclodextrin and nystatin— comparative analysis of biochemical and physiological consequences for plants. *FEBS Journal* **281**, 2051-2060.
- Valot, B., Negroni, L., Zivy, M., Gianinazzi, S., and Dumas-Gaudot, E. (2006). A mass spectrometric approach to identify arbuscular mycorrhiza-related proteins in root plasma membrane fractions. *Proteomics* **6 Suppl 1**, S145-155.
- Valot, B., Dieu, M., Recorbet, G., Raes, M., Gianinazzi, S., and Dumas-Gaudot, E. (2005). Identification of membrane-associated proteins regulated by the arbuscular mycorrhizal symbiosis. *Plant molecular biology* **59**, 565-580.
- Van den Berg, B., Clemons, W.M., Jr., Collinson, I., Modis, Y., Hartmann, E., Harrison, S.C., and Rapoport, T.A. (2004). X-ray structure of a protein-conducting channel. *Nature* **427**, 36-44.
- van Esse, W.G., Westphal, A., Surendran, R., Albrecht, C., Veen, B., Borst, J., and Vries, S. (2011). Quantification of the Brassinosteroid Insensitive1 Receptor in *Planta*. *Plant Physiology* **156**, 1691-1700.
- van Meer, G., Voelker, D.R., and Feigenson, G.W. (2008). Membrane lipids: where they are and how they behave. *Nature Reviews* **9**, 112-124.
- van Meer, G., Stelzer, E.H., Wijnaendts-van-Resandt, R.W., and Simons, K. (1987). Sorting of sphingolipids in epithelial (Madin-Darby canine kidney) cells. *The Journal of Cell Biology* **105**, 1623-1635.
- Vanhamme, L., Lecordier, L., and Pays, E. (2001). Control and function of the bloodstream variant surface glycoprotein expression sites in *Trypanosoma brucei*. *International Journal for Parasitology* **31**, 523-531.
- Vanholme, R., Demedts, B., Morreel, K., Ralph, J., and Boerjan, W. (2010). Lignin Biosynthesis and Structure. *Plant Physiology* **153**, 895-905.
- Veatch, S.L., Cicuta, P., Sengupta, P., Honerkamp-Smith, A., Holowka, D., and Baird, B. (2008). Critical Fluctuations in Plasma Membrane Vesicles. *ACS Chemical Biology* **3**, 287-293.
- Vidal, A., and McIntosh, T.J. (2005). Transbilayer peptide sorting between raft and nonraft bilayers: comparisons of detergent extraction and confocal microscopy. *Biophysical journal* **89**, 1102-1108.
- Wagner, T.A., and Kohorn, B.D. (2001). Wall-associated kinases are expressed throughout plant development and are required for cell expansion. *The Plant Cell* **13**, 303-318.
- Walker, J. (1994). Structure and function of the receptor-like protein kinases of higher plants. *Plant Molecular Biology* **26**, 1599-1609.
- Wallin, E., and von Heijne, G. (1998). Genome-wide analysis of integral membrane proteins from eubacterial, archaean, and eukaryotic organisms. *Protein Science : A Publication of the Protein Society* **7**, 1029-1038.
- Wan, Y., Ash, W.M., Fan, L., Hao, H., Kim, M.K., and Lin, J. (2011). Variable-angle total internal reflection fluorescence microscopy of intact cells of *Arabidopsis thaliana*. *Plant Methods* **7**, 7-27.
- Wang, L., Hukin, D., Pritchard, J., and Thomas, C. (2006a). Comparison of plant cell turgor pressure measurement by pressure probe and micromanipulation. *Biotechnology Letters* **28**, 1147-1150.
- Wang, W., Wen, Y., Berkey, R., and Xiao, S. (2009). Specific targeting of the *Arabidopsis* resistance protein RPW8.2 to the interfacial membrane encasing the fungal haustorium renders broad-spectrum resistance to powdery mildew. *The Plant Cell* **21**, 2898-2913.
- Wang, X., Teng, Y., Wang, Q., Li, X., and Sheng, X. (2006b). Imaging of dynamic secretory vesicles in living pollen tubes of *Picea meyeri* using evanescent wave microscopy. *Plant Physiology* **141**, 1591-1603.

- Wang, Z.-Y., Seto, H., Fujioka, S., Yoshida, S., and Chory, J. (2001). BRI1 is a critical component of a plasma-membrane receptor for plant steroids. *Nature* **410**, 380-383.
- Wisniewska, J., Xu, J., and Seifertova, D. (2006). Polar PIN Localization Directs Auxin Flow in Plants. *Science* **312**, 883-883.
- Wolf, S., Hématy, K., and Höfte, H. (2012). Growth Control and Cell Wall Signaling in Plants. *Plant Biology* **63**, 381-407.
- Xiang, T., Zong, N., Zou, Y., Wu, Y., Zhang, J., Xing, W., Li, Y., Tang, X., Zhu, L., Chai, J., and Zhou, J.-M. (2008). *Pseudomonas syringae* Effector AvrPto Blocks Innate Immunity by Targeting Receptor Kinases. *Current Biology* **18**, 74-80.
- Xu, S.-L., Rahman, A., Baskin, T., I., and Kieber, J., J. . (2008). Two leucine-rich repeat receptor kinases mediate signaling, linking cell wall biosynthesis and ACC synthase in *Arabidopsis*. *The Plant cell* **20**, 3065-3079.
- Yang, Z., and Lavagi, I. (2012). Spatial control of plasma membrane domains: ROP GTPase-based symmetry breaking. *Current Opinion in Plant Biology* **15**, 601-607.
- Yernool, D., Boudker, O., Jin, Y., and Gouaux, E. (2004). Structure of a glutamate transporter homologue from *Pyrococcus horikoshii*. *Nature* **431**, 811-818.
- Yonghua, L.-B., Basil, S., Fred, B., Mats, X.A., Vincent, A., Philip, D.B., Sébastien, B., David, B., Allan, D., Timothy, P.D., Rochus, B.F., Ian, A.G., Kenta, K., Amélie, A.K., Tony, L., Jonathan, E.M., Martine, M., Isabel, M., Ikuo, N., Owen, R., Lacey, S., Katherine, M.S., Hajime, W., Ruth, W., Changcheng, X., Rémi, Z., and John, O. (2013). Acyl-Lipid Metabolism. *The Arabidopsis Book*.
- Yoshida, S., Ohya, Y., Goebel, M., Nakano, A., and Anraku, Y. (1994). A novel gene, STT4, encodes a phosphatidylinositol 4-kinase in the PKC1 protein kinase pathway of *Saccharomyces cerevisiae*. *The Journal of Biological Chemistry* **269**, 1166-1172.
- Yue, J., Li, C., Liu, Y., and Yu, J. (2014). A Remorin Gene SiREM6, the Target Gene of SiARDP, from Foxtail Millet (*Setaria italica*) Promotes High Salt Tolerance in Transgenic *Arabidopsis*. In PLoS ONE.
- Zeng, Q., Wang, X., and Running, M.P. (2007). Dual lipid modification of *Arabidopsis* Ggamma-subunits is required for efficient plasma membrane targeting. *Plant Physiology* **143**, 1119-1131.
- Zhang, F.L., and Casey, P.J. (1996). Protein prenylation: molecular mechanisms and functional consequences. *Annual Review of Biochemistry* **65**, 241-269.
- Zhang, W., Sommers, C.L., Burshtyn, D.N., Stebbins, C.C., DeJarnette, J.B., Tribble, R.P., Grinberg, A., Tsay, H.C., Jacobs, H.M., Kessler, C.M., Long, E.O., Love, P.E., and Samelson, L.E. (1999). Essential role of LAT in T cell development. *Immunity* **10**, 323-332.
- Zhou, L.-Z.Z., Li, S., Feng, Q.-N.N., Zhang, Y.-L.L., Zhao, X., Zeng, Y.-L.L., Wang, H., Jiang, L., and Zhang, Y. (2013). PROTEIN S-ACYL TRANSFERASE10 Is Critical for Development and Salt Tolerance in *Arabidopsis*. *The Plant Cell* **25**, 1093-1107.
- Zhu, J.Y., Sae-Seaw, J., and Wang, Z.Y. (2013). Brassinosteroid signalling. *Development* **140**, 1615-1620.
- Zinchuk, V., Zinchuk, O., and Okada, T. (2007). Quantitative colocalization analysis of multicolor confocal immunofluorescence microscopy images: pushing pixels to explore biological phenomena. *Acta Histochemica et Cytochemica* **40**, 101-111.
- Zurzolo, C., van Meer, G., and Mayor, S. (2003). The order of rafts. Conference on microdomains, lipid rafts and caveolae. *EMBO Reports* **4**, 1117-1121.

